LM-04K130
October 18, 2004

Delayed Fission Product Gamma-Ray Transmission Through Low Enriched UO_2 Fuel Pin Lattices in Air

TH Trumbull

NOTICE

DELAYED FISSION PRODUCT GAMMA-RAY TRANSMISSION THROUGH LOW ENRICHED UO_2 FUEL PIN LATTICES IN AIR

By

Timothy H. Trumbull

A Thesis Submitted to the Graduate
Faculty of Rensselaer Polytechnic Institute
in Partial Fulfillment of the Requirements
for the Degree of

DOCTOR OF PHILOSOPHY

Major Subject: Nuclear Engineering and Science

Approved by the
Examining Committee:

_____
Dr. Donald Harris, Thesis Co-Advisor

_____
Dr. Don Steiner, Thesis Co-Advisor

_____
Dr. George Xu, Member

_____
Dr. Yaron Danon, Member

_____
Dr. Mark Embrechts, Member

Rensselaer Polytechnic Institute
Troy, New York

December, 2004

TABLE OF CONTENTS

LIST OF FIGURES

LIST OF TABLES

ACKNOWLEDGMENTS

I would like to thank Jonathan Stephens, Glenn Winters, and the rest of the staff at the RPI Reactor Critical Facility for supporting this research effort and assisting me with the experimental measurements. I would also like to extend my gratitude to the Mechanical, Aerospace, and Nuclear Engineering department at RPI for their continued support of RCF operations.

This work would not have been possible without the Lockheed Martin Tuition Reimbursement Program and the support of KAPL, Inc. I would like to specifically thank Mr. Jeff Hoole and Dr. Ray Gamino for their support throughout this endeavor.

I wish to acknowledge my thesis committee for their time and efforts in support of this research. In particular, I would like to thank Dr. Don Steiner for his assistance without which I could not have completed this work as a part-time graduate student. Special thanks go to Dr. Donald Harris whose constant encouragement and excellent advice was instrumental in developing this work and guiding it to completion.

Over the years I have benefited immensely from the influence of my family. I offer special thanks to my parents for fostering an atmosphere of learning and stressing the values of education and hard work.

To my incredible wife, Virgine, I offer my deepest thanks. Her unwavering optimism pulled me through the periods of doubt. Without question, her support was as valuable in completing this work as anything I contributed.

Finally, to my wonderful children, Sebastian and Claire, I dedicate this thesis. It is my sincerest wish that one day they understand how meaningful it is to have such devoted fans.

ABSTRACT

The transmission of delayed fission-product gamma rays through various arrangements of low-enriched UO_2 fuel pin lattices in an air medium was studied. Experimental measurements, point-kernel and Monte Carlo photon transport calculations were performed to demonstrate the shielding effect of ordered lattices of fuel pins on the resulting gamma-ray dose to a detector outside the lattice. The variation of the gamma-ray dose on the outside of the lattice as a function of radial position, the so-called "channeling" effect, was analyzed.

Techniques for performing experimental measurements and data reduction at Rensselaer Polytechnic Institute's Reactor Critical Facility (RCF) were derived. An experimental apparatus was constructed to hold the arrangements of fuel pins for the measurements. A gamma-ray spectroscopy system consisting of a sodium-iodide scintillation detector was used to collect data. Measurements were made with and without a collimator installed.

A point-kernel transport code was developed to map the radial dependence of the gamma-ray flux. Input files for the Monte Carlo code, MCNP, were also developed to accurately model the experimental measurements. The results of the calculations were compared to the experimental measurements. In order to determine the delayed fission-product gamma-ray source for the calculations, a technique was developed using a previously written code, DELBG and the reactor state-point data obtained during the experimental measurements.

Calculations were performed demonstrating the effects of material homogenization on the gamma-ray transmission through the fuel pin lattice.

Homogeneous and heterogeneous calculations were performed for all RCF fuel pin lattices as well as for a typical commercial pressurized water reactor fuel bundle.

The results of the study demonstrated the effectiveness of the experimental measurements to isolate the channeling effect of delayed fission-product gamma-rays through lattices of RCF fuel pins in an air medium. The calculational results support the measurements and suggest that under certain conditions material homogenization of fuel pin lattices does not introduce significant error in the dose rate calculation.

CHAPTER 1
INTRODUCTION

Calculations and measurements of delayed fission-product gamma-ray dose rates from spent nuclear fuel and operating reactors have been conducted for many different purposes. In many applications, the fuel pins are in water, as is the case for the operating reactor. In other cases, the fuel pins are in air. These include determination of personnel exposure from shipping and storage casks, gamma scanning to determine fuel pin depletion, non-destructive methods to determine fuel pin integrity, non-destructive methods to determine individual pin power profiles and other tomography-based non-destructive analysis. These analyses are of high value in supporting the commercial nuclear industry. Thus, it is of major importance to verify the methods used to predict these effects. Among the effects requiring verification is the streaming of gamma rays through dry fuel pin lattices; specifically, the effect of approximating the fuel pin lattice as a homogeneous region. The importance of this effect is reinforced by recent calculations showing large differences in the calculated gamma-ray dose from homogeneous and actual fuel bundles [**Bozkurt**].

The Reactor Critical Facility (RCF) at Rensselaer Polytechnic Institute, Troy, NY, offers a unique opportunity to perform detailed measurements of fission-product gamma-ray transport through fuel pin lattices closely approximating those used in the commercial nuclear industry [**Harris1**]. The high-enriched fuel-plate core at the RPI RCF was refueled in 1986 with low-enriched Special Power Excursion Reactor Test (SPERT) fuel pins [**Harris2**]. The SPERT fuel pins used in the RCF contain UO_2 pellets enriched to 4.81 weight percent ^{235}U, clad in stainless steel. The effective fuel height is 36 inches

and the pins are 0.466” in outside diameter. The fuel pin enrichment and lattice spacing are close to those used in pressurized light water and boiling light water reactors, constituting the great majority of reactors worldwide.

The core itself contains on the order of 330 fuel pins, arranged in an octagon, with four perimeter control rods constructed of boron-impregnated iron, clad with stainless steel. The pins are arranged in the RCF core on a 0.640” square pitch. The RCF maintains an inventory of fuel pins that have not been irradiated allowing the unique opportunity to study lattice arrangements of mixed irradiated and unirradiated fuel pins in an air medium.

Because the RCF operates at very low power, usually less than three watts, the power history on the core is very low resulting in low levels of radiation during and after operation. Activated pins can be easily removed from the core and placed in the measurement apparatus with very little dose being received by the experimenters.

Utilizing the RCF to further characterize and experimentally verify fission-product gamma-ray transmission through pin lattices in air will help to provide analysts with unique data and perspectives in evaluating fission-product gamma-ray transport. One such perspective involves accurate modeling, or the representation of the actual problem within the framework of a calculational tool. This is an essential part of obtaining meaningful results in the calculation of radiation transport problems. The analyst usually has little control over some of the approximations made in the model, such as approximations in the nuclear physics, cross section libraries, or transport theory solution technique used in the solver code.

However, the analyst is often compelled to make additional simplifications of the model. Examples of such simplifications include the representation of curvilinear shapes in rectilinear geometry, such as representing curves as steps of rectangular blocks, and the homogenization of materials, or the "smearing" of the materials in several discrete geometric regions to create a new material in a larger, less detailed geometric region.

Approximations of model geometry, specifically the homogenization of materials in geometrically complex regions, has been shown in one study to significantly affect the Monte Carlo calculated dose rates from gamma radiation of a spent PWR fuel assembly [**Bozkurt**]. This implies that explicit modeling of commercial pin lattice geometries and the subsequent investment of the analyst's time and computer calculation time is necessary to obtain accurate gamma radiation dose rate calculations.

Therefore, it is necessary to analyze and verify the underlying physics of the problem in order to determine to what extent the homogeneous approximation affects the solution. With this understanding, the analyst can better choose the level of geometric detail to include in the calculational model. Of particular interest in the evaluation of homogeneous and heterogeneous models is the radial angular dependence of the channeling effect of gamma rays through the lattice spaces, irradiated pin self-shielding effects, and non-irradiated pin shielding effects.

The effects of material homogenization for these types of calculations have been characterized and experimental data of gamma-ray transmission through dry fuel pin lattices have been collected and analyzed. The results of this research will benefit analysts in determining appropriate modeling strategies for similar pin lattice calculations including calculating gamma-ray dose rates for dry storage containers, gamma-ray

fluence calculations on structures exterior to the core, and radial gamma scanning of spent nuclear fuel bundles.

CHAPTER 2
HISTORICAL REVIEW

The total gamma-ray energy released by the delayed fission-product decay chains at times greater than about 50 ns after fission is comparable to the energy released by prompt fission gamma photons [**Shultis**]. Determining the delayed fission-product source, therefore, is of great importance. Accurate estimates of the delayed fission-product gamma-ray source are required for a variety of reasons, e.g., determining reactor shielding, planning outage maintenance and personnel exposure, design of spent fuel storage and shipping containers, and gamma scanning of irradiated fuel.

Gamma rays are released from the fission process as "prompt" or "delayed." Prompt gamma rays are emitted at times less than 5.0×10^{-8} seconds following fission. The fission fragments themselves may remain in isomeric states, emitting gamma rays, as they decay to their ground states. The time interval for isomeric transformation is on the order of 10^{-6} to 10^{-3} seconds after fission [**Jaeger**]. Following isomeric transformation of the fission fragments, gamma-ray emission due to beta decay becomes the dominant source of delayed fission-product gamma rays after about 0.1 second following fission, as illustrated in Figure 2.1.

A great deal of work has been performed in determining the delayed fission-product gamma-ray source spectra as functions of time after shutdown, as well as applications of this knowledge for reactor shielding and gamma-ray tomography of fuel rods. A survey of this work is provided in this chapter.

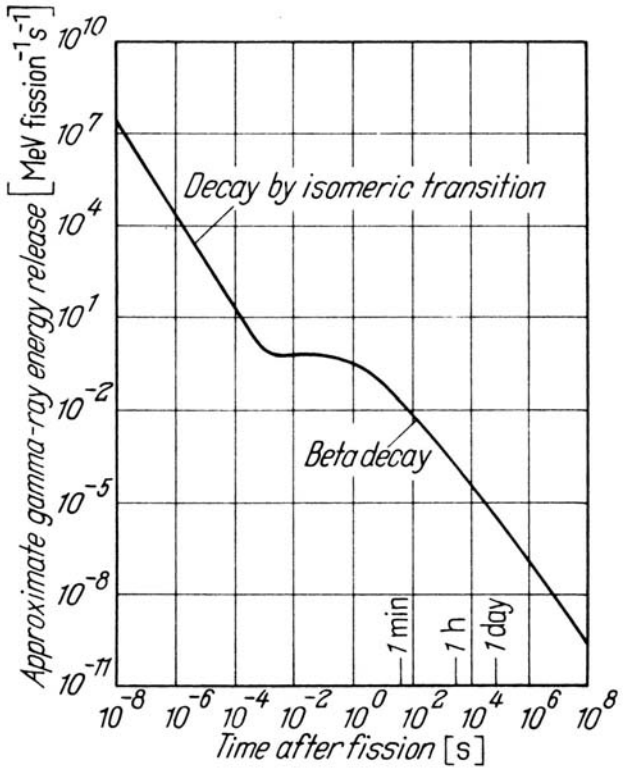

Figure 2.1: Gamma-ray energy release from fission of ^{235}U as a function of time after fission **[Jaeger].**

2.1 Experimental Measurements of Delayed Fission-Product Gamma Rays

For reactors after shutdown, the longer lived fission-product gamma rays become the dominant source of radiation and decay heat. For this reason, these long-lived fission products have been considered in detail. In particular, two sets of experiments were performed in the early 1960's to study fission-product gamma-ray emissions for times after fission greater than about one second.

The first of these was conducted at Oak Ridge National Laboratory (ORNL). The ORNL study measured the gamma-ray spectra as a function of time after fission for gamma rays emitted primarily from thermal neutron induced fission of ^{235}U in the Oak Ridge Graphite Reactor [**Maienschein**]. The ORNL experiment used two types of multiple scintillation spectrometers to cover the energy range of 0.28 to 5.0 MeV.

The second set of measurements was performed at Los Alamos Scientific Laboratory, now Los Alamos National Laboratory (LANL), using a single-crystal scintillation spectrometer to examine the gamma-ray spectra after fission of several isotopes in a bare critical assembly [**Fisher**]. The time after fission ranged from 0.2 to 45 seconds in this study.

For times greater than about 1000 seconds after fission, the delayed fission-product decay rate can be predicted on the basis of the beta-decay information for the individual isotopes. Figure 2.2 shows the ORNL and LANL data along with predictions using beta-decay information [**Perkins**] for gamma-ray energy release rates at times from one to about 2000 seconds after fission.

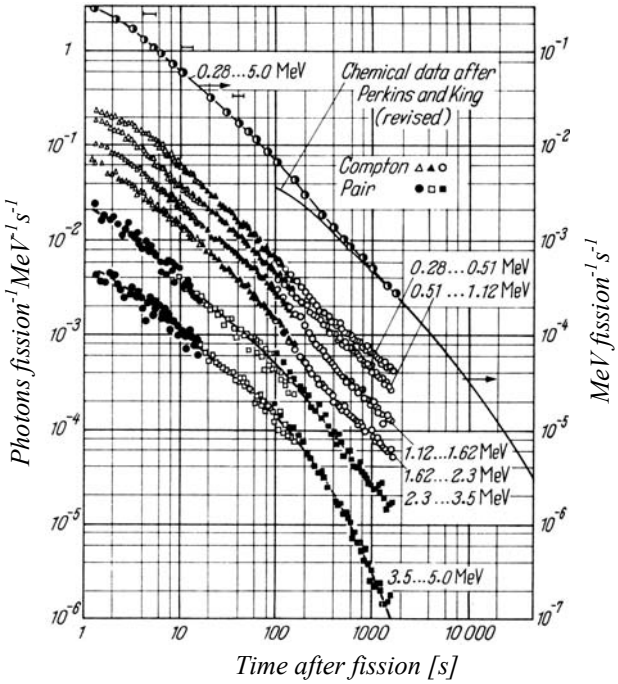

Figure 2.2: Gamma-ray energy release from fission of ^{235}U as a function of time after fission for selected energy groups [**Jaeger**].

In Figure 2.2, the ORNL data are represented as points, the LANL data are represented by the bars, and the beta-decay predictions are represented by the solid line.

The gamma-ray energy release rates as a function of time after fission shown in Figure 2.2 are well-behaved curves which suggest that they can be described by single, continuous functions. This is an important aspect of delayed fission-product behavior which is exploited in this research, as described in later chapters.

2.2 Gamma Scanning of Irradiated Nuclear Fuel

A great deal of work has been done in the area of post-irradiation gamma ray measurement of fuel pins and fuel pin bundles (see [**Matsson**] for comprehensive list). Gamma scanning of fuel pins and bundles offers a non-destructive analysis alternative for determining several key parameters of reactor and fuel performance, such as fuel pin power distribution, axial power profile, determination of fission gas release, and determination of fuel utilization.

Post-irradiation gamma scanning is usually accomplished with the fuel pin or bundle submerged in wet storage, due to the high dose rates. An apparatus similar to the one shown in Figure 2.3 is required to perform the measurements. Recent improvements in gamma scanning by [**Matsson**] at ABB, Sweden have produced measurements with excellent agreement to calculations in the non-destructive prediction of fission gas release, axial cesium redistribution, burnup comparison and relative axial power distributions, as well as loss of uranium from failed fuel rods. In total, some 20 measurement programs spanning the last 10 years, involving over 400 objects (fuel pins and assemblies) have been carried out by ABB Atom, Sweden.

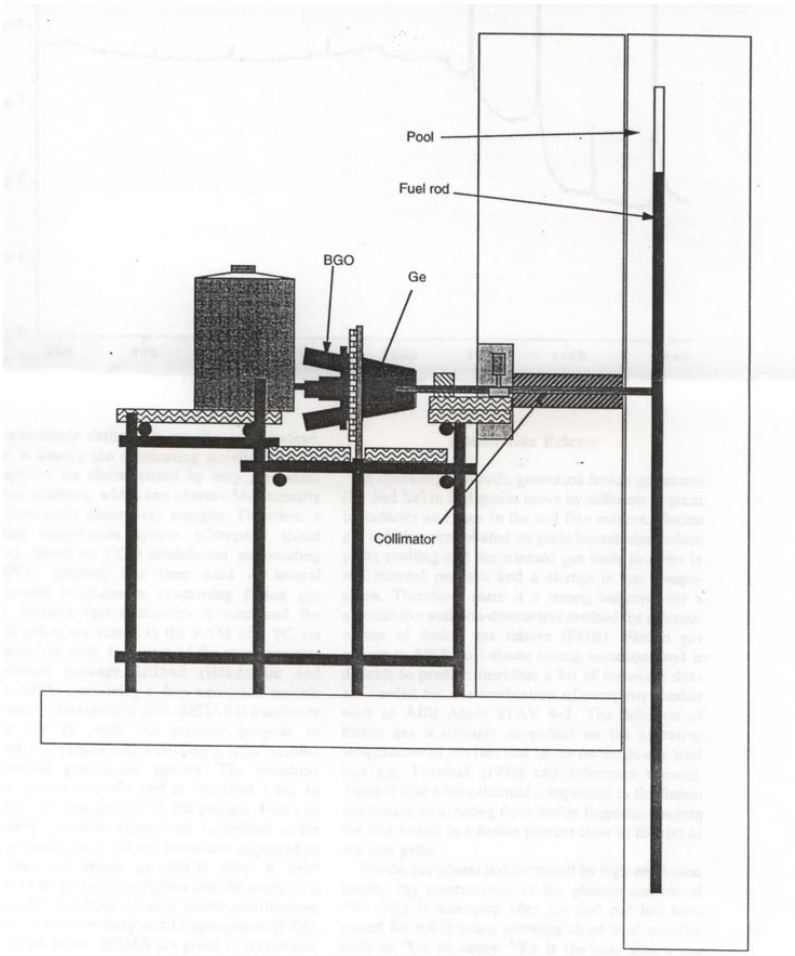

Figure 2.3: Experimental apparatus used for measurements in ABB Atom BWR plants, in this case with a Compton shield detector (BGO-type) surrounding the main Germanium detector [**Matsson**].

Additional gamma scanning applications involve the principles of tomography to provide information about the fuel bundle without destructive disassembly [**Lee**, **Jacobsson1,2**].

In these methods, a number of scans with a collimated detector are performed at various positions relative to the fuel bundle and parameters are then reconstructed using tomographic algorithms. The principles of 2-D, point-kernel transport are applied to determine the contribution to the detector, at each position, from each pin in the lattice. In the study of the HANARO fuel bundle [**Lee**], 36 measurements at equally spaced

intervals around the bundle were performed. The bundle itself contained 36 pins creating a set of 36 equations with 36 unknowns.

The studies performed by Jacobsson [**Jacobsson1,2**] involve a larger number of measurement locations than fuel pins, leading to a highly overdetermined set of linear equations. In order to solve the system of equations, least-squares fitting techniques [**Trefethen**] or algebraic reconstruction techniques (ART) [**Kak**] are required.

Results measured by Lee [**Lee**] in predicting the pin power distributions within a HANARO fuel bundle were shown to agree well with similar MCNP calculations. Similarly, measurements performed by Jacobsson [**Jacobsson2**] show good agreement with calculations in predicting the pin power distributions in a typical 8x8 pin BWR fuel assembly.

Tomographic reconstruction of pin power distributions is a significant capability because it provides a means of determining pin powers, pin integrity, and the actual presence of fuel pins in various lattice positions, without costly disassembly of the fuel bundle. The basis of gamma scanning fuel bundles for tomography relies on knowledge of the channeling effect of radiation through the fuel pin lattice. The channeling effect for neutrons in a fuel pin/water medium has previously been studied [**Harris3**] and no significant anisotropy in the neutron migration parallel and perpendicular to the pin was noted. Water is not as transparent to neutrons as air is to gamma rays, and so this conclusion is not directly extendable to gamma-rays in an air medium. A major focus of this research is the direct measurement of the gamma ray-air channeling effect and development of a 2-D point-kernel calculational tool capable of predicting the contribution from each pin in a lattice to a detector at various positions.

2.3 Modeling Gamma-Ray Dose Rate from a Spent Pressurized Water Reactor Fuel Assembly

Perhaps the single most important application of quantifying the delayed fission-product gamma-ray source is in the determination of the dose rate from spent nuclear fuel. This is of particular importance when the fuel has been removed from wet storage for storage in dry casks or in the final geologic repository. Once the fuel is removed from the wet storage facility any shielding benefit from the water is removed. Therefore, it is important to characterize the fission-product gamma-ray dose rate for spent fuel in an air medium.

One such calculation was performed [**Bozkurt**] on a typical pressurized water reactor (PWR) fuel bundle using the MCNP™ [**Briesmeister**] Monte Carlo code. In this study, a Westinghouse Vantage-5™, 17x17 pin PWR fuel bundle was modeled. The fission-product source was taken from literature [**Chilton**] for both one year and 10 years following removal from the core using a seven-group energy structure covering the range of 0.0 to 20.0 MeV. MCNP ring detector tallies were used to calculate the gamma-ray flux at various radii from the center of the bundle and at three axial heights. A flux-to-dose response function was used to convert the flux to a dose rate.

Of particular interest in this study was the effect of material homogenization on the calculated dose rate on the outside of the fuel bundle. The homogeneous dose rate, as computed in this work, was shown to be significantly higher than the heterogeneous calculation for detector radii out to approximately one meter from the center of the assembly.

The difference in the homogeneous and heterogeneous dose rates was attributed to a combination of effects. In the heterogeneous case, preferential paths through a lattice

of fuel pins exist giving rise to radiation "channeling." The channeling results in a greater number of outwardly directed gamma rays reaching the detector. Once the fuel bundle is homogenized into a "solid," uniformly dense region of material, the channeling effect is effectively eliminated.

However, another competing effect serves to increase the dose rate in the homogeneous case. The source sites for gamma rays are no longer constrained to be within the meat of a fuel pin, which is highly attenuating. Instead, the gamma-ray birth sites can exist anywhere in the homogeneous core. This essentially removes the "self shielding" effect of the fuel meat on the gamma-ray source and serves to increase the dose rate on the outside of the bundle.

In this particular study, the authors claim that removing the self shielding is the dominant effect causing the homogeneous dose rate to be significantly larger than that calculated in the heterogeneous case. Because of the results shown in this reference, the effects of homogenization of materials on the calculated dose rate for fuel pin lattices became an additional focus area for this research.

CHAPTER 3
THE EFFECTS OF CHANNELING ON THE CALCULATED GAMMA-RAY DOSE OUTSIDE OF A PIN LATTICE

Given the nature of a lattice, the transport of radiation from within the lattice to some position outside the lattice will depend on the path traversed. Radiation emanating from one position within a lattice may find a favorable path, reaching the exterior with little attenuation, or the radiation may encounter several attenuating masses on its journey and arrive at the exterior with little of its original intensity. The degree of attenuation along any path traveled by the radiation is a function of its starting position, material attenuation factors, lattice spacing, lattice configuration, and lattice materials.

Thus, the dose calculated at various positions on the exterior of a lattice is not expected to be constant. Rather, the dose outside of the lattice is expected to have an angular dependence reflecting the differing paths that the radiation must take to reach the outside of the lattice. This characteristic of radiation transport through lattices is referred to here as the "channeling effect."

In order to assess the importance of the lattice channeling effect, point kernel transport calculations and Monte Carlo calculations of various lattice configurations were performed. These calculations were based on experimental measurements of the channeling effect (discussed in Chapter 4), and are therefore based on the same geometry and source strength of those measurements.

3.1 Determination of the Fission-Product Source Term

In order to perform a calculation which effectively models the experimental measurements, an accurate estimation of the source term was necessary. The source for all the measurements performed is solely due to gamma rays released from fission-

product decay. Since all the experiments were conducted using a single activated fuel pin as the source, the fission-product source strength was determined using the power history (peak power, reactor period, time of activation) for that single pin for each particular experiment.

Several commercial codes are available to determine the after-shutdown inventory of fission products, e.g., CINDER and ORIGEN, both based on more detailed nuclear decay data. Additional work has been performed to develop methods to calculate the time-dependent energy release rate from fission-product gamma rays in order to characterize decay heat. Corrections based on observed decay data ("integral data") have been developed [**Wilson**]. The time-dependent energy release rate from fission-product beta and gamma rays is, at any time, due to a large collection of many different fission products at many different concentrations. This proves problematic in describing the time dependence of the energy release rate in terms of a set of known fission products. Instead, a series of exponential functions have been developed that describe the total energy release rate for a set of discrete energy intervals [**Wilson**]. Least-squares fitting of the exponential parameters was performed based on results of CINDER calculations. The number of terms in the exponential series was extended until the desired degree of agreement with beta-decay calculations and observations was obtained. This technique was repeated for all desired energy groups.

3.1.1 Calculating the Delayed Beta and Gamma-Ray Energy Released From Fission Using the DELBG Code

For this work, a code developed and written by Dr. D.R. Harris called DELBG (DELayed Beta and Gamma) was utilized. DELBG uses a published library of derived

exponential constants [**Wilson**] to calculate the beta and gamma-ray source, based on the power history, fission rate, and report times included in the input file. The method of solution used in DELBG is explained below.

DELBG allows the user to describe a power history in "blocks" of time. Each block represents a period of time, starting at t_a and ending at t_b, when the power of the reactor is either at a constant level or changing with a constant period. The energy release rate at some time t, as a result of a fission occurring at time, t', where $t_a < t' \le t_b$, is given by

$$E(t,t') = \alpha e^{-\lambda(t-t')} \quad , \tag{3.1}$$

where α and λ are constants describing the time dependence of a particular fission-product energy range and E has units of MeV per fission per second. The total energy release rate as a result of all fissions occurring within the power block is obtained by integrating Equation (3.1) over the range t_a to t_b,

$$E(t) = \int_{t_a}^{t_b} dt' \alpha e^{-\lambda(t-t')} \quad . \tag{3.2}$$

Equation (3.2) is easily integrated and when evaluated over the limits of integration becomes

$$E(t) = \frac{\alpha}{\lambda}\left(e^{-\lambda(t-t_b)} - e^{-\lambda(t-t_a)}\right) . \tag{3.3}$$

Calculating the energy release rate given a block with power changing on a constant period is performed in a similar manner. In this case, however, Equation (3.1) includes an additional term to describe the change in power over the interval

$$E(t,t') = \alpha e^{-\lambda(t-t')} e^{\Lambda(t'-t_b)} \quad , \tag{3.4}$$

where Λ is the inverse reactor period. The total energy release rate as a result of all fissions occurring within the power block is again obtained by integrating the equation over the range t_a to t_b,

$$E(t) = \int_{t_a}^{t_b} dt' \alpha e^{-\lambda(t-t')} e^{\Lambda(t'-t_b)} \quad . \tag{3.5}$$

It is convenient to perform a transformation of variables in Equation (3.5) where $T = t' - t_b$, the time after shutdown. Applying the transformation yields

$$E(t) = \alpha e^{-\lambda t} \int_{t_a - t_b}^{0} dT e^{\lambda(T+t_b)} e^{\Lambda T} \quad , \tag{3.6}$$

which is again easily integrated to obtain

$$E(t) = \alpha e^{-\lambda t} e^{\lambda t_b} \left(\frac{1}{\lambda + \Lambda} \right) e^{T(\lambda+\Lambda)} \Bigg|_{t_a - t_b}^{0} \quad . \tag{3.7}$$

Evaluating Equation (3.7) over the specified limits results in the final form of the energy release rate

$$E(t) = \frac{\alpha}{\lambda + \Lambda} e^{-\lambda(t-t_b)} \left(1 - e^{(t_a - t_b)(\lambda+\Lambda)} \right) . \tag{3.8}$$

In most practical cases (and as certainly the case in this work) the interval $(t_a - t_b) >> (\lambda + \Lambda)$, and is negative. Therefore, an excellent approximation to Equation (3.8) is

$$E(t) = \frac{\alpha}{\lambda + \Lambda} e^{-\lambda(t-t_b)} \quad . \tag{3.9}$$

DELBG uses Equations (3.3) and (3.9) to determine the energy release rate for eighteen beta and nineteen gamma-ray energy groups, at a specified number of report times, given a specified number of power blocks and fission reaction rates. Allowable fission reaction

rates in DELBG include those for fast ^{232}Th, thermal ^{233}U, thermal ^{235}U, fast ^{238}U, thermal ^{239}Pu, and thermal ^{241}Pu.

Pseudo code describing the process followed by DELBG to calculate the total energy release rate is shown in Figure 3.1. DELBG source code, library, and sample input file are included in Appendix A.

Loop over # of report times, *t*.
  Loop over # of energy groups, *g*.
    Loop over # of power history blocks, *h*.
      Loop over # of fissionable materials, *m*.
        Loop over # of terms for gamma-ray production, *i*.
          Calculate the gamma-ray energy released for energy group, *g*, at report time, *t*.
          If constant power block,

$$E_{g,t} = E_{g,t} + \frac{R_{h,m}\alpha_{i,g,m}}{\lambda_{i,g,m}}\left[e^{-\lambda_{i,g,m}(t-t_b)} - e^{-\lambda_{i,g,m}(t-t_a)}\right], \tag{3.10}$$

          else if on a constant period, τ_h,

$$E_{g,t} = E_{g,t} + \frac{R_{h,m}\alpha_{i,g,m}}{\lambda_{i,g,m} + \frac{1}{\tau_h}}\left[e^{-\lambda_{i,g,m}(t-t_b)}\right]. \tag{3.11}$$

          End if.
        End do.
      End do.
    End do.
  End do.
End do.

Figure 3.1: Pseudo code for calculating gamma-ray energy emission using DELBG.

Equations (3.10) and (3.11) are identical to the previously derived Equations (3.3) and (3.9), where the following notation is used:

$E_{g,t}$ = Gamma-ray energy release rate (MeV/s) in energy group, *g*, at report time, *t*,

$R_{h,m}$ = Fission rate (fissions/s) over the power history block, *h,* for material, *m*,

$\alpha_{i,g,m}$ = Gamma-ray production coefficient for term, *i,* energy group, *g*, and material, *m*,

$\lambda_{i,g,m}$ = Decay constant for term, *i,* energy group, *g*, and material, *m*,

t = time at which gamma-ray energy release is requested,

t_a = time at the beginning of power history block, *h*,

t_b = time at the end of power history block, *h*,

τ_h = reactor period over power history block, *h*.

Energy breakpoints for the nineteen energy groups used in DELBG are shown in Table 3.1. DELBG also divides the energy release rate by the average energy of the group to obtain the gamma-ray release rate (γ/s) for each energy group.

Table 3.1: DELBG nineteen energy group structure.

Energy Group	$E_{bot.}$ (MeV)	E_{top} (MeV)	$E_{avg.}$ (MeV)
1	0	0.1	0.05
2	0.1	0.2	0.15
3	0.2	0.4	0.3
4	0.4	0.6	0.5
5	0.6	0.8	0.7
6	0.8	1.0	0.9
7	1.0	1.2	1.1
8	1.2	1.4	1.3
9	1.4	1.6	1.5
10	1.6	1.8	1.7
11	1.8	2.0	1.9
12	2.0	2.2	2.1
13	2.2	2.4	2.3
14	2.4	2.6	2.5
15	2.6	3.0	2.8
16	3.0	4.0	3.5
17	4.0	5.0	4.5
18	5.0	6.0	5.5
19	6.0	7.5	6.75

Previous validation work [**Stephens**] has shown that DELBG results compare well to similar calculations performed using gamma-ray decay data published by Shultis and Faw [**Shultis**].

For the experimental measurements, the RCF core was used to activate the fuel pins with a known power history. This was accomplished by increasing reactor power on a constant period to a desired peak power level and then scramming the reactor. Typically, the core was activated to approximately 75 W·s, with sufficient excess reactivity to obtain a constant reactor period of about 26 seconds with all control rods withdrawn.

What is important in the calculation of the delayed fission-product gamma-ray spectra is the *time* of the activation. The target activation energy of 75 W·s was chosen because of the time of irradiation, given the predicted 26 second period. The time of irradiation for all the measurements conducted in this work was estimated from the nuclear instrumentation to be 200 seconds.

The target peak power level was calculated by using the relationship

$$P(t) = P_{-\infty} e^{\frac{t}{\tau}} \quad , \tag{3.12}$$

where,

$P(t)$ = target peak power at time, t,

$P_{-\infty}$ = reactor power at beginning of history,

τ = reactor period.

The activation energy is the product of the power level and the time at that power level,

$$E = \int_{-\infty}^{t} dt' P_{-\infty} e^{\frac{t'}{\tau}} \quad . \tag{3.13}$$

Integrating Equation (3.4) is simple and results in

$$E = \tau \cdot P_{-\infty} e^{\frac{t'}{\tau}} \Big|_{-\infty}^{t} = \tau \cdot P_{-\infty} e^{\frac{t}{\tau}} \quad . \tag{3.14}$$

Substituting Equation (3.12) into Equation (3.14), the activation energy, E, given a constant period, τ, and a peak power, $P(t)$, is simply expressed as

$$E = \tau \cdot P(t) \ . \tag{3.15}$$

Using Equation (3.15), it is now a simple matter to calculate the desired peak power level given the expected reactor period and activation energy desired. In the majority of measurements, the period was assumed to be approximately 26 seconds and the desired activation energy was 75 W·s, giving a peak power target of approximately 2.88 W. For reactor operator convenience, the target peak power level was set at 3 watts. Because measurements were only conducted using the center fuel pin as the source, the actual power level used as DELBG input was adjusted by the calculated power fraction for the center pin.

An example of the gamma-ray source spectrum calculated by DELBG is shown in Table 3.2 for the nineteen energy groups. The spectrum shows the number of gamma rays emitted within an energy group of average energy, $E_{avg.}$, plotted at ten minutes following reactor scram, with an irradiation time of 200 seconds, power history of 75 W·s, and peak power of 3.0 W. The data in Table 3.2 can be used directly in deterministic calculations to provide the energy group dependent gamma-ray source or arranged to represent a histogram probability density function (PDF).

Table 3.2: DELBG calculated gamma-ray spectrum ten minutes after reactor scram for center fuel pin of RCF following a 200 second irradiation resulting in 75 W·s activation.

$E_{avg.}$ (MeV)	Gamma-Ray Source Strength (γ/s)
0.05	6.51E+05
0.15	8.48E+05
0.3	1.72E+06
0.5	1.25E+06
0.7	1.44E+06
0.9	1.67E+06
1.1	7.96E+05
1.3	6.16E+05
1.5	4.05E+05
1.7	3.36E+05
1.9	2.55E+05
2.1	2.37E+05
2.3	1.57E+05
2.5	1.48E+05
2.8	1.79E+05
3.5	1.64E+05
4.5	7.45E+04
5.5	1.00E+04
6.75	4.29E+02

Given gamma-ray source strength, Γ_i, for i=1..n energy bins of width $(x_i - x_{i-1})$, the probability of gamma rays being released within an energy bin is given by

$$p(i) = \frac{\Gamma_i(x_i - x_{i-1})}{\sum_{i=1}^{n} \Gamma_i(x_i - x_{i-1})} \ . \tag{3.16}$$

Assuming that the gamma-ray energy within an energy bin varies uniformly, the probability of a gamma ray with energy x being released is then expressed as

$$p(x) = \sum_{i=1}^{n} p(i) \frac{[\Theta(x - x_{i-1}) - \Theta(x - x_i)]}{(x_i - x_{i-1})} \ , \tag{3.17}$$

where Θ is the Heaviside unit "step function" [**Duderstadt**] defined by the properties

$$\Theta(x) = \begin{cases} 0 & x < 0 \\ 1 & x \geq 0. \end{cases}$$

Alternatively, the PDF can be integrated with respect to energy to generate a cumulative probability density function (CDF). PDFs and CDFs are useful in generating source definition input for stochastic transport codes. Figure 3.2 shows the data of Table 3.2 represented as a discrete PDF and Figure 3.3 shows the same data represented by a CDF.

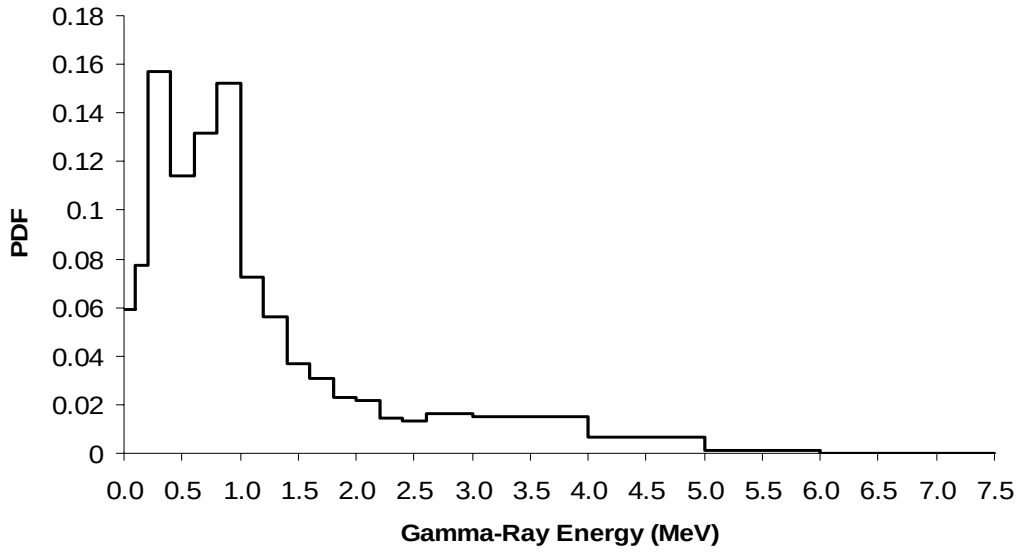

Figure 3.2: Probability density function for DELBG calculated gamma-ray spectrum ten minutes after reactor scram following 75 W•s activation.

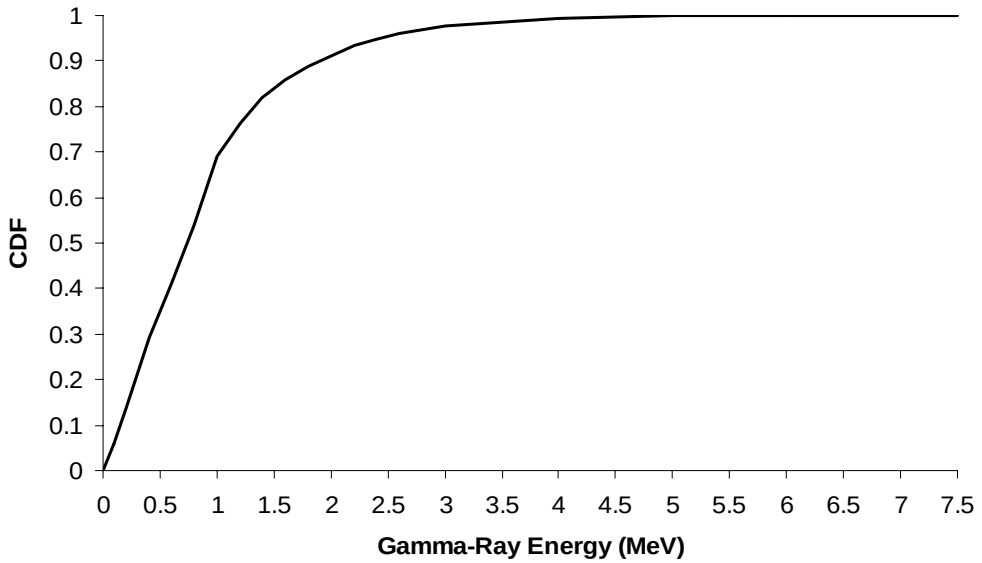

Figure 3.3: Cumulative probability density function for DELBG calculated gamma-ray spectrum ten minutes after reactor scram following 75 W•s activation.

In the manner described in the preceding paragraphs, DELBG was used to produce gamma-ray source input to point-kernel and stochastic transport codes, as described in the following two sections.

3.2 Calculating the Lattice Effects Using Point-Kernel Techniques

For this work, point-kernel methods were used to first evaluate the radiation transport through pin lattices. It was anticipated that an analysis of the uncollided dose at various points outside of the lattice, from a point residing within the lattice, would demonstrate not only the effect of channeling through the lattice but also the relative magnitude of the effect. The specific method used to develop the point-kernel is explained below.

3.2.1 The Point-Kernel for Calculating the Uncollided Gamma-Ray Flux and Dose from Isotropic, Polyenergetic, Gamma-Ray Sources

Consider first the case of an isotropic point source emitting monoenergetic radiation with strength, *S*, in a vacuum. The flux, Φ, of the source at a distance *r* varies as

$$\Phi(r) = \frac{S}{4\pi \cdot r^2} \ . \tag{3.18}$$

This effect is simply due to the sphere surface area subtended by a single steradian increasing as the square of the sphere's radius. Therefore, the radiation flux given by Equation (3.18) is a purely geometric effect and says nothing as to the effect of materials that may be involved in the problem.

In the point-kernel analysis, all materials are assumed to be exponential attenuators. That is, for particles starting at *x=0* and streaming through a homogeneous

medium, the probability that a particle will travel at least a distance x without colliding can be expressed as

$$p(x) = e^{-\mu x}, \tag{3.19}$$

where μ is the attenuation coefficient for the material. If n materials having thicknesses, t_i, and attenuation coefficients, μ_i, are "stacked" or "layered" than the probability of traveling a distance x through all the materials without interaction is given by

$$p(x) = e^{-\mu_1 t_1} e^{-\mu_2 t_2} ... e^{-\mu_n t_n}, \tag{3.20}$$

which can be written as

$$p(x) = e^{\sum_{i=1}^{n} -\mu_i t_i}. \tag{3.21}$$

By combining Equations (3.18) and (3.21), the final form of the equation describing the uncollided radiation flux, Φ, at a distance, r, from a monoenergetic point source, S, through n materials of thickness, t_i, and attenuation coefficient, μ_i, is

$$\Phi(r) = \frac{S}{4\pi \cdot r^2} e^{\sum_{i=1}^{n} -\mu_i t_i}, \tag{3.22}$$

where

$$\sum_{i=1}^{n} t_i = r .$$

A dose rate, D, can be calculated if an appropriate response function, $\Re$, is introduced into Equation (3.22),

$$D(r) = \frac{S\Re}{4\pi \cdot r^2} e^{\sum_{i=1}^{n} -\mu_i t_i}. \tag{3.23}$$

In general, the response function and attenuation factors are dependent on the source energy. Therefore, rewriting Equations (3.22) and (3.23) as functions of energy, E,

$$\Phi(r,E) = \frac{S}{4\pi \cdot r^2} e^{\sum_{i=1}^{n} -\mu_i(E) t_i} \quad , \tag{3.24}$$

and

$$D(r,E) = \frac{S\Re(E)}{4\pi \cdot r^2} e^{\sum_{i=1}^{n} -\mu_i(E) t_i} \quad . \tag{3.25}$$

In the case of a source comprised of j discrete energies, the total flux and dose rate are

$$\Phi(r) = \sum_j \frac{S \cdot f_j}{4\pi \cdot r^2} e^{\sum_{i=1}^{n} -\mu_i(E_j) t_i} \quad , \tag{3.24}$$

and

$$D(r) = \sum_j \frac{S \cdot f_j \cdot \Re(E)}{4\pi \cdot r^2} e^{\sum_{i=1}^{n} -\mu_i(E_j) t_i} \quad , \tag{3.25}$$

where f_j is the fraction of the total source, S, with energy E_j.

Generalizing the geometric attenuation is useful for defining the point-kernel in terms of an arbitrarily positioned source and target, described by the position vectors, $\mathbf{r_s}$ and $\mathbf{r_t}$, respectively. Applying this generalization to Equations (3.24) and (3.25) yields the final form of the point-kernel equations used in this work:

$$\Phi(\mathbf{r_t}) = \sum_j \frac{S \cdot f_j}{4\pi \cdot \left|\mathbf{r_s} - \mathbf{r_t}\right|^2} e^{\sum_{i=1}^{n} -\mu_i(E_j) t_i} \quad , \tag{3.26}$$

and

$$D(\mathbf{r_t}) = \sum_j \frac{S \cdot f_j \cdot \Re(E)}{4\pi \cdot \left|\mathbf{r_s} - \mathbf{r_t}\right|^2} e^{\sum_{i=1}^{n} -\mu_i(E_j) t_i} \quad , \tag{3.27}$$

where the region thicknesses, t_i, satisfy

$$\sum_{i=1}^{n} t_i = \left|\mathbf{r_s} - \mathbf{r_t}\right| \ .$$

The use of an additional factor in point-kernel calculations – the build-up factor – is often used to account for the contribution to the flux or dose from multiple scattering events, as shown in Figure 3.4. The build-up factor, B, is simply defined as

$$B = 1 + \frac{\Phi_s}{\Phi_0} \ , \tag{3.28}$$

where the contribution to the total flux, Φ_T, due to scattered photons is Φ_s and the contribution from uncollided photons is Φ_0.

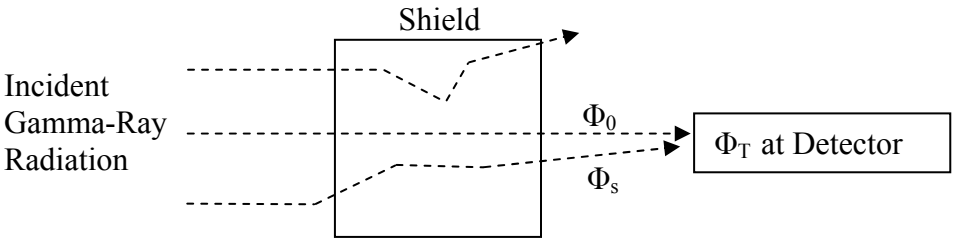

Figure 3.4: Contribution to the Total Flux from Scattering

A large volume of work has been performed in the calculation of build-up factors for many commonly encountered materials in radiation shielding applications [**Jaeger, Rockwell, Shultis**]. Typically, build-up factors are tabulated as a function of material properties (linear attenuation coefficient, μ) and thickness, t, for a given incident gamma-ray energy. Build-up factors are applied to the point-kernel equations as direct multipliers on the flux,

$$\Phi(\mathbf{r_t}, E) = \frac{S}{4\pi \cdot \left|\mathbf{r_s} - \mathbf{r_t}\right|^2} B(\mu t, E) e^{-\mu(E)t} \ . \tag{3.29}$$

Much of the data are applicable to homogeneous media only, however. Various techniques have been suggested for the calculation of suitable build-up factors in multi-layer shields of varying compositions but the practice is somewhat dubious [**Shultis**].

To the extent that the point-kernel is applied in this work, only uncollided flux and dose are considered and the application of build-up factors is not necessary. This is consistent with other similar point-kernel calculations of gamma-ray transport through fuel pin lattices [**Jacobsson1, Jacobsson2, Lee**].

3.2.2 Gamma-Ray Attenuation Coefficients for use in Point-Kernel Calculations

The linear attenuation coefficient, μ, for any particular interaction is a function of material properties and incident gamma-ray energy. In order to apply the equations derived for the point-kernel in §3.2.1, the linear attenuation coefficients for all the materials, interactions and energies of interest must be obtained.

The linear attenuation coefficient can be defined as the factor by which the radiation intensity, I, is reduced over a differential distance of travel, dx,

$$\frac{dI}{I} = \mu dx. \tag{3.30}$$

Assuming an initial radiation intensity of I_0, and integrating Equation 3.30, the radiation intensity at a position t within the slab is given by

$$I(t) = I_0 e^{-\int_0^t \mu(x)dx}, \tag{3.31}$$

or for a homogeneous region,

$$I(t) = I_0 e^{-\mu t}. \tag{3.32}$$

Some have suggested that the term "attenuation coefficient" be replaced with "interaction coefficient" because, as shown in §3.2.2.1, not all photon interactions with matter are attenuating. For consistency, however, this work will maintain the standard convention and use the term attenuation coefficient.

3.2.2.1 Interaction of Gamma Rays with Matter

The major photon interactions with matter are shown in block-diagram form in Figure 3.5. Of particular importance are incoherent (Compton) scattering, coherent (Rayleigh) scattering, photoelectric effect, and pair production. Additional photon scattering is possible through nuclear Thomson Scattering and nuclear resonance scattering. However, these interactions are mostly considered insignificant compared to Compton Scattering [**Price**].

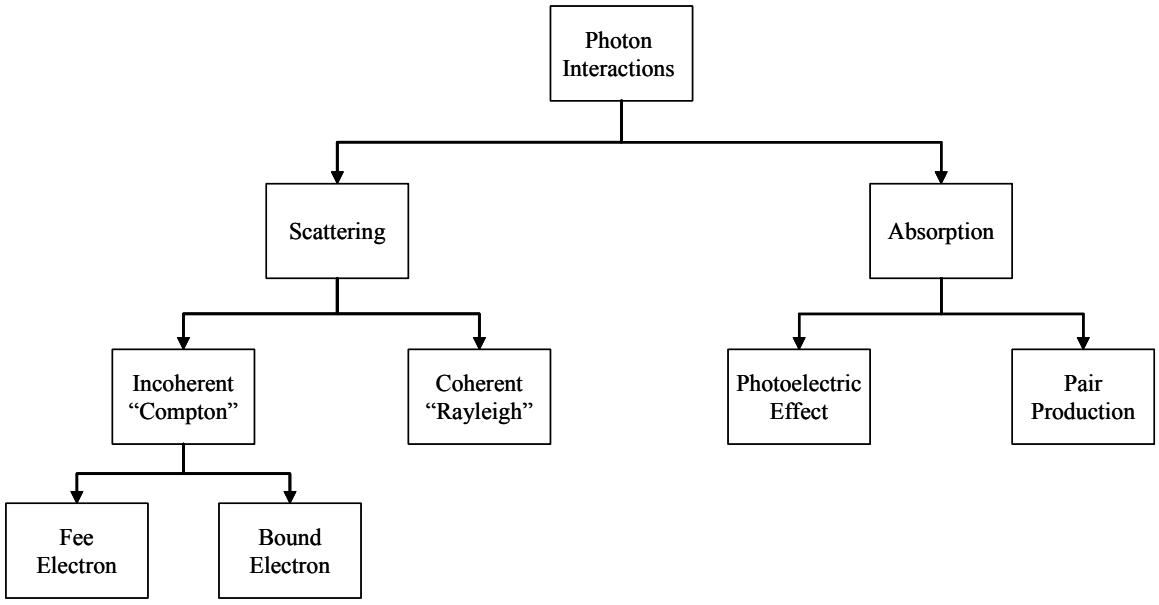

Figure 3.5: Block Diagram of Basic Photon Interactions with Matter

Compton scattering is treated as a photon interaction with a single electron of an atom, as depicted in Figure 3.6.

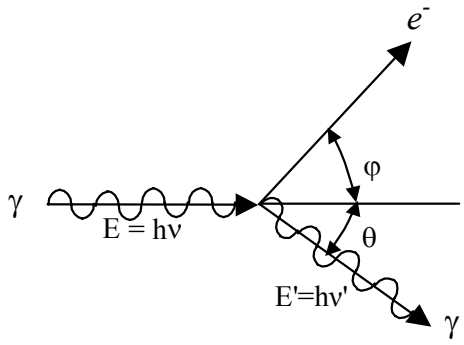

Figure 3.6: Compton scattering of a photon, γ, scattering from a single electron, e-, through an angle, θ.

If the incident photon energy is sufficiently greater than the binding energy of the electron, the binding energy effects on the scattering of the photon can be neglected and the reaction assumed to be from a free electron at rest. Generally, free-electron scattering can be assumed for photon energies greater than about 500 keV [**Schultis**]. In such cases when the energy is below about 500 keV, the effects of electron binding are noticeable in the cross section and must be considered. However, in the range of energies where electron binding effects are important, photoelectric interactions greatly exceed incoherent scattering. It is therefore generally accepted that the error from neglecting electron binding effects is small [**Schultis**].

Given a Compton scattering event as shown in Figure 3.6, the final energy of the gamma ray can be calculated using two-body kinematics to be

$$E' = \frac{E}{1 + \frac{E}{m_0 c^2}\left(1 - \cos\theta\right)} \ . \tag{3.33}$$

The scattering angle, θ, for most materials and incident energies is highly forward peaked. The Compton differential scattering cross section can be computed using the *Klein-Nishina* formula for unpolarized photons [**Schultis, Knoll**]

$$\sigma_C(E,E',\mu)=\frac{3}{16\pi}\sigma_T\left(\frac{E'^2}{E^2}\right)\left(\frac{E}{E'}+\frac{E'}{E}-\sin^2\theta\right) \tag{3.34}$$

where μ is the cosine of the scattering angle, σ_T is the Thomson cross section for photon scattering by the nucleus

$$\sigma_T=\frac{8\pi}{3}r_e^2, \tag{3.35}$$

and r_e is the classical electron radius, 2.8179x10^{-13} cm [**Chart**].

It is convenient to make use of Equation 3.33 to eliminate *E'* obtaining the final form of the differential scattering cross section

$$\sigma_C(E,\mu)=\frac{3}{16\pi}\sigma_T\left(\frac{1}{1+\alpha_0(1-\mu)}\right)^2\left(\mu^2+\alpha_0(1-\mu)+\frac{1}{1+\alpha_0(1-\mu)}\right), \tag{3.36}$$

where

$$\alpha_0=\frac{E}{m_0c^2}\ . \tag{3.37}$$

Figure 3.7 shows the differential scattering cross section energy-angle relationship for five incident photon energies. The forward peaked scattering tendency is clearly visible in the figure.

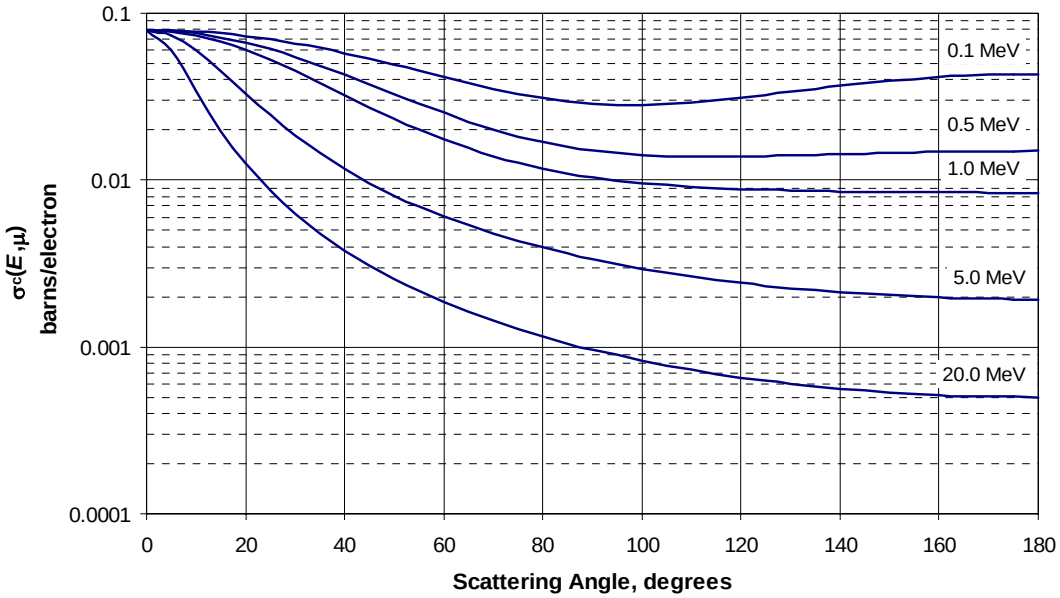

Figure 3.7: Compton scattering differential cross section (barns/electron) for five incident photon energies.

Integrating Equation (3.36) over all angles gives the value of the total Compton scattering cross section for photons of energy *E*, and is shown in Figure 3.8 for natural uranium.

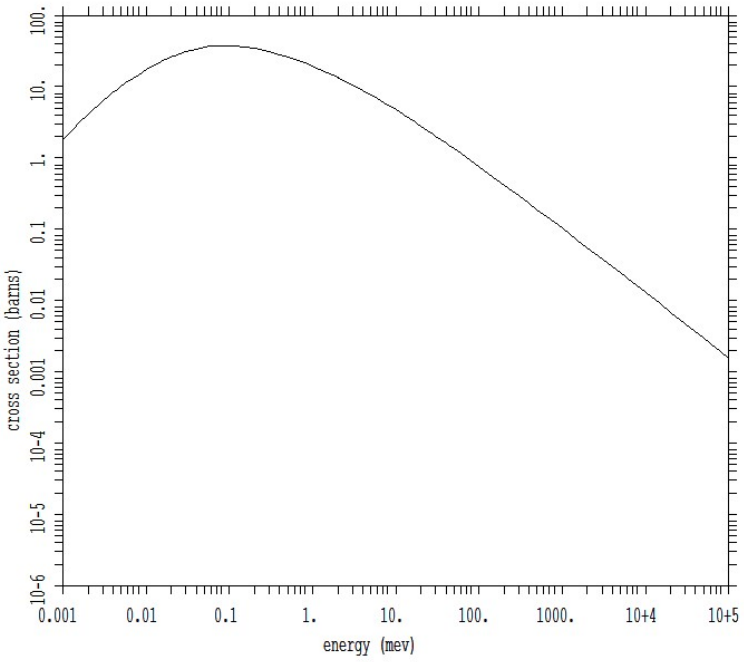

Figure 3.8: Incoherent scattering cross section as a function of energy for Uranium.[1]

[1] Cross section plotted using MCNP4C2 [Breismiester] and data library mcplib02 with ZAID of 92000.02p.

Coherent or Rayleigh scattering occurs when the photon interacts with all the electrons of an atom, collectively. The probability of coherent scattering of photons is dependent on the material and the incident photon energy. For example, in lead only about 10% of 500 keV photons experience coherent scattering. To achieve the same value in iron, the incident photon energy would have to drop to 150 keV [**Price**].

Rayleigh scattering is only important at low incident photon energies and for materials with high atomic number. However, in energy ranges where coherent scattering is more probable than incoherent scattering, the photoelectric effect will be the dominate reaction type for most materials. Additionally, the energy loss and scattering angle of the incident photon are small for coherent scattering, e.g., 75% of 1 MeV photons scattering coherently from iron are scattered within a cone of less than 4° half-angle [**Shultis**]. Therefore, it is common practice to ignore Rayleigh scattering.

Thus far the discussion has centered on photon scattering, shown on the left side of Figure 3.5. Now, the mechanisms for photon absorption (right side of Figure 3.5) are discussed.

The photoelectric effect describes the case where an incident photon is completely absorbed within the target atom, liberating an energetic photoelectron from one of the atom's electron shells. The energy of the emitted electron, E_{e^-}, is the difference between the incident photon energy, $h\nu$, and the binding energy of the electron, E_b,

$$E_{e^-} = h\nu - E_b \ . \tag{3.37}$$

Since the binding energy is usually small compared to the photon energy (> ~300 keV), the photoelectron carries away a large fraction of the original incident photon energy [**Knoll**]. The vacancy created by the emission of the photoelectron can be filled one of

two ways, each of which produces secondary radiation: 1) an electron from a lower shell may make the transition to the shell to fill the vacancy directly, emitting an X-ray (fluorescence), or 2) an electron may be ejected from one of the outer shells in the form of an Auger electron.

The photoelectric process is the dominant reaction for low photon energies and, in general, increases rapidly for decreasing photon energy. For a given photon energy, the probability of photoelectric absorption is increased with increasing atomic number of the target atom. Therefore, the photoelectric absorption cross section, σ_{ph}, can be considered to vary roughly as

$$\sigma_{ph} \propto \frac{Z^4}{E^3} \ . \tag{3.38}$$

The photoelectric cross section, however, is not monotonic, as suggested by Equation (3.38) but is characterized by discrete changes in magnitude at low photon energies, as shown in Figure 3.9. The cross section for photoelectric absorption will typically increase as the photon energy decreases toward an energy corresponding to the binding energy of the electron shell. Once the photon energy drops below the electron binding energy for a particular shell, the reaction is no longer energetically possible and the cross section drops sharply. This pattern is repeated for all electron shells for the target atom.

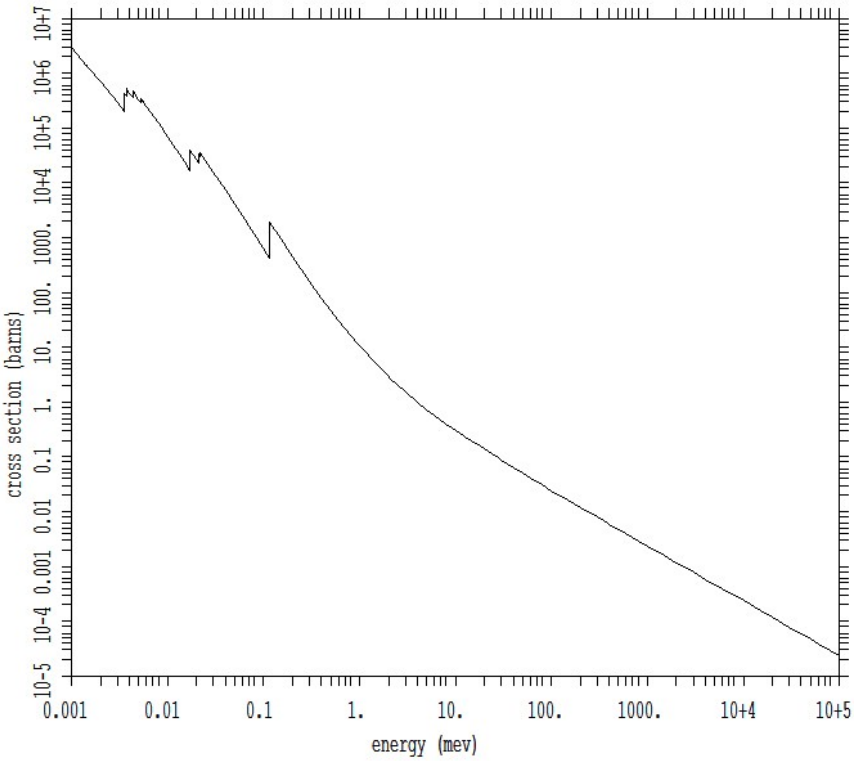

Figure 3.9: Photoelectric absorption cross section as a function of energy for Uranium.[2]

Photoelectric absorption will preferentially occur within the most tightly bound electron shell for which the reaction is energetically possible [**Price**], with 80% of the ionizations occurring within the *K* electron shell [**Evans, Price**].

Pair production is the process that occurs when the incident photon is completely absorbed within the target atom and in its place a positron-electron pair is emitted. This reaction must take place within the strong electric field of the nucleus, or less probable, an atomic electron (triplet production) [**Schultis**]. In order for nuclear pair production to occur, the incident photon must have energy greater than 1.022 MeV or, twice the rest-mass energy of an electron. The kinetic energy of the electron-positron pair is equal to the incident gamma-ray energy minus 1.022 MeV. The recoil energy of the nucleus is neglected due to its large mass [**Evans**].

[2] Cross section plotted using MCNP4C2 [Breismiester] and data library mcplib02 with ZAID of 92000.02p.

In the case of electron pair production, the recoil energy of the electron must be considered and a triplet is produced containing the electron-positron pair plus the recoil electron. The threshold energy for triplet production is 2.044 MeV.

For any given energy, nuclear pair production can be considered to vary with the square of the atomic number of the target material [**Knoll, Price**]. This is modified somewhat by electron pair production at high energies but, in general, this effect is negligible. Figure 3.10 shows the pair production cross section, σ_{pp}, as a function of energy for uranium.

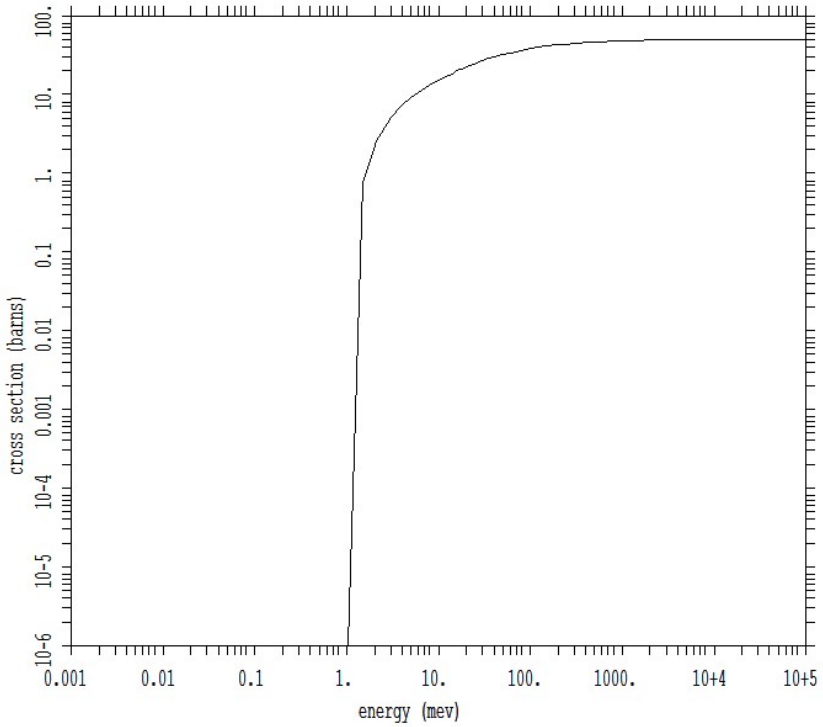

Figure 3.10: Pair production cross section as a function of energy for Uranium.[3]

The probability of a photon of energy *E* experiencing Compton scattering, photoelectric absorption or pair production within a material is simply the sum of the individual cross sections and is termed the total cross section, $\sigma_T(E)$:

[3] Cross section plotted using MCNP4C2 [Breismiester] and data library mcplib02 with ZAID of 92000.02p.

$$\sigma_T(E) = \sigma_C(E) + \sigma_{ph}(E) + \sigma_{pp}(E) \ . \tag{3.39}$$

Figure 3.11 shows the total cross section as a function of incident energy for photons in uranium. The figure also shows over which energy range each of the three major interaction types is dominant.

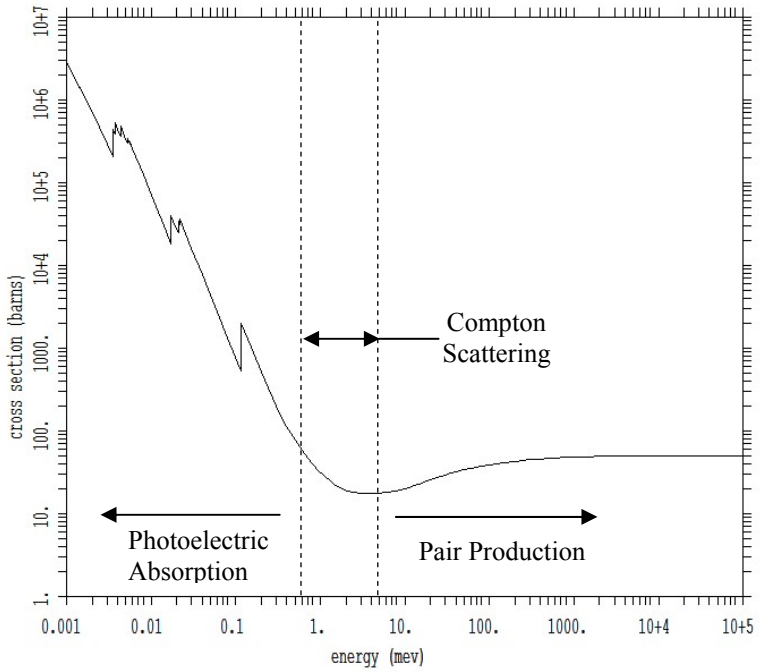

Figure 3.11: Total cross section as a function of energy for Uranium[4] and the energy ranges over which each interaction type is dominant.

3.2.2.2 Linear and Mass Attenuation Coefficients

Given Equation (3.39), the *linear attenuation coefficient*, μ, can be defined as

$$\mu(E) = N\sigma_C(E) + N\sigma_{ph}(E) + N\sigma_{pp}(E) \ , \tag{3.40}$$

where N is the atom density. The linear attenuation coefficient is the probability per unit path length of travel that a photon will experience one of the interactions included in the sum of Equation (3.40). Minor reactions such as Rayleigh scattering are excluded when calculating linear attenuation coefficients in this work. Use of Equation (3.40) ignores

[4] Cross section plotted using MCNP4C2 [Breismiester] and data library mcplib02 with ZAID of 92000.02p.

secondary gamma rays from Compton scattering and pair production because they are unlikely to be emitted in the pre-collision direction.

It is often convenient to represent the probability of photon interaction independent of the material density, ρ, by defining the *mass attenuation coefficient,*

$$\frac{\mu(E)}{\rho} = \left[\frac{N\sigma_C(E) + N\sigma_{ph}(E) + N\sigma_{pp}(E)}{\rho} \right] . \tag{3.41}$$

The mass attenuation coefficient is independent of the material density and does not depend on the physical state of the material, e.g., liquid water and water vapor. It is more common to find mass attenuation coefficient data rather than linear attenuation coefficient data.

For a given composition containing *n* materials, the linear attenuation coefficient is simply the sum of each constituent's linear attenuation coefficient or,

$$\mu = \sum_{i=1}^{n} \mu_i \ . \tag{3.42}$$

The mass attenuation coefficient for a composition containing *n* materials can be expressed as

$$\frac{\mu}{\rho} = \sum_{i=1}^{n} w_i \left(\frac{\mu}{\rho} \right)_i \ , \tag{3.43}$$

where w_i is the weight fraction of the i^{th} material in the composition. The energy dependency of the linear and mass attenuation coefficients has been dropped from Equations (3.42) and (3.43) to simplify the discussion.

3.2.3 LATDOSE - A 2D Point-Kernel Code for Calculating the Channeling Effect for Photons in a Pin Lattice

The computer program, LATDOSE, was written for the purpose of calculating the gamma-ray flux at a point outside a pin lattice. Specifically, the variation of the flux as a function of angle within the plane of the lattice was of interest. The flux variation will represent the degree of channeling for any given path from within the lattice to a point outside the lattice, as shown in Figure 3.12. Clearly, gamma rays emitted at (x_0,y_0) traveling a fixed distance toward a detector traverse less fuel when the detector is rotated an angle θ from position (x_1,y_1) to (x_2,y_2).

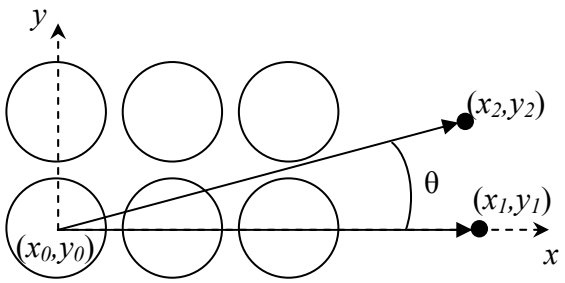

Figure 3.12: Ray trace through a pin lattice showing that the amount of fuel pin encountered by a gamma ray is dependent on the direction of travel.

Source code and an example input deck for LATDOSE are included in Appendix B. Pseudo code demonstrating the method of solution for LATDOSE is shown in Figure 3.13.

Loop over energy groups, *ie*.
  Loop over detector positions, *ipos*.
    Loop over pins in lattice, *n*.
      If n^{th} pin is a source,
        Loop over pins in lattice, *m*.
          If gamma ray intersects m^{th} pin,
            Calculate distance traveled in fuel and cladding.
          End if.
        End do.
        Calculate distance traveled in air.
        Calculate flux at detector, $\Phi(ie,ipos,n)$.
      End if.
    End do.
    Calculate total flux at detector position *ipos* from all source pins,

$$\Phi(ie,ipos) = \sum_{n} \Phi(ie,ipos,n) .$$

  End do.
End do.

Figure 3.13: LATDOSE pseudo code for calculating flux at a point outside a pin lattice.

LATDOSE computes the contribution from each pin inside the lattice to a point, representing a detector, located at some distance outside the lattice. At each pin location within the lattice, a ray is extended to the point detector, as shown in Figure 3.14.

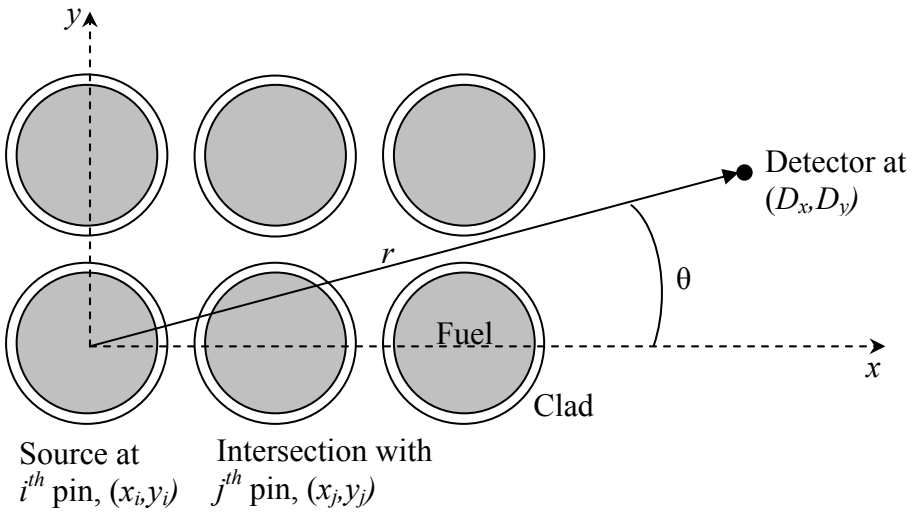

Figure 3.14: Ray trace through a pin lattice showing intersection of a fuel pin.

The slope-intercept form for the ray equation is substituted into the equation for the cladding circle,

$$\left(x_j - x\right)^2 + \left[y_j - \left(mx + b\right)\right]^2 - r_{clad}^2 = 0 \ , \tag{3.44}$$

where

$$m = \frac{D_y - y_i}{D_x - x_i} \ ,$$

and

$$b = y_i - mx_i \ .$$

Inspection of Equation (3.44) reveals that given the detector location, pin lattice parameters, clad radius, and fuel radius (all of which are supplied as input to LATDOSE), values of x satisfying the equation can be easily determined.

Defining a constant, $\xi = y_j - b$, is convenient for the ensuing algebra and when substituted in Equation (3.44) gives

$$\left(x_j - x\right)^2 + \left[\xi - mx\right]^2 - r_{clad}^2 = 0 \ . \tag{3.45}$$

Expanding the binomials and collecting similar terms yields a second order polynomial in the variable x,

$$\left(1 + m^2\right)x^2 + \left(-2x_j - 2\xi m\right)x + \left(x_j^2 - \xi^2 - r_{clad}^2\right) = 0 \, . \tag{3.46}$$

Using the quadratic formula, the solution to Equation (3.46) can be written as

$$x = \frac{-b \pm \sqrt{b^2 - 4ac}}{2a} \ , \tag{3.47}$$

with

$$a = 1 + m^2 ,$$
$$b = -2x_j - 2\xi m ,$$
$$c = x_j^2 - \xi^2 - r_{clad}^2 \ .$$

LATDOSE tests the discriminant, $b^2 - 4ac$, and performs one of the following. If the discriminant is less than zero, no real solutions exist and the next pin is tested for intersection. If the discriminant is greater than zero, two unique solutions exist, x_a and x_b, representing the entry and exit points of the ray on the circle. LATDOSE treats the unlikely case of a tangent (discriminant exactly equals zero), as an intersection with zero path-length. The corresponding y-axis values, y_a and y_b, are calculated by substitution into the slope-intercept form of the equation of the ray. LATDOSE computes the total distance traveled within the pin as the difference between these two points,

$$d_{tot} = \sqrt{(x_a - x_b)^2 + (y_a - y_b)^2} \ . \tag{3.48}$$

In order to determine the fraction of d_{tot} traveled in fuel, the fuel region radius is substituted into Equation (3.46) and the process is repeated. It is possible that the ray will intersect the pin at such an angle that no fuel is traversed making the new discriminant less than zero. In that case, the distance traveled in cladding for that pin, d_{clad}, is just d_{tot}. Otherwise, given that the new discriminant is greater than zero, two unique solutions exist, $x_{a'}$ and $x_{b'}$, representing the ray entry and exit of the fuel region. The corresponding y-axis values, $y_{a'}$ and $y_{b'}$, are calculated by substitution and the total distance traveled in the fuel region is

$$d_{fuel} = \sqrt{(x_{a'} - x_{b'})^2 + (y_{a'} - y_{b'})^2} \ . \tag{3.49}$$

It is a simple matter now to calculate the distance the ray traveled in the clad,

$$d_{clad} = d_{tot} - d_{fuel} \ . \tag{3.50}$$

Given a source at one pin location, the above method is repeated for every pin in the lattice to determine the total fuel distance and cladding distance traveled by the gamma ray *en route* to the detector.

The problems solved by LATDOSE are predetermined to contain only three material regions, i.e., clad, fuel, and air, as shown in Figure 3.14. Using the above equations the distance traveled by the ray in cladding and fuel is determined leaving only the distance traveled in air to be calculated. LATDOSE calculates this quantity by first solving the equation

$$d_{air} = \sqrt{\left(x_i - D_x\right)^2 + \left(y_i - D_y\right)^2} \quad . \tag{3.51}$$

However, this is the total distance traveled by the ray from source to detector and the distance traveled in the fuel and clad, for all pins that the ray intersects, must be subtracted from d_{air}.

With the total distance traveled by the gamma ray known and the individual distances traveled within clad, fuel and air, the gamma-ray flux at the detector can be calculated using the previously defined expression [Equation (3.26)],

$$\Phi(\mathbf{r_t}) = \sum_j \frac{S \cdot f_j}{4\pi \cdot \left|\mathbf{r_s} - \mathbf{r_t}\right|^2} e^{\sum_{i=1}^{n} -\mu_i(E_j) t_i} \quad ,$$

LATDOSE uses Equation (3.26) exactly with the number of energy groups, j, equal to the 19 groups provided by DELBG (§3.1.1), the source term, $S \cdot f_j$, taken from the DELBG calculated gamma rays released per second for the j^{th} energy group, and the number of heterogeneous regions, n, equal to three (air, clad, fuel). The linear attenuation factors are also calculated for the three materials at each of the 19 energies. Region thicknesses, t_i, are set equal to the calculated distance traveled by the gamma ray in air, clad, or fuel.

The geometric attenuation factor, $|\mathbf{r}_s - \mathbf{r}_t|$, equals the total distance from the source pin to the detector as found in Equation (3.51).

3.2.3.1 Linear Attenuation Coefficients Used in LATDOSE Calculations

Tabulated data for mass attenuation coefficients as a function of incident photon energy are available in several references [**ANSI/ANS-6.4.3, NIST, Hubbell**]. These data were used to generate either 19-group average (DELBG energy group structure) or 7-group average ([**Bozkurt**] energy group structure) mass attenuation coefficients for the three materials designated in the LATDOSE problem. These data are beneficial to others seeking to perform similar group-structure calculations.

A flat-energy weighting scheme was used to average the mass attenuation coefficients giving

$$\frac{\mu(E_{avg})}{\rho} = \frac{\int_{E_i}^{E_{i+1}} dE' \left(\frac{\mu(E')}{\rho} \right)}{\int_{E_i}^{E_{i+1}} dE'} , \tag{3.52}$$

where

$$E_{avg} = \frac{E_{i+1} + E_i}{2} . \tag{3.53}$$

Table 3.3 shows the 19-group energy averaged values for dry air, uranium, iron, and oxygen.

Table 3.3: 19-group energy averaged mass attenuation coefficients (cm^2/g) for dry air, oxygen, iron, and uranium.

Eavg , MeV	Dry Air <μ/ρ>	Oxygen <μ/ρ>	Iron <μ/ρ>	Uranium <μ/ρ>
0.05	2.2777E+01	2.9212E+01	8.3349E+01	1.1751E+02
0.15	1.3715E-01	1.3775E-01	2.2763E-01	2.7935E+00
0.30	1.4041E-01	1.4082E-01	1.5775E-01	1.1433E+00
0.50	1.3812E-01	1.3840E-01	1.3581E-01	4.1195E-01
0.70	1.1756E-01	1.1778E-01	1.1231E-01	2.1195E-01
0.90	1.4281E-01	1.4308E-01	1.3549E-01	2.1558E-01
1.10	1.2806E-01	1.2832E-01	1.2084E-01	1.6314E-01
1.30	1.1678E-01	1.1701E-01	1.0998E-01	1.3518E-01
1.50	9.3398E-02	9.3574E-02	8.8062E-02	1.0231E-01
1.70	7.4349E-02	7.4508E-02	7.0464E-02	8.0615E-02
1.90	9.4764E-02	9.4988E-02	9.0244E-02	1.0323E-01
2.10	8.9530E-02	8.9770E-02	8.5892E-02	9.8547E-02
2.30	8.5476E-02	8.5732E-02	8.2724E-02	9.5836E-02
2.50	8.2012E-02	8.2284E-02	8.0148E-02	9.4112E-02
2.80	5.7612E-02	5.7834E-02	5.7213E-02	6.8645E-02
3.50	4.8317E-02	4.8563E-02	4.9664E-02	6.2328E-02
4.50	6.2450E-02	6.2870E-02	6.6955E-02	8.8470E-02
5.50	5.5515E-02	5.6030E-02	6.3305E-02	8.9505E-02
6.75	4.1683E-02	4.2200E-02	5.0999E-02	7.7093E-02

Using the mass densities for dry air, oxygen, iron, and uranium given in Table 3.4 and Equation (3.43) to combine the uranium and oxygen, the linear attenuation coefficients for iron, UO_2, and dry air can be calculated.

Table 3.4: Mass densities (g/cm^3) for dry air, oxygen, iron, and uranium.

Dry Air	Oxygen	Iron	Uranium
1.21E-03	1.33E-03	7.874	18.95

The final calculated linear attenuation coefficients for the 19-group DELBG energy mesh are tabulated in Table 3.5 and shown graphically in Figure 3.15.

Table 3.5: Calculated 19-group energy averaged linear attenuation coefficients (cm^{-1}) for iron, UO_2, and dry air.

Eavg , MeV	Iron	UO_2	Dry Air
0.05	6.5629E+02	1.0691E+03	2.7447E-02
0.15	1.7923E+00	2.4748E+01	1.6527E-04
0.3	1.2421E+00	1.0230E+01	1.6919E-04
0.5	1.0693E+00	3.7912E+00	1.6643E-04
0.7	8.8433E-01	2.0065E+00	1.4166E-04
0.9	1.0668E+00	2.0688E+00	1.7208E-04
1.1	9.5149E-01	1.5896E+00	1.5431E-04
1.3	8.6599E-01	1.3300E+00	1.4072E-04
1.5	6.9340E-01	1.0126E+00	1.1255E-04
1.7	5.5483E-01	7.9882E-01	8.9591E-05
1.9	7.1058E-01	1.0224E+00	1.1419E-04
2.1	6.7631E-01	9.7494E-01	1.0788E-04
2.3	6.5137E-01	9.4624E-01	1.0300E-04
2.5	6.3109E-01	9.2693E-01	9.8824E-05
2.8	4.5050E-01	6.7347E-01	6.9422E-05
3.5	3.9106E-01	6.0676E-01	5.8222E-05
4.5	5.2720E-01	8.5398E-01	7.5252E-05
5.5	4.9846E-01	8.5488E-01	6.6896E-05
6.75	4.0157E-01	7.2906E-01	5.0228E-05

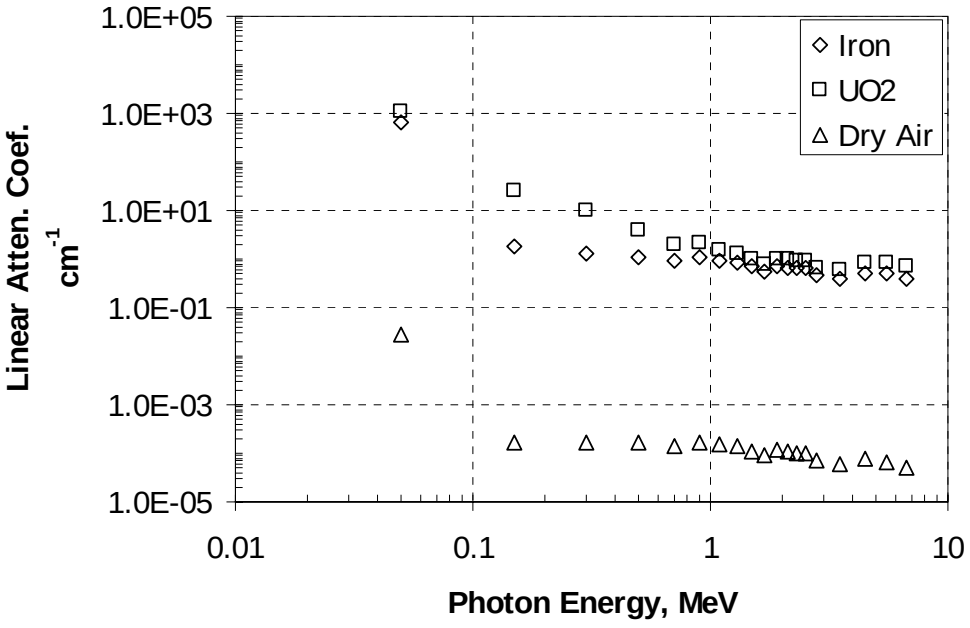

Figure 3.15: Plot of the calculated 19-group energy averaged linear attenuation coefficients (cm^{-1}) for iron, UO_2, and dry air as a function of energy.

The linear attenuation coefficient data shown in Table 3.5 is used directly in the LATDOSE input file (see Appendix B). For the purpose of this calculation, the pin cladding is assumed to be all iron. This is not a significant simplification given that nearly 70 weight-percent is iron and the other major nuclides in stainless steel are close in atomic number to iron, suggesting that their attenuation properties are similar.

3.2.4 Results of Pin Lattice Calculations using LATDOSE

Sections 3.2.1, 3.2.2, and 3.2.3 have developed the basis for performing calculations of various pin lattice configurations using LATDOSE. It is important to note that LATDOSE is calculating the solution for a very specific problem. Therefore, the magnitudes of the calculated fluxes are not expected to provide highly accurate predictions of 3-D fuel bundles in general. However, LATDOSE should provide a very good relative flux calculation. Of particular interest in this work is comparing fluxes at various positions, based on the position of a detector outside a pin lattice. The relative fluxes, calculated as a function of detector position, can effectively demonstrate the lattice effect and are the main objective of these calculations. In addition, the LATDOSE results provide a basis to anticipate the behavior of the real experiment (Chapter 5) and MCNP Monte Carlo calculations (§3.3).

In all calculations performed using LATDOSE, the problem is assumed to have 45 degree symmetry. Therefore, LATDOSE calculates the flux at one degree increments over a range of 0 to 45 degrees.

3.2.4.1 Calculations for 3x3, 5x5, and 7x7 Pin Lattices

The most simple lattice arrangement studied in this work consists of nine pins arranged in a square lattice, 0.613 inch pitch, with the center pin activated and the remaining pins inactive. The axis of rotation for the detector is about the z-axis of the activated fuel pin. The arrangement is shown in Figure 3.16.

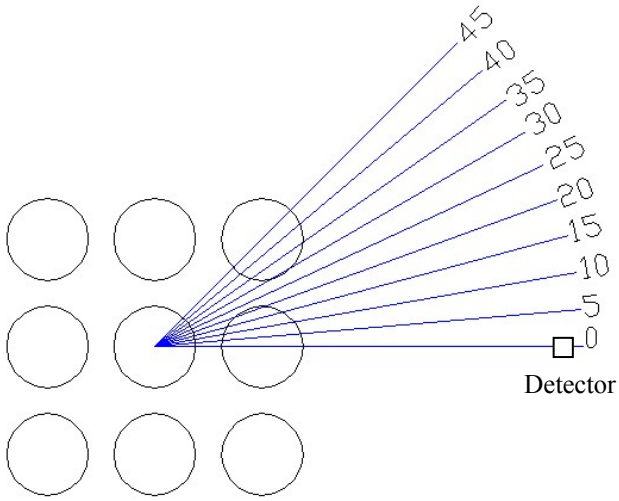

Figure 3.16: The 3x3 pin lattice with center fuel pin active. Rays are provided from 0 to 45 degrees in 5 degree increments showing the different paths through the lattice.

A quick inspection of Figure 3.16 shows that for any detector position only a single pin in the lattice will ever be in line between the source and detector. In fact, for several detector positions the source has an unimpeded path to the detector location. It is reasonable, therefore, to assume that the LATDOSE calculation will show an increase in dose moving from the 0 degree position, peaking out at a little above 20 degrees. From this position to a little under 30 degrees, the flux should be a constant and the maximum seen by the detector. From this position to 45 degrees, the flux should decrease back to the original level, in that the distance to the detector has not changed and the amount of fuel and cladding seen by the ray on its way to the detector is identical to the 0 degree case. The LATDOSE results are shown in Figure 3.17.

The source was generated using the DELBG code with an irradiation time of 200 seconds and a core power history equal to that of the experimental measurement. Similarly, the distance from the center of the activated fuel pin to the detector was taken from the experimental measurement, 13.58 cm. These values, as well as others, are supplied in Table 3.6.

Table 3.6: Core activation, time after SCRAM, and distance to detector for 3x3, 5x5 and 7x7 lattice LATDOSE Calculations.

Lattice Configuration	Irradiation Time (s)	Peak Power Observed (W)	Reactor Period Measured (s)	Time after SCRAM (s)	Distance to Detector (cm)
3x3, center pin active	200	3.1	29	383	13.58
3x3, corner pin active	200	3.2	25	512	15.93
5x5, center pin active	200	3.4	26	471	15.30
5x5, corner pin active	200	3.1	26	425	20.31
7x7, center pin active	200	3.1	27	400	15.74
7x7, corner pin active	200	3.2	24	470	25.97

Table 3.6 shows the parameters used in the DELBG source calculation and LATDOSE calculation for 3x3, 5x5 and 7x7 lattices. The values in the table are based on the actual experimental measurements (Chapter 4). DELBG input files are provided in Appendix A. Input files for LATDOSE calculations are provided in Appendix B.

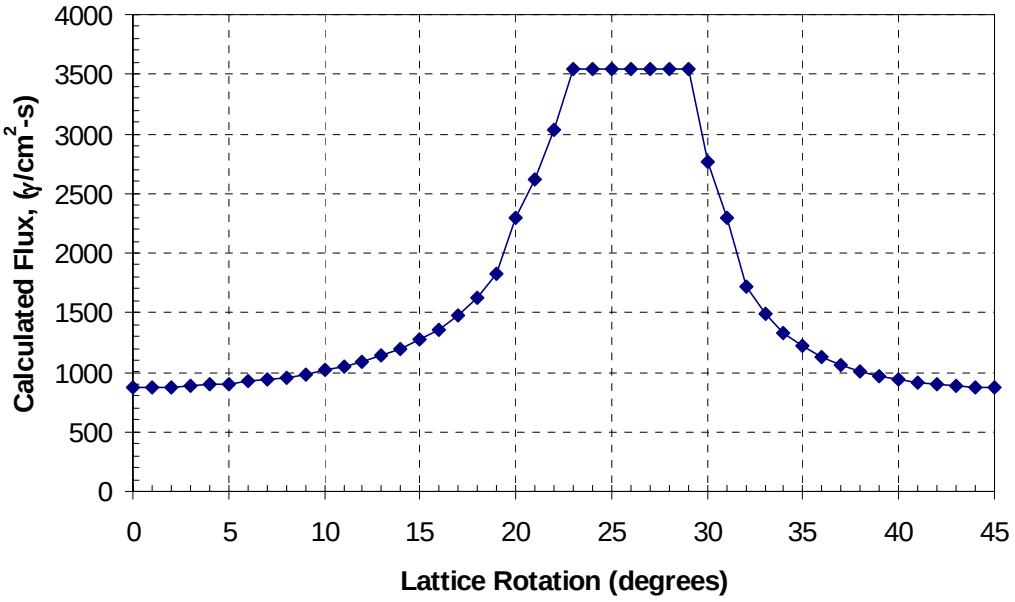

Figure 3.17: LATDOSE calculated gamma-ray flux as a function of angle as the detector is rotated about the center pin of a 3x3 pin lattice. The center pin is active and the surrounding pins are inactive.

The behavior of the flux at the detector as calculated by LATDOSE is exactly as anticipated. The change in slope of the flux at 19 degrees is due to the source rays striking the incident pin at such an angle where only cladding material is traversed by the ray. Since cladding material has a much different linear attenuation coefficient, the slope of the increase in flux changes. At the 22 degree position, the ray sees the last of the cladding from the right-most fuel pin and reaches its maximum value between 22 and 23 degrees rotation. This maximum value is held until the ray begins to see the cladding material in the upper right pin, between 29 and 30 degrees. The flux continues to drop as more cladding material becomes incident on the ray's path. At about 32 degrees, the ray begins to intersect fuel material causing the flux to drop, ultimately reaching the same value as the 0 degree position.

The good agreement of the LATDOSE results with the expected flux behavior, coupled with extensive verification performed using hand calculations, gives a high degree of confidence that the LATDOSE code is accurately predicting the flux at a point outside a lattice, as intended.

To increase the level of complexity, the activated pin was moved to the lower left lattice position and the calculation was repeated. Figure 3.18 shows the new arrangement. In this arrangement, the source gamma rays travel through a more varied set of conditions than in the previous arrangement. Therefore, it is reasonable to assume that the LATDOSE results will show a much more interesting dependence of the calculated flux on the detector position.

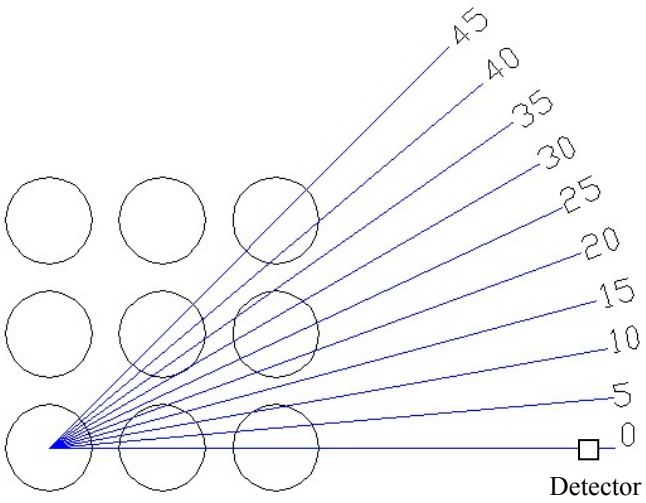

Figure 3.18: The 3x3 pin lattice with lower left fuel pin active. Rays are provided from 0 to 45 degrees in 5 degree increments showing the different paths through the lattice.

By examination of Figure 3.18, the flux is expected to reach a maximum around 15 degrees rotation, with minimum values at the 0 and 45 degree positions. However, given the increased complexity, other maxima and minima are also expected, as well. The source used was generated using the DELBG code with a core power history equal to that

of the experimental measurement. Similarly, the distance from the center of the activated fuel pin to the detector was taken from the experimental measurement, 15.93 cm. The LATDOSE results for this arrangement are shown in Figure 3.19.

The calculated flux as a function of detector position, shown in Figure 3.19, is in good agreement with the expectations, given the ray traces in Figure 3.18.

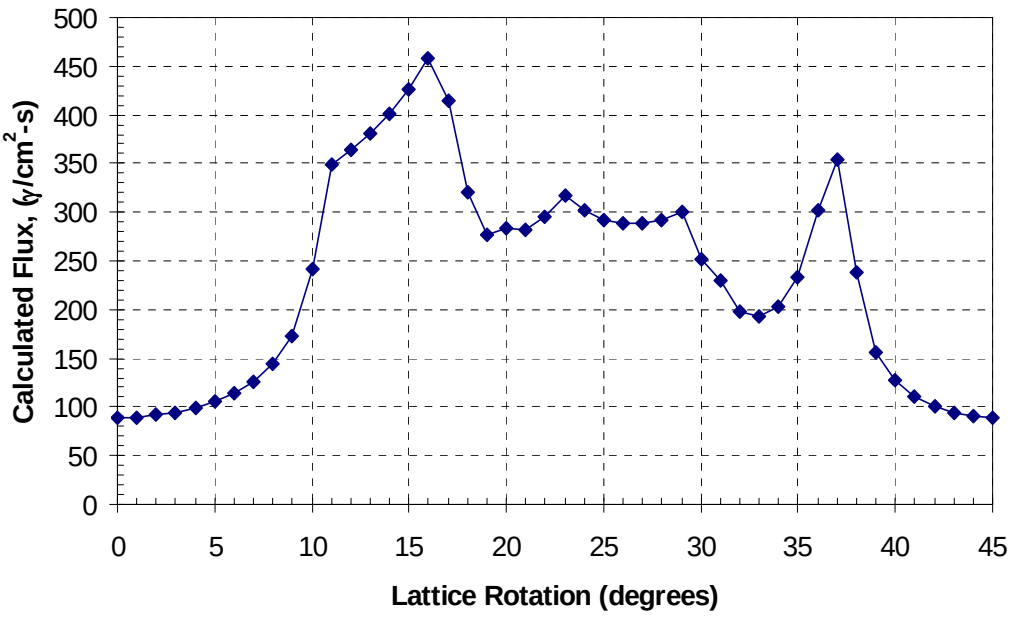

Figure 3.19: LATDOSE calculated gamma-ray flux as a function of angle as the detector is rotated about the lower left pin of a 3x3 pin lattice. The lower left pin is active and the surrounding pins are inactive.

A clear maximum value is shown at the expected position (16 degrees) with other maxima and minima values observed as the source rays encounter various amounts of cladding and fuel material on the way to the detector. The calculations confirm expectations for this lattice arrangement.

The next set of calculations was performed on a 5x5 pin lattice. Two additional rows and columns of pins were added to the lattices for a total of 25 pins. A single

activated fuel pin was placed either in the center or the lower left corner of the lattice and the remaining 24 pins were inactive.

The 5x5 lattice arrangement with center pin active is shown in Figure 3.20 and is identical, as far as LATDOSE is concerned, to the 3x3 lattice with the lower left pin activated. This is because LATDOSE calculates the *uncollided* flux at a detector outside the lattice, as previously mentioned. Contributions to the flux at a detector outside the 5x5 lattice due to pins below and to the left of the active pin would be a result of scattering (most likely multiple scattering) and therefore are not included in the LATDOSE calculation.

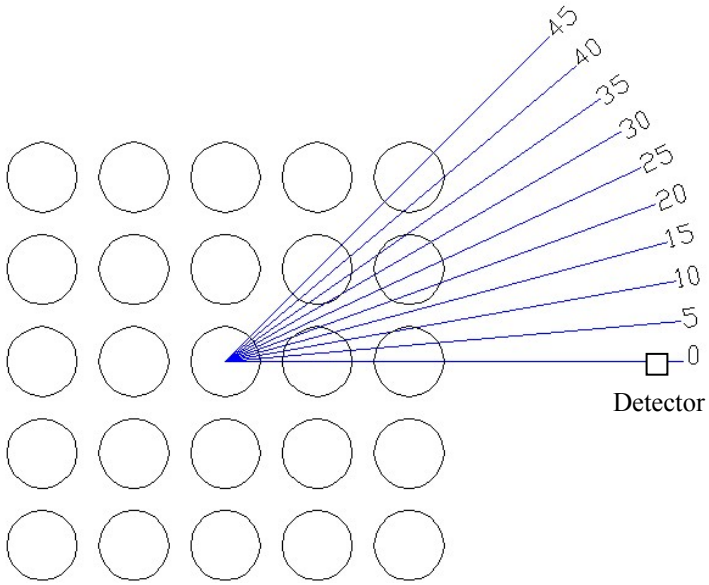

Figure 3.20: The 5x5 pin lattice with center fuel pin active. Rays are provided from 0 to 45 degrees in 5 degree increments showing the different paths through the lattice.

Because geometrically this is an identical problem to the 3x3, center pin active case, the expectation is that LATDOSE will give the exact same result as shown in Figure 3.19. However, the source used in the 5x5 calculation is based on a different core power history, different times after shutdown, and the distance of the detector from the activated

pin is not identical for the two cases. Nevertheless, the results are expected to be very similar. The LATDOSE results for this case are shown in Figure 3.21.

The shape of the flux versus angle of rotation curves in Figure 3.21 is identical to that in Figure 3.19, as expected. Comparison of the maximum values also follows the expected trend given that the source used in the calculation of Figure 3.21 was taken form a higher core power history and shorter time after reactor SCRAM than that used in Figure 3.19.

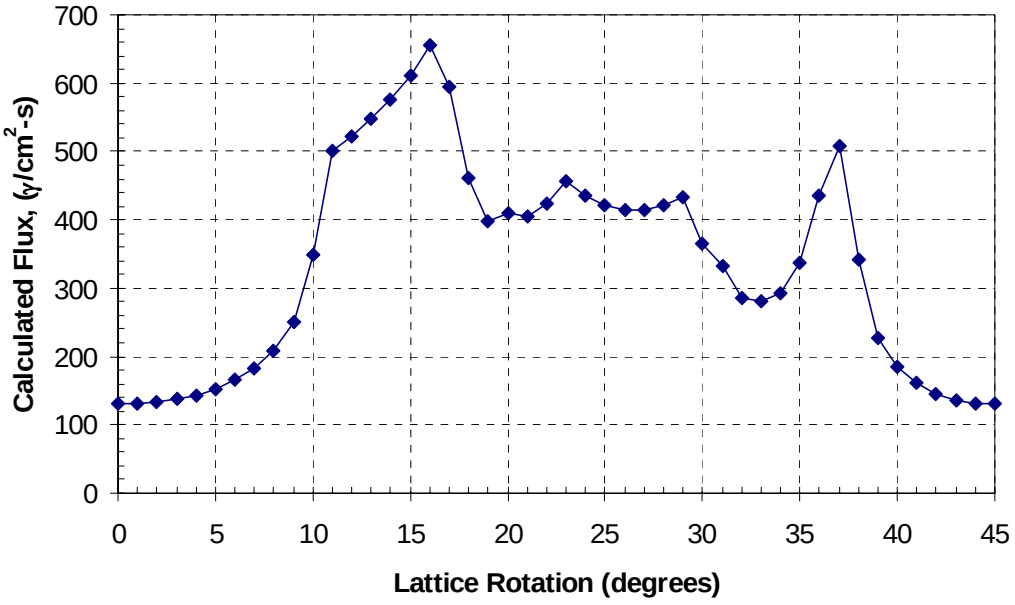

Figure 3.21: LATDOSE calculated gamma-ray flux as a function of angle as the detector is rotated about the center pin of a 5x5 pin lattice. The center pin is active and the surrounding pins are inactive.

The 5x5 lattice calculation with the lower left corner pin activated provides the next level of detail for the LATDOSE calculations. This arrangement is shown in Figure 3.22.

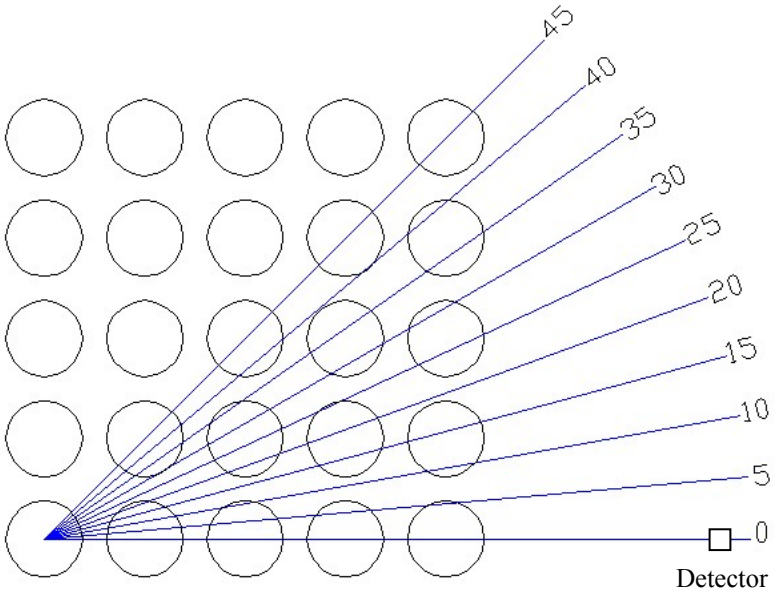

Figure 3.22: The 5x5 pin lattice with lower left fuel pin active. Rays are provided from 0 to 45 degrees in 5 degree increments showing the different paths through the lattice.

By inspection of Figure 3.22, the LATDOSE results of flux as a function of detector position is expected to exhibit much more structure than for previous lattices. Based on the number of pins now potentially within the path of the ray, it is increasingly difficult to predict *a priori* the shape of the detector flux curve. However, it is reasonable to conclude from Figure 3.22 that the maximum flux should occur at a detector position of between 5 and 10 degrees. Other potentially favorable angles for channeling can also be observed in the lattice.

Figure 3.23 shows the LATDOSE solution for this 5x5 lattice. The jump in flux from 10 to 11 degrees rotation is somewhat conspicuous. However, LATDOSE reports a steep reduction in clad material with only a small increase in fuel material traversed for a ray at 11 degrees, with respect to a ray at 10 degrees. This would account for the jump in flux. The "jagged" shape near the jump is a function of the one-degree resolution of the LATDOSE calculation.

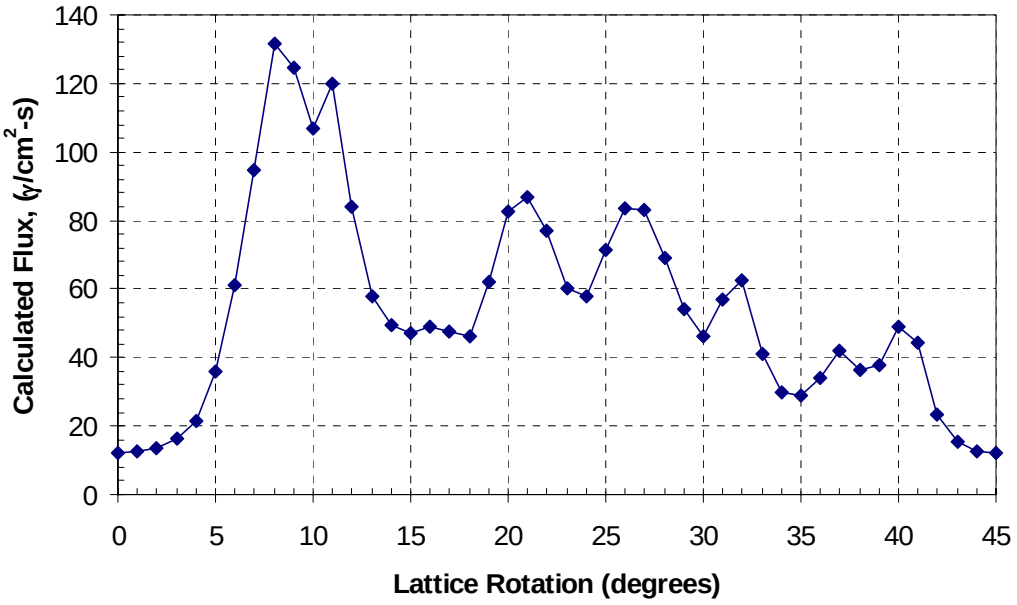

Figure 3.23: LATDOSE calculated gamma-ray flux as a function of angle as the detector is rotated about the lower left corner pin of a 5x5 pin lattice. The lower left corner pin is active and the surrounding pins are inactive.

The jump in flux from 10 to 11 degrees rotation is somewhat conspicuous. However, LATDOSE reports a steep reduction in clad material with only a small increase in fuel material traversed for a ray at 11 degrees, with respect to a ray at 10 degrees. This would account for the jump in flux. The "jagged" shape near the jump is a function of the one-degree resolution of the LATDOSE calculation.

The final lattice arrangements examined consisted of a 7x7 array of fuel pins. As in previous lattices, calculations were performed with the center pin active and lower left corner pin active. The remaining 48 pins in the array were inactive. Figure 3.22 shows the arrangement of the 7x7 lattice with center pin active.

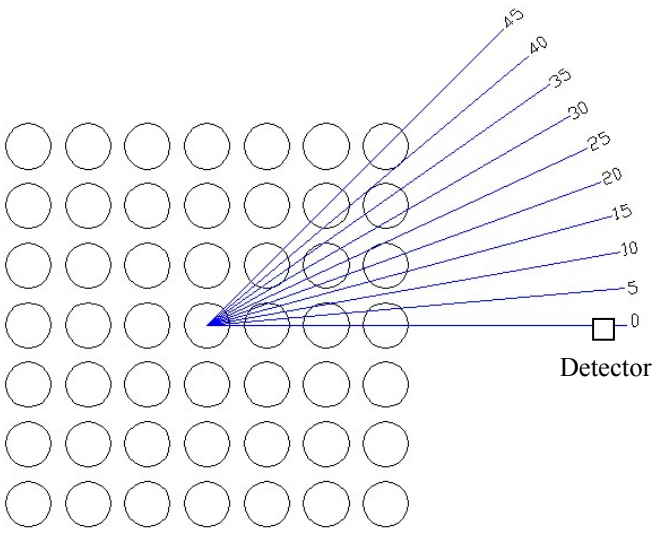

Figure 3.24: The 7x7 pin lattice with center fuel pin active. Rays are provided from 0 to 45 degrees in 5 degree increments showing the different paths through the lattice.

By inspection of the number of pins and ray traces in Figure 3.24, it is expected that the calculated flux versus detector position will exhibit greater structure than shown in Figure 3.21 but less than that shown in Figure 3.23. A maximum value is expected at a detector position of about 10 degrees. Additional local maxima and minima are anticipated as the detector is rotated through the different positions. The positions at 0 and 45 degrees should be identical and representative of the source transported through a total of 3.5 fuel pins. The LATDOSE results for the 7x7 lattice with center pin activated are shown in Figure 3.25.

As expected, Figure 3.25 shows a maximum flux value at a detector position of 11 degrees. In this position, only a fraction of a pin in the first row is intersected by the ray. A second large flux value occurs at a detector position of between 26 and 27 degrees where the ray encounters only a single fuel pin. Detector positions in which the ray intersects several fuel pins are becoming more numerous as the lattice becomes more

complex. This trend leads to higher peaks and lower valleys in the calculated flux as a function of detector position.

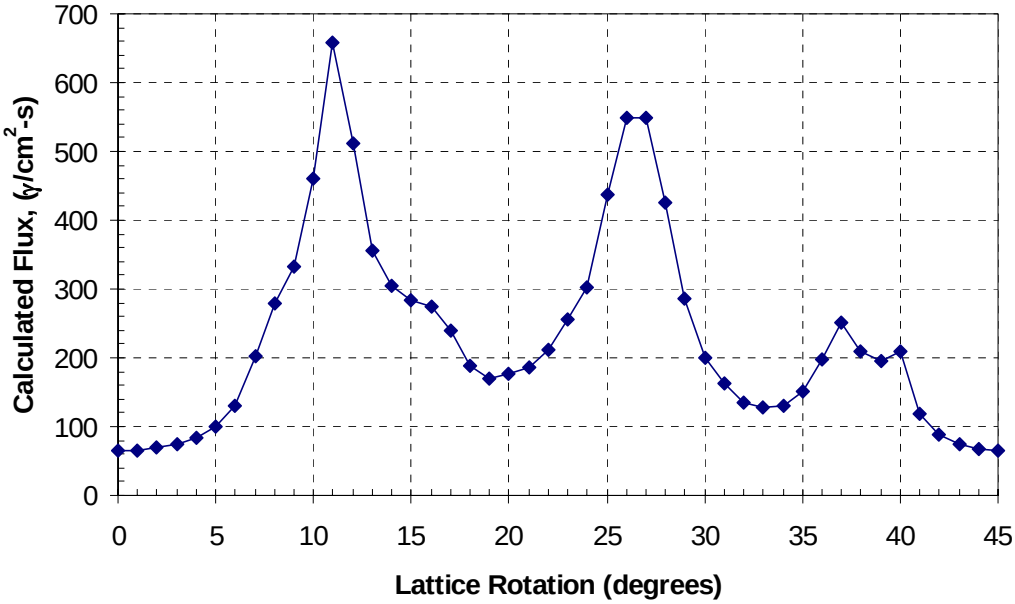

Figure 3.25: LATDOSE calculated gamma-ray flux as a function of angle as the detector is rotated about the center pin of a 7x7 pin lattice. The center pin is active and the surrounding pins are inactive.

The most complex lattice analyzed with LATDOSE was the 7x7 arrangement with the lower left corner pin activated, shown in Figure 3.26. This configuration is expected to exhibit the greatest amount of structure in the flux versus detector position results. The maximum flux value seen be the detector in this case is anticipated to be much less than in previous lattices. By observation of Figure 3.26, no path through the lattice without intersecting multiple pins is readily apparent. The LATDOSE results for this case are shown in Figure 3.27.

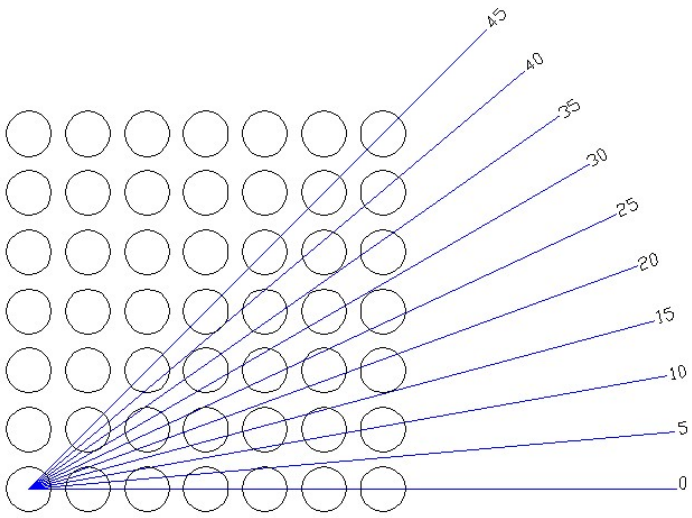

Figure 3.26: The 7x7 pin lattice with lower left corner fuel pin active. Rays are provided from 0 to 45 degrees in 5 degree increments showing the different paths through the lattice.

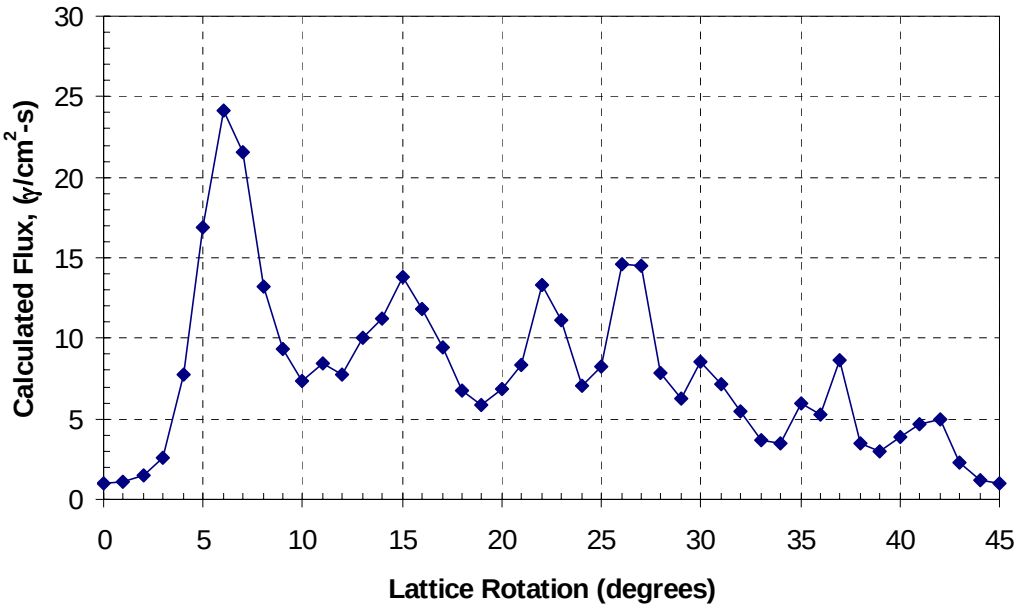

Figure 3.27: LATDOSE calculated gamma-ray flux as a function of angle as the detector is rotated about the lower left corner pin of a 7x7 pin lattice. The lower left pin is active and the surrounding pins are inactive.

3.3 Calculating the Lattice Effects Using Monte Carlo

The MCNP™ code [**Briesmeister**] was used to calculate the lattice effects demonstrated using the LATDOSE code. A higher degree of fidelity in the calculation is possible in Monte Carlo given the full 3-D geometry modeling capability, continuous particle tracking in space and energy, and continuous cross-section treatment. In fact, the Monte Carlo calculation is considered to yield results that are the closest to "truth" for a given model.

The calculations performed using MCNP were modeled as closely as practical to the experimental measurements discussed in Chapter 4. By comparing LATDOSE results to MCNP results, a qualitative comparison of the LATDOSE calculated lattice effects can be preformed. Additionally, the MCNP results are expected to follow the experimental results. By comparison, the MCNP calculations provide information on the precision and accuracy of the experimental results.

3.3.1 MCNP Photon Transport

The MCNP code developed at Los Alamos National Laboratory is a general, Monte Carlo transport code. The code system comes with a complete set of cross-section libraries for neutron, photon, and electron transport. The code system is distributed through the Radiation Safety Information Computational Center (RSICC). Version 4C2 of MCNP was used for this work.

MCNP can be run in various "modes," to simulate particle transport, e.g., neutrons only, gamma rays only, coupled neutron – gamma ray, coupled gamma ray – electron, or coupled neutron – gamma ray – electron. This functionality makes it convenient to track fission-product gamma rays during a neutron criticality problem, or

track electrons created during a photon tracking problem. For this work, the DELBG code (§3.1.1) was used to generate a starting photon source and MCNP was run in photon only mode.

Photon transport in MCNP can be performed at two levels of complexity: (1) "simple" physics, and (2) "detailed" physics. The detailed physics treatment is the default option and is recommended for most applications, especially deep penetration problems and those involving high *Z* materials. In the detailed physics option, MCNP models both incoherent (Compton) and coherent (Rayleigh) scattering and applies appropriate form factors to account for bound electron effects. Fluorescence as a result of photoelectric absorption is tracked explicitly. Ejected electrons created as a result of photoelectric absorption, incoherent scattering, and pair production are also modeled explicitly in the detailed physics treatment. However, in a photon only problem, a thick-target bremmstrahlung (TTB) model is used by default for the ejected electrons. The electron is created and assumed to travel in the same direction as the incoming photon but the electron is immediately annihilated. The TTB method has the benefit of modeling the electron creation and annihilation without the expensive electron transport. In a coupled photon – electron problem, the electron is explicitly tracked to its demise using the appropriate physics.

The simple physics treatment ignores coherent scattering, assumes free-electron scattering, and assumes secondary energy from fluorescence and ejected electrons is deposited locally. The simple physics treatment is intended for high energy gamma-ray transport where the free-atom scattering approximation is valid. For this work, the detailed physics treatment was used.

3.3.2 MCNP Model Description

A major strength of MCNP is the ability to model the physical reality of a problem with minimal approximations. For instance, the combinatorial geometry features in MCNP allow for very accurate representations of the physical geometry to be created. For this work, the MCNP geometry was modeled as closely as practical to the experimental measurements.

Details regarding the experimental apparatus are described in §4.2, however, a brief description follows. Two steel lattice plates, a bottom and top, are held in place and separated by a wooden frame. Depending on the experiment, various arrangements of fuel pins are placed within the lattice plates. A sodium iodide, (NaI(Tl)) detector within a lead shield is located on another wooden frame and held at a fixed position relative to the pins in the lattice. The lead shield contains a rectangular collimator that is 0.953 cm wide by 10.16 cm deep by 5.08 cm high. The wooden frame holding the pins and lattice plates can be rotated about the vertical axis of a selected pin, thus providing a method to measure the detector response as a function of lattice rotation, emulating the LATDOSE calculations.

Figure 3.28 shows the geometry model for the 7x7 (corner pin active) case as rendered by the MCNP plotter in the x-y plane at the mid-point of the z-axis. Figure 3.29 provides a view of the same model in the y-z plane at the model mid-plane. The NaI(Tl) crystal is modeled in full detail but the photomultiplier and associated electronics located behind the detector have not been included in the model. The wooden frame structures supporting the lattice plates and detector are also not modeled in the MCNP geometry.

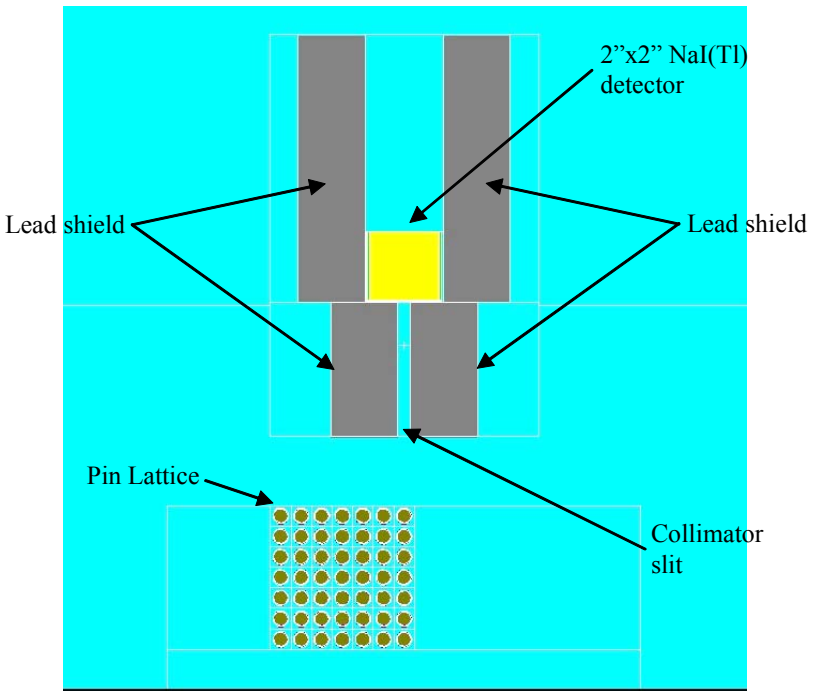

Figure 3.28: MCNP plotter rendering of the x-y plane at the axial center height for the 7x7 pin lattice with lower right pin active.

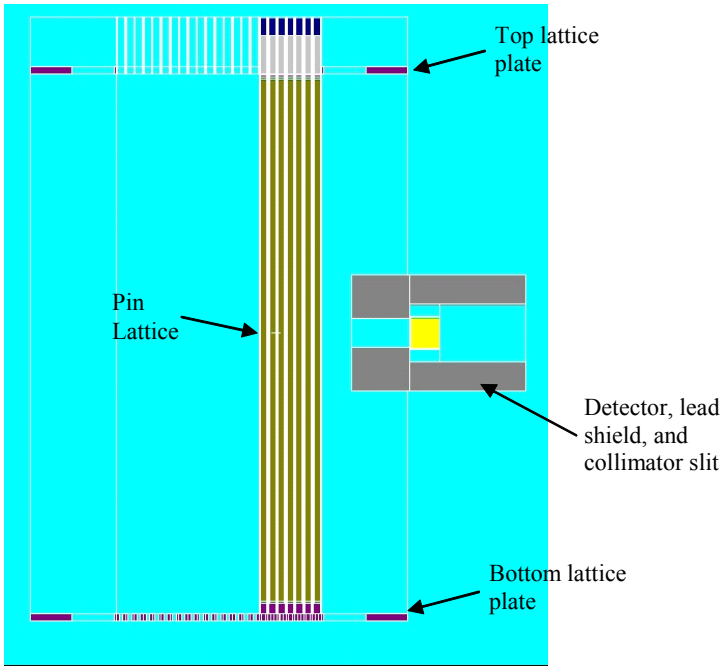

Figure 3.29: MCNP plotter rendering of the y-z plane at x = 0 for the 7x7 pin lattice with lower right pin active.

As previously mentioned, in the experimental apparatus the lattice is rotated about the z-axis of the activated fuel pin and the detector is held stationary. In order to simulate the lattice rotation with respect to the detector in the MCNP model it was necessary to fix the lattice in place and rotate the shield, detector, and collimator assembly instead. This was accomplished in the MCNP model by using the "universe" construct. The shield, detector, and collimator assembly are created inside a universe. The universe boundaries are created from a closed set of surfaces which can then undergo translations and rotations relative to the pin lattice. This feature provides a very convenient way to manipulate the detector relative to the pin lattice in that the necessary translation and rotation need only be applied to the universe boundaries. All surface definitions inside the universe will then automatically receive the proper translation and rotation, based on the new universe orientation. Figure 3.30 shows the 7x7 (corner pin active) lattice with the detector assembly universe rotated 45 degrees.

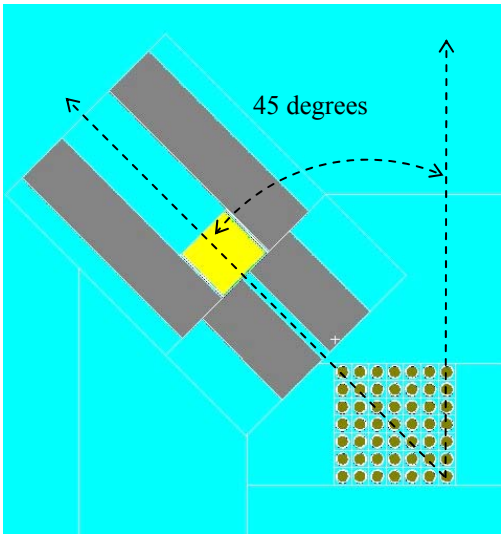

Figure 3.30: MCNP plotter rendering of the x-y plane at the axial center height for the 7x7 pin lattice with lower right pin active and detector rotated 45 degrees.

The MCNP model contains 106 cells, 87 surfaces, and 12 materials. Appendix C contains the MCNP input decks for several of the models run in the calculation.

3.3.2.1 Tallies Used

MCNP has several options for tallying various results including current integrated over a surface, flux averaged over a surface, flux averaged over a volume, flux at a point or ring detector, energy deposition averaged over a cell, fission energy deposition averaged over a cell, and energy distribution of pulses created in a detector ("pulse-height tally"). For this work, both the gamma-ray flux averaged over the detector crystal volume and pulse-height tally within the detector crystal volume were tallied.

The flux averaged over a volume tally (F4) is a straight forward tally in any Monte Carlo particle transport algorithm and is given by

$$\mathrm{F4} = \int_V \int_t \int_E \Phi(\mathbf{r}, E, t) dE dt \frac{dV}{V} \quad , \tag{3.54}$$

usually referred to as a track-length estimator of the cell flux. Given that $\Phi(\mathbf{r},E,t) = vN(\mathbf{r},E,t)$, where v is particle velocity and $N(\mathbf{r},E,t)$ is the particle density, Equation (3.54) can be written as

$$\mathrm{F4} = \int_V \int_s \int_E N(\mathbf{r}, E, t) dE ds \frac{dV}{V} \quad , \tag{3.55}$$

where the substitution $ds=vdt$ has been made to change the equation to an integral over track-length, s. Integrating Equation (3.55) over energy, track-length, and volume, and recognizing that the particle weight per unit volume, $W/V = N(\mathbf{r},E,t)$, the track-length estimate of the flux averaged over a volume is

$$\mathrm{F4} = \frac{WT_l}{V} \quad , \tag{3.56}$$

where, W = particle weight, T_l = track length, and V = volume.

The pulse-height tally (F8) is a highly specialized tally in MCNP designed to represent the energy deposited in an actual physical detector. The energy bin results of an F8 tally correspond to the total energy deposited in a detector in the specified channel by a physical particle. The process is inherently analog in nature and therefore does not work well with neutron tracking and most variance reduction techniques [**Briesmeister**]. To illustrate the analog nature of this process, consider Figure 3.31 showing a particle born at energy E_0 and with weight W_0 and passing through two volumes with pulse-height tallies. As the particle crosses into the first tally volume, Cell 1, an account of particle energy is initiated within the cell and is set to E_1W_1. Similarly, when the particle passes into Cell 2, an account is initiated and set to E_2W_2. However, upon leaving Cell 1 and entering Cell 2, the account in Cell 1 is decremented by E_2W_2, giving the energy deposited within Cell 1 as $E_1W_1 - E_2W_2$. The same process is repeated for Cell 2 when the particle exits, giving the energy deposited in Cell 2 as $E_2W_2 - E_3W_3$. The process is repeated until the particle history is terminated, at which time the energy deposition tallies are normalized by the birth-weight of the particle, W_0.

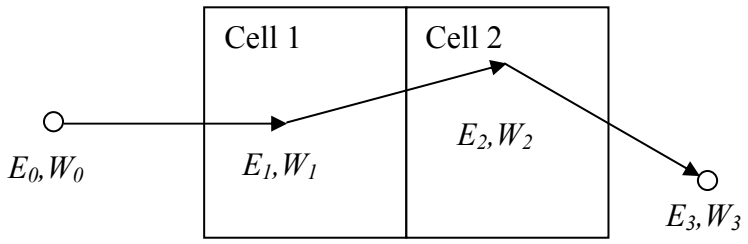

Figure 3.31: Pictorial representation of a particle passing through two cells each with a pulse-height tally.

It is clear to see that variance reduction games and non-analog processes that affect particle weight can have adverse effects on the veracity of a pulse-height tally.

Consider the example of a particle with $W=1$ and E=10 MeV undergoing a 2 for 1 split when crossing from Cell 1 to Cell 2. Suppose that one of the two resulting particles of weight 0.5 does not deposit any energy into Cell 2 but the other particle deposits all of its energy in the cell. The pulse-height tally would incorrectly score this in the energy bin for W_2E_2 = (0.5)(10 MeV) = 5 MeV. Suppose that both particles deposited all their energy in Cell 2. The pulse-height tally would incorrectly calculate two contributions to the 5 MeV energy bin rather than the correct 10 MeV value. Therefore, extreme caution must be exercised when using the pulse-height tally feature in MCNP.

3.3.2.1 Variance Reduction

Because the pulse-height tally in MCNP is incompatible with non-analog processes, the techniques available to accomplish variance reduction are limited. For this work, directional biasing of the source gamma rays was the single variance reduction technique used.

This technique samples the source using a modified probability distribution function that is preferential to a certain specified direction. The birth-weight of the particle is subsequently adjusted by the ratio of the true probability to that of the modified probability, ensuring a fair game. In MCNP, an exponential biasing function is used

$$p(\mu) = Ce^{K\mu}, \tag{3.57}$$

where C is a normalization constant,

$$C = \frac{K}{e^{K} - e^{-K}},$$

K is the biasing parameter, and μ=cosθ, with the angle θ relative to the biasing direction. For this work a biasing parameter of 3.0 was used. Figure 3.32 shows the resulting probability density function for the source biasing.

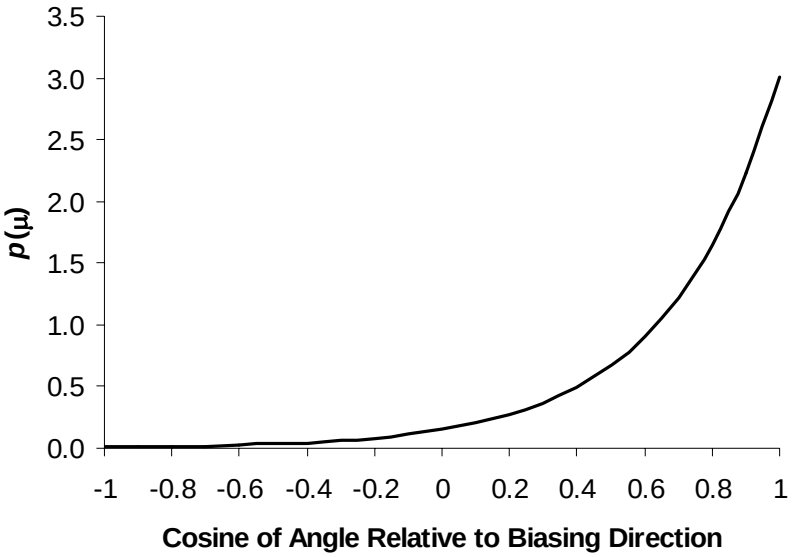

Figure 3.32: Probability density function for directional biasing of the source using biasing parameter of 3.0.

The biasing angle was chosen to correspond to the degrees of rotation of the detector relative to the pin lattice.

The effectiveness of source biasing can be seen be examining Figure 3.33. The figure shows the 7x7 lattice (corner pin active) with the detector rotated 45 degrees relative to the lattice, as rendered by the Visual Editor [**Carter**]. Collision sites for photons are shown as colored points superimposed on the MCNP geometry. A total of 100,000 photons were run to generate the images. Figure 3.33(a) shows the photon collisions from the unbiased model and Figure 3.33(b) shows the collisions from the biased model. It is readily observable that the biased model serves to transport more

particles in the direction of the detector, thus increasing the probability of particles contributing to the cell average flux tally and pulse-height tally.

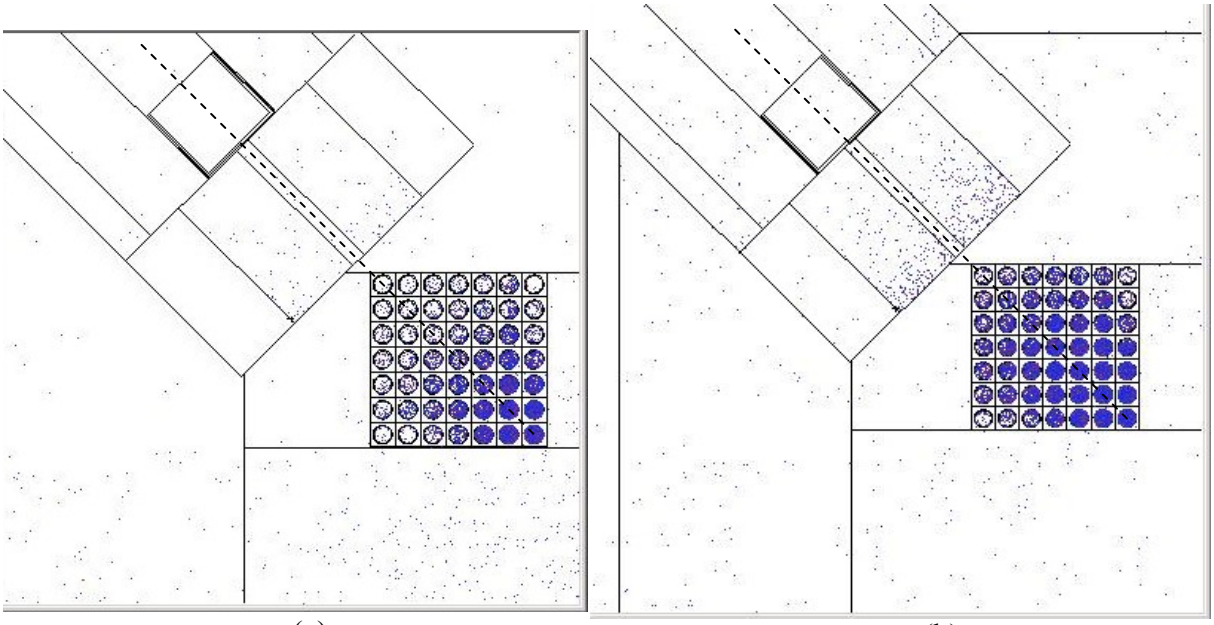

(a) (b)

Figure 3.33: Collision density plots for source with (a) unbiased direction sampling and (b) biased directional sampling at the axial mid-plane of the 7x7 lattice with the lower right pin activated.

3.3.2.2 Modeling the Fission-product Gamma-Ray Source

MCNP calculations for this work were performed using a fixed-source for fission-product gamma rays. Source gamma-ray location in the model was determined using both axial and radial probability functions. Source gamma-ray energy was determined from sampling an additional probability function. In order to accurately describe the probability functions for sampling the source in MCNP, information pertaining to the spatial location and energy of the source gamma rays was required.

A separate MCNP neutron tracking run was performed for a model of the SPERT fuel pins as loaded into the RCF. This run was intended to model the reactor as closely

as practical to the configuration used to activate fuel pins for use in this work. Neutron flux tallies were set up on three inch axial nodes for a total of 12 bins. The tally results of the 12 bins were normalized and entered into the MCNP source definition as a histogram. MCNP samples the histogram bin with probability specified from the tally results, and then samples uniformly within the bin to determine the actual axial height of the source site. To determine the radial location within the pin, a flat source guess along the pin radius was chosen. Arguably, given the flux depression within a fuel pin, a better guess would be a quadratic function with increasing probability toward the pin edge. However, this was judged to be an insignificant modeling error. This treatment is consistent with other similar studies [**Bozkurt**].

To determine the energy of the source gamma ray, a probability function was generated using the results of DELBG (§3.1). As previously described, The DELBG results for a given power history can be used to create a probability density function (Figure 3.2) which can then be entered in the MCNP source definition as a histogram. MCNP samples first the energy bin, with specified probability, and then samples uniformly within the bin to determine the final gamma-ray energy.

Gamma rays released from the decay of fission products are isotropic. However, as previously discussed in §3.3.2.2, a directional bias is added in the MCNP source definition for variance reduction. Examples of the entire MCNP source definition used in this work are found in the input files of Appendix C.

3.3.3 MCNP Results

MCNP calculations were performed for the 3x3, 5x5, and 7x7 lattice configurations described in §3.2.4.1. The power history used to generate the source for each run was taken from the experimental measurements described in Chapter 4 and shown in Table 3.6. For each lattice configuration, ten runs were performed in which the detector was rotated from 0 degrees to 45 degrees, in five degree increments. This mimics the data taken in Chapter 4 so as to provide the best comparisons to experiment.

Figure 3.34 shows the calculated total photon flux averaged over the detector volume for the 3x3 lattice with center pin active, with two-sigma (95% confidence interval) error bars.

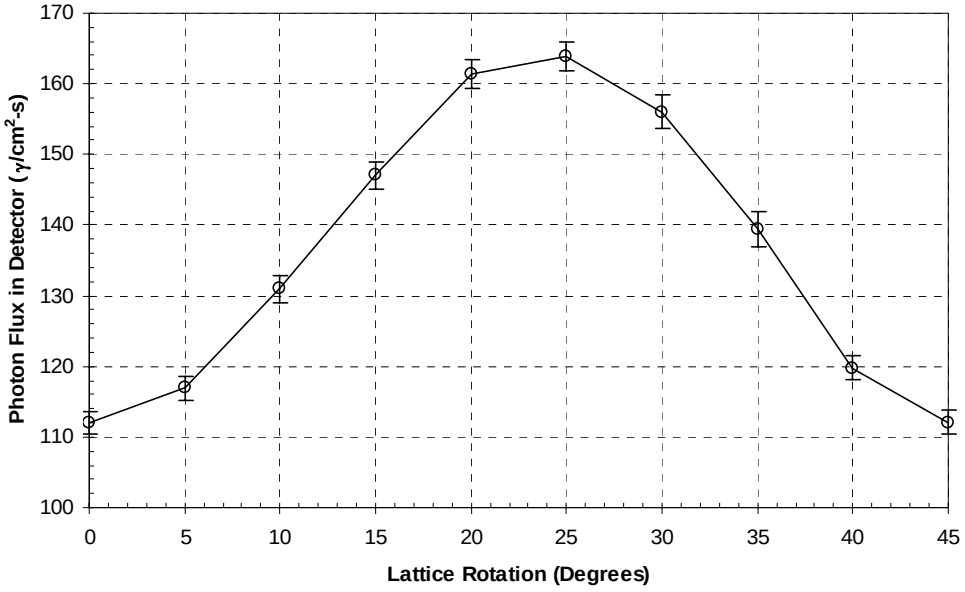

Figure 3.34: MCNP calculated photon flux averaged over the detector volume for the 3x3 pin lattice with center pin activated.

The results for the same case using the pulse-height tally are shown in Figure 3.35.

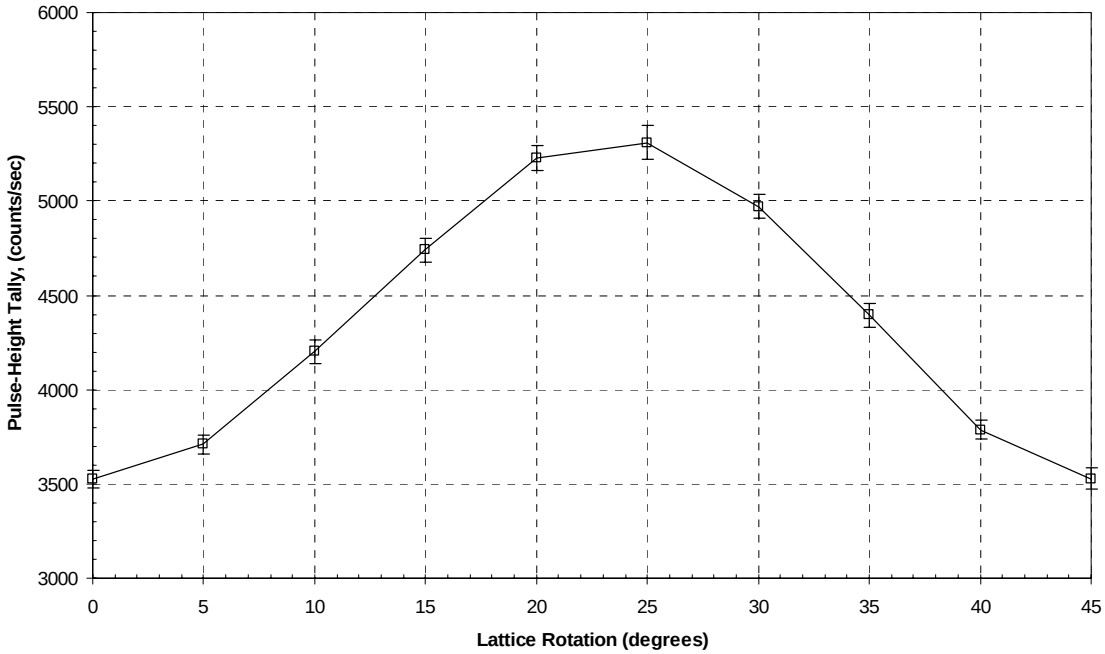

Figure 3.35: MCNP calculated total pulse height in the detector volume for the 3x3 pin lattice with center pin activated.

By inspection, the cell average flux and total pulse height shown in the figures agree well in shape, demonstrating that the two tallies are consistent in showing the effect of rotating the detector around the pin lattice.

To validate the LATDOSE results, it is useful to compare to the MCNP calculated results. However, the fundamental differences between the 2-D code and 3-D code produce unavoidably different answers. In LATDOSE, the entire source and detector volumes are collapsed to points and the effects of multiple scattering and other 3-D effects are lost. These 2-D simplifications affect the magnitude of the calculated flux but should have minimal impact on the *shape* of the flux, that is, the channeling effect as the detector is rotated about the lattice. To compare the flux shapes, the calculated flux for all angles is normalized to the zero degree position. Additionally, the LATDOSE results are averaged over a five-degree interval to better emulate the MCNP tally results. Figure

3.36 shows the normalized results of for MCNP with the LATDOSE results superimposed.

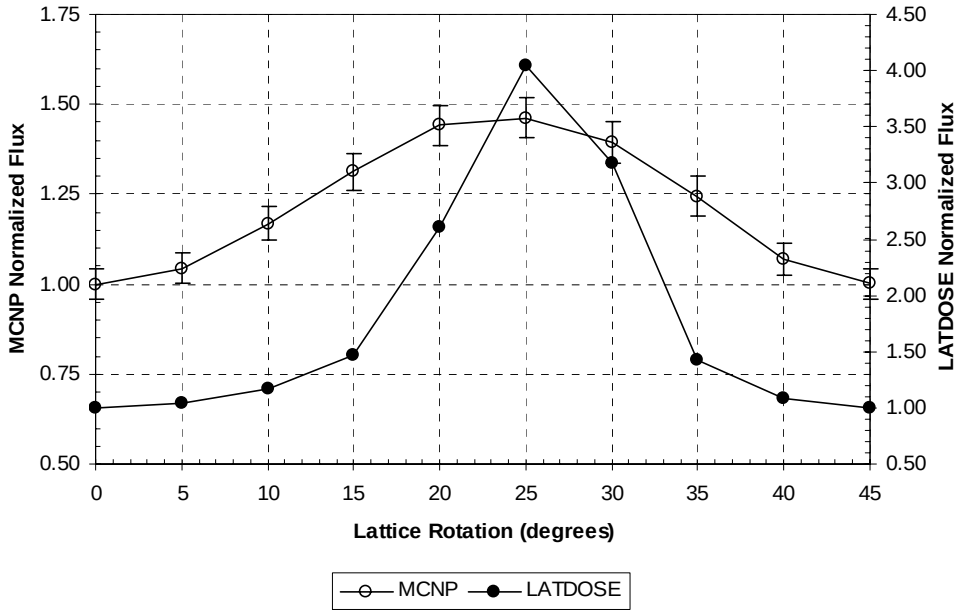

Figure 3.36: Comparison of MCNP calculated and LATDOSE calculated flux ratios for the 3x3 pin lattice with center pin active. The flux at each detector position is normalized to the flux at the 0 degree position.

The figure shows that the change in flux as a function of detector position is considerably less in the MCNP model than for the LATDOSE model. This is not surprising and, in fact, is the expected result. The setup of the source, collimator, and detector in the MCNP model will not demonstrate the same severe changes in flux vs. position as in the LATDOSE point-model. The 3-D model of the source in MCNP is not as concentrated, the collimator does not produce the same focused rays as in LATDOSE, and the MCNP detector is a 3-D volume rather than a point. The overall result will be to "smooth" the flux vs. position curve. The experimental results are expected to more closely follow the MCNP model results rather than the LATDOSE results. However, LATDOSE is effective in predicting the "special" angles where channeling is the highest, as shown in the following figures.

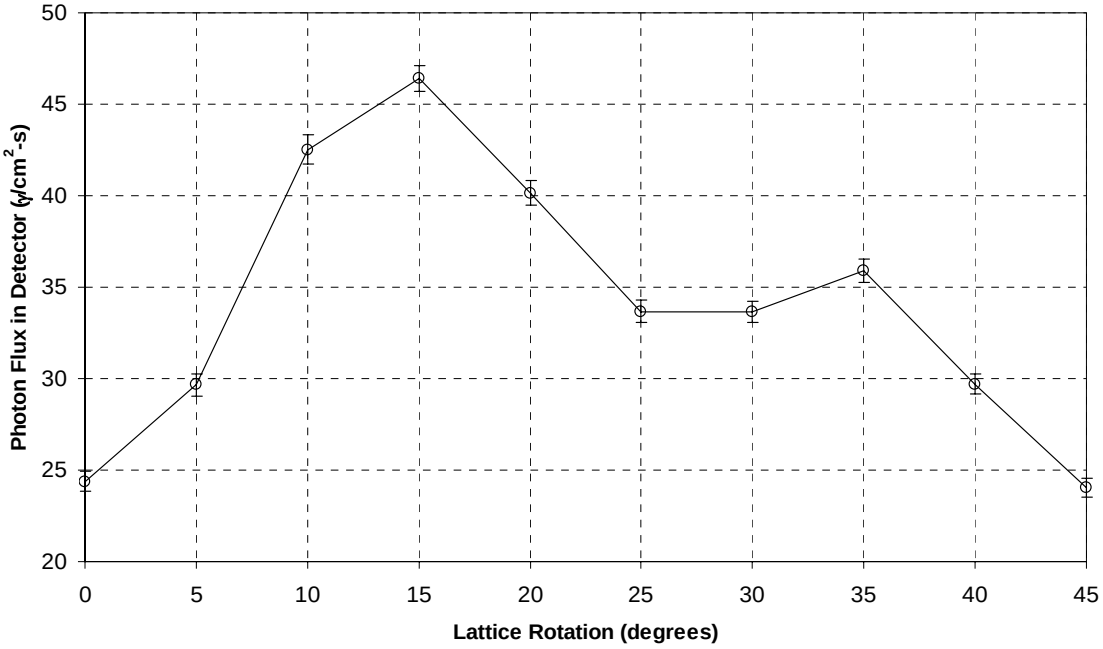

Figure 3.37: MCNP calculated photon flux averaged over the detector volume for the 3x3 pin lattice with corner pin activated.

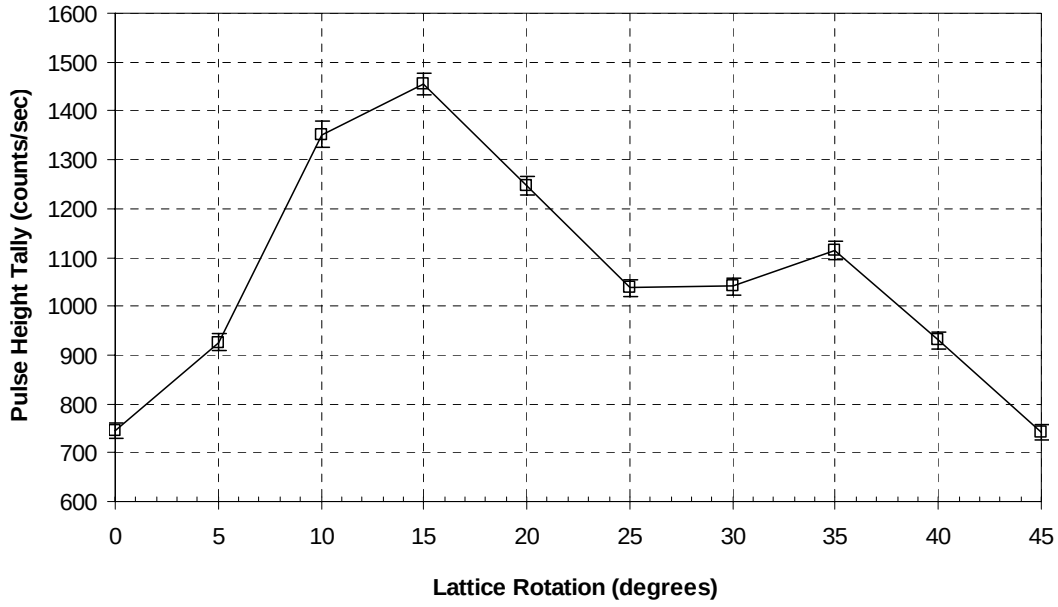

Figure 3.38: MCNP calculated total pulse height in the detector volume for the 3x3 pin lattice with corner pin activated.

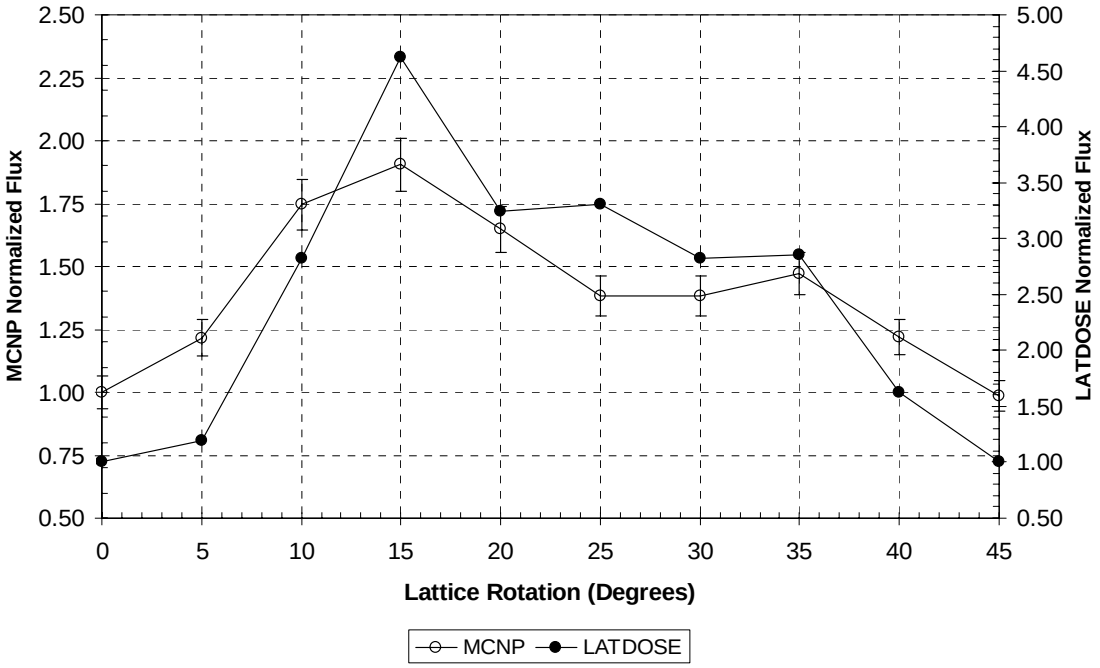

Figure 3.39: Comparison of MCNP calculated and LATDOSE calculated flux ratios for the 3x3 pin lattice with corner pin active. The flux at each detector position is normalized to the flux at the 0 degree position.

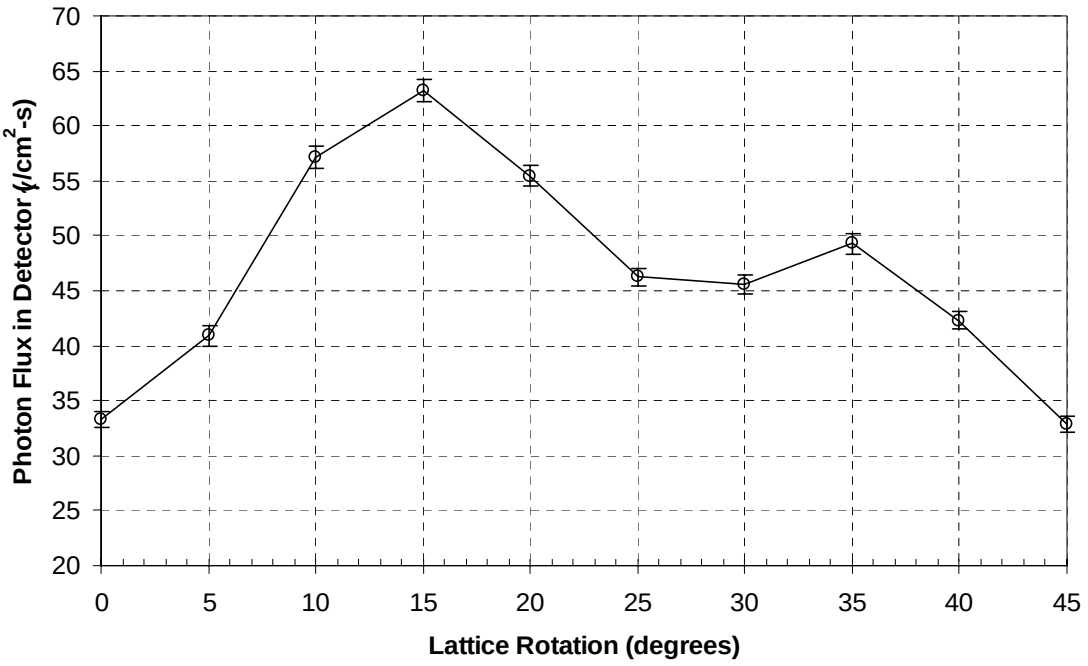

Figure 3.40: MCNP calculated photon flux averaged over the detector volume for the 5x5 pin lattice with center pin activated.

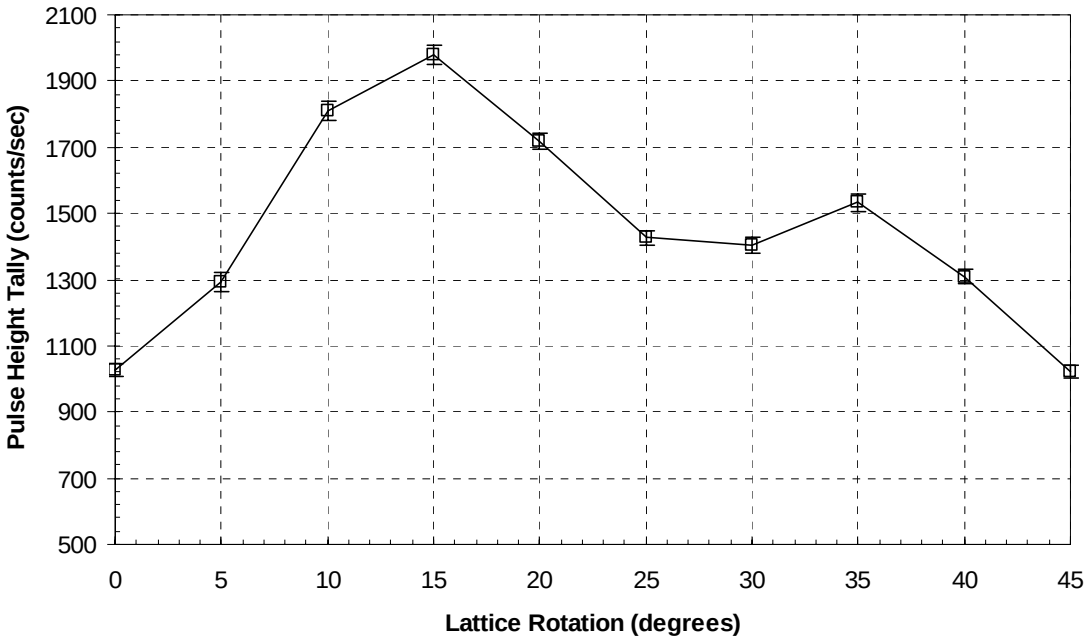

Figure 3.41: MCNP calculated total pulse height in the detector volume for the 5x5 pin lattice with center pin activated.

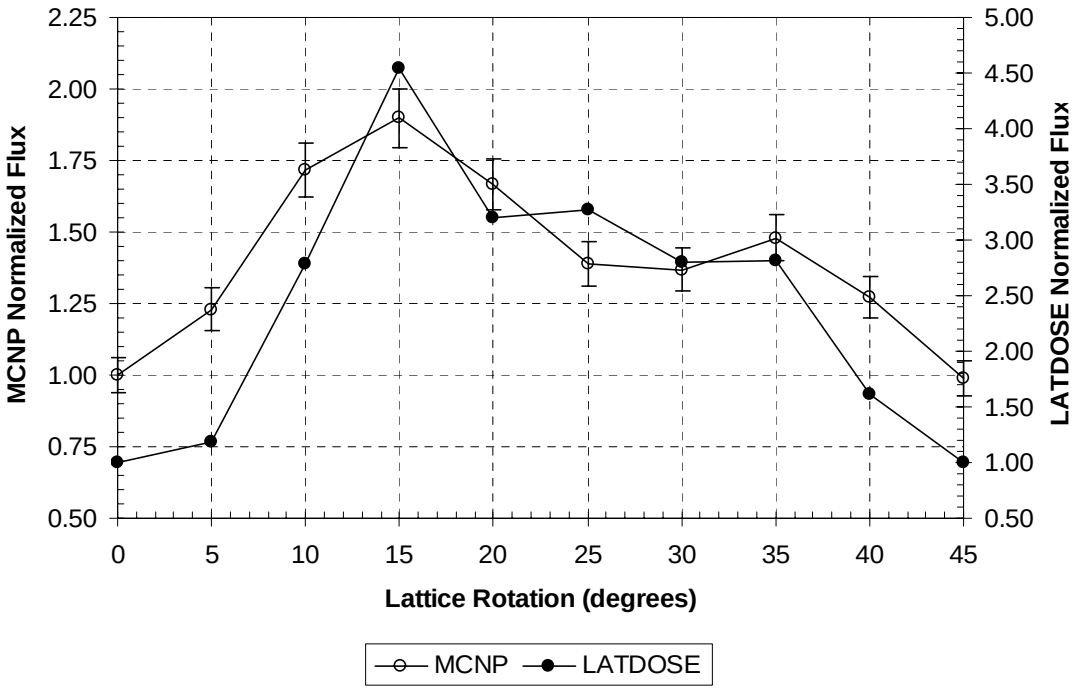

Figure 3.42: Comparison of MCNP calculated and LATDOSE calculated flux ratios for the 5x5 pin lattice with center pin active. The flux at each detector position is normalized to the flux at the 0 degree position.

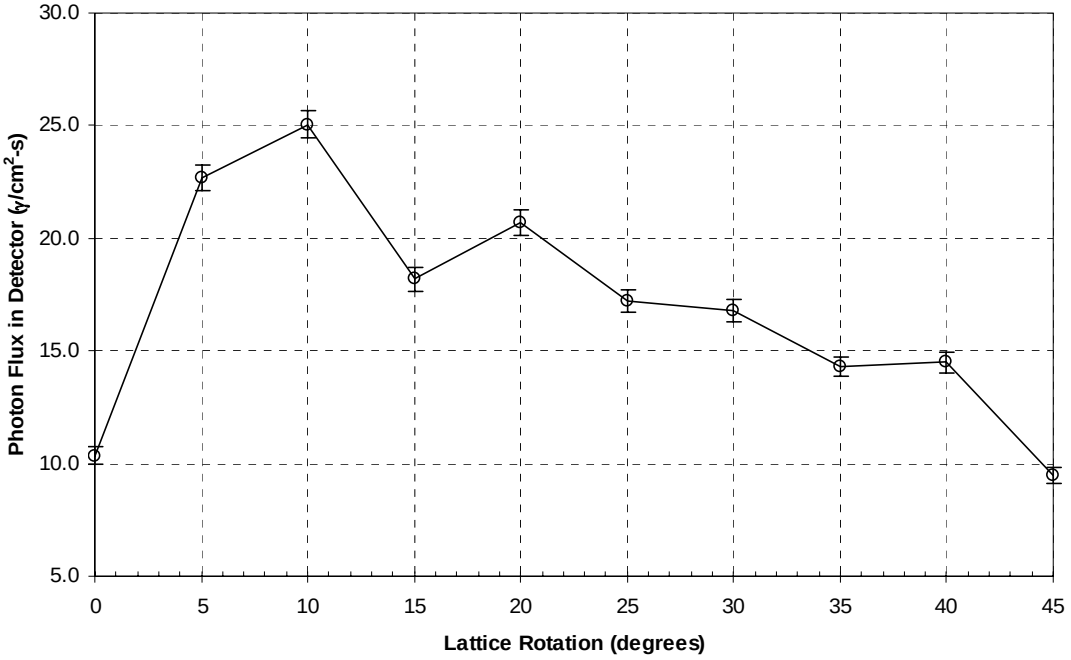

Figure 3.43: MCNP calculated photon flux averaged over the detector volume for the 5x5 pin lattice with corner pin activated.

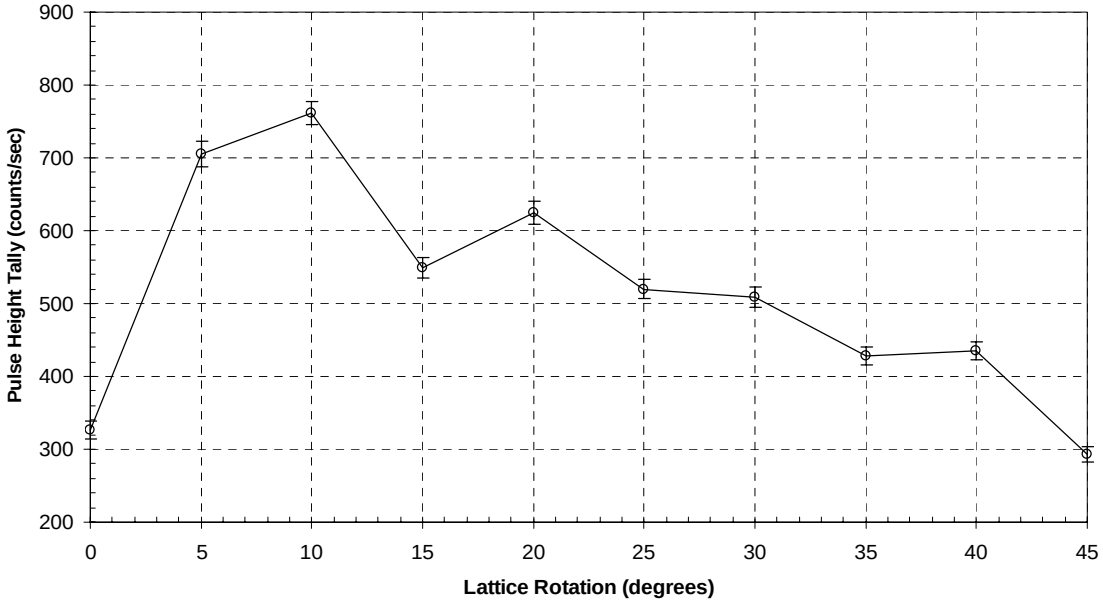

Figure 3.44: MCNP calculated total pulse height in the detector volume for the 5x5 pin lattice with corner pin activated.

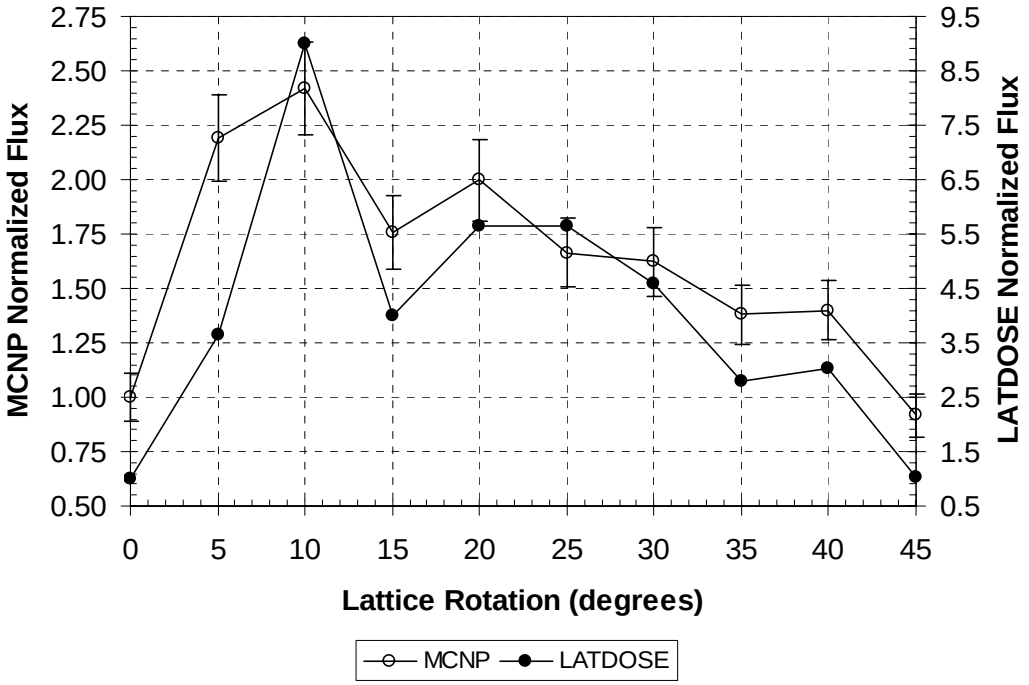

Figure 3.45: Comparison of MCNP calculated and LATDOSE calculated flux ratios for the 5x5 pin lattice with corner pin active. The flux at each detector position is normalized to the flux at the 0 degree position.

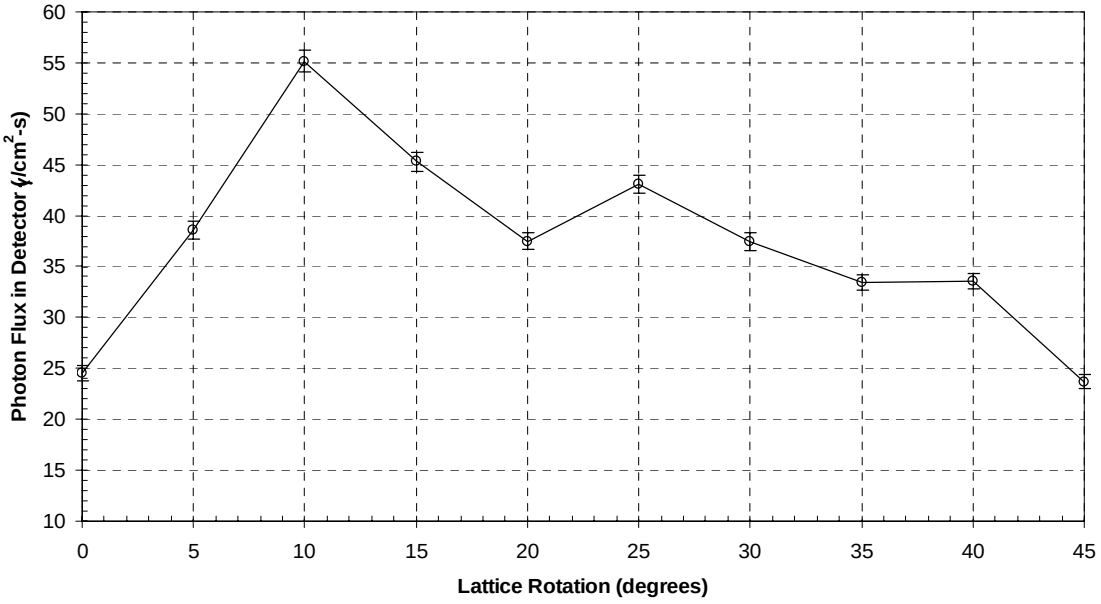

Figure 3.46: MCNP calculated photon flux averaged over the detector volume for the 7x7 pin lattice with center pin activated.

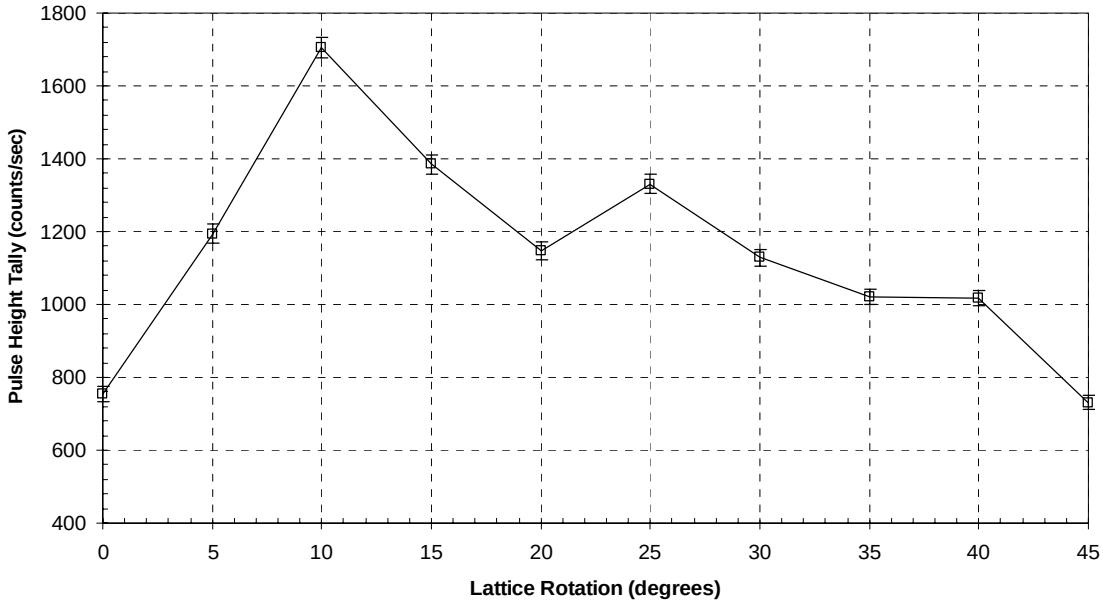

Figure 3.47: MCNP calculated total pulse height in the detector volume for the 7x7 pin lattice with center pin activated.

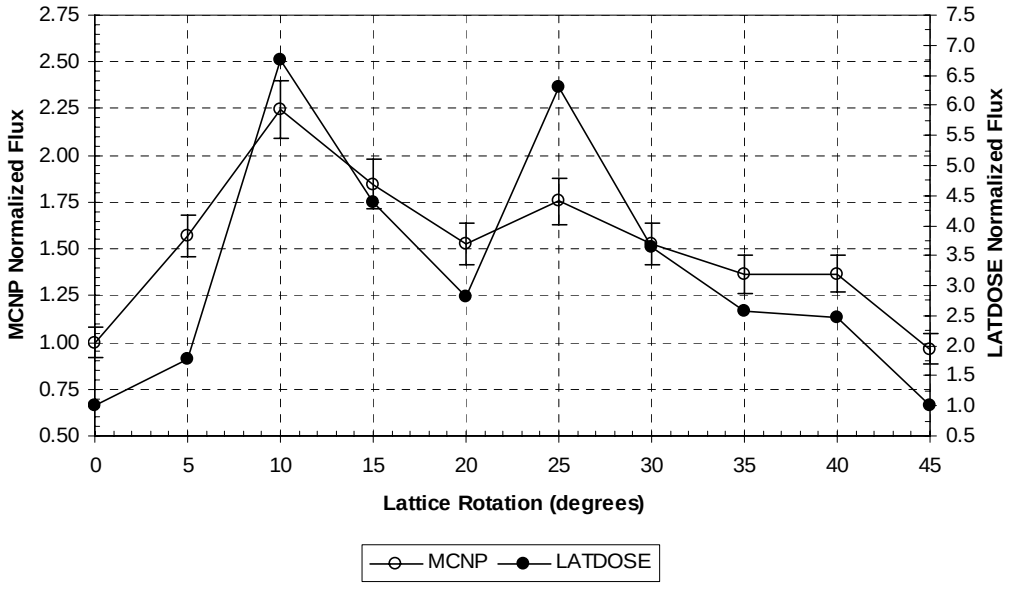

Figure 3.48: Comparison of MCNP calculated and LATDOSE calculated flux ratios for the 7x7 pin lattice with center pin active. The flux at each detector position is normalized to the flux at the 0 degree position.

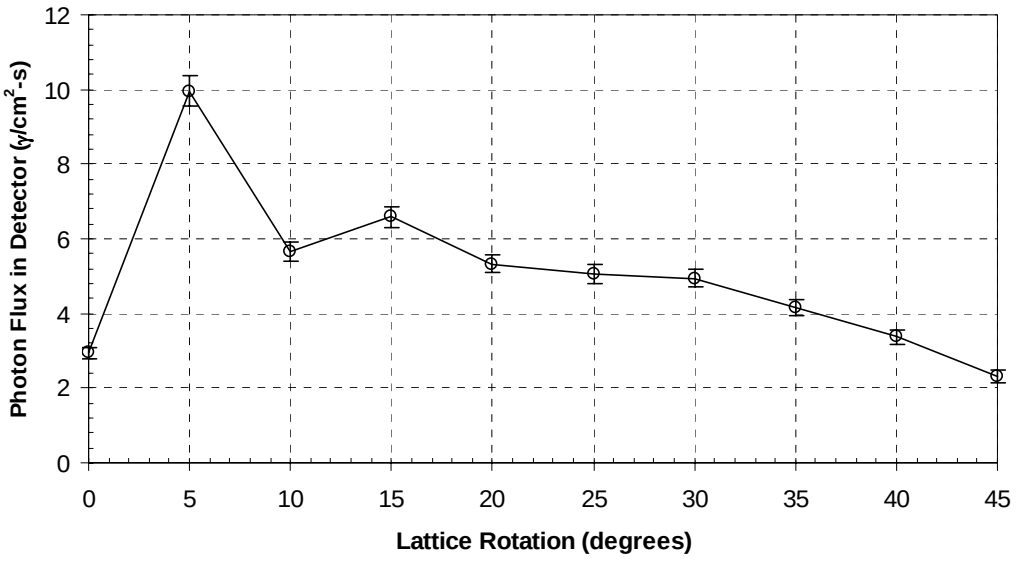

Figure 3.49: MCNP calculated photon flux averaged over the detector volume for the 7x7 pin lattice with corner pin activated.

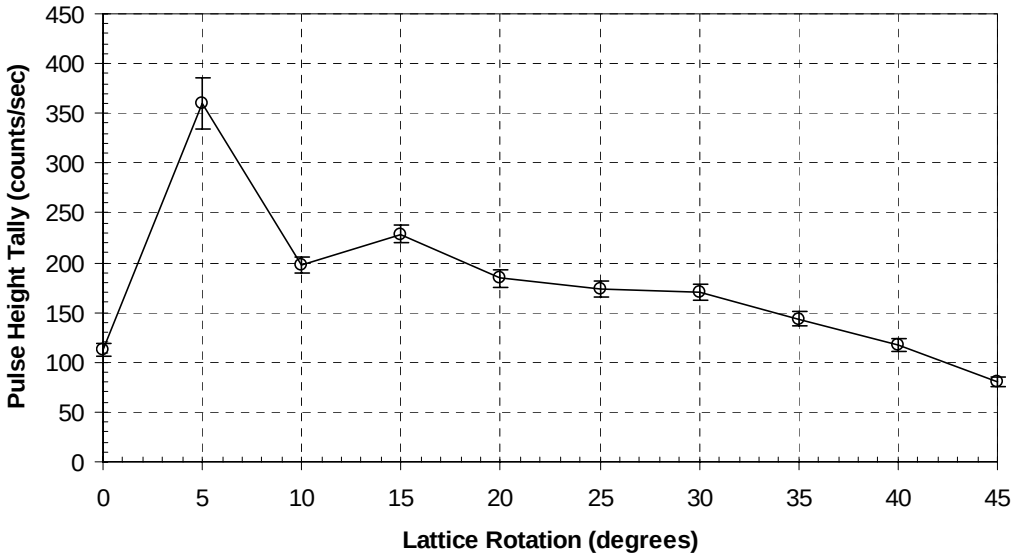

Figure 3.50: MCNP calculated total pulse height in the detector volume for the 7x7 pin lattice with corner pin activated.

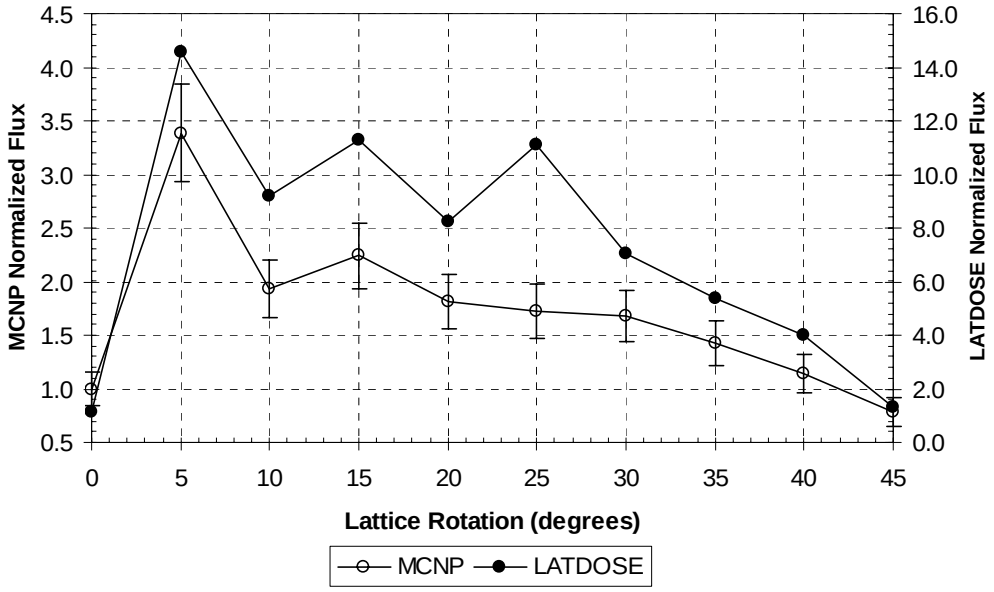

Figure 3.51: Comparison of MCNP calculated and LATDOSE calculated flux ratios for the 7x7 pin lattice with corner pin active. The flux at each detector position is normalized to the flux at the 0 degree position.

The preceding figures clearly show that LATDOSE is effective at determining the angles of lattice rotation at which the channeling effect of radiation through the lattice is the greatest. The MCNP model is a much more accurate representation of the physical geometry and a higher-order solution to the gamma-ray transport equation. The collimator arrangement, source modeling and detector modeling in MCNP all serve to reduce the sharp peaks in gamma-ray flux present in the LATDOSE solution.

It is also apparent from the figures of total pulse-height tally versus lattice rotation that energy deposition in the detector closely follows the gamma-ray flux, as expected. In later discussions (Chapter 4), the pulse-height tally will be further utilized by comparing energy deposition in specific energy ranges to experimental values.

CHAPTER 4
EXPERIMENTAL MEASUREMENTS OF FISSION-PRODUCT GAMMA-RAY TRANSMISSION THROUGH SPERT FUEL PINS

Experimental measurements of the detector response verses degrees of lattice rotation were performed in order to characterize the photon transport through SPERT fuel pins, as calculated by LATDOSE and MCNP in Chapter 3. Measurements were performed on several arrangements of unirradiated pins with a single activated fuel pin as the gamma-ray source. A sodium iodide detector (NaI(Tl)) coupled with gamma spectroscopy software were used to generate results over several energy ranges.

Given that the gamma-ray source used in these measurements was from the decay of fission products in the activated pin, the source intensity was time-dependent. Therefore, a suitable "decay-correction" strategy was necessary in order to normalize the measurements to a fixed point in time.

4.1 Gamma-Ray Spectroscopy at the Reactor Critical Facility

The RCF gamma-ray spectroscopy system consists of a NaI(Tl) detector with a 2" by 2" crystal (Canberra Model 802-2x2) connected to a photomultiplier tube and preamp (Canberra Model 2007P). The detector interfaces with a PC using a multichannel analyzer card (Canberra Model ASA-100). Data are collected, displayed and processed with spectroscopy software (Canberra GENIE-2000).

4.1.1 Basics of Gamma-Ray Spectroscopy Using Sodium Iodide Detectors

NaI(Tl) detectors belong to a group of detectors referred to as inorganic scintillators. Inorganic scintillator detectors are Alkali Halide crystals, doped with an impurity such as Thallium. Incoming radiation interacts with the detector crystal, which potentially causes

a valence electron to be excited into the conduction band, creating a vacancy ("hole") in the normally filled valence band. Upon return of an electron to the valence band, a photon is released. The probability of a valence electron being excited into the conduction band and the wave length of the photon created from filling the hole in the valence band are determined by the crystal properties of the detector. To achieve an efficient detector and increase the probability of a photon being released in the visual spectrum, these crystals are often doped with an impurity. The impurity, or *activator*, modifies the energy structure within the crystal lattice, creating energy bands within the normally "forbidden band," between the valence band and conduction band. As a result, incoming radiation is much more likely to cause a visible photon to be emitted from the detector crystal. NaI(Tl) detectors have an excellent light yield, near linear response to electrons and gamma-rays (over the most significant energy ranges) and have become the standard for standard gamma-ray spectroscopy [**Knoll**].

In order for an electronic signal to be produced as a result of photons created from the interaction of radiation with the NaI(Tl) crystal, a *photomultiplier tube* is used. The photomultiplier tube contains two primary sections, the photocathode and electron multiplier. Photons created in the detector crystal impinge on the photocathode, creating low energy electrons. The electrons migrate through the electron multiplier section, increasing in strength, until reaching a collector. An electronic pulse is then created, proportional to the number of incident visible spectrum photons from the detector, which is in turn proportional to the incident radiation on the detector. A block diagram of the instrumentation used at the RCF is provided in Figure 4.1.

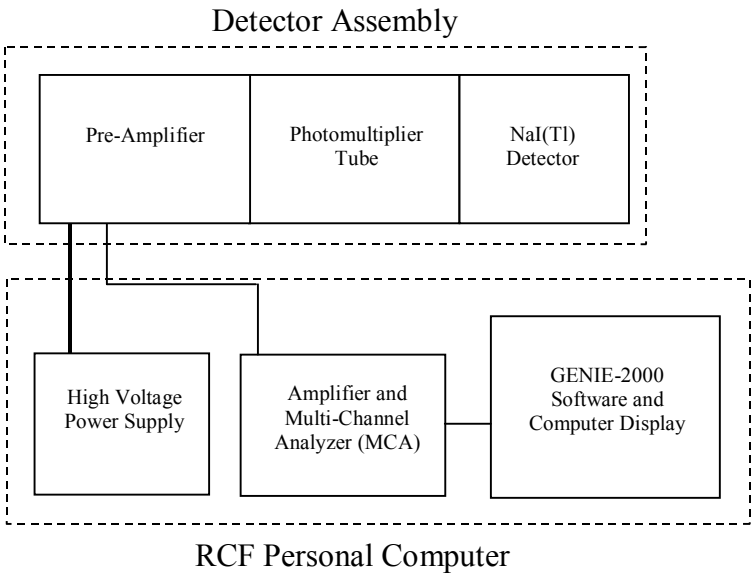

Figure 4.1: Block Diagram of NaI(Tl) Detector and Instrumentation at RCF.

If photons of energy E_0 are incident on the detector, the ideal detector response would by a "line" on the spectrum generated from the instrumentation at a channel corresponding to E_0. The magnitude of the line would exactly match the number of incident gamma rays on the detector. However, many processes occur within the detector (and shield, if present) that prevent the ideal response.

Consider first that photons incident on the detector will undergo interactions, as previously discussed in §3.2.2.1, with the detector crystal, detector housing, and lead shielding (if present). Depending on the physical size of the detector with respect to the mean free path of the secondary radiations created from these interactions, different amounts of the original photon's energy will be deposited within the detector crystal, contributing to the pulse heights at various energies in the spectrum. Figure 4.2 illustrates some of the different radiation interactions for a detector system similar to the one used at the RCF for this work.

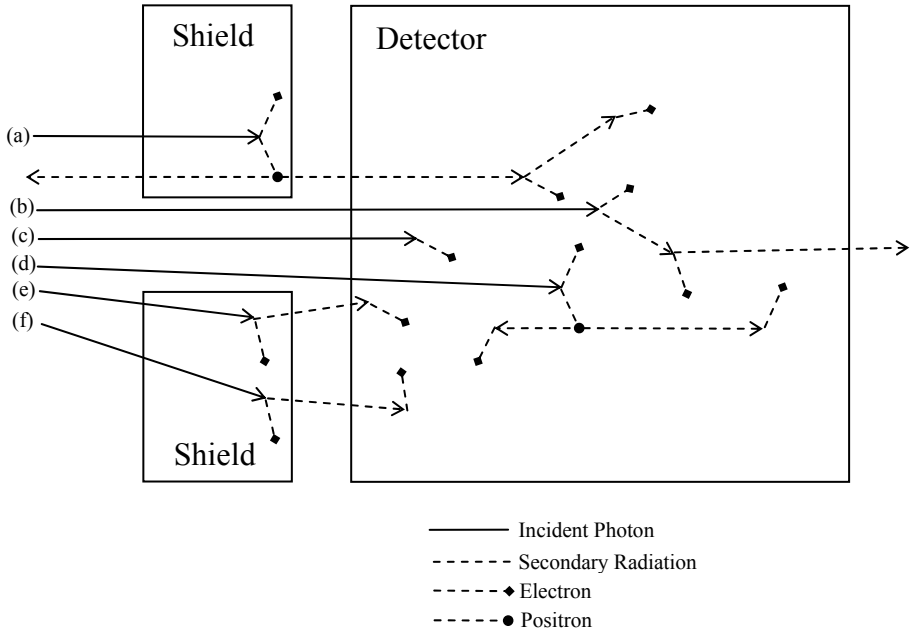

Figure 4.2: Schematic representation of photon reactions in a shielded detector of "intermediate" size such as used at the RCF.

Regardless of detector size, if a photon undergoes capture via photoelectric absorption (Figure 4.2(c)), it is highly likely that the entire energy of the photon will be deposited within the detector. If the absorption occurs extremely close to the detector boundary there is a non-zero probability that the resulting photoelectron will migrate out of the crystal without depositing all of its energy. However, photoelectric absorption is the "best case scenario" for gamma rays incident on the detector and provides for a well defined pulse, or "photopeak" at the expected energy.

Photons undergoing Compton scattering will deposit a spectrum of energies to the detector, based on the energy transferred during the scattering event to the target electron (Figure 4.2(b)). If the detector is "small" the scattered photon may exit with no further collisions. The net transfer of energy to the small detector is therefore less than that of the incident photon. Compton scattering within the shield may also contribute a source

of secondary radiation to the detector (Figure 4.2(e)). The net result is to create the "Compton Continuum" below the photopeak whereby scattered photons of various energies contribute to the pulse-height spectrum of the detector system.

Pair production events result in different energy depositions to the detector depending on the interaction of the secondary radiation produced. In Figure 4.2(a), a photon of energy $E_0 = h\nu$ undergoes pair production in the shield. The energy deposited in the shield is due to the kinetic energy of the electron and positron, $h\nu - 2m_oc^2$. The positron is annihilated creating two gamma rays, each with energy $m_oc^2 = 0.511$ MeV. A single annihilation gamma ray then enters the detector where it is subsequently absorbed, depositing all of its energy. The result is a contribution to the pulse height at the detector channel corresponding to 0.511 MeV. Figure 4.2(d) shows the incident gamma ray undergoing pair production with subsequent absorption of both annihilation gamma rays in the detector. In this case, the full energy of the incident gamma is deposited in the detector. Depending on the size of the detector, however, one or both of the annihilation gamma rays may escape the detector without further interaction, resulting in energy depositions of $h\nu - m_oc^2$ and $h\nu - 2m_oc^2$, respectively.

Photoelectric absorption within the detector shield (Figure 4.2(f)) will produce x-rays at a discrete energy corresponding to the binding energy of the ejected photoelectron, referred to as the "characteristic" energy. Usually, the x-rays are absorbed in the immediate vicinity of the reaction. However, if the reaction takes place close to the surface of the shield, the x-ray may escape and enter the detector contributing to the pulse height at a channel corresponding to the characteristic energy for the shielding material.

In the case of a source emitting gamma rays with a broad spectrum of energies, such as from fission products, the detector response becomes a very complicated function of all incident gamma rays and their secondary reactions within the detector and in the shielding surrounding the detector.

Figure 4.3 shows a pulse-height spectrum generated by the RCF detector system for a typical fuel pin activation without the shielded collimator installed between the source and detector. Figure 4.4 shows the pulse-height spectrum for another typical fuel pin activation but with the shielded collimator installed between the source and detector.

The resulting spectrum in Figure 4.3 lacks any real "structure," or sharp peaks, which would correspond to a significant contribution from a single particular fission-product isotope because of the large spread in gamma-ray energies resulting from the variety of fission products created. Using the DELBG calculated spectrum for fission-product energy in Figure 3.2, a peak is predicted around 300 keV and 1.1 MeV. Although a small peak may be discerned in the spectrum at approximately these energies in Figure 4.3, the contribution to the pulse-height spectrum from scattered photons yields a detector spectrum that is smeared-out relative to the predicted signal. However, the characteristic x-ray for the lead shielding is clearly present in the spectrum, however, at approximately 88 keV.

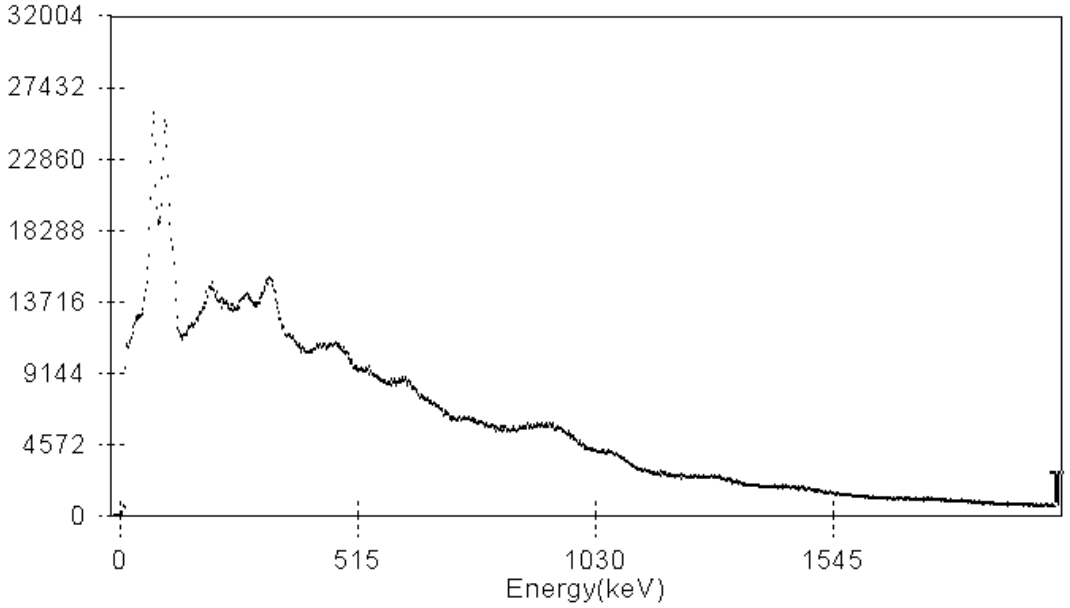

Figure 4.3: Typical Pulse-Height Spectrum up to 2 MeV for SPERT Fuel Pin Following Activation to ~80 watt-sec. without shielded collimator installed.

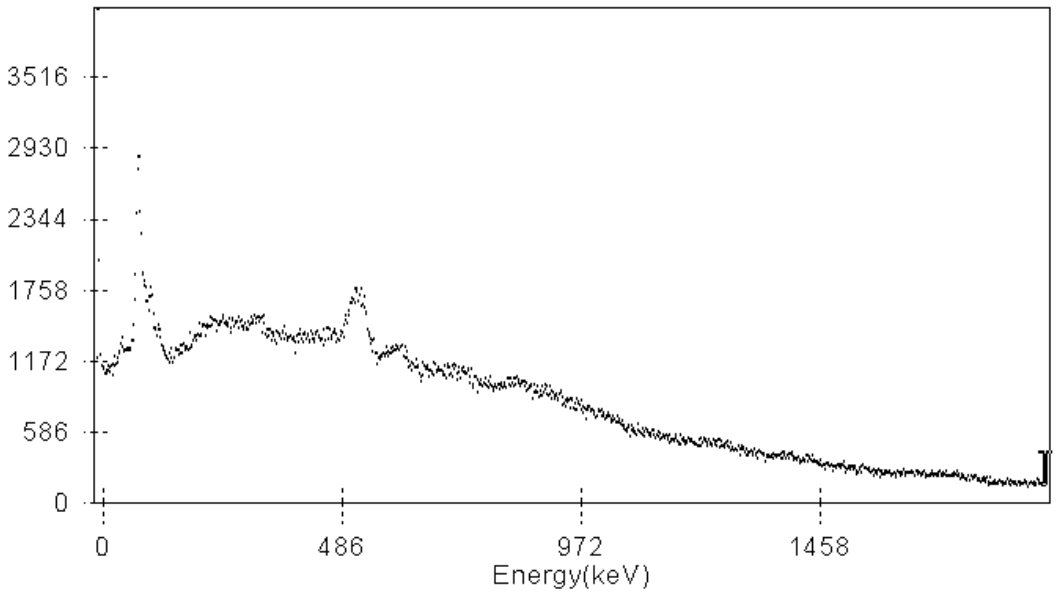

Figure 4.4: Typical Pulse-Height Spectrum up to 2 MeV for SPERT Fuel Pin Following Activation to ~80 watt-sec. with shielded collimator installed.

The obvious effect of adding the collimator is to reduce the overall intensity of the radiation incident on the detector, as shown in Figure 4.4 when compared to Figure 4.3.

Additionally, what little structure existed is lost except for the very noticeable peak at 0.511 MeV, due to the annihilation gamma ray resulting from pair production in the shielded collimator. However, this work does not require well-defined pulse-height spectra and, as discussed later in this section, NaI(Tl) detectors have some advantages for the types of measurements performed in this work.

The major limitation of NaI(Tl) detectors is their relative poor energy resolution, *R*, defined as

$$R = \frac{FWHM}{H_0} \ , \tag{4.1}$$

where *FWHM* is the "full width at half maximum" for a pulse with mean pulse-height value, H_0. The energy resolution for NaI(Tl) is limited primarily due to the sequence of low efficiency events that must occur in order to convert incident radiation to pulses, as detailed above. This sequence of events serves to introduce photoelectron statistical fluctuations, broadening the peaks. For example, under the best circumstances, NaI(Tl) can only be expected to provide energy resolution of 5-10% [**Knoll**]. Examples of the broad peaks typical of NaI(Tl) detectors are seen in Figure 4.5.

If better energy resolution (sharper peaks) is desired, a different detector must be employed. The detector must be capable of providing far greater numbers of carriers per radiation event than NaI(Tl), lowering the statistical uncertainties and providing sharper pulses. Usually, this implies semiconductor diode type detectors; specifically, high purity germanium detectors.

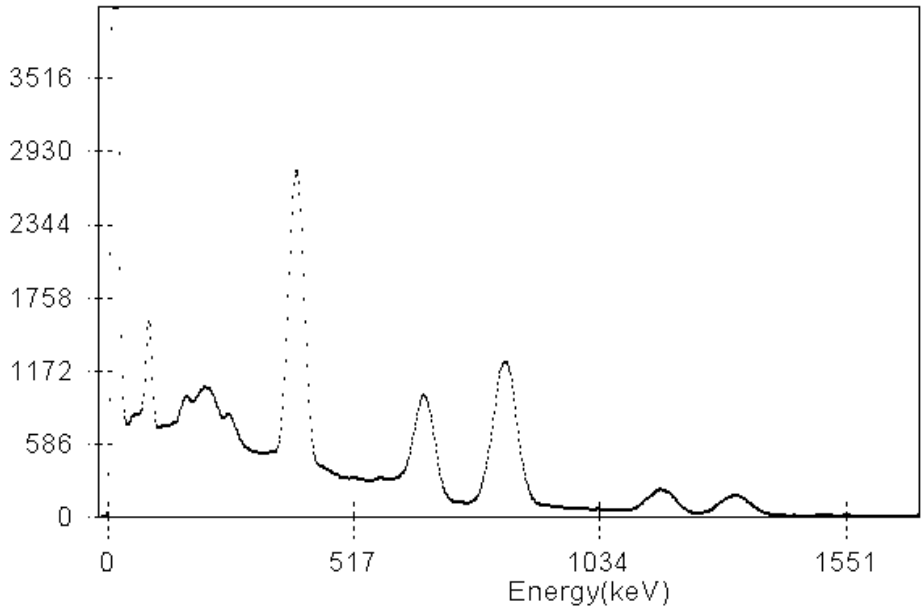

Figure 4.5: Pulse-height Spectrum generated using the RCF detector system and a multi-gamma standard source used for calibration.

In semiconductor detectors, the carriers are electron – hole pairs created along the path of a charged particle through the detector. By applying a high potential across the detector, these carriers migrate to their opposite poles, creating a flow of current, or pulse. The number of electron – hole pairs created are large compared to the number of photoelectrons produced in scintillator detectors for a given radiation event and therefore the pulses are much sharper and the energy resolution is greatly improved. Typically, HPGe resolutions are on the order of a few tenths of a percent compared to 5-10% of NaI(Tl).

The choice between using scintillators or semiconductor detectors depends on the application. Scintillators have a much better counting efficiency, given the high probability that incident radiation will undergo a reaction within the detector crystal but poor energy resolution. Semiconductor detectors have superior energy resolution but poor counting efficiency. Therefore, germanium is usually a better choice when

examining complex gamma-ray spectra and identifying individual peaks within the spectra. NaI(Tl) can be a better choice when only a few well known peaks are present and the emphasis of the measurement is intensity rather than identifying specific pulse energies. Additional consideration must be given to the fact that NaI(Tl) detectors are widely available, lower in cost, and easier to use compared to expensive HPGe detectors which require liquid nitrogen cooling.

The use of NaI(Tl) detectors for this work was judged to be adequate given that the goal was to determine the overall intensity of radiation along a path through a pin lattice rather than to identify the spectrum for specific fission-product isotopes. The high efficiency of the NaI(Tl) detector was also valuable given that the source was constantly changing due to decay. Therefore, it was beneficial to use a NaI(Tl) detector and get the greatest number of counts in the shortest counting time.

The potential loss of counts due to instrument dead time was considered. Count losses occur when the intensity of the incident radiation produces a large enough number of radiation events such that the capability of the detector electronics to resolve the individual counts is exceeded. The higher the radiation intensity, the greater the count-loss potential. The GENIE-2000 system, coupled with the ASA-100, reduces the potential for count losses by sensing when the ASA-100 can no longer resolve the individual counts. The system stops collecting data for a period of time, termed "dead time," until the electronics can again discern the individual counts. The dead time is added to the requested counting interval so that the actual amount of "real" time spent counting is the same as the requested counting interval. However, the "elapsed" time of

the counting interval will be the requested counting interval plus the accumulated dead time.

Therefore, in order to collect the maximum amount of data in the shortest counting intervals, in general it is necessary to limit the radiation intensity such that the counting electronics do not require a large amount of dead time. For the measurements at the RCF in support of this work, this was not an issue. The use of the collimator and the low radiation levels of the activated pins did not result in significant count loss corrections for the measurements.

4.2 Experimental Apparatus for Measuring Fission-product Gamma-Ray Transmission through SPERT Fuel Pins at the RCF

An apparatus was constructed consisting primarily of four components: the lattice plates, lattice plate support assembly, lattice plate support base, and detector support assembly. The lattice plates themselves had been constructed previously for use in the RCF core support structure as part of the conversion from high-enriched plate fuel to low-enriched SPERT fuel pins.

The lattice plates are constructed of stainless steel with the top lattice plate pin holes bored to 0.5 inch diameter. The bottom lattice plate has holes bored to accommodate the "nipple" on the lower end of the fuel pin. Both plates are drilled with the identical hole pattern with hole centers on a 0.613 inch square pitch.

The lattice plate support assembly is constructed entirely of wood, holds the top and bottom lattice plates in the correct position, and mounts to the lattice plate support base. The lattice plate support base is also constructed of wood. The mounting connection allows for the lattice plate support assembly to be rotated about a specific pin

position's vertical axis, relative to the detector support assembly, from 0 to 45 degrees. The lattice plate support base is marked off in 5 degree increments for rotating the lattice plate support assembly. It is also marked as necessary to facilitate positioning the detector support assembly as required for the experiment.

The detector support assembly is also constructed of wood and is designed to accommodate a heavy cantilevered load, based on the expected weight of the detector and shielded collimator assembly. The detector support assembly is constructed such that when the detector is positioned inside the shielded collimator assembly, the center of the detector is at the axial midpoint of the fueled region of the pins mounted in the lattice plates.

Wood was chosen for the support structures because of its relatively low mass density (and therefore low mass attenuation coefficient) as compared to steel, its availability and ease of construction. Figure 4.6 shows scanned photographs of two views of the experimental apparatus.

(a)

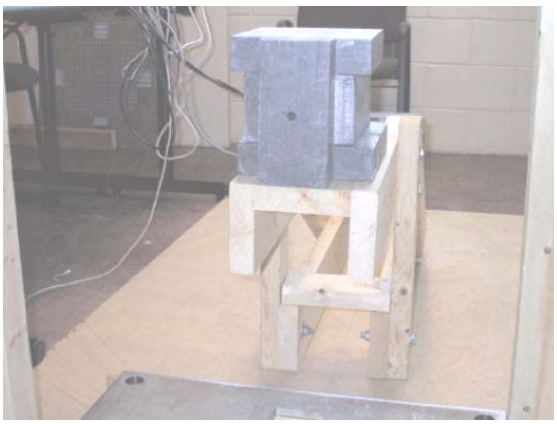

(b)

Figure 4.6: Experimental Apparatus (a) behind detector looking at lattice plates and (b) looking at collimator brick[5] between lattice plates.

4.3 Experimental Procedures

Experiments performed at the RCF for this work were essentially performed in two phases: the "exploratory" phase and the "final" phase. The exploratory phase consisted of simple measurements and served to work out any problems with the detector system, procedure, and experimental apparatus. The second phase of experiments involved the measurement of channeling through the six arrangements of fuel pin lattices, identical to the configurations discussed in the LATDOSE and MCNP calculations of Chapter 3.

4.3.1 Exploratory Measurements

The primary objective in this phase of testing was to develop the necessary procedures and knowledge to successfully setup the detector system, perform the pin activation, transfer the activated pin to the experimental apparatus, and collect data with the detector system. The typical sequence involved the on-watch Senior Reactor Operator (SRO) performing the pre-startup checklist while the experimental apparatus was readied and detector system calibrated. If needed for the experiment, unirradiated fuel pins were loaded into the experimental apparatus in accordance with RCF fuel pin handling procedure.

The RCF core was used to activate the source pin for the measurements. Using normal reactor operational procedures, all control rods were fully withdrawn from the core to achieve a slightly supercritical condition. The reactor was allowed to increase

[5] This photo was taken when a collimator brick with a 0.5 inch x 2 inch long cylindrical collimator was used. For most of the experiments discussed in this work, this collimator was replaced with a slit-type collimator having dimensions 0.375 inch x 4 inch long x 2 inch high.

power on a constant period to a desired power level. The power level was determined by the amount of activation energy desired and the reactor period (see §3.1.1 for details). When the specified power level was reached, the reactor was scrammed and a stopwatch started. The stopwatch provided the "time after scram" values for all data collected.

In order to minimize personnel exposure, several minutes were allotted after reactor scram for the radiation levels to decay prior to withdrawing the activated fuel pin from the core. Once the radiation level on the reactor deck area radiation monitor was judged acceptable, the center pin was removed from the core and transferred to the experimental apparatus.

Data collection was performed by initiating a counting cycle on the detector system and noting the time after scram that the counting cycle started. Counting cycles were generally of either 60 or 100 second duration, depending on the experiment. All counting results were saved on disk prior to beginning another counting cycle. This allowed for maximum flexibility in data handling using the GENIE-2000 software, i.e., setting and changing regions of interest, determining live-time and dead-time intervals for each collection cycle.

4.3.1.1 Single Pin Measurements

Two separate experiments were planned using just a single activated pin in the experimental apparatus. The first involved the detector system without a collimator brick installed between the source pin and detector. Otherwise, the detector was shielded on the top, bottom, and sides using lead bricks. The detector face was measured to be 8.25 inches (21 cm) from the center of the activated pin, as shown in Figure 4.7.

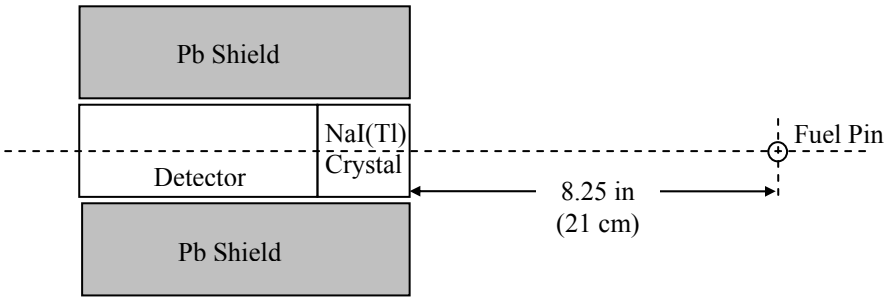

Figure 4.7: Top (x-y plane) view schematic of single activated fuel pin measurement showing arrangement of fuel pin, detector, and shielding[6].

For activating the source pin, the reactor was brought to a power level of 2.6 W on a constant period of 32 seconds. Using Equation (3.15), the activation energy was calculated to be 83.2 W•s. Data collection commenced at 660 seconds after scram with 60 second collection intervals.

For this experiment, two "regions of interest" (ROI's) were specified in the energy domain of the spectrum. The GENIE-2000 software automatically integrates the pulse heights within the energy range of the ROI and displays a value for the entire ROI. The two ROI's examined in this experiment spanned from 180 keV to 450 keV and 550 keV to 1000 MeV. The 450 keV to 550 keV interval was avoided because of the annihilation gamma ray from pair production in the lead shield. The collected data are shown in Table 4.1.

[6] Note that in this view the top and bottom shielding configuration is not shown.

Table 4.1: Experimental data showing the time dependent counts of two regions of interest in the delayed fission-product gamma-ray spectrum for a single SPERT fuel pin. No collimator was installed.

Count	Start Time After SCRAM (sec)	Count Duration (sec)	Effective Time After SCRAM (sec)	180 - 450 KeV (counts)	2σ	550 - 1000 KeV (counts)	2σ
1	660	256	788	2294500	3030	1967558	2805
2	1020	198	1119	1787680	2674	1499907	2449
3	1260	170	1345	1530458	2474	1276119	2259
4	1470	150	1545	1358511	2331	1119810	2116
5	1650	137	1719	1239786	2227	1012773	2013
6	1815	126	1878	1151444	2146	929337	1928
7	1965	117	2024	1071442	2070	861548	1856
8	2160	107	2214	973029	1973	785618	1773
9	2295	101	2346	912121	1910	740654	1721
10	2420	96	2468	867915	1863	703235	1677
11	2540	92	2586	825888	1818	671692	1639
12	2690	87	2734	780409	1767	634172	1593
13	2805	83	2847	745638	1727	607943	1559
14	2910	81	2951	711486	1687	583894	1528
15	3020	80	3060	678755	1648	560535	1497
16	3120	79	3160	654644	1618	541494	1472
17	3240	78	3279	627458	1584	521081	1444
18	3360	77	3399	600057	1549	501857	1417
19	3480	76	3518	575463	1517	484493	1392
20	3600	75	3638	554571	1489	466920	1367

The start time after scram was taken from the stopwatch and count duration was reported by the GENIE-2000 software. The GENIE-2000 will suspend counting to avoid lost counts due to detector "dead-time." Therefore, the count duration represents the time required to obtain 60 seconds of actual counting time. The effective time after scram is calculated by adding one half the count duration to the start time after scram. This places the data at the midpoint of the data collection interval. The pulse height results (counts) for the two ROI's chosen for this experiment are shown next with their associated standard deviation.

The standard deviation was calculated by applying counting statistics to the collected data [**Knoll**]. An estimate of the standard deviation of a single measurement can be made by assuming that the measured value is the mean, $\bar{x} = x$, and the count distribution follows a Poisson distribution. In making these two assumptions, the

distribution is completely described and an estimate of the variance can be made where $\sigma^2 = \bar{x}$, or simply, $\sigma = \sqrt{x}$. This is a frequently used method and has been applied to other similar experiments at the RCF [**Galayda**]. A plot of the data presented in Table 4.1 is shown in Figure 4.9. The error bars showing the 95% confidence interval (2σ) are too small to show on the points.

The results of the experiment show that the gamma-ray energy deposited in the detector decays as a function of time, as expected. The well-behaved shape of the curves suggests that a decay-correction curve can be generated to normalize the measured values of each ROI to a fixed point in time. Further, the exponential shape of the decay curve supports the veracity of the DELBG algorithms and agrees with expectations based on previous work (§2.1).

The ability to decay correct the gamma-ray source is essential to performing the subsequent lattice channeling experiments. By applying a decay correction to the measured data, the effects of changing the lattice orientation can be isolated from the effects of the reduction in delayed fission-product gamma-ray intensity with increasing time after scram.

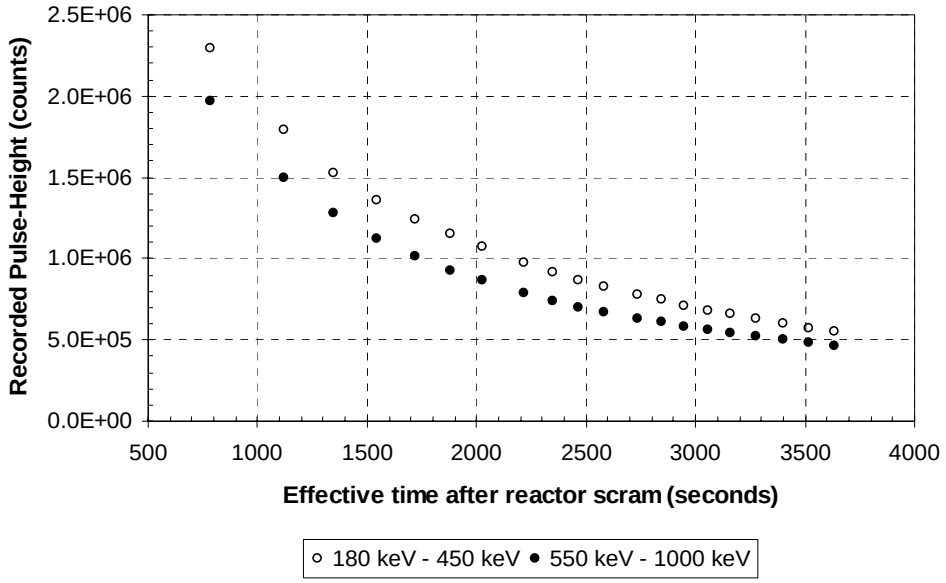

Figure 4.9: Plot of counts versus time for two regions of interest in the delayed fission-product gamma-ray spectrum for a single SPERT fuel pin. No collimator was installed.

Goldstein's Expression [**Jaeger**] suggests that the time-dependent, total gamma-ray energy released from delayed fission-product gamma rays, from about 20 seconds to 30 days after fission, can be approximated by an equation of the form

$$E(t) = At^{-B} \quad , \tag{4.2}$$

where A and B are constants. The energy released from delayed fission-product gamma rays at some time after fission will correspond to the number of counts recorded in the detector for a specific ROI. Therefore, the detector counts in each ROI will exhibit the same time-dependent behavior. Using the data provided in Table 4.2 and performing a least-squares curve fit to obtain the constants A and B, equations can be generated to fit the data.

Trial fits of several function types were performed on the data and correlation coefficients for the various fits were compared. For both ROI's, a *shifted-power* fit of the form

$$C(t) = A(t - B)^{-C} \quad , \tag{4.3}$$

where $C(t)$ are the time-dependent counts for an ROI and t is the effective time after fission (seconds), provided an improved fit to the experimental data, relative to the power-fit form of Equation (4.2). Table 4.2 shows the constants for the shifted-power fits.

Table 4.2: Calculated coefficients for shifted-power fit to measured pulse-height data collected from SPERT fuel pin. No collimator was installed.

ROI	A	B	C
180 - 450 keV	3.0255E+10	-693.8117	1.2984
550 - 1000 keV	1.1976E+10	-476.4024	1.2193

Figure 4.10 shows the measured data with the fitted curves superimposed.

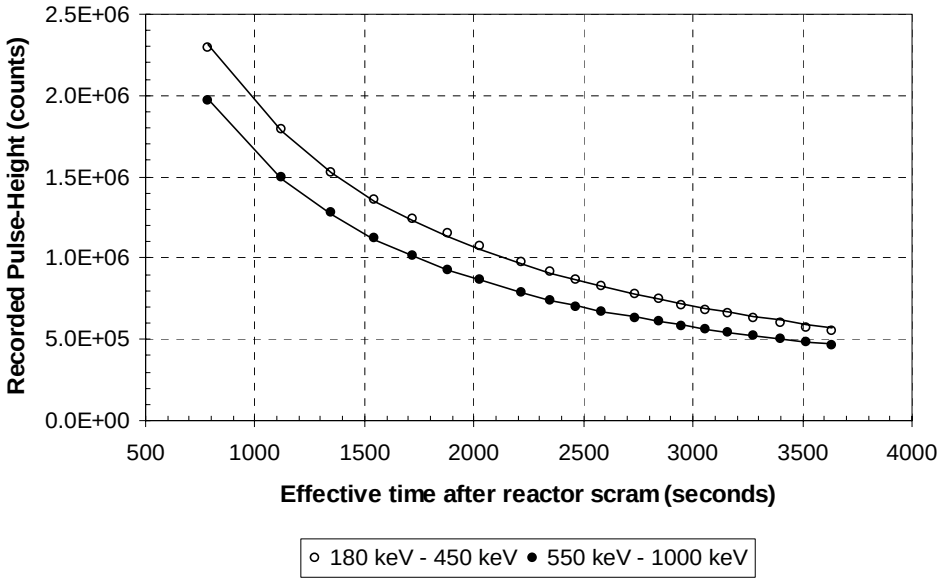

Figure 4.10: Plot of counts versus time and fitted curve for two regions of interest in the delayed fission-product gamma-ray spectrum for a single SPERT fuel pin. No collimator was installed.

This experiment was repeated with the collimator brick installed, a shown in the schematic of Figure 4.11. The solid angle of incident gamma rays on the detector has been reduced by approximately a factor of 16.

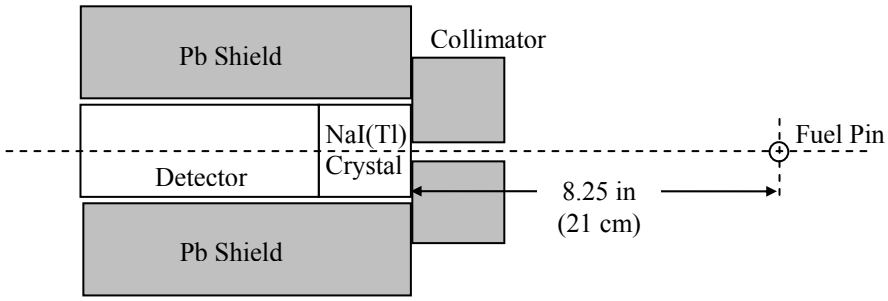

Figure 4.11: Top (x-y plane) view schematic of single activated fuel pin measurement showing arrangement of fuel pin, detector, collimator, and shielding[7].

Therefore, if the collimator were 100% efficient and the pin were activated to exactly the same energy, the measured pulse heights would be reduced by a factor of 16. Obviously, the collimator is not 100% effective. Its effectiveness varies with the energy of the incident gamma rays – less for higher energy gamma rays, more for lower energy gamma rays.

The results for the second measurement are shown in Table 4.3. The recorded period and peak power for this experiment were 32 seconds and 2.6 W, respectively, with an irradiation time of 200 seconds. The activation energy and irradiation time is the same for the two experiments, within the accuracy of the reactor operator's ability to read the nuclear instrumentation and initiate a scram at the desired peak power level. A conscious attempt was made to begin the measurements earlier after reactor scram to compensate for the expected reduction in source intensity due to the collimator. A greater number of data points were also collected because the lower intensity resulted in lower dead-times and shorter real-times for the given counting interval (60 seconds). By comparing similar effective times after scram in Table 4.1 and Table 4.3, the pulse-height magnitude for the

[7] Note that in this view the top and bottom shielding configuration is not shown. This measurement used the cylindrical collimator.

lower ROI is affected to a greater degree than the higher ROI, and in general, the reductions in measured pulse heights are as expected.

Table 4.3: Experimental data showing the time dependent counts of two regions of interest in the delayed fission-product gamma-ray spectrum for a single SPERT fuel pin. A 0.5 inch x 2 inch cylindrical collimator was installed.

Count	Start Time After SCRAM (sec)	Count Duration (sec)	Effective Time After SCRAM (sec)	180 - 450 KeV (counts)	2σ	550 - 1000 KeV (counts)	2σ
1	225	77.0	263.5	358694	1198	416849	1291
2	410	74.5	447.3	206177	908	243559	987
3	500	74.3	537.2	175885	839	207273	911
4	585	74.3	622.2	152947	782	181329	852
5	671	74.0	708.0	136925	740	161842	805
6	765	74.1	802.1	122307	699	145827	764
7	850	74.2	887.1	112115	670	132811	729
8	940	74.2	977.1	102615	641	122117	699
9	1030	74.4	1067.2	95269	617	114050	675
10	1120	74.5	1157.3	89063	597	104677	647
11	1210	74.5	1247.3	83383	578	98038	626
12	1295	74.3	1332.2	78378	560	92324	608
13	1380	74.2	1417.1	73841	543	87076	590
14	1470	74.5	1507.3	69632	528	82722	575
15	1560	74.4	1597.2	65183	511	77833	558
16	1645	74.2	1682.1	61621	496	73721	543
17	1730	74.3	1767.2	59297	487	70357	530
18	1815	74.5	1852.3	56722	476	67306	519
19	1900	74.5	1937.3	54630	467	64709	509
20	1985	74.8	2022.4	52845	460	61814	497
21	2075	74.7	2112.4	50766	451	59214	487
22	2160	74.8	2197.4	48674	441	57035	478
23	2245	74.8	2282.4	46267	430	54849	468
24	2330	74.9	2367.5	44941	424	52514	458
25	2416	75.0	2453.5	43291	416	50821	451
26	2500	74.8	2537.4	42330	411	49512	445
27	2590	75.0	2627.5	40602	403	47320	435
28	2675	75.1	2712.6	38608	393	45704	428
29	2760	75.1	2797.6	37205	386	44225	421
30	2850	74.7	2887.4	35814	378	42386	412
31	2940	74.8	2977.4	34691	373	41082	405
32	3025	74.7	3062.4	33483	366	39667	398
33	3115	74.8	3152.4	32796	362	38761	394
34	3200	74.6	3237.3	31501	355	37747	389
35	3290	75.0	3327.5	30661	350	36520	382
36	3380	75.1	3417.6	29593	344	35820	379
37	3470	75.0	3507.5	28832	340	34434	371
38	3560	75.1	3597.6	27667	333	33308	365
39	3645	74.8	3682.4	26959	328	32483	360
40	3735	74.8	3772.4	26113	323	31643	356
41	3825	74.9	3862.5	25303	318	30520	349
42	3915	75.0	3952.5	25011	316	30201	348

A plot of the data presented in Table 4.3 is shown in Figure 4.12. Again, the error bars showing the 95% confidence interval (2σ) are too small to show on the points and have therefore been omitted. The shapes of the curves are consistent with the first experiment and further suggest that the data can be decay-corrected by fitting a curve to the data points.

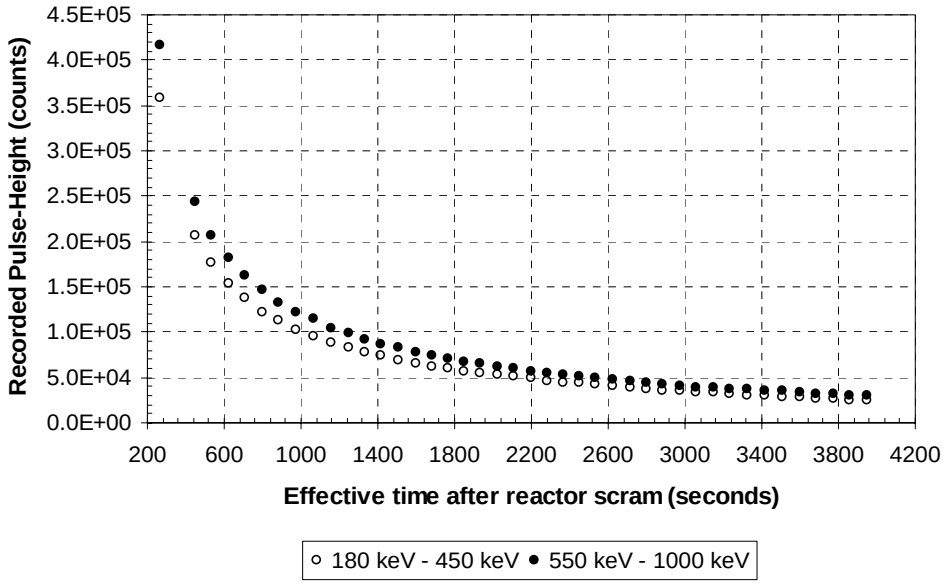

Figure 4.12: Plot of counts versus time for two regions of interest in the delayed fission-product gamma-ray spectrum for a single SPERT fuel pin. A 0.5 inch x 2 inch cylindrical collimator was installed.

A shifted-power fit was again applied to the measured data. Table 4.4 shows the resulting coefficients.

Table 4.4: Calculated coefficients for shifted power fit to measured pulse-height data collected from SPERT fuel pin. A 0.5 inch x 2 inch cylindrical collimator was installed.

ROI	A	B	C
180 - 450 keV	5.2823E+07	24.4610	0.9125
550 - 1000 keV	7.8246E+07	0.0000	0.9408

Figure 4.13 shows the resulting curve fits superimposed over the measured data.

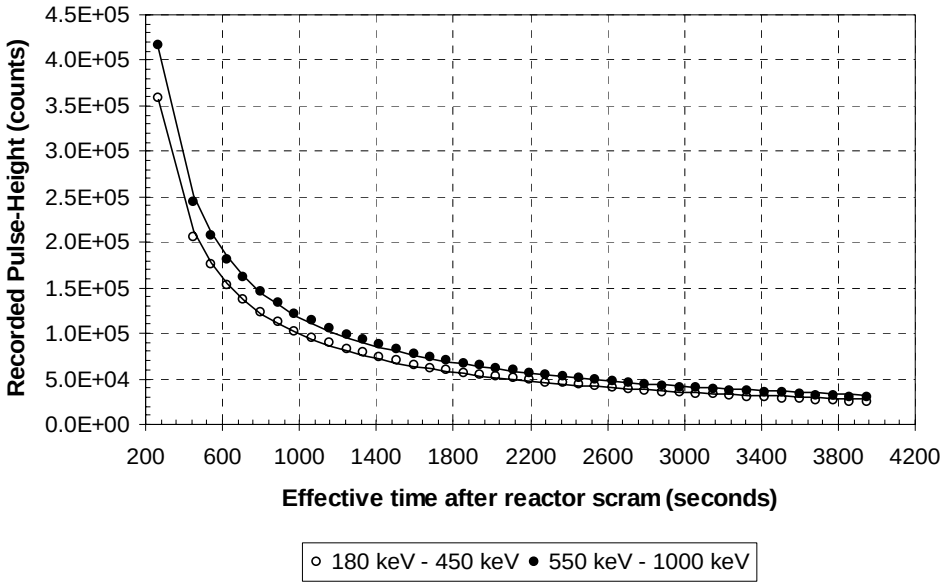

Figure 4.13: Plot of counts versus time and fitted curve for two regions of interest in the delayed fission-product gamma-ray spectrum for a single SPERT fuel pin. A 0.5 inch x 2 inch cylindrical collimator was installed.

Figures 4.13 and 4.10 show that aside from the count magnitudes and differences in time span, the curves are very similar in shape. The counts are normalized to a common effective time after scram, C_i / C, (the closest data point is at 2020 seconds for the no-collimator case and 2024 seconds with the collimator) and plotted together in Figure 4.14. The figure clearly shows that a common decay curve, generated from normalized data, can be used to correct measured data taken with and without the collimator installed.

Because the time span is larger for the measurements taken with a collimator and the time between measurements is less (better precision), the decay curve generated for this case was chosen to decay-correct subsequent data.

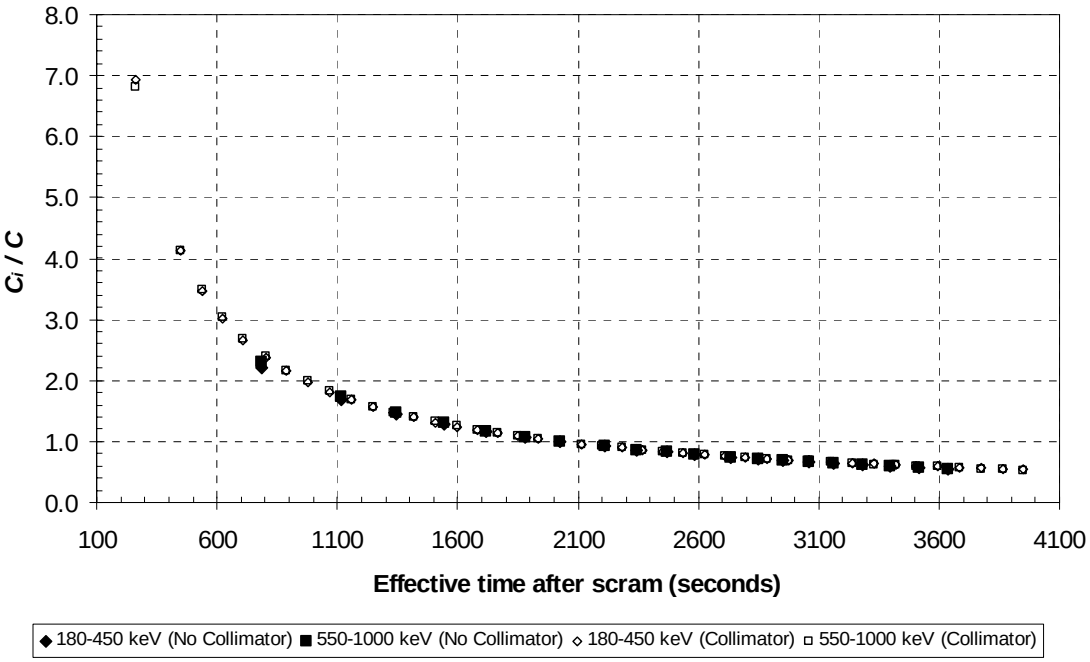

Figure 4.14: Plot of fitted decay curves normalized to a near common effective time after scram for two regions of interest in the delayed fission-product gamma-ray spectrum for a single SPERT fuel pin.

4.3.1.2 In-Line Pin Shielding Experiments

The next measurement involved placing a series of unirradiated fuel pins in line between the activated fuel pin and the detector. During the measurement, the inactive fuel pins were removed one-by-one. Counts were measured for the five, four, three, two, one and no unirradiated pin cases. A schematic is shown in Figure 4.15.

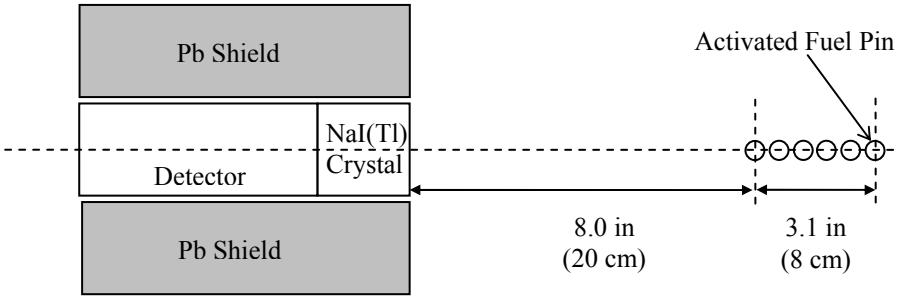

Figure 4.7: Top view schematic of single activated fuel pin measurement with five unirradiated fuel pins in line showing arrangement of fuel pins, detector, and shielding[8].

[8] Note that in this view the top and bottom shielding configuration is not shown.

The core was irradiated for 200 seconds in this measurement, reaching a peak power of 2.5 W on a 32 second period. Multiple counts were taken at each configuration. The raw experimental data are shown in Table 4.5.

Table 4.5: Raw experimental data showing the shielding effectiveness of SPERT fuel pins in-line between the detector and a single fuel pin.

Count	Number of Unirradiated Pins In Line	Start Time After SCRAM (sec)	Count Duration (sec)	Effective Time After SCRAM (sec)	180 - 450 keV (counts)	2σ	550 - 1000 keV (counts)	2σ
1	5	600	74.3	637	408077	1278	203124	901
2	5	700	74.0	737	355742	1193	173790	834
3	4	810	73.9	847	321899	1135	156037	790
4	4	900	74.0	937	301235	1098	162452	806
5	4	1000	73.9	1037	279078	1057	149612	774
6	3	1100	74.2	1137	282901	1064	184530	859
7	3	1200	74.1	1237	265226	1030	171638	829
8	2	1320	74.7	1357	307548	1109	251025	1002
9	2	1425	74.3	1462	284081	1066	232413	964
10	1	1530	76.1	1568	408836	1279	396230	1259
11	1	1660	75.9	1698	387023	1244	372998	1221
12	0	1800	105.2	1853	980439	1980	707997	1683
12a	0	1940	98.2	1989	914984	1913	654323	1618
13	1	2040	74.9	2077	306033	1106	287763	1073
14	1	2140	74.6	2177	293403	1083	275400	1050
15	2	2260	74.1	2297	189202	870	144532	760
16	2	2350	73.9	2387	182872	855	139602	747
17	3	2470	73.9	2507	146775	766	86227	587
18	3	2560	73.8	2597	142619	755	82856	576
19	4	2660	74.1	2697	130953	724	63015	502
20	4	2760	74.1	2797	126889	712	61545	496
21	5	2880	74.2	2917	121695	698	53243	461
22	5	2970	74.2	3007	119108	690	51870	455
23	4	3075	74.4	3112	116590	683	56496	475
24	4	3180	74.3	3217	113677	674	54230	466
25	3	3280	74.4	3317	116813	684	67710	520
26	3	3380	74.1	3417	114055	675	65381	511
27	2	3480	74.2	3517	132101	727	96989	623
28	2	3570	74.2	3607	129707	720	95428	618
29	1	3660	74.1	3697	184753	860	164567	811
30	1	3760	73.9	3797	179818	848	160849	802
31	0	3865	74.8	3902	426739	1307	310272	1114
32	0	3960	74.8	3997	414962	1288	303949	1103

Table 4.6 shows the decay-corrected data calculated when applying the correction curves generated from the single pin activations in §4.3.1.1.

Table 4.6: Decay-corrected data showing the shielding effectiveness of SPERT fuel pins in-line between the detector and a single fuel pin.

Effective Time After SCRAM (seconds)	Number of Unirradiated Pins In Line	180 - 450 keV (counts)	2σ	550 - 1000 keV (counts)	2σ
637	5	138754	434	68506	306
737	5	138855	466	67232	325
847	4	143231	505	68804	352
937	4	147357	537	78772	394
1037	4	150106	568	79808	416
1137	3	165817	624	107340	504
1237	3	168159	653	108081	525
1357	2	212526	766	172458	692
1462	2	210377	789	171269	714
1568	1	323071	1011	311864	995
1698	1	329253	1059	316423	1039
1853	0	904303	1827	652056	1552
1989	0	901023	1884	644145	1593
2077	1	313657	1134	295063	1100
2177	1	314053	1160	295160	1123
2297	2	212795	978	162922	855
2387	2	213096	997	163159	871
2507	3	178942	934	105537	716
2597	3	179618	951	104832	725
2697	4	170766	944	82614	655
2797	4	171106	961	83498	669
2917	5	170571	978	75147	647
3007	5	171678	995	75332	657
3112	4	173439	1016	84743	707
3217	4	174345	1034	83924	714
3317	3	184269	1078	107847	821
3417	3	184897	1095	107088	829
3517	2	219905	1210	163229	1037
3607	2	220991	1227	164466	1053
3697	1	321984	1498	290276	1414
3797	1	321161	1515	290932	1433
3902	0	781502	2393	575787	2040
3997	0	776905	2412	576963	2064

The decay-correction algorithm is less accurate at correcting counts at times less than about 1100 seconds. The corrected counts for configurations measured prior to 1100 seconds are not close to the values for the same configurations measured after 1100 seconds. Closer examination of Figure 4.14 shows a divergence between the no-collimator and collimator decay-correction curves starting below approximately 1100 seconds.

This decay-correction algorithm assumes that the exact irradiation time and power history can be reproduced, from measurement to measurement, to achieve exactly the same source. Practically speaking, this is not possible. The apparent sensitivity of the decay-correction curves to these factors dictated that another technique be developed for

the final phase of measurements, although this technique was deemed satisfactory for the remainder of the exploratory experiments.

The data shown in Table 4.6 was averaged for each configuration, with the error propagated using root-sum-squares, and is shown graphically in Figure 4.8. The 95% confidence interval error bars are too small to show on the figure and are therefore omitted.

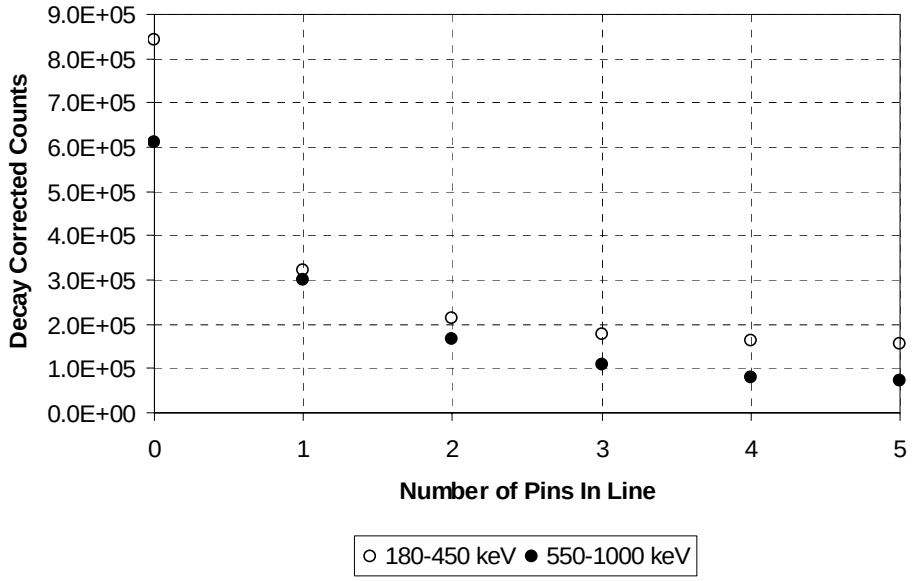

Figure 4.8: Plot of decay-corrected counts showing the shielding effectiveness for unirradiated fuel pins in-line between the detector and activated fuel pin for two regions of interest in the delayed fission-product gamma-ray spectrum for a single fuel pin.

This figure shows the shielding effect for each pin as it is inserted between the detector and the activated pin. The asymptotic behavior of the curve matches expectations given that without the collimator installed, each pin added in line shadows less and less of the solid angle subtended by the detector.

4.3.1.3 Static Lattice Measurements

Measurements were performed on two different nine-pin lattice configurations. The measurements are referred to as "static lattice" because the lattice is not rotated with respect to the detector. Instead, the activated fuel pin swapped into each lattice position while the remaining lattice positions are occupied by unirradiated fuel pins.

The first static lattice experiment consisted of a 3x3 pin lattice, as shown in Figure 4.9. The activated pin was again taken from the center lattice position of the RCF core following an irradiation time of 200 seconds, a peak power of 2.6 W, and constant period of 32 seconds.

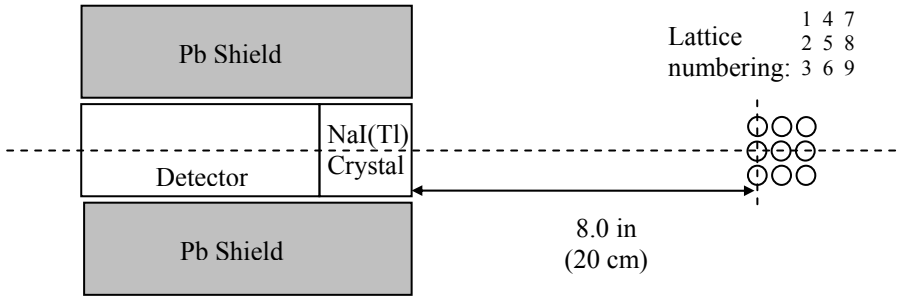

Figure 4.9: Top view schematic of 3x3 static lattice measurement showing arrangement of fuel pins, detector, and shielding[9].

The lattice positions are numbered starting with the upper left position and progress by rows. The raw experimental data are shown in Table 4.7 and the decay-corrected data are shown in Table 4.8.

[9] Note that in this view the top and bottom shielding configuration is not shown.

Table 4.7: Raw experimental data of the measured counts for the 3x3 static lattice as the activated fuel pin is moved to each lattice position.

Count	Lattice Position	Start Time After SCRAM (sec)	Count Duration (sec)	Effective Time After SCRAM (sec)	180 - 450 keV (counts)	2σ	550 - 1000 keV (counts)	2σ
1	7	450	140.7	520	1149413	2144	1048120	2048
2	8	630	111.3	686	931302	1930	770863	1756
3	9	785	95.6	833	789189	1777	655868	1620
4	4	920	134.2	987	1104147	2102	1026589	2026
5	5	1090	117.7	1149	968901	1969	883820	1880
6	6	1260	101.2	1311	816652	1807	750312	1732
7	1	1420	201.1	1521	1797778	2682	1429735	2391
8	2	1660	183.6	1752	1655233	2573	1273453	2257
9	3	1880	164.0	1962	1465652	2421	1137579	2133
10	7	2080	76.0	2118	466597	1366	354880	1191
11	8	2200	74.9	2237	402078	1268	288039	1073
12	9	2320	74.6	2357	374024	1223	280393	1059
13	4	2440	77.9	2479	526325	1451	448885	1340
14	5	2570	77.2	2609	501059	1416	417963	1293
15	6	2700	77.8	2739	537334	1466	444907	1334
16	1	2820	115.5	2878	1013706	2014	783872	1771
17	2	2970	113.1	3027	987977	1988	755337	1738
18	3	3135	107.0	3189	924567	1923	714373	1690

Table 4.8: Decay-corrected data of the measured counts for the 3x3 static lattice as the activated fuel pin is moved to each lattice position.

Effective Time After SCRAM (sec)	Lattice Position	180 - 450 keV (counts)	2σ	550 - 1000 keV (counts)	2σ
520	7	322093	601	293708	574
686	8	339695	704	281174	640
833	9	345697	778	287297	710
987	4	567062	1079	527230	1041
1149	5	573490	1165	523130	1113
1311	6	546531	1210	502134	1159
1521	1	1381118	2060	1098374	1837
1752	2	1449561	2253	1115219	1977
1962	3	1425179	2354	1106165	2074
2118	7	486931	1426	370345	1243
2237	8	441310	1392	316144	1178
2357	9	430787	1409	322946	1220
2479	4	635068	1751	541628	1617
2609	5	633732	1791	528634	1635
2739	6	710736	1939	588482	1765
2878	1	1403348	2788	1085172	2451
3027	2	1432749	2883	1095378	2521
3189	3	1406649	2926	1086857	2572

Figure 4.10 shows the decay-corrected counts as a function of location of the activated pin within the lattice. The expected response is observed in that the measured counts drop off as the activated pin is moved to lattice positions further from the detector and behind unirradiated pins. Error bars showing the 95% confidence interval for the counts at each point are too small to show on the plot and have therefore been omitted.

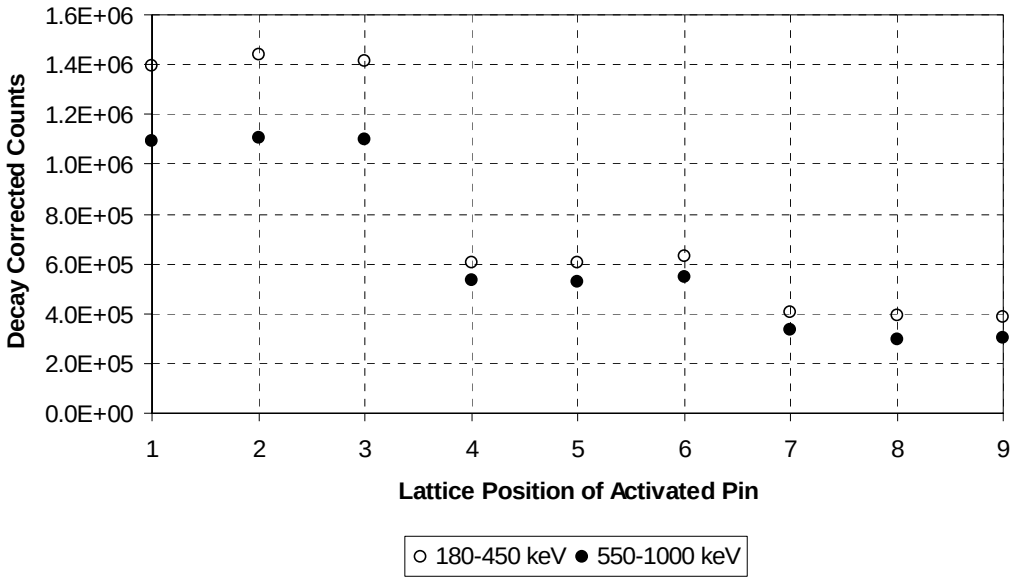

Figure 4.10: Plot of decay-corrected counts versus lattice position of activated fuel pin in the 3x3 static lattice for two regions of interest in the delayed fission-product gamma-ray spectrum for a single SPERT fuel pin.

The final exploratory experiment involved a static lattice with the fuel pins arranged in a triangle, as shown in Figure 4.11. The active pin was taken from the center lattice position of the RCF core following a 200 second irradiation time, and placed in each of the nine lattice positions. The remaining eight pins were unirradiated.

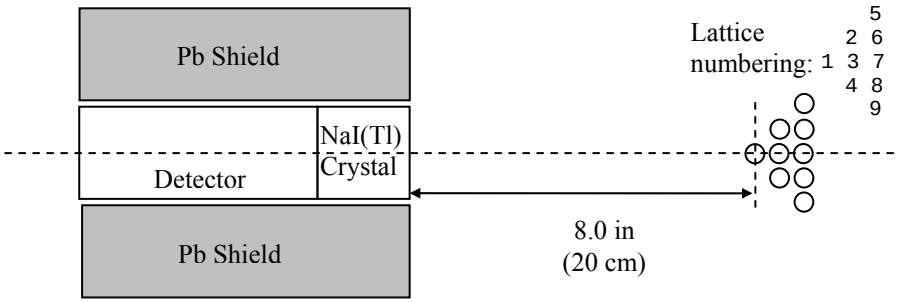

Figure 4.11: Top view schematic of triangular 9-pin static lattice measurement showing arrangement of fuel pins, detector, and shielding[10].

The raw experimental data are shown in Table 4.9 and the decay-corrected data are shown in Table 4.10.

Table 4.9: Raw experimental data of the measured counts for the triangular 9-pin static lattice as the activated fuel pin is moved to each lattice position.

Count	Lattice Position	Start Time After SCRAM (sec)	Count Duration (sec)	Effective Time After SCRAM (sec)	180 - 450 keV (counts)	2σ	550 - 1000 keV (counts)	2σ
1	7	382	165.5	465	1429431	2391	1132820	2129
2	6	600	175.1	688	1438534	2399	1355974	2329
3	8	830	139.6	900	1152420	2147	1058732	2058
4	5	1010	237.1	1129	2123165	2914	1734482	2634
5	9	1290	203.4	1392	1848580	2719	1447656	2406
6	3	1540	95.6	1588	816591	1807	661494	1627
7	2	1675	181.7	1766	1665655	2581	1260793	2246
8	4	1910	164.8	1992	1514094	2461	1134019	2130
9	1	2120	160.7	2200	1472713	2427	1096620	2094

[10] Note that in this view the top and bottom shielding configuration is not shown.

Table 4.10: Decay-corrected data of the measured counts for the triangular 9-pin static as the activated fuel pin is moved to each lattice position.

Effective Time After SCRAM (sec)	Lattice Position	180 - 450 keV (counts)	2σ	550 - 1000 keV (counts)	2σ
465	7	359788	602	285131	536
688	6	526156	877	495959	852
900	8	542842	1011	498711	969
1129	5	1236285	1697	1009961	1534
1392	9	1308012	1924	1024328	1703
1588	3	652913	1445	528903	1301
1766	2	1469471	2277	1112294	1981
1992	4	1493070	2427	1118272	2100
2200	1	1591726	2623	1185240	2264

Figure 4.12 shows the decay-corrected counts as a function of position in the lattice of the activated fuel pin.

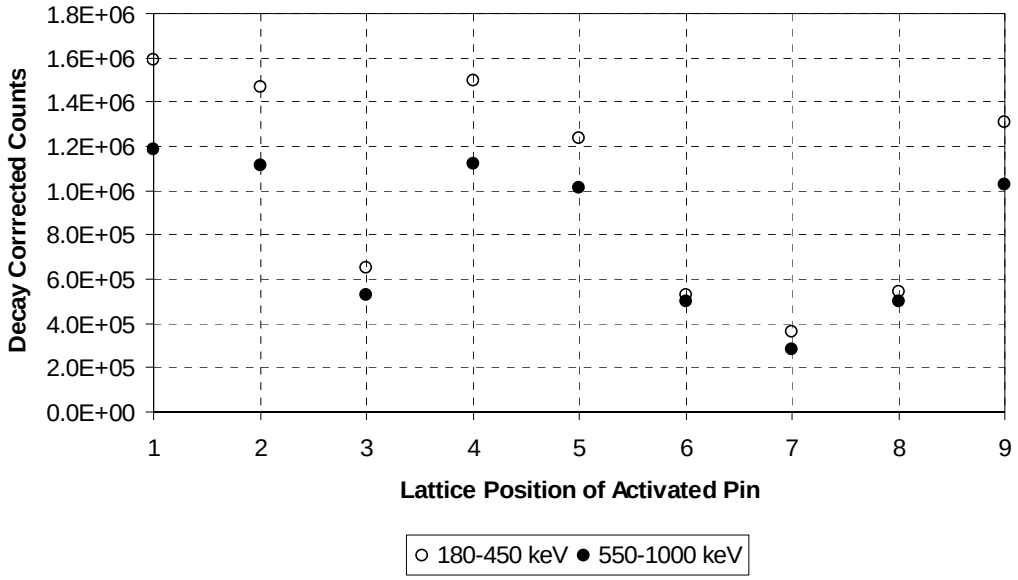

Figure 4.12: Plot of decay-corrected counts versus lattice position of activated fuel pin in the 9-pin triangular lattice for two regions of interest in the delayed fission-product gamma-ray spectrum for a single SPERT fuel pin.

The behavior of the decay-corrected counts as a function of lattice position of the activated pin is as expected. Because of the symmetry of the lattice, positions 2 and 4, 5 and 9, and 6 and 8 are identical, relative to the detector. The decay-corrected counts

show consistent agreement between the corresponding pairs of identical lattice positions. Error bars showing the 95% confidence interval on the measured and corrected counts are too small to show on the plots and therefore have been omitted.

4.3.1.4 Conclusions

The exploratory experiments proved invaluable in evaluating whether the rotating lattice measurements of the next phase could reasonably be performed. In particular,

- valuable experience with the counting system and experimental apparatus was gained,
- the irradiation time and amount of activation necessary for the source pin in order to achieve the desired counts on the detector was determined,
- methods of how to correct measured data to account for fission-product decay were explored,
- experience with collimators was gained, and
- the measured data can be used to benchmark calculations by others.

It was determined that the current method of decay correction was not robust enough for the next phase of experiments. Instead, it was decided that a separate decay curve would be generated for each lattice measurement in the next phase of experiments rather than applying the decay-correction curve from the single-pin measurement to all data. This would eliminate errors introduced as a result of unavoidable changes in key parameters from measurement to measurement.

The cylindrical collimator was also replaced with a deeper, slit-type collimator. The slit-type collimator provides better resolution of the lattice effect and is more consistent with previous work [**Jacobsson1, Jacobsson2, Lee**].

Additionally, the number of ROI's established in the detector system was increased to cover a larger fraction of the delayed fission-product spectrum. Two additional bins were added covering 1000 keV – 2000 keV and 2000 keV – 3000 keV.

4.3.2 Pin Lattice Experiments

Using the experimental apparatus described in §4.2, measurements were performed on lattice configurations matching those of Chapter 3, i.e., 3x3, 5x5, 7x7, to determine the channeling of fission-product gamma rays through the lattice. The degree to which channeling occurs, as a function of radial position relative to the plane of the lattice, was of greatest interest.

For each experiment, only a single pin has been activated with the other pins in the lattice being unirradiated. The lattice is rotated about the z-axis of the activated pin with respect to the detector from 0 to 45 degrees in 5 degree increments. Several measurements are made at the 0 degree position to facilitate generating a specific decay-correction curve for each set of measured data.

4.3.2.1 The 3x3 Lattice Measurements

The experimental setup for the 3x3 lattice with center pin activated is shown in Figure 4.13. This set of measurements was expected to have the least "structure" to the measured counts versus lattice rotation because of the simple nature of the lattice. At any one time, only a single shielding pin is rotating in or out of the path from source pin to detector.

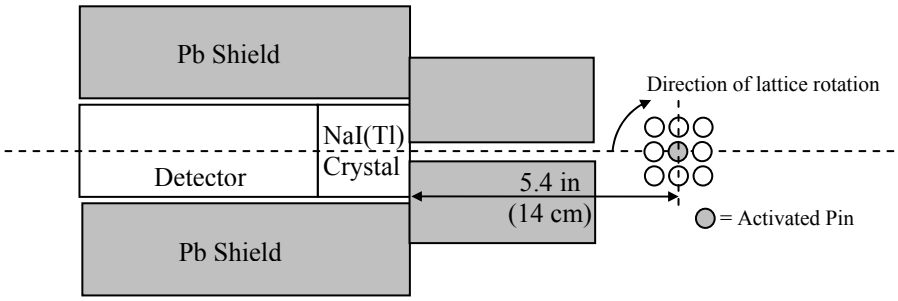

Figure 4.9: Top view schematic of 3x3 lattice measurements with center pin activated showing arrangement of fuel pins, detector, and shielding[11].

For this set of measurements, the RCF core was irradiated for 200 seconds and expended 90 W•s of energy. Raw experimental data are shown in Table 4.11.

Table 4.11: Raw experimental data of the measured counts as a function of lattice rotation with respect to the detector for the 3x3 lattice with center pin activated.

Count	Lattice Rotation (deg.)	Start Time After SCRAM (sec)	Count Duration (sec)	Effective Time After SCRAM (sec)	180-450 keV (counts)	2σ	550-1000 keV (counts)	2σ	1000-2000 keV (counts)	2σ	2000-3000 keV (counts)	2σ
1	0	353	60	383	308209	1110	423028	1301	300313	1096	60066	490
2	0	446	60	476	250160	1000	343779	1173	234908	969	43945	419
3	0	532	60	562	213559	924	292870	1082	197443	889	35097	375
4	5	630	60	660	190563	873	249832	1000	166821	817	28023	335
5	0	733	60	763	159131	798	218010	934	144630	761	23413	306
6	10	841	60	871	189235	870	222333	943	141071	751	21582	294
7	15	949	60	979	207436	911	227933	955	140888	751	20857	289
8	0	1052	60	1082	116879	684	159369	798	104902	648	15195	247
9	20	1162	60	1192	204526	904	215151	928	128560	717	18262	270
10	25	1268	60	1298	194842	883	206860	910	123957	704	17107	262
11	0	1373	60	1403	93492	612	126918	713	82617	575	11431	214
12	30	1495	60	1525	157440	794	171467	828	102526	640	13805	235
13	35	1604	60	1634	120969	696	138904	745	85492	585	11347	213
14	0	1710	60	1740	76462	553	103036	642	66951	517	9017	190
15	40	1814	60	1844	74208	545	97839	626	63179	503	8496	184
16	45	1924	60	1954	65734	513	85948	586	55568	471	7500	173
17	0	2025	60	2055	64693	509	87194	591	55905	473	7482	173
18	0	2102	60	2132	62919	502	83832	579	53507	463	7238	170
19	0	2181	60	2211	60820	493	80607	568	52002	456	6883	166

Notice that over the course of conducting the measurements for this experiment, the lattice was repositioned several times to 0 degrees. This was necessary to generate a decay curve specific to this set of measurements.

It is assumed that the decay behavior is independent of lattice orientation relative to the detector so that any single position is equally valid for collecting decay curve data. In this work the 0 degree position was always used as the reference position. By periodically taking data at the reference position during the measurements and plotting counts versus time, a decay curve can be generated. What is actually plotted is the ratio

[11] Note that in this view the top and bottom shielding configuration is not shown.

of the counts at the reference position at any time over the initial counts at the reference position, $C(t)/C(t_0)$. Curves of the form described in §4.3.1.1 are fitted to the ratio data and used to decay correct the counts for measurements taken at every lattice position. The measured data are divided by the correction factor for that time as determined by the appropriate decay curve. This is a consistent approach to decay-correcting data based on similar measurements conducted at the RCF [**Galayda**].

A plot of the 0 degree data versus time is shown in Figure 4.10 with the fitted curves superimposed. Notice that each energy group of interest gets its own decay curve. Error bars representing a 95% confidence interval around the plotted data are too small to show and are therefore omitted.

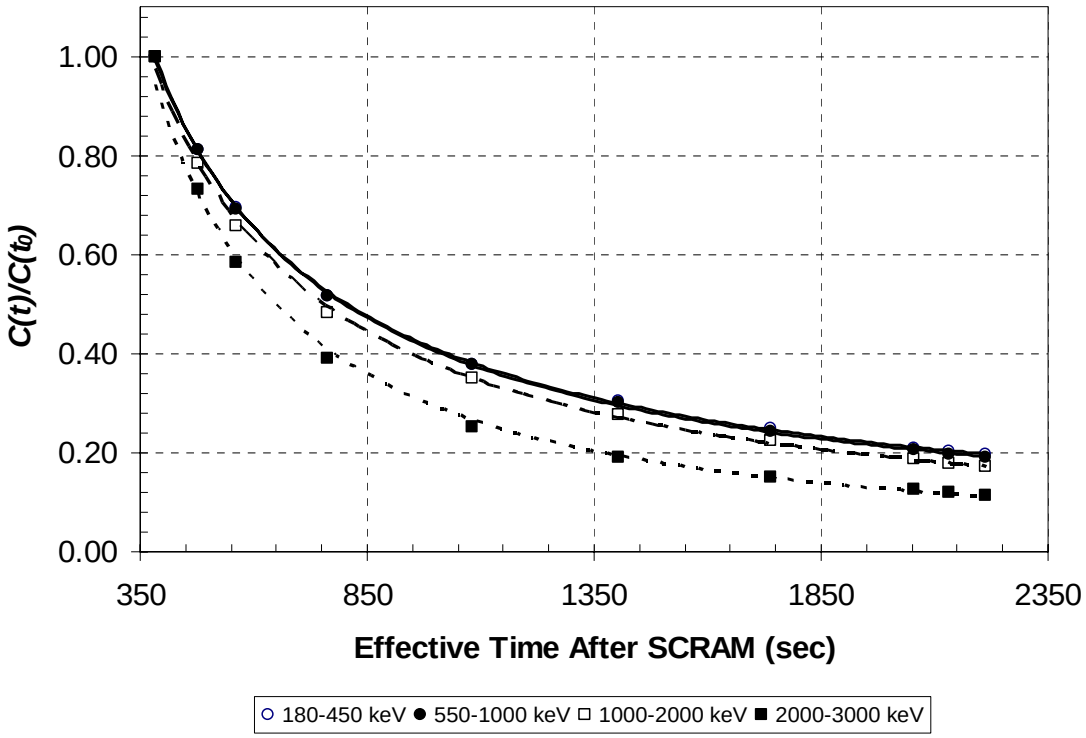

Figure 4.13: Plot of counts versus time and fitted curves for four regions of interest in the delayed fission-product gamma-ray spectrum at a reference position of 0 degrees lattice rotation for the 3x3 lattice measurements with center pin activated.

A plot of the decay-corrected counts vs. lattice rotation for all four ROI's is shown in Figure 4.14. From Chapter 3, Figures 3.34 through 3.36, provide the expected shape of the curve for the experiment. Error bars representing the 95% confidence interval are included in Figure 4.14 but for the most part are obscured by the markers.

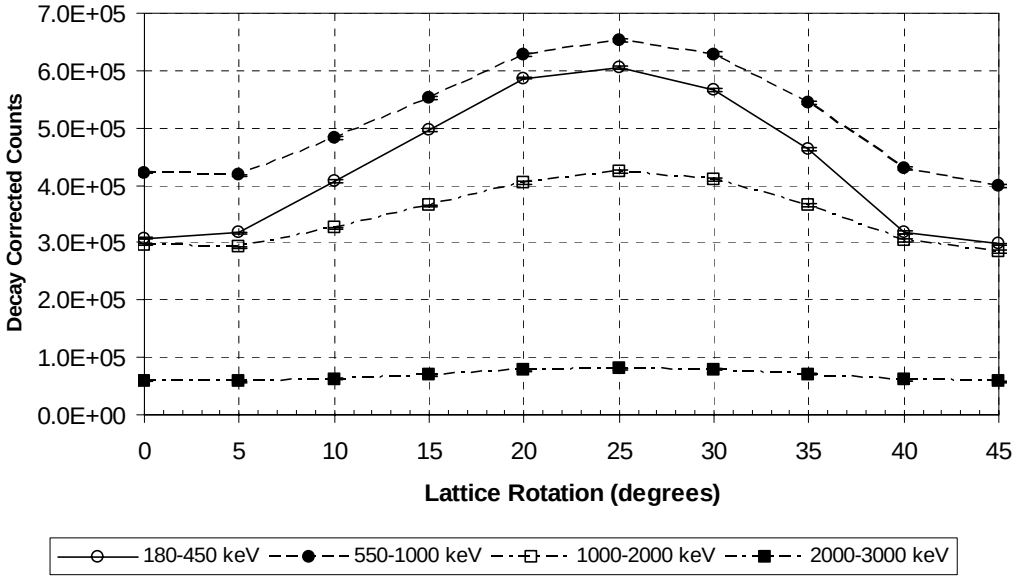

Figure 4.14: Plot of decay-corrected counts versus lattice rotation for four regions of interest in the delayed fission-product gamma-ray spectrum for the 3x3 lattice measurements with center pin activated.

The shapes of the curves follow the expectations set out in Chapter 3. The magnitude of the pulse heights is a function of the detector system efficiency for the ROI, the delayed gamma-ray spectrum for the ROI, and the penetrating power of the gamma rays in each ROI. From Chapter 3, Figure 3.2 and Figure 3.3, there is a high probability that gamma rays will be emitted with energy spanned by the first three ROI's. Gamma rays with energy in the range of the fourth ROI will be emitted with much lower probability. Additionally, the efficiency of the detector system decreases as the incident gamma-ray energy increases. Considering these factors, it is expected that the highest energy ROI will be well bellow the other three.

The MCNP pulse-height spectrum calculations are the closest analogy to the data collected in the experiment. It is presumed that MCNP will accurately model the interactions of the gamma rays within the detector crystal and closely predict the energy deposition that is seen by the physical detector crystal. In this regard, the intrinsic efficiency of the MCNP detector and physical detector should be the same. What is not accounted for, on the other hand, is the efficiency of converting the light pulses to photoelectrons and the corresponding peak generated in the instrumentation. Therefore, it is not expected that the magnitudes of the curves will agree. The shapes of the curves and relative magnitudes are most important in determining the lattice effect. In this regard, the measured data and MCNP calculations are expected to agree. Calculational results for the same ROI's as the measurement are shown in Figure 4.15. The MCNP problem geometry and source were modeled as closely as practical to the experiment.

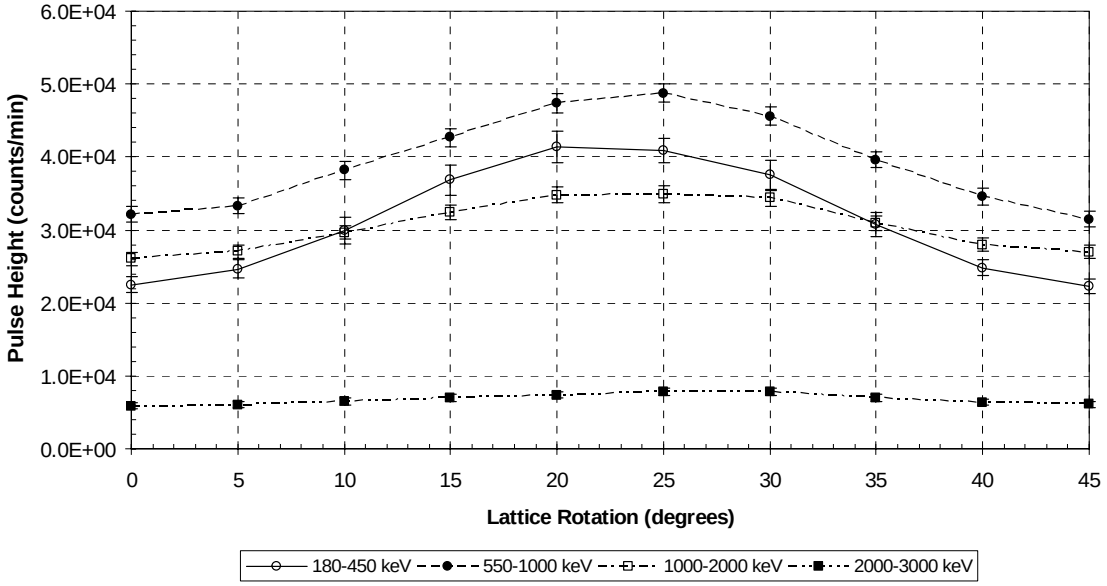

Figure 4.15: MCNP calculated counts versus lattice rotation for four regions of interest in the delayed fission-product gamma-ray spectrum for the 3x3 lattice measurements with center pin activated.

What is of primary interest in this work is the channeling of the radiation through the lattice. The degree to which the channeling depends on the angle of rotation of the lattice can be determined by normalizing the data to a reference position, *C(θ)/C(0)*.

Again, the zero degree rotation was chosen as the reference position. In the zero degree position all possible pins are in-line between the detector and source and the minimum dose is expected at the detector. Figure 4.16 shows the normalized pulse-height data as a function of lattice rotation for the experiment and Figure 4.17 shows the normalized MCNP calculated pulse-height data.

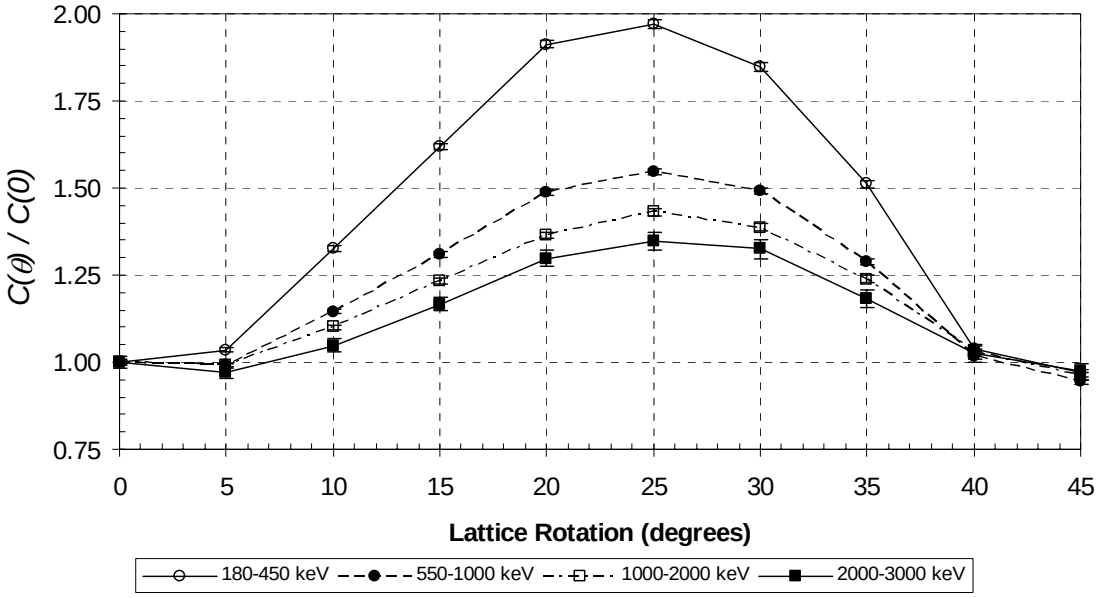

Figure 4.16: Decay-corrected counts versus lattice rotation normalized to the zero degree position for four regions of interest in the delayed fission-product gamma-ray spectrum for the 3x3 lattice measurements with center pin activated.

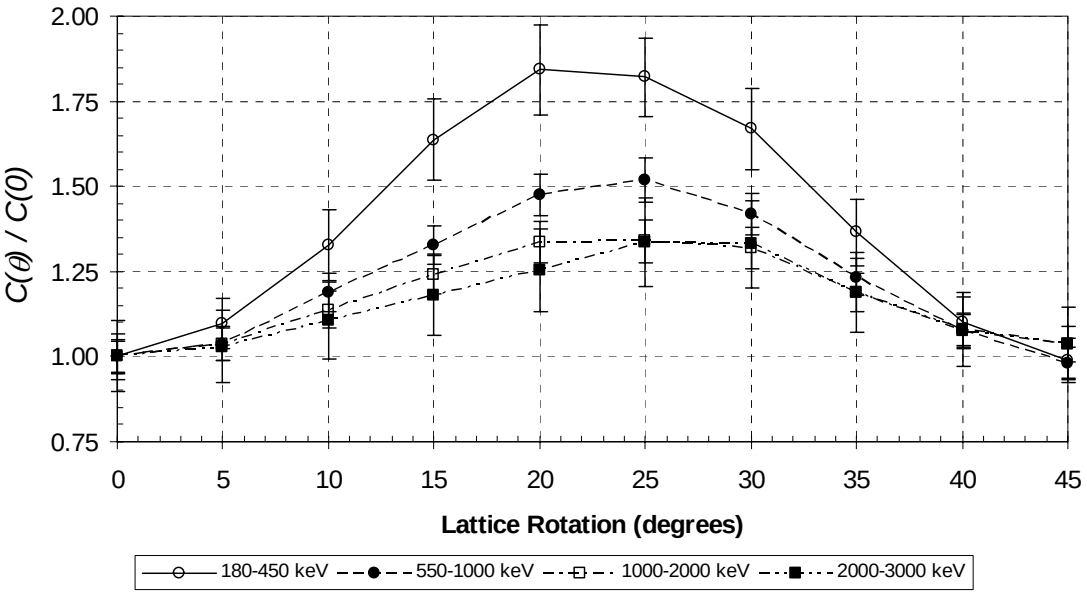

Figure 4.17: MCNP calculated counts versus lattice rotation normalized to the zero degree position for four regions of interest in the delayed fission-product gamma-ray spectrum for the 3x3 lattice measurements with center pin activated.

The figures show the sensitivity of the lower energy gamma rays to the path through the lattice. As the energy of the gamma rays increase, the shielding effectiveness of the pins lessens resulting in less of an increase in counts when a favorable path through the lattice is available. The net result is a "flatter" curve for higher energy gamma rays and a more "peaked" curve for lower energy gamma rays.

The next experiment was performed on the same lattice configuration but with the source located at the corner pin instead of the center pin, as shown in Figure 4.18. The point of rotation for the lattice was the corner pin. For this set of measurements, the RCF core was irradiated for 200 seconds and expended 79.2 W•s of energy.

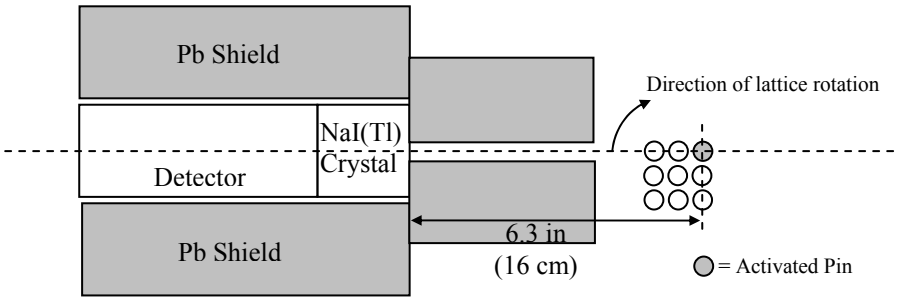

Figure 4.18: Top view schematic of 3x3 lattice measurements with corner pin activated showing arrangement of fuel pins, detector, and shielding[12].

With additional pins moving in and out of line between the source and detector as the lattice is rotated, the resulting data were expected to be more interesting than the previous case. The raw experimental data are shown in Table 4.12.

Table 4.12: Raw experimental data of the measured counts as a function of lattice rotation with respect to the detector for the 3x3 lattice with corner pin activated.

Count	Lattice Rotation (deg.)	Start Time After SCRAM (sec)	Count Duration (sec)	Effective Time After SCRAM (sec)	180-450 keV (counts)	2σ	550-1000 keV (counts)	2σ	1000-2000 keV (counts)	2σ	2000-3000 keV (counts)	2σ
1	0	482	60	512	103337	643	132247	727	93666	612	22432	300
2	0	574	60	604	88607	595	113572	674	78892	562	17133	262
3	0	654	60	684	79139	563	101077	636	69380	527	14134	238
4	5	757	60	787	105245	649	118310	688	74250	545	14078	237
5	0	968	60	998	56142	474	71551	535	49086	443	8494	184
6	10	1133	60	1163	115643	680	121411	697	69619	528	10731	207
7	15	1236	60	1266	103069	642	119182	690	68767	524	10496	205
8	0	1346	60	1376	50154	448	58602	484	38078	390	5994	155
9	20	1453	60	1483	63445	504	83398	578	50622	450	7563	174
10	25	1721	60	1751	44208	421	57896	481	37179	386	5381	147
11	0	1830	60	1860	32216	359	40479	402	27452	331	3938	126
12	30	1934	60	1860	37829	389	50068	448	32245	359	4597	136
13	35	2045	60	2075	34704	373	45969	429	30110	347	4411	133
14	0	2149	60	2179	26650	326	33779	368	23081	304	3382	116
15	40	2263	60	2293	27184	330	34618	372	23061	304	3354	116
16	45	2379	60	2409	24830	315	30732	351	20852	289	2952	109
17	0	2481	60	2511	24622	314	30337	348	20346	285	2844	107
18	0	2563	60	2593	24001	310	29281	342	19294	278	2788	106
19	0	2644	60	2674	23626	307	28630	338	18492	272	2656	103

The data were decay corrected in the same manner as in the previous measurements using specific decay-correction curves for each ROI generated from the zero degree data. Figure 4.19 shows the decay-corrected data, normalized to the zero degree position for each ROI. Figure 4.20 shows the corresponding MCNP calculated data.

[12] Note that in this view the top and bottom shielding configuration is not shown.

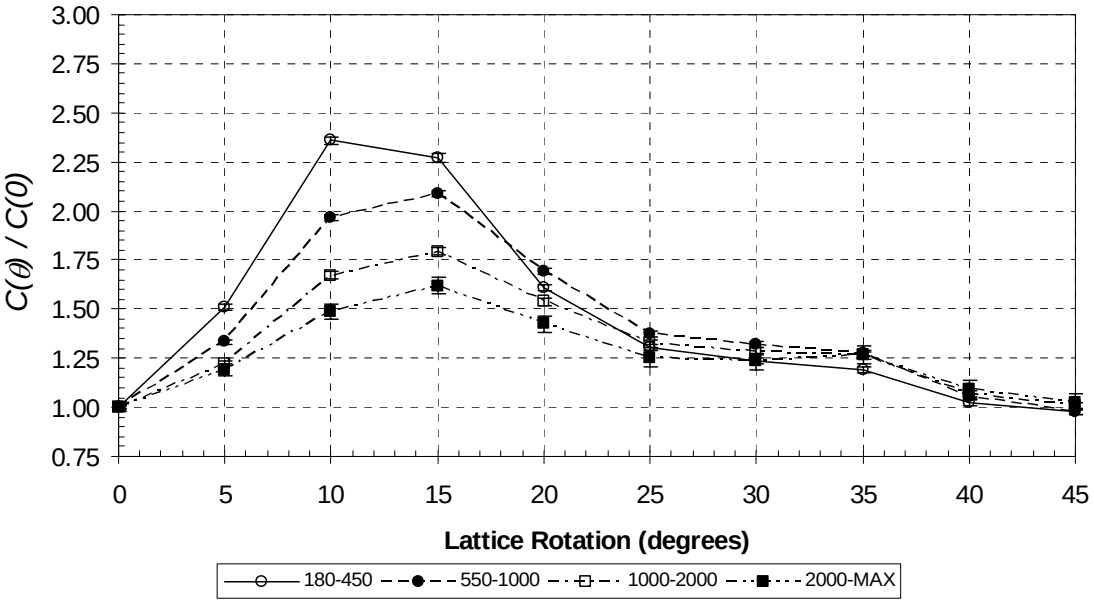

Figure 4.19: Decay-corrected counts versus lattice rotation normalized to the zero degree position for four regions of interest in the delayed fission-product gamma-ray spectrum for the 3x3 lattice measurements with corner pin activated.

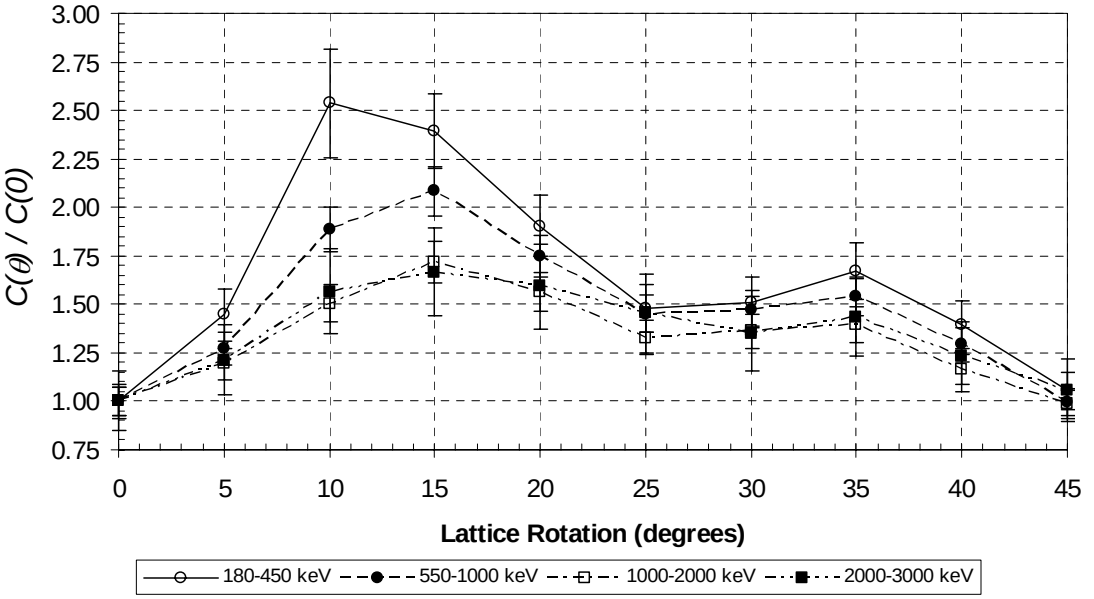

Figure 4.20: MCNP calculated counts versus lattice rotation normalized to the zero degree position for four regions of interest in the delayed fission-product gamma-ray spectrum for the 3x3 lattice measurements with corner pin activated.

The curves contain more structure, as expected. The lower energy gamma rays again show more sensitivity to the change in shielding as pins move in and out of line to the detector.

In comparing the two curves, MCNP predicts a slight peak at 35 degrees. In this region, the experimental data tends to be flatter and of slightly lower magnitude. This is likely due to sources of error in the experiment which will be addressed in §4.4.

4.3.2.2 The 5x5 Lattice Measurements

The next series of experiments involved a 5x5 lattice. The first measurement was performed with the center pin as the source, as shown in Figure 4.21. The source pin was taken from the center of the RCF core following a 200 second irradiation resulting in 88.5 W•s of activation.

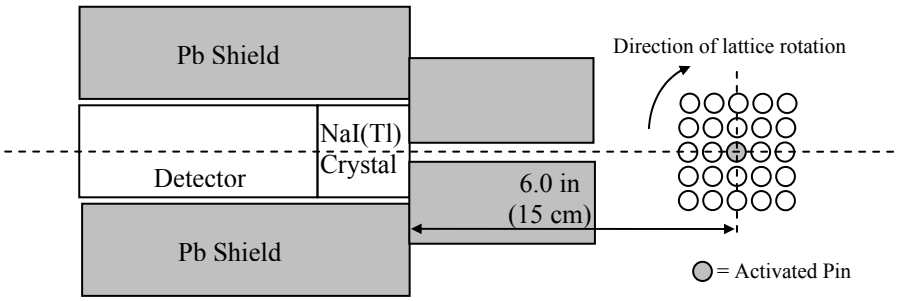

Figure 4.21: Top view schematic of 5x5 lattice measurements with center pin activated showing arrangement of fuel pins, detector, and shielding[13].

In many respects this arrangement is similar to the 3x3 with the corner pin activated. Therefore, it was expected that the measurement would be similar to the 3x3, corner pin activated case with some subtle differences potentially from the scattering off pins above and to the right of the source pin that were not present in the 3x3 lattice. The experimental data are shown in Table 4.13.

[13] Note that in this view the top and bottom shielding configuration is not shown.

Table 4.13: Raw experimental data of the measured counts as a function of lattice rotation with respect to the detector for the 5x5 lattice with center pin activated.

Count	Lattice Rotation (deg.)	Start Time After SCRAM (sec)	Count Duration (sec)	Effective Time After SCRAM (sec)	180-450 keV (counts)	2σ	550-1000 keV (counts)	2σ	1000-2000 keV (counts)	2σ	2000-3000 keV (counts)	2σ
1	0	441	60	471	125944	710	164370	811	115733	680	24689	314
2	0	523	60	553	108372	658	141079	751	96641	622	19429	279
3	0	602	60	632	95702	619	124082	705	84190	580	16052	253
4	5	710	60	740	124562	706	142377	755	87501	592	15131	246
5	0	821	60	851	73250	541	95796	619	64290	507	10733	207
6	10	927	60	957	163068	808	171129	827	96088	620	14928	244
7	15	1039	60	1069	147973	769	169048	822	94199	614	13720	234
8	0	1141	60	1171	56870	477	73823	543	48759	442	7266	170
9	20	1263	60	1293	90856	603	119481	691	69857	529	10302	203
10	25	1382	60	1412	67201	518	89680	599	55455	471	7843	177
11	0	1485	60	1515	44370	421	58030	482	38586	393	5660	150
12	30	1603	60	1633	56636	476	76207	552	47637	437	6582	162
13	35	1718	60	1748	52632	459	71034	533	44939	424	6406	160
14	0	1830	60	1860	37374	387	48046	438	32332	360	4414	133
15	40	1940	60	1970	37803	389	49767	446	33480	366	4806	139
16	45	2038	60	2068	32758	362	43297	416	29515	344	4092	128
17	0	2140	60	2170	32451	360	41551	408	28425	337	4180	129
18	0	2224	60	2254	30964	352	39941	400	27544	332	3875	124
19	0	2319	60	2349	29879	346	38075	390	26388	325	3831	124

A plot of the decay-corrected data is shown in Figure 4.22 with the corresponding MCNP results plotted in Figure 4.23.

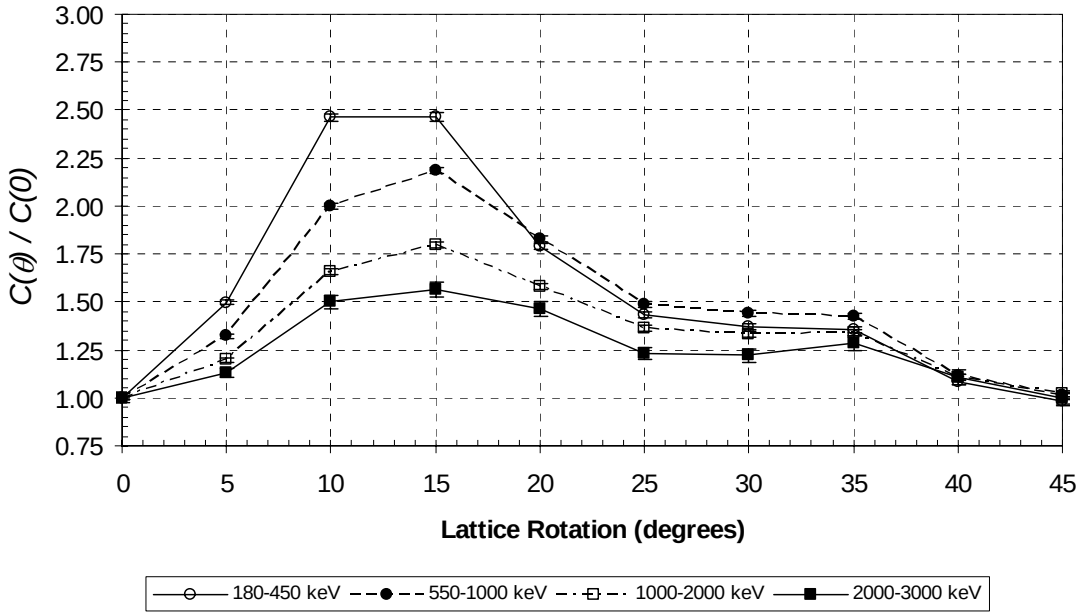

Figure 4.22: Decay-corrected counts versus lattice rotation normalized to the zero degree position for four regions of interest in the delayed fission-product gamma-ray spectrum for the 5x5 lattice measurements with center pin activated.

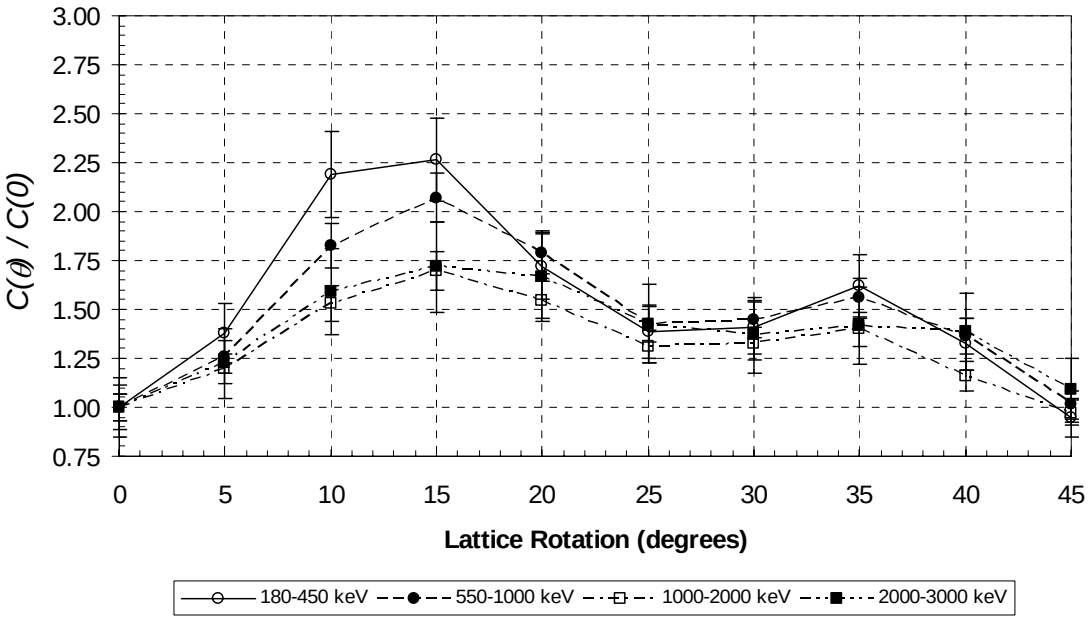

Figure 4.23: MCNP calculated counts versus lattice rotation normalized to the zero degree position for four regions of interest in the delayed fission-product gamma-ray spectrum for the 5x5 lattice measurements with center pin activated.

In general, the figures compare favorably with expectations and follow the 3x3, corner pin active case. There are some subtle differences, however. For example, in the 5x5 case, the lower two ROI's show slightly higher magnitudes from approximately 20 degrees rotation onward. The increased scattering from pins on both sides of the source pin (5x5 case) as opposed to only on one side (3x3 case) cause additional photons to enter the detector. The multiple scatterings necessary to redirect the photons to the detector, however, results in an increased number of lower energy photons incident on the detector.

The next increment in complexity involved the same 5x5 lattice but with the source and center of rotation moved to the corner pin, as shown in Figure 4.24.

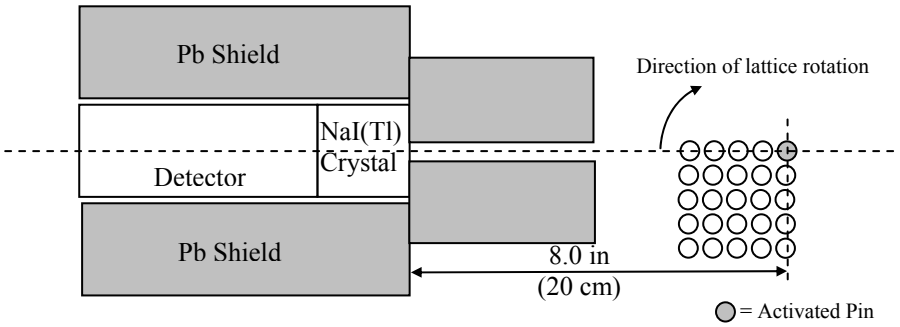

Figure 4.24: Top view schematic of 5x5 lattice measurements with corner pin activated showing arrangement of fuel pins, detector, and shielding[14].

The source pin was again taken from the center lattice position of the RCF core following a 200 second irradiation resulting in an activation of 80.7 W•s.

This arrangement should provide data with a high degree of structure because of the number of shielding pins that move in and out of line to the detector as the lattice rotated. The raw experimental data are shown in Table 4.14.

Table 4.14: Raw experimental data of the measured counts as a function of lattice rotation with respect to the detector for the 5x5 lattice with corner pin activated.

Count	Lattice Rotation (deg.)	Start Time After SCRAM (sec)	Count Duration (sec)	Effective Time After SCRAM (sec)	180-450 keV (counts)	2σ	550-1000 keV (counts)	2σ	1000-2000 keV (counts)	2σ	2000-3000 keV (counts)	2σ
1	0	395	60	425	41170	406	46879	433	33533	366	7933	178
2	0	480	60	510	35453	377	39077	395	27135	329	5466	148
3	0	570	60	600	30120	347	33848	368	22742	302	4148	129
4	5	678	60	708	68143	522	67387	519	37302	386	6007	155
5	0	776	60	806	26152	323	28307	336	17861	267	2696	104
6	10	932	60	962	40983	405	54526	467	33070	364	4652	136
7	15	1037	60	1067	27220	330	35258	376	22223	298	2849	107
8	0	1144	60	1174	19522	279	20684	288	12809	226	1612	80
9	20	1260	60	1290	24489	313	32265	359	20098	284	2558	101
10	25	1365	60	1395	20063	283	25688	321	16062	253	1935	88
11	0	1461	60	1491	16045	253	16848	260	10174	202	1172	68
12	30	1561	60	1591	18574	273	23374	306	14307	239	1732	83
13	35	1674	60	1704	15428	248	19092	276	11724	217	1406	75
14	0	1772	60	1802	14303	239	14728	243	8458	184	948	62
15	40	1889	60	1919	13474	232	16531	257	9871	199	1193	69
16	45	1984	60	2014	11178	211	12581	224	7112	169	798	56
17	0	2082	60	2112	12007	219	12936	227	7220	170	820	57
18	0	2163	60	2193	11857	218	12389	223	7030	168	797	56
19	0	2240	60	2270	11549	215	12064	220	6674	163	800	57

A plot of the decay-corrected data is shown in Figure 4.25 with the corresponding MCNP results plotted in Figure 4.26.

[14] Note that in this view the top and bottom shielding configuration is not shown.

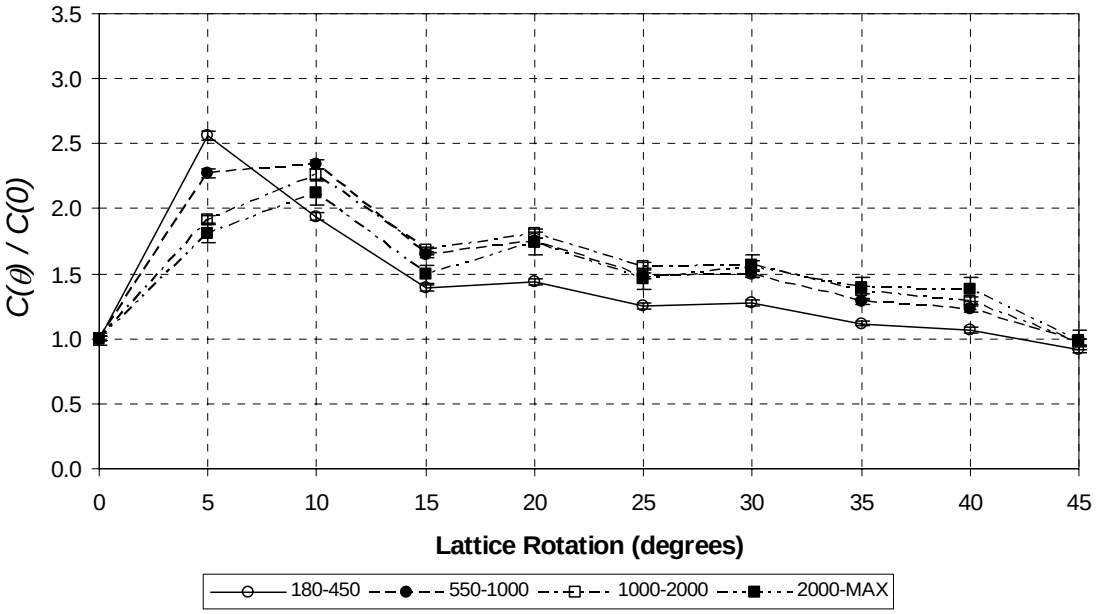

Figure 4.25: Decay-corrected counts versus lattice rotation normalized to the zero degree position for four regions of interest in the delayed fission-product gamma-ray spectrum for the 5x5 lattice measurements with corner pin activated.

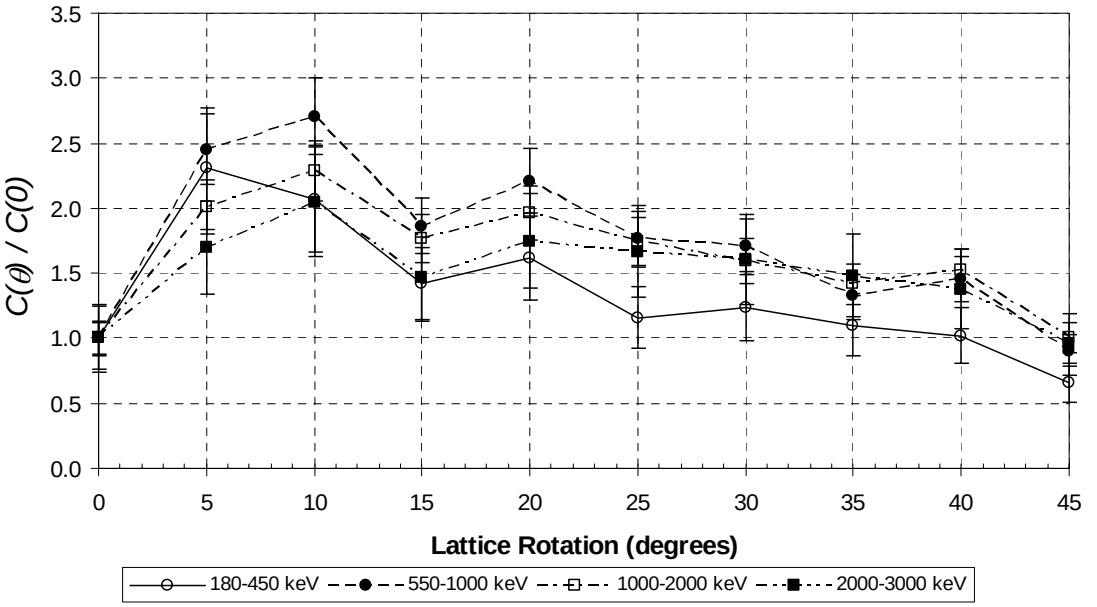

Figure 4.26: MCNP calculated counts versus lattice rotation normalized to the zero degree position for four regions of interest in the delayed fission-product gamma-ray spectrum for the 5x5 lattice measurements with corner pin activated.

From inspection of the curves it is apparent that a greater number of "peaks," or preferential paths through the lattice, exist as the lattice becomes more complicated. However, the relative magnitude of the peaks are lower since there are more pins from the lattice in line between the detector and source pin at the various rotational positions measured.

An increase in the uncertainty on the MCNP calculations is also noticeable. This is a result of the decrease in numbers of particles reaching the detector due to the increased shielding provided by the additional pins. A reduction in particles reaching the detector will yield a reduction in collisions and tracks through the detector and, regardless of whether a collision or path-length estimator is used, result in worse statistics.

4.3.2.3 The 7x7 Lattice Measurements

The final series of experiments involved a 7x7 lattice. The first measurement was performed with the center pin as the source, as shown in Figure 4.27. The source pin was taken from the center of the RCF core following a 200 second irradiation resulting in 83.0 W•s of activation.

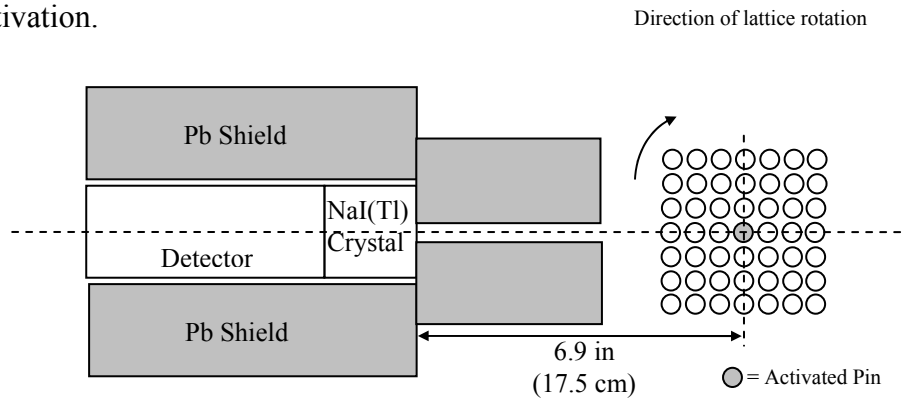

Figure 4.27: Top view schematic of 7x7 lattice measurements with center pin activated showing arrangement of fuel pins, detector, and shielding[15].

[15] Note that in this view the top and bottom shielding configuration is not shown.

In terms of the number of pins between the detector and source pin, this is a simpler lattice than the 5x5 with the corner pin case of Figure 4.24. It is therefore expected that the results will exhibit slightly less structure than seen in Figures 4.25 and 4.26. The raw experimental data are shown in Table 4.15. Figure 4.28 shows the decay-corrected data plotted versus lattice rotation and Figure 4.29 shows the corresponding MCNP results.

Table 4.15: Raw experimental data of the measured counts as a function of lattice rotation with respect to the detector for the 7x7 lattice with center pin activated.

Count	Lattice Rotation (deg.)	Start Time After SCRAM (sec)	Count Duration (sec)	Effective Time After SCRAM (sec)	180-450 keV (counts)	2σ	550-1000 keV (counts)	2σ	1000-2000 keV (counts)	2σ	2000-3000 keV (counts)	2σ
1	0	370	60	400	85620	585	102977	642	80642	568	14297	239
2	0	446	60	476	70756	532	85637	585	65287	511	11082	211
3	0	522	60	552	61921	498	74093	544	56068	474	9082	191
4	5	618	60	648	59124	486	74570	546	53946	465	8290	182
5	0	717	60	747	47649	437	56641	476	41651	408	6147	157
6	10	816	60	846	82137	573	107174	655	68893	525	9262	192
7	15	918	60	948	61761	497	88474	595	59899	489	8038	179
8	0	1019	60	1049	36756	383	43053	415	30449	349	3903	125
9	20	1128	60	1158	42583	413	58751	485	40698	403	5327	146
10	25	1234	60	1264	41756	409	58370	483	39544	398	5060	142
11	0	1358	60	1388	29521	344	34149	370	23806	309	2919	108
12	30	1492	60	1522	32434	360	44558	422	30064	347	3629	120
13	35	1627	60	1657	27674	333	36857	384	25442	319	3039	110
14	0	1782	60	1812	24683	314	27641	333	18315	271	2186	94
15	40	1921	60	1951	24159	311	31920	357	21037	290	2595	102
16	45	2044	60	2074	18699	273	22843	302	15325	248	1799	85
17	0	2215	60	2245	20815	289	23362	306	14948	245	1754	84
18	0	2302	60	2332	20293	285	22088	297	14278	239	1636	81
19	0	2386	60	2416	20136	284	21658	294	13861	235	1567	79

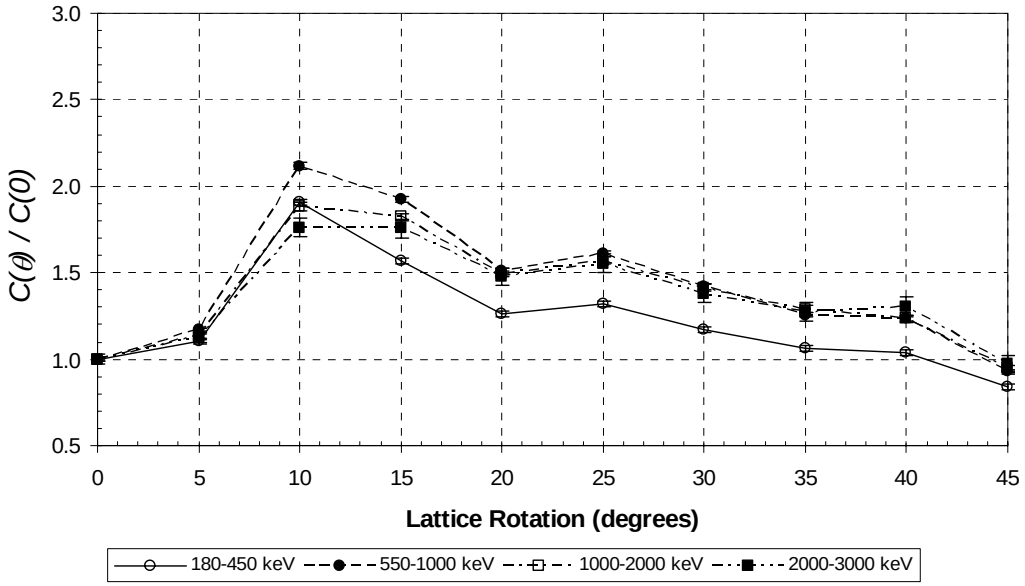

Figure 4.28: Decay-corrected counts versus lattice rotation normalized to the zero degree position for four regions of interest in the delayed fission-product gamma-ray spectrum for the 7x7 lattice measurements with center pin activated.

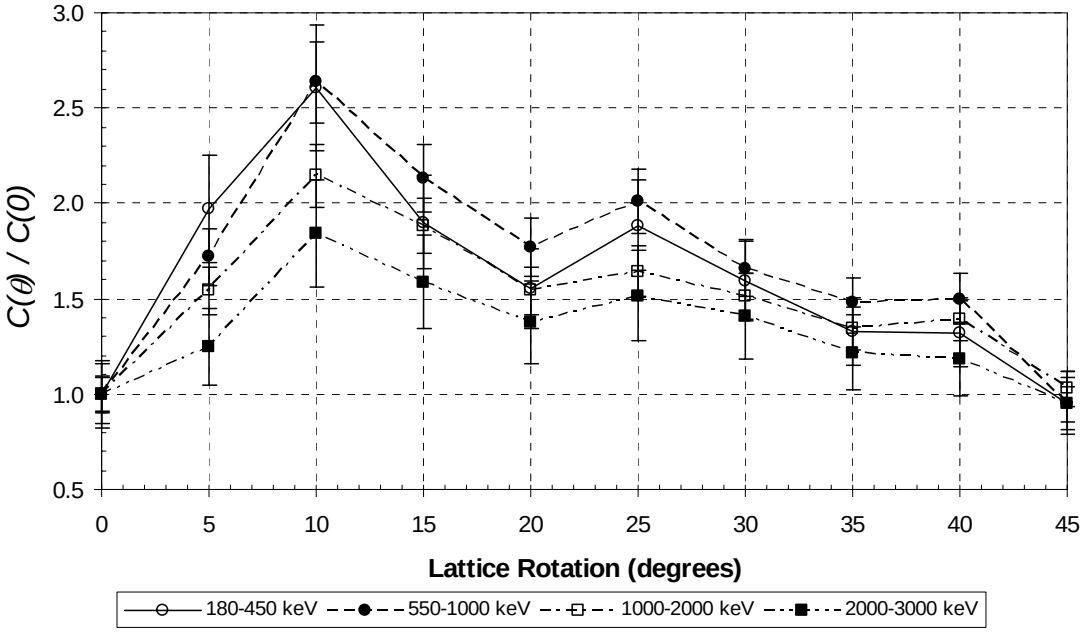

Figure 4.29: MCNP calculated counts versus lattice rotation normalized to the zero degree position for four regions of interest in the delayed fission-product gamma-ray spectrum for the 7x7 lattice measurements with center pin activated.

The final measurement was performed with the corner pin as the source, as shown in Figure 4.30. The source pin was taken from the center of the RCF core following a 200 second irradiation resulting in 76.0 W•s of activation.

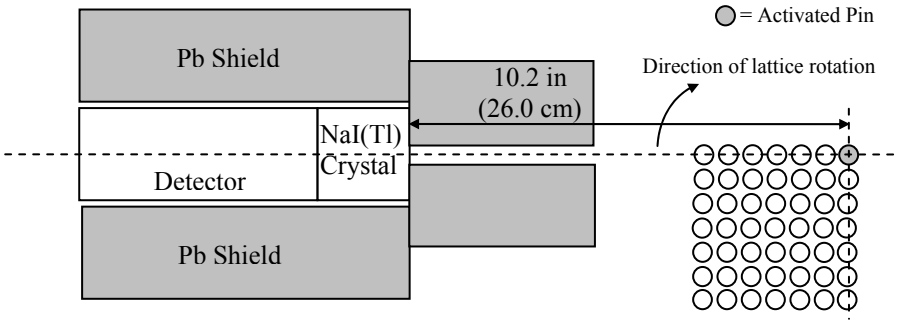

Figure 4.30: Top view schematic of 7x7 lattice measurements with corner pin activated showing arrangement of fuel pins, detector, and shielding[16].

[16] Note that in this view the top and bottom shielding configuration is not shown.

In terms of the number of pins between the detector and the source, this is the most complicated lattice investigated in this work. The raw experimental data are shown in Table 4.16.

Table 4.16: Raw experimental data of the measured counts as a function of lattice rotation with respect to the detector for the 7x7 lattice with corner pin activated.

Count	Lattice Rotation (deg.)	Start Time After SCRAM (sec)	Count Duration (sec)	Effective Time After SCRAM (sec)	180-450 keV (counts)	2σ	550-1000 keV (counts)	2σ	1000-2000 keV (counts)	2σ	2000-3000 keV (counts)	2σ
1	0	440	60	470	19205	277	18734	274	12557	224	2157	93
2	0	536	60	566	16488	257	16304	255	10221	202	1640	81
3	0	619	60	649	15143	246	14613	242	8963	189	1403	75
4	5	720	60	750	26377	325	32453	360	21506	293	3497	118
5	0	815	60	845	12847	227	12091	220	7046	168	987	63
6	10	923	60	953	13154	229	15377	248	10814	208	1677	82
7	15	1038	60	1068	12033	219	13796	235	9241	192	1400	75
8	0	1222	60	1252	10249	202	9479	195	5091	143	600	49
9	20	1322	60	1352	11078	211	11916	218	7741	176	1068	65
10	25	1420	60	1450	10097	201	10910	209	6784	165	922	61
11	0	1526	60	1556	9364	194	8471	184	4247	130	470	43
12	30	1830	60	1860	9275	193	9385	194	5453	148	714	53
13	35	1953	60	1983	8336	183	7893	178	4112	128	481	44
14	0	2054	60	2084	8089	180	7133	169	3395	117	337	37
15	40	2208	60	2238	7970	179	7348	171	3220	113	339	37
16	45	2314	60	2344	8095	180	7473	173	3655	121	352	38
17	0	2414	60	2444	7536	174	6631	163	3074	111	266	33
18	0	2503	60	2533	7435	172	6610	163	2882	107	276	33
19	0	2583	60	2613	7386	172	6505	161	2953	109	261	32

The additional shielding provided by the greater number of pins in this lattice is evident in the lower magnitudes of counts as compared to previous lattice experiments. The decay-corrected data are plotted in Figure 4.31 and the MCNP results shown in Figure 4.32. The error associated with the counts and the uncertainties in the MCNP results are highest for this case. Also evident in comparing the measurement to the calculation is a tendency of the ratios to be lower for the measurements. This suggests that this complicated lattice configuration is testing the limits of the measurement capability. Additionally, a higher level of activation for the source pin would increase the number of counts in the detector and may improve the results.

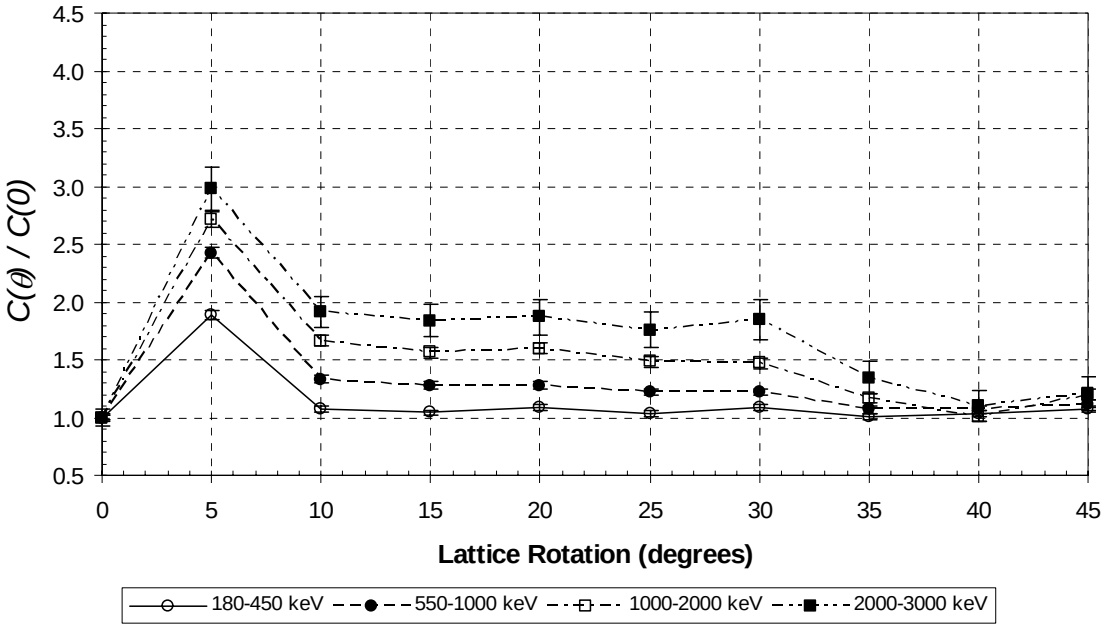

Figure 4.31: Decay-corrected counts versus lattice rotation normalized to the zero degree position for four regions of interest in the delayed fission-product gamma-ray spectrum for the 7x7 lattice measurements with corner pin activated.

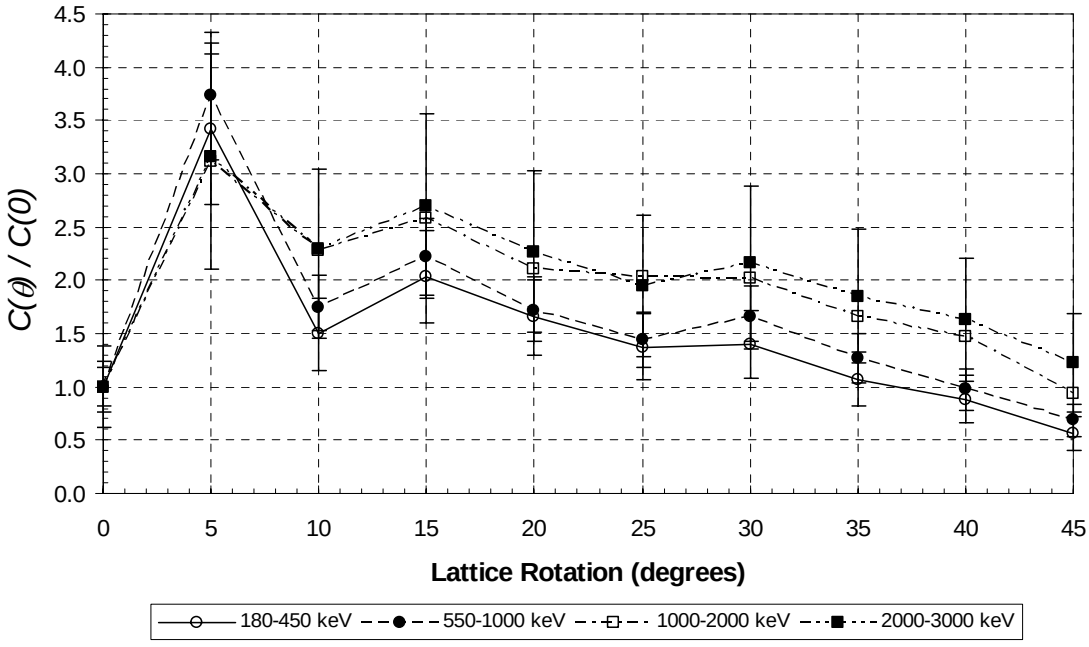

Figure 4.32: MCNP calculated counts versus lattice rotation normalized to the zero degree position for four regions of interest in the delayed fission-product gamma-ray spectrum for the 7x7 lattice measurements with corner pin activated.

4.4 Sources of Experimental Error

Thus far the only error attributed to the experimental measurements has been the counting error. In fact, however, the measurements are subject to many more sources of error based on the experimental setup used to collect the data.

In order to quantify some of the major sources of experimental error, a best estimate was made of the precision of some key parameters in the experimental setup: collimator slit width (Δw), detector offsets in the x and y axes (Δx and Δy), and lattice rotation (Δθ). Figure 4.33 shows the potential sources of error investigated and Table 4.17 shows the estimated precision of the measured parameters.

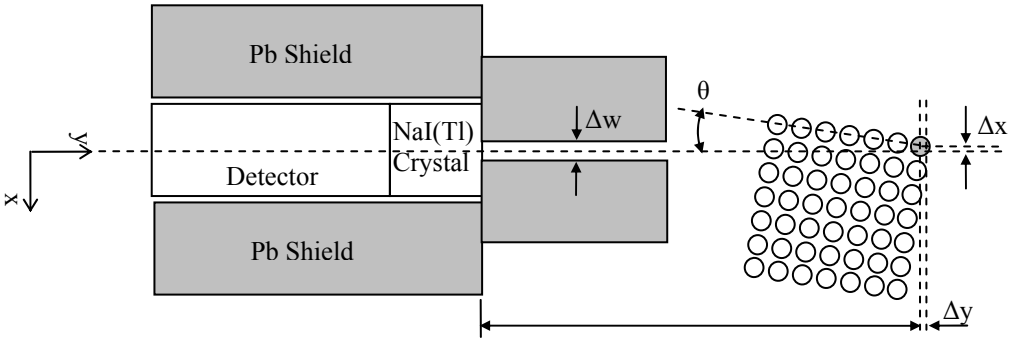

Figure 4.33: Top view schematic of 7x7 lattice measurements with corner pin activated showing potential sources of error in the experimental setup.

Table 4.17: Estimated precision for key parameters in the experimental setup.

Parameter	Symbol	Precision
Collimator Width	Δw	± 0.1 cm
X axis	Δx	± 0.2 cm
Y axis	Δy	± 0.2 cm
Lattice Rotation	Δθ	± 1.0 degree

It was expected that the most complicated lattice would be the most sensitive to the sources of error in the experimental setup because of the greater number of preferential paths that exist and the lower magnitude of the ratio of counts at those locations. MCNP

calculations were performed using the 7x7 lattice with the corner pin as the source and with the estimated errors applied to the parameters in the computational model. The results were then compared to a "base case" that had no errors applied. Table 4.18 shows the results of the error analysis. The estimated error is with respect to the base case. The 95% confidence intervals based on the uncertainties of the MCNP calculations are in the range of approximately 4% to 5%.

Table 4.18: Estimated percent errors in measured counts as a function of lattice rotation for various sources of error in key parameters of the experimental setup.

	Lattice Rotation (degrees)									
Case	0	5	10	15	20	25	30	35	40	45
Collimator slit + 0.1 cm	14%	6%	10%	9%	9%	14%	8%	9%	8%	11%
y-axis offset = + 0.2 cm	3%	-3%	0%	1%	1%	1%	-2%	-2%	-5%	-1%
x-axis offset = + 0.2 cm	3%	-5%	2%	2%	-3%	3%	0%	1%	-4%	0%
lattice rotation = + 1 deg	11%	-13%	-2%	-6%	3%	2%	-2%	1%	6%	12%
lattice rotation = - 1 deg	15%	-9%	8%	4%	-4%	6%	-1%	0%	-5%	14%
x-axis offset = - 0.2 cm	7%	-6%	-5%	-4%	0%	0%	0%	1%	1%	2%

Based on this analysis, the largest sources of error are the uncertainty in collimator slit width and lattice rotation. The x and y axes offsets have less effect on the measurement, particularly after the first 10 degrees of lattice rotation.

During the course of any one particular set of measurements, any offset in the x or y axes and collimator slit are constant for each measurement. The error in rotating the lattice, however, will be random as the lattice is moved from position to position. Therefore, if all the parameters were at their presumed worst-case values, the error expected in the measurement would be 14% + 3% + 15% + 7% = 39%. For all the sources of error to be simultaneously at their maximum is unlikely, but the potential for large errors helps to explain the differences observed between Figure 4.31 and 4.32, particularly in the first 10 degrees of lattice rotation.

CHAPTER 5
THE EFFECT OF MATERIAL HOMOGENIZATION ON LATTICE CALCULATIONS

The fuel pin lattice problem is, in many ways, similar to a shielding problem composed of an array of two heterogeneous compositions: a highly attenuating medium (fuel pin) and low attenuating medium (air). In many practical analytical situations, it is beneficial to combine the two mediums into a single, homogeneous smear of fuel pin and air.

Although material homogenization saves time in eliminating detail from the calculational model and/or may be unavoidable given limitations of the analysis code being employed, this type of simplification can lead to errors in the calculated gamma-ray transmission through the lattice. As discussed in §2.3, large differences in calculated dose have been reported [**Bozkurt**] between the results of heterogeneous and homogeneous models of a PWR fuel pin lattice.

Consider the case shown in Figure 5.1 where a "shield" of continuous material contains a random dispersion of a second material with different attenuation characteristics. Instances of the second material in the shield can be considered as discontinuities. Discontinuities within shields can be either random or ordered and can consist of highly attenuating material, "lumps," or low attenuating material, "voids." The magnitude of the discontinuity can be classified as large or small based on its optical thickness relative to the mean-free path of the continuous phase.

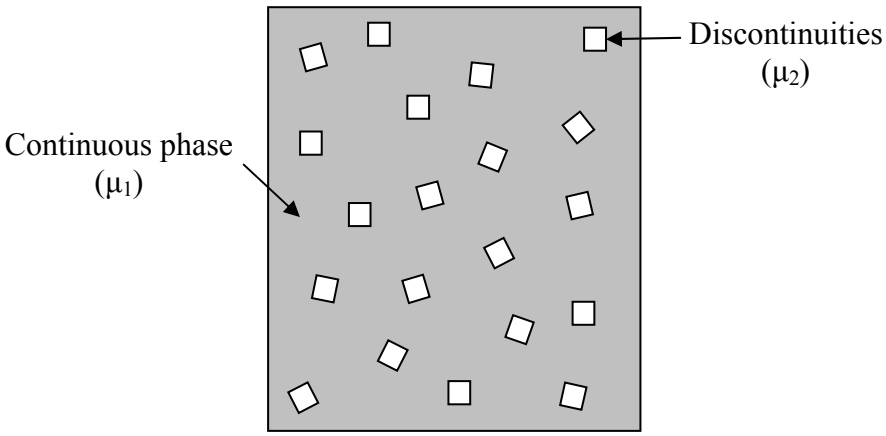

Figure 5.1: Example of a shield containing random dispersion of discontinuities.

Various techniques have been derived to calculate the effect of discontinuities using ray theory [**Shultis, Jaeger, Rockwell**] on random and ordered discontinuities. However, to rigorously study the effect of discontinuities it is convenient to use Monte Carlo techniques. Work has recently been performed on particle transmission through binary stochastic media using Monte Carlo [**Donovan**].

In lieu of formally addressing the discontinuities, it is common practice to simply mix the two materials into a single, homogeneous, composition with an average attenuation coefficient given by equation 3.43. Although this technique may produce adequate results in some circumstances, it can also lead to errors such as over prediction of shield effectiveness in the case of void discontinuities [**Shultis**].

In this work, it is convenient to consider the fuel pin regions in the lattice as the discontinuities and the air surrounding the pins in the lattice as the continuous material. Clearly, the discontinuities are "large" and regularly spaced within the continuous air medium. Homogenization of materials within the lattice will serve to eliminate the

channeling effect by removing the discontinuities. It is expected that this will tend to lower the outwardly directed gamma-ray transmission through the lattice.

A second effect is to redefine the source volume. Typically, the birth sites of all source photons are restricted to the cylindrical volume of the fuel pins. Once the fuel pin, cladding, and surrounding air are homogenized, the birth sites can exist at any location within the homogenized volume (source redistribution). This implies that outwardly directed source photons born close to the edge of the homogenized volume will undergo less attenuation. This effect is coupled to the traditional self-shielding effect where the attenuation of gamma rays born within fuel regions is reduced. Therefore, the resulting gamma-ray transmission in a homogeneous model will depend on the competing effects of eliminating the channeling and the self shielding.

5.1 SPERT Pin Lattice Calculations with Homogenized Materials Using the LATDOSE Computer Code

LATDOSE calculates the gamma-ray transmission through a lattice either using a heterogeneous treatment, as described in §3.2.3, or a homogeneous treatment of the materials. The type of calculation is specified with the first entry in the SETUP file (Appendix B). If this entry is set to .false. then LATDOSE will perform calculations using a homogeneous treatment of the lattice.

Figure 5.2 shows a schematic of the 2-D pin lattice as solved by LATDOSE. In Figure 5.2(a), the lattice is represented with heterogeneous materials and geometry. For a given source location and detector location, LATDOSE solves for the intersection of the ray with pins in the lattice explicitly. In the homogeneous case, as represented in Figure 5.2(b), LATDOSE assumes a unit cell having sides equal to the lattice pitch (provided by

entry seven in the SETUP file). The unit cell boundaries are shown as dotted lines in Figure 5.2(b). Given the area of the fuel region, clad region, and surrounding air in the unit cell, LATDOSE automatically calculates an effective linear attenuation coefficient through the entire unit cell. One limitation of the LATDOSE code is that it assumes that all pins in the lattice are identical in dimension and material and are in a square array.

Based on the equation of a ray from the source pin to the detector, LATDOSE determines the side of the lattice that is intersected by the ray and the point at which the intersection occurs. It is then a straight-forward calculation to determine the distance traveled by the ray in the homogeneous medium of the lattice and in the air medium between the lattice and the detector.

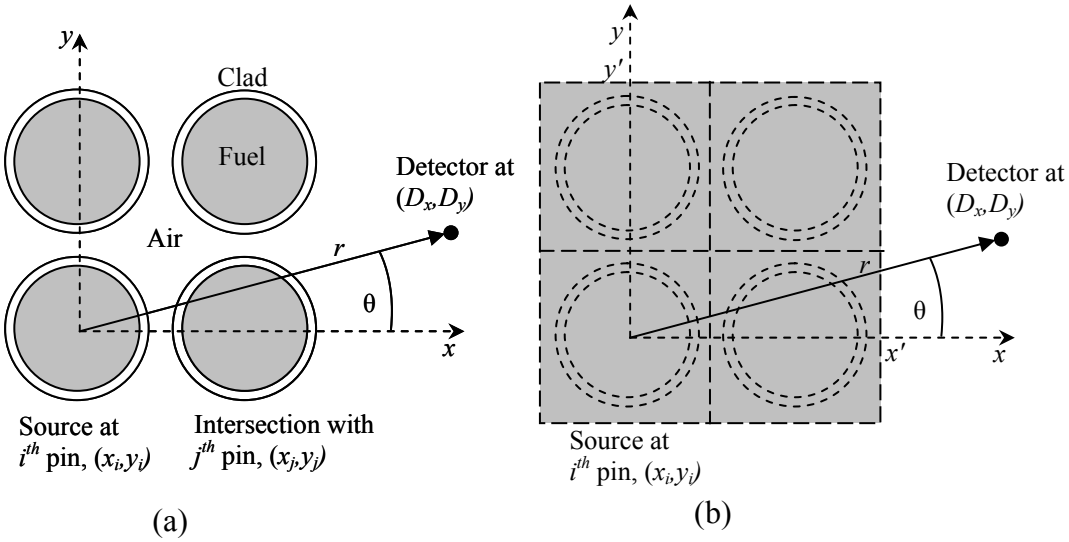

Figure 5.2: 2-D pin lattice represented with (a) heterogeneous and (b) homogeneous materials and geometry.

Since the material has been homogenized (which essentially eliminates channeling), it is not expected that the LATDOSE calculated photon flux versus detector position will exhibit the sharp peaks and valleys characteristic of the heterogeneous solutions in §3.2.4. Instead, the homogeneous solution should be a smoothly varying

function of the angle between the lattice x-axis and the ray, with the flux decreasing as a greater amount of the lattice is traversed by the ray. The distance from the source at (x_i,y_i) to a plane perpendicular to the x-axis at x' defining the edge of the lattice can be shown to be

$$r' = (x' - x_i)\sqrt{1 + \tan^2 \theta} \ . \tag{5.1}$$

LATDOSE was used to calculate the gamma-ray flux versus detector position for the same pin lattice configurations as §3.2.4 but with the materials homogenized. Aside from the material treatment, the heterogeneous and homogeneous problems are identical. Figure 5.3 shows the homogeneous solution superimposed on the heterogeneous solution for the 3x3 lattice with center pin activated.

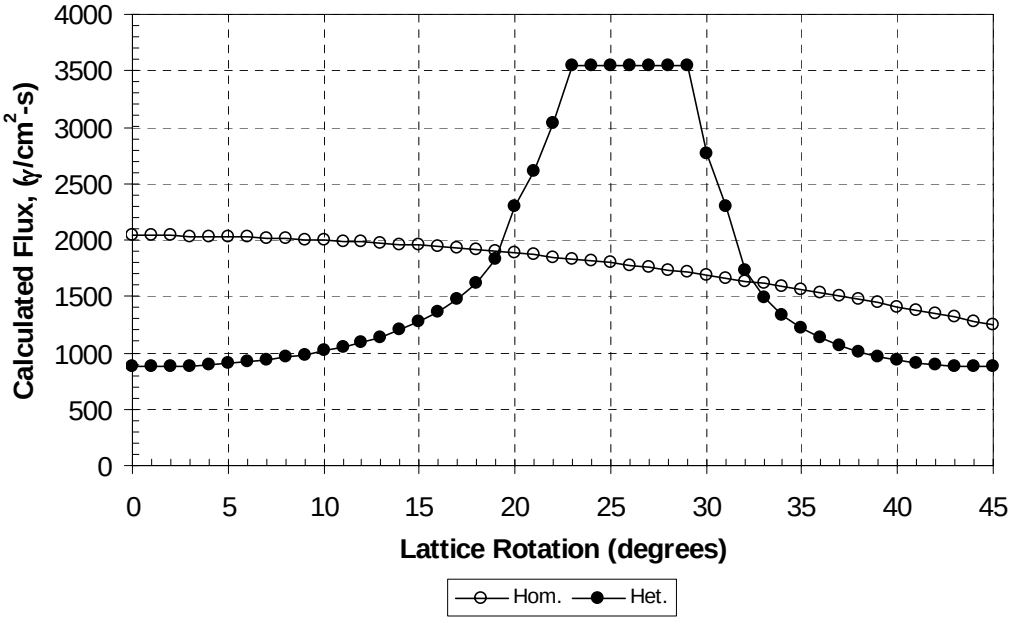

Figure 5.3: LATDOSE calculated gamma-ray flux as a function of angle as the detector is rotated about the center of a 3x3 homogeneous and heterogeneous pin lattice.

The expected behavior of the gamma-ray flux is observed in the figure. The maximum occurs at 0 degree lattice rotation where the path through the homogenized lattice is the shortest. The fraction of the ray passing through the homogenized lattice increases as the

lattice is rotated with respect to the detector, in accordance with Equation (5.1), and the calculated flux decreases. Figures 5.4, 5.5, 5.6, 5.7, and 5.8 show the homogeneous solution superimposed on the heterogeneous solution for the remaining lattice configurations.

From LATDOSE perspective, the 3x3 corner pin source and 5x5 center pin source are identical cases. Figure 5.4 and 5.5 show the identical shape but with magnitudes specific to the power history of the pin activation.

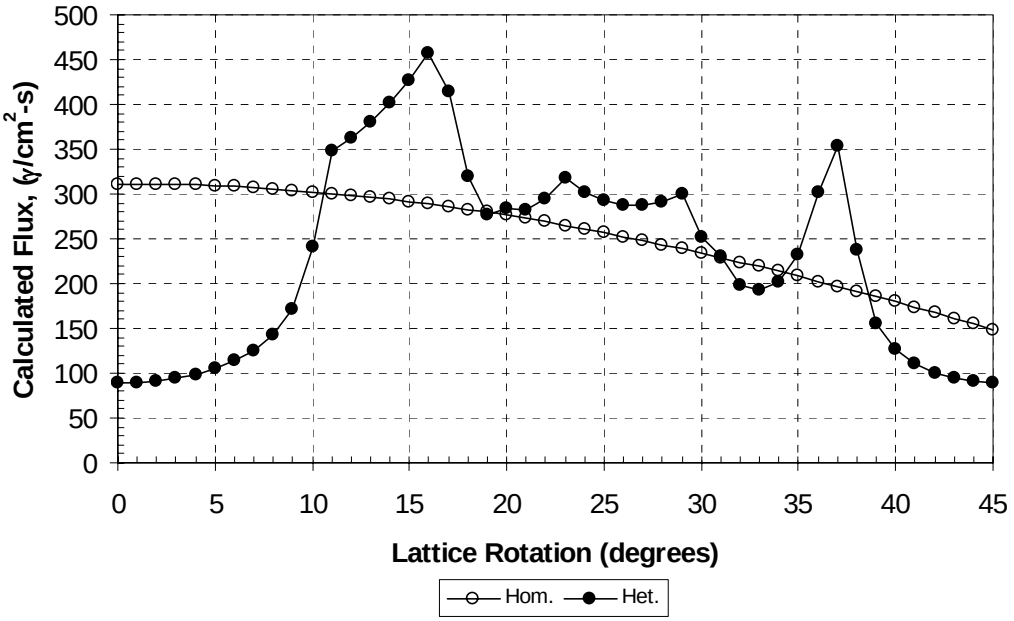

Figure 5.4: LATDOSE calculated gamma-ray flux as a function of angle as the detector is rotated about the corner of a 3x3 homogeneous and heterogeneous pin lattice.

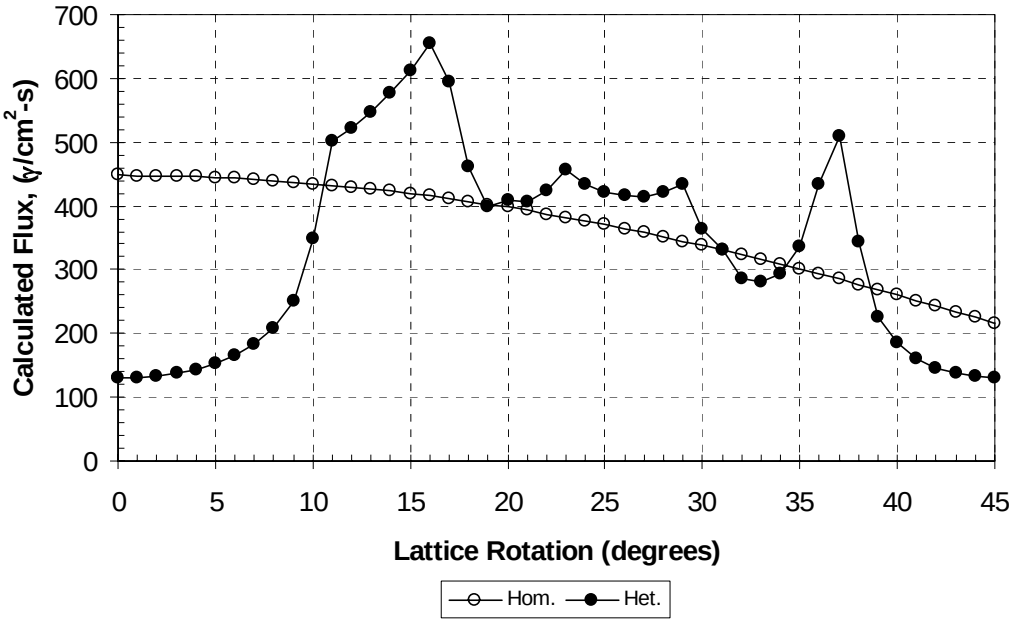

Figure 5.5: LATDOSE calculated gamma-ray flux as a function of angle as the detector is rotated about the center of a 5x5 homogeneous and heterogeneous pin lattice.

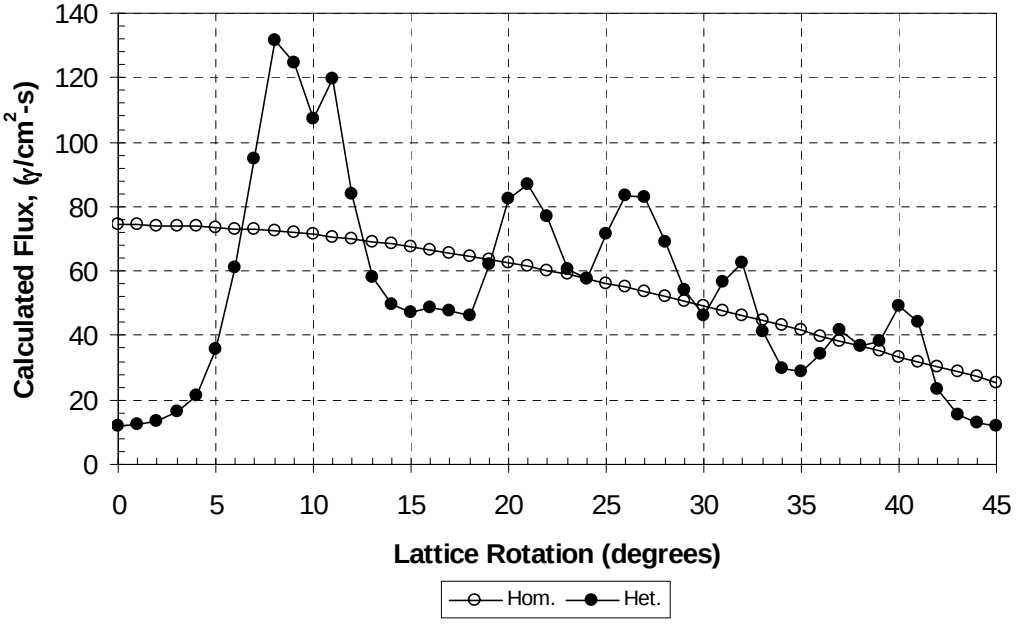

Figure 5.6: LATDOSE calculated gamma-ray flux as a function of angle as the detector is rotated about the corner of a 5x5 homogeneous and heterogeneous pin lattice.

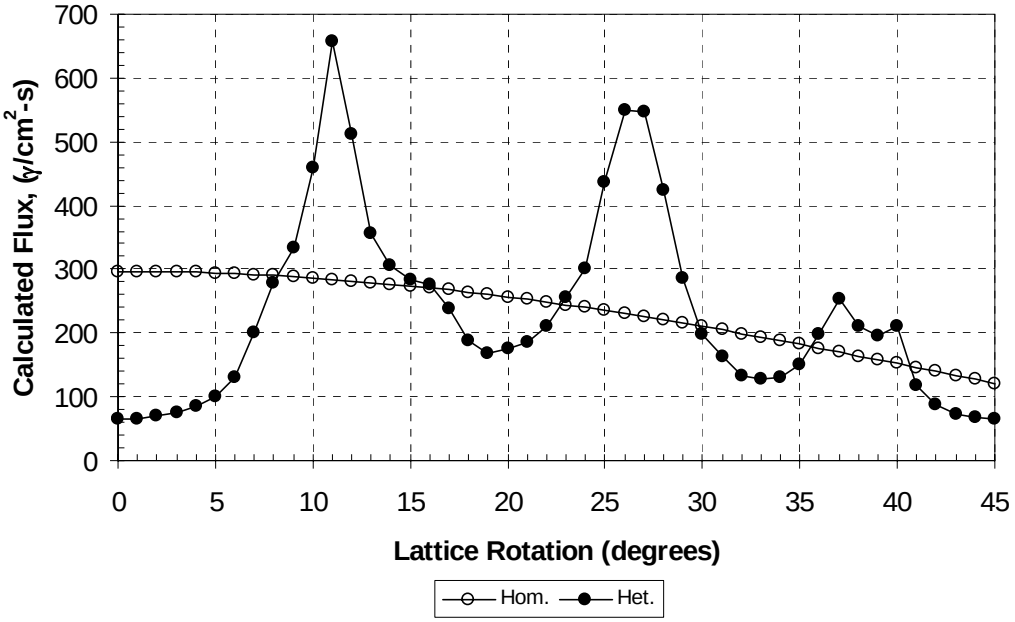

Figure 5.7: LATDOSE calculated gamma-ray flux as a function of angle as the detector is rotated about the center of a 7x7 homogeneous and heterogeneous pin lattice.

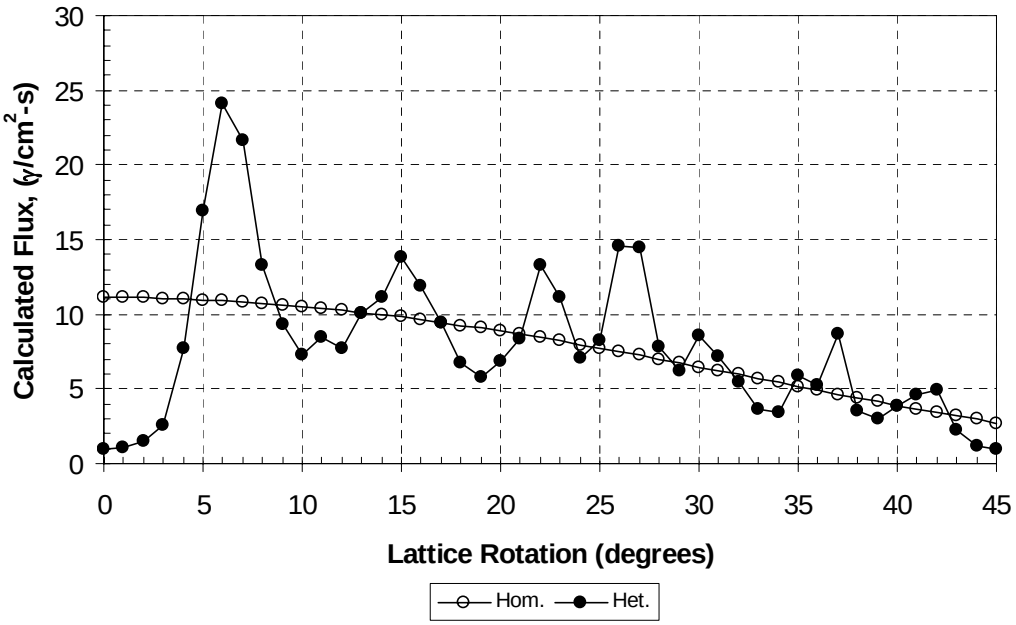

Figure 5.8: LATDOSE calculated gamma-ray flux as a function of angle as the detector is rotated about the corner of a 7x7 homogeneous and heterogeneous pin lattice.

Table 5.1 provides a comparison of the gamma-ray flux through both the homogeneous and heterogeneous lattices, integrated (using trapezoidal rule) over the entire 45 degrees of rotation. The result of material homogenization can lead to an over-prediction the integrated gamma-ray flux by as much as 8% in the lattices studied.

Table 5.1: Comparison of LATDOSE Calculated gamma-ray flux for 3x3, 5x5, and 7x7 lattices, integrated from 0 to 45 degrees lattice rotation, for heterogeneous and homogeneous cases.

Lattice Case	Gamma-Ray Flux (γ/cm^2-s)		Ratio
	Heterogeneous	Homogeneous	(Hom. / Het.)
3x3, Center Pin Source	7.4432E+04	7.9837E+04	1.07
3x3, Corner Pin Source	1.0575E+04	1.1451E+04	1.08
5x5, Center Pin Source	1.5253E+04	1.6511E+04	1.08
5x5, Corner Pin Source	2.4802E+03	2.5288E+03	1.02
7x7, Center Pin Source	1.0537E+04	1.0506E+04	0.997
7x7, Corner Pin Source	3.6113E+02	3.5223E+02	0.975

The LATDOSE code captures the effect of homogenization with respect to the elimination of channeling adequately, based on its ray-tracing algorithm. However, in its current form it has two main disadvantages. The first is that it does not model the effect of source redistribution. For both the heterogeneous and homogeneous LATDOSE calculation, the entire source is modeled as a point at the center of the fuel pin or unit cell. The second disadvantage is that it does not model the effect of scattering. In order to determine the magnitude of these effects on lattice problems, it is necessary to use higher order transport codes, such as Monte Carlo.

5.2 SPERT Pin Lattice Calculations with Homogenized Materials Using MCNP

To assess the impact of material homogenization on the SPERT fuel pin lattices, new MCNP models were generated in which the pin cell materials were homogenized. The fuel, cladding, fill gas and surrounding air for a given pin cell were uniformly blended into a unit cell. The unit cell was chosen to have length and width dimensions equal to the pitch of the lattice, 0.613 in. Following the blending procedure, a check of the isotopic masses in the model was performed to ensure that the mass was conserved in both the homogeneous and heterogeneous models.

The source redistribution was accomplished by extending the radius of the sampling cylinder from the fuel radius to a radius that completely enclosed the unit cell, as shown in Figure 5.9. As in the heterogeneous model, the sample cylinder radius was sampled uniformly. However, source-sites sampled outside of the unit cell were rejected, constraining the source within the unit cell. MCNP input decks for the homogeneous cases are found in Appendix C.

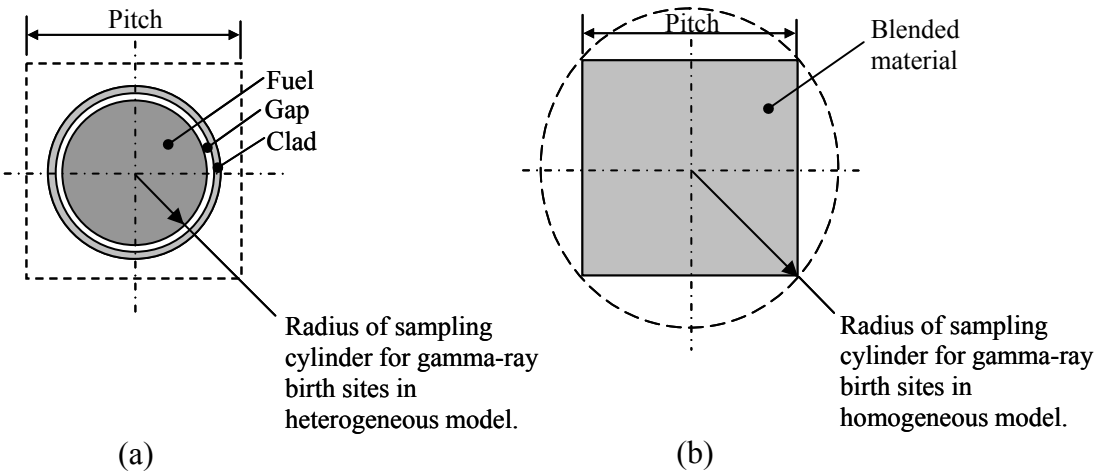

Figure 5.9: Schematic representation of (a) heterogeneous pin cell and (b) homogeneous unit cell with source sampling radii shown.

The MCNP homogenized results were expected to follow the LATDOSE homogeneous calculations, with the addition of the effect of the source redistribution and multiple scattering effects. Calculations for the homogeneous models were performed at exactly the same lattice positions as the heterogeneous cases for a total of 10 positions. Figures 5.10, 5.11, 5.12, 5.13, 5.14, and 5.15 show the results of the homogeneous MCNP calculations with the heterogeneous results superimposed for comparison.

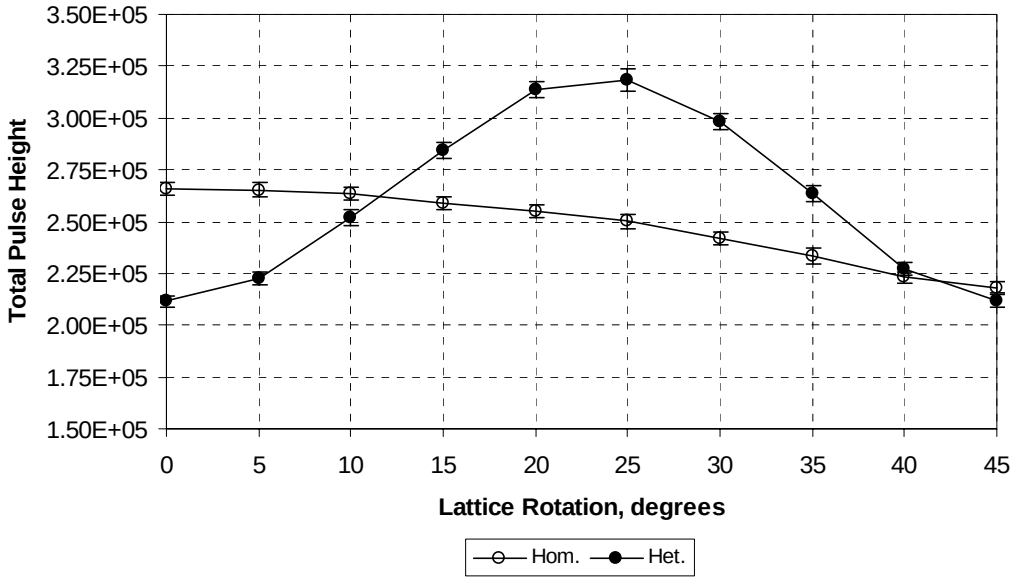

Figure 5.10: MCNP calculated total pulse height for a homogenized 3x3 SPERT fuel pin lattice with center pin activated. Heterogeneous results are shown for comparison.

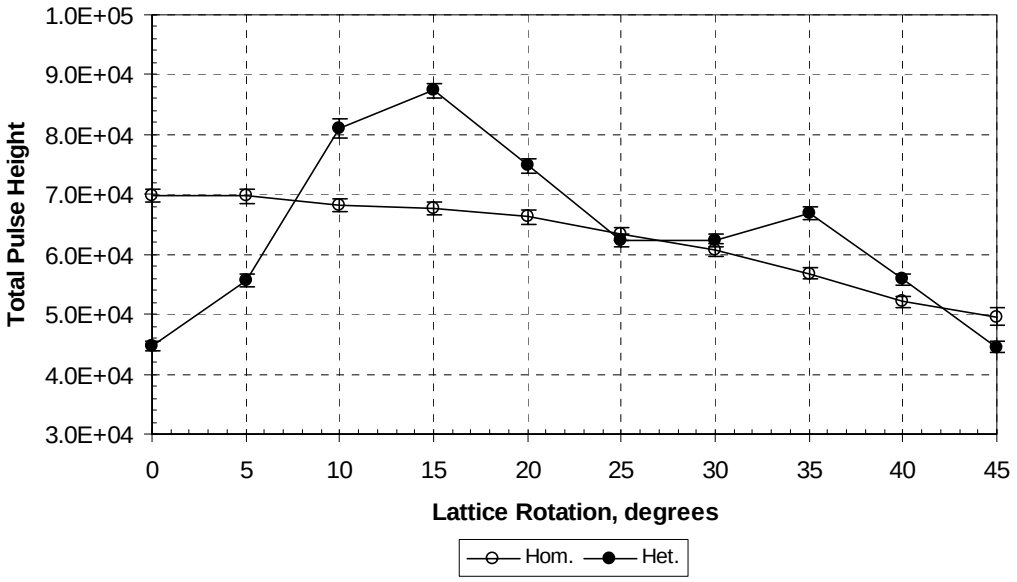

Figure 5.11: MCNP calculated total pulse height for a homogenized 3x3 SPERT fuel pin lattice with corner pin activated. Heterogeneous results are shown for comparison.

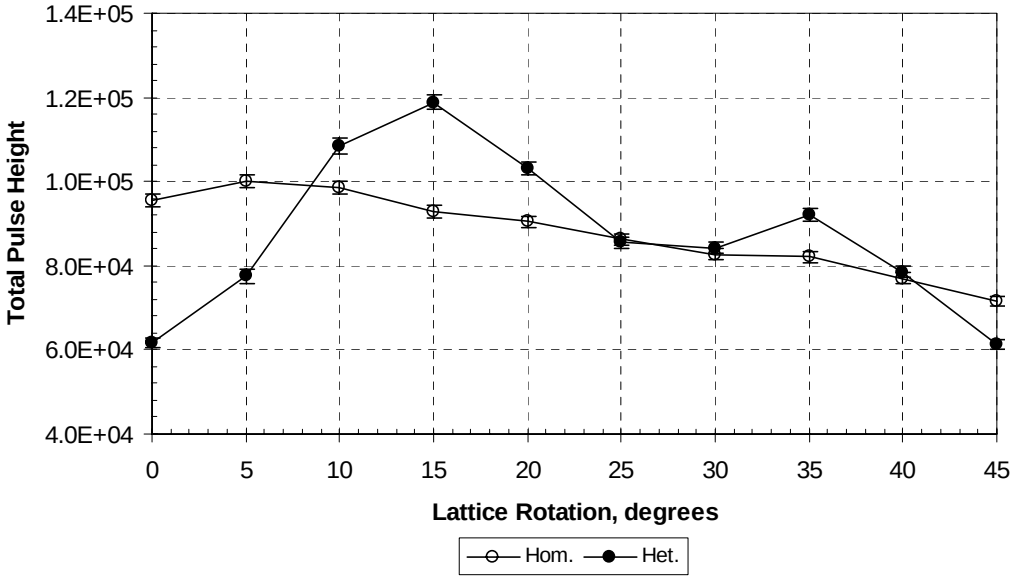

Figure 5.12: MCNP calculated total pulse height for a homogenized 5x5 SPERT fuel pin lattice with center pin activated. Heterogeneous results are shown for comparison.

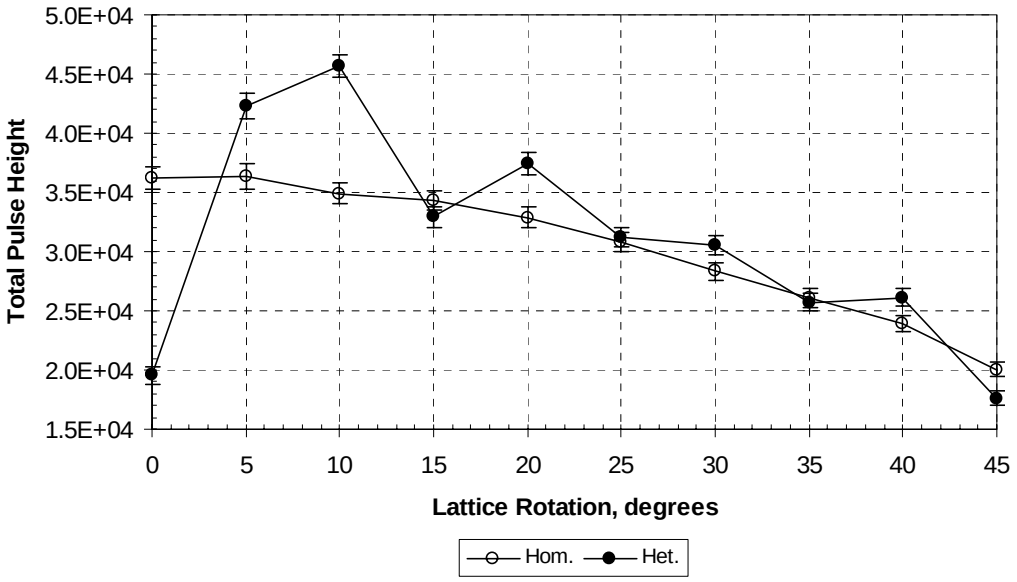

Figure 5.13: MCNP calculated total pulse height for a homogenized 5x5 SPERT fuel pin lattice with corner pin activated. Heterogeneous results are shown for comparison.

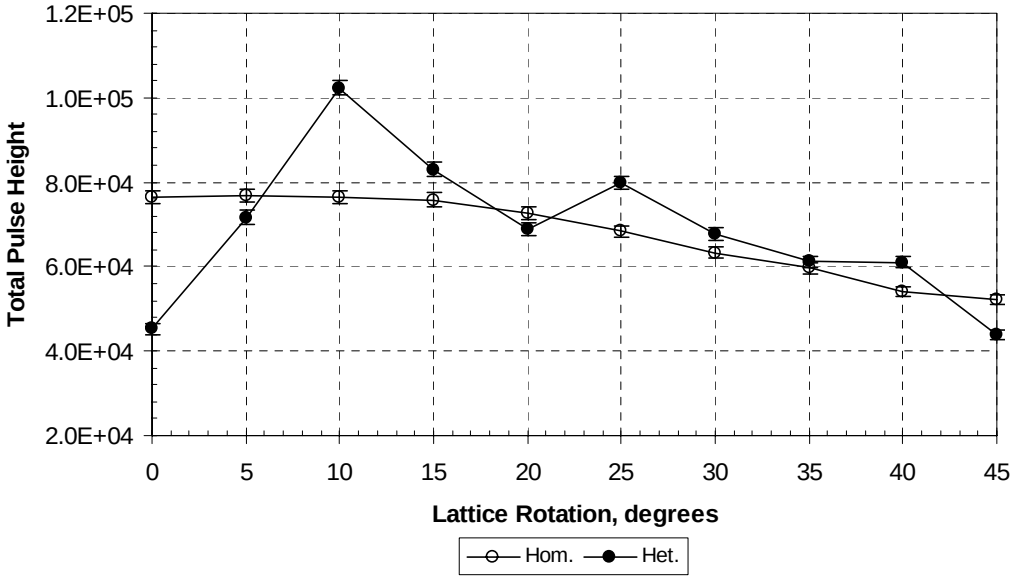

Figure 5.14: MCNP calculated total pulse height for a homogenized 7x7 SPERT fuel pin lattice with center pin activated. Heterogeneous results are shown for comparison.

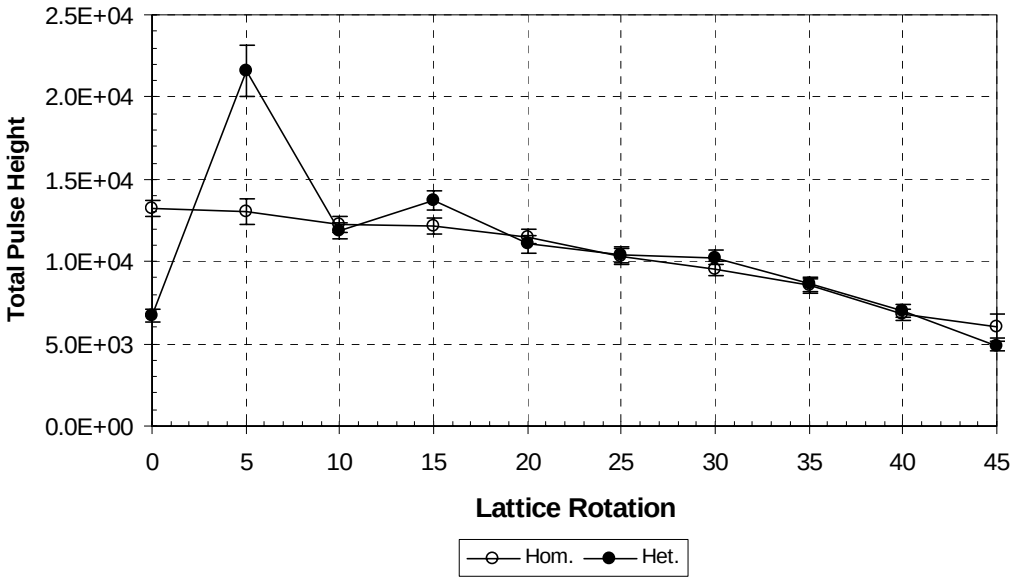

Figure 5.15: MCNP calculated total pulse height for a homogenized 7x7 SPERT fuel pin lattice with corner pin activated. Heterogeneous results are shown for comparison.

The homogeneous results shown in the preceding figures agree with the LATDOSE predicted behavior. The calculated pulse height as a function of lattice rotation is a smoothly varying function, without the sharp peaks of the heterogeneous solution attributable to the channeling effect. As the lattice grows in size, the heterogeneous and homogeneous results approach each other, as observed in Figure 5.15 and to a lesser degree in Figure 5.13 and 5.14.

Table 5.2 provides a comparison of the MCNP calculated total pulse height in the detector for both the homogeneous and heterogeneous lattices, integrated (using trapezoidal rule) over the entire 45 degrees of rotation. In every case MCNP under-predicts the integrated pulse height as a result of material homogenization. It is apparent that the channeling effect in the heterogeneous model outweighs the source redistribution of the homogeneous model for these particular cases of a single activated pin in a lattice.

Table 5.2: Comparison of MCNP calculated detector pulse height for 3x3, 5x5, and 7x7 lattices, integrated from 0 to 45 degrees lattice rotation, for heterogeneous and homogeneous cases.

Lattice Case	Total Pulse Height		Ratio
	Heterogeneous	Homogeneous	(Hom. / Het.) ± 95% CI
3x3, Center Pin Source	1.1963E+07	1.1164E+07	0.93 ± 0.01
3x3, Corner Pin Source	2.9536E+06	2.8221E+06	0.96 ± 0.01
5x5, Center Pin Source	4.0495E+06	3.9672E+06	0.98 ± 0.01
5x5, Corner Pin Source	1.4525E+06	1.3786E+06	0.95 ± 0.02
7x7, Center Pin Source	3.2007E+06	3.0572E+06	0.96 ± 0.01
7x7, Corner Pin Source	5.0160E+05	4.6868E+05	0.93 ± 0.03

The homogeneous to heterogeneous total pulse-height ratios calculated by MCNP differs from the LATDOSE calculated ratio of gamma-ray fluxes. Given the higher fidelity, 3-D detailed geometry and transport capability of MCNP relative to LATDOSE, the results in Table 5.2 provide the best indication of the effect of material homogenization on SPERT fuel pin lattices with a single activated pin.

5.3 The Pressurized Water Reactor Fuel Bundle Problem

Up to this point this work has focused on the particular case of a single source, or activated, fuel pin in a lattice of unirradiated fuel pins. The focus is now expanded to include MCNP calculations of a typical pressurized water reactor (PWR) fuel pin bundle.

As previously discussed, the effect of material homogenization on dose outside the PWR bundle will depend on the competing effects of the removal of the channeling effect, tending to lower the dose, and the redistribution of the source, tending to increase the dose. By comparing MCNP Results from heterogeneous material calculations and homogeneous material calculations, a determination can be made as to which effect dominates for a typical PWR bundle.

The fuel bundle used for this study is a Westinghouse Vantage-5 ™, 17x17 array with control rods and instrument tube. This is the same bundle used in a previous study of the effect of material homogenization on calculated dose [**Bozkurt**] and the fuel bundle characteristics shown in Table 5.3 are taken directly from the reference.

Table 5.3: Characteristics of PWR fuel bundle used in this study.

Fuel element array	17 x 17
Number of fuel elements	264
Number of control rod channels	24
Number of instrument tubes	1
Assembly dimension (cm)	21.42 x 21.42
Pellet-pellet gap (cm)	0.3456
Fuel element outside diameter (cm)	0.9144
Fuel element height (cm)	386.80
Cladding thickness (cm)	0.0572
Pellet-clad gap (cm)	0.0082
Top and Bottom plenum length (cm)	19.37
Fuel pellet outside diameter (cm)	0.7836
Fuel rod length (cm)	365.76
Control rod channel outside diameter (cm)	1.0922
Cladding thickness (cm)	0.04064
Instrumentation tube outside diameter (cm)	1.204
Cladding thickness (cm)	0.04064

Also for consistency, the gamma-ray source and material compositions used in the PWR calculations are taken from the reference [**Bozkurt**] and are shown in Table 5.4 and Table 5.5, respectively. The source position was sampled uniformly in the fuel pellet and a cosine probability density function (at the beginning of exposure) was used to sample the axial position in the pin. Each pin in the bundle was assumed to have the same power density and therefore assumed to have equal probability of emitting a delayed fission-product gamma ray.

Table 5.4: Energy group structure and gamma-ray emission rates for PWR bundle.

Group	Energy Range (MeV)	Average Energy (MeV)	Energy Release Rate[17] (MeV/fission)	Photon Release Rate (γ/s)
1	0.0 to 1.0	0.5	7.54E-3	1.511E-2
2	1.0 to 2.0	1.5	1.52E-4	1.013E-4
3	2.0 to 3.0	2.5	3.78E-4	1.511E-4
4	3.0 to 4.0	3.5	1.38E-7	3.935E-8
5	4.0 to 5.0	4.5	4.34E-22	9.640E-23
6	5.0 to 7.5	6.25	1.83E-22	2.937E-23
7	7.5 to 20.0	13.75	6.44E-24	4.689E-25

Table 5.5: PWR Fuel bundle material compositions.

Material	Fuel	Air	Zircaloy	Type 304 Stainless Steel
Density (g/cm^3)	10.5	1.296E-3	6.5	0.972
Element	Weight Fractions			
Uranium	0.8815			
Oxygen	0.1185	0.2315		
Nitrogen		0.7552		
Argon		0.0133		
Zirconium			0.9850	
Tin			0.0120	
Iron			0.0030	0.6950
Chromium				0.1900
Manganese				0.0200
Nickel				0.0950

Ring detectors perpendicular to the vertical axis were used to tally the gamma-ray flux on the outside of the bundle at various radial distances from its center. A flux-to-dose function [**ANSI/ANS-6.1.1**] was added to convert the MCNP tally to dose. The geometry, source, compositions, and tallies in this study are all consistent with that in the previous work by [**Bozkurt**]. The MCNP input decks used for this study are found in Appendix C.

[17] Energy release rates are given after 1 yr cooling time following 40000 h of service in the core [Chilton].

5.3.1 Single Pin and Small Lattice Calculations

The SPERT fuel pin measurements and calculations shown previously demonstrate that the channeling effect decreases as the lattice becomes larger. It is expected that this will be true for the PWR bundle. However, the effect of the source redistribution on the PWR bundle, given that every pin in the lattice is now a source, is unknown.

The effect of source redistribution is to essentially reduce the attenuation of gamma rays that are born in the fuel. The nearer the birth site to the center of the fuel pin, the greater the attenuation before the gamma ray exits the source volume. This phenomenon is sometimes referred to as "self shielding." In the homogeneous case, the entire unit cell is the source volume. It is possible for the gamma-ray birth site to reside closer to the edges of the unit cell, in a medium of reduced attenuation coefficient, relative to that of fuel. It is reasonable then to expect that more gamma rays will exit the unit cell as a result of homogenization. If these unit cells are close to the perimeter of the fuel bundle, the increase in exiting gamma rays will produce an increase in dose.

To isolate the effect of source redistribution, a heterogeneous and homogeneous model of a single PWR fuel bin was constructed. In the absence of any other pins to provide a channeling effect, the difference in the calculated dose should be a direct result of the source redistribution. Similarly, to isolate the channeling effect, 3x3, 5x5, and 7x7 PWR pin lattices were modeled with both homogeneous and heterogeneous materials.

Table 5.6 shows the results of the single pin and small lattice calculations using a set of five ring detectors. The detector radii start at a minimum value, determined by adding 0.1 cm to the diagonal of the entire lattice, and increase to a value of 19.0 cm

beyond the minimum radius. Two additional ring detectors are placed at 100.0 cm and 200.0 cm distance from the center of the pin or lattice. All the ring detectors are at the mid-point of the model relative to the vertical axis.

Table 5.6: Dose comparison for single PWR fuel bundle pin modeled heterogeneously and homogeneously.

Ring Detector Position	Distance from Center of Pin (cm)	Heterogeneous Dose (Sv)	Homogeneous Dose (Sv)	Ratio (Hom. / Het.) ± 95% CI
Minimum	1.0	1.1515E-15	1.5525E-15	1.35 ± 0.05
+ 1.0	2.0	5.7146E-16	7.2275E-16	1.26 ± 0.03
+ 4.0	5.0	2.2470E-16	2.8118E-16	1.25 ± 0.02
+ 9.0	10.0	1.1227E-16	1.3872E-16	1.24 ± 0.01
+ 19.0	20.0	5.4690E-17	6.7154E-17	1.23 ± 0.01
100.0	100.0	8.2131E-18	9.7579E-18	1.188 ± 0.004
200.0	200.0	2.8383E-18	3.3214E-18	1.170 ± 0.004

The ratios versus detector distance from Table 5.6 are plotted in Figure 5.16.

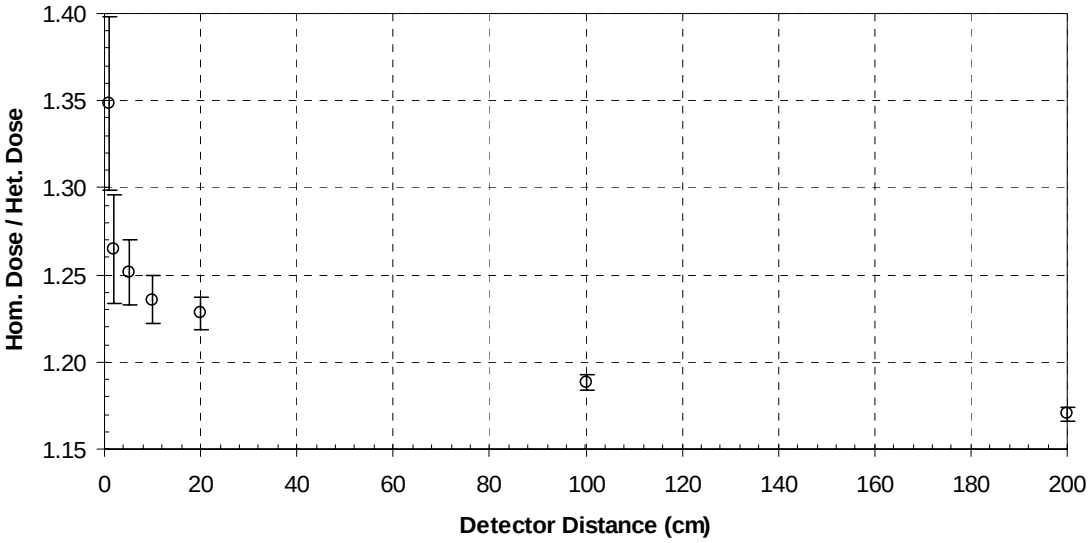

Figure 5.16: Ratio of MCNP calculated doses for homogeneous and heterogeneous models of a single PWR bundle fuel pin as a function of detector distance.

The data confirm the effect of source redistribution (lessening of the self-shielding) results in a higher dose for the homogeneous model. As the distance to the

detector increases, this effect lessens due to the source volumes in both cases approaching a line-source, parallel to the axis of the ring detector. The effect, however, remains significant even at 200.0 cm where the homogeneous dose is 17% higher than that calculated in the heterogeneous model.

The results of the 3x3 PWR fuel bundle pin lattice are shown in Table 5.7. These results begin to show the effect of homogenization of materials in a lattice. The channeling in the heterogeneous model competes with the source redistribution of the homogeneous model, resulting in a lower ratio of the homogeneous to heterogeneous dose.

Table 5.7: Dose comparison for a 3x3 lattice of PWR fuel bundle pins modeled heterogeneously and homogeneously.

Ring Detector Position	Distance from Center of Lattice (cm)	Heterogeneous Dose (Sv)	Homogeneous Dose (Sv)	Ratio (Hom. / Het.) ± 95% CI
Minimum	2.78	3.2553E-16	3.6942E-16	1.13 ± 0.03
+ 1.0	3.78	2.2634E-16	2.5513E-16	1.13 ± 0.03
+ 4.0	6.78	1.2125E-16	1.3534E-16	1.12 ± 0.02
+ 9.0	11.78	6.8764E-17	7.6477E-17	1.11 ± 0.01
+ 19.0	21.78	3.6251E-17	4.0026E-17	1.10 ± 0.01
100.0	100.0	6.1116E-18	6.7094E-18	1.098 ± 0.005
200.0	200.0	2.1473E-18	2.3453E-18	1.092 ± 0.004

Figure 5.17 shows the homogeneous dose to heterogeneous dose ratio as a function of distance from the center of the lattice. Again, the ratios decrease with distance as the two source volumes appear more as a line-source relative to the detectors. However, the dose calculated in the homogeneous case remains nearly 10% higher than the heterogeneous dose.

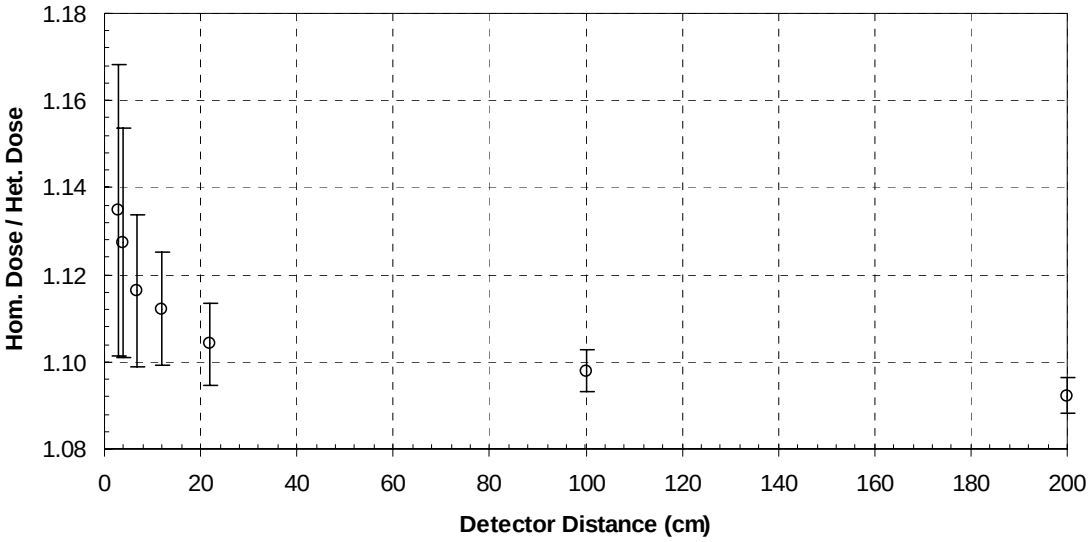

Figure 5.17: Ratio of MCNP calculated doses for homogeneous and heterogeneous models of a 3x3 lattice of PWR bundle fuel pins as a function of detector distance.

As the lattices grow in size, previous calculations suggest that the magnitude of the channeling effect is reduced. However, the data shown in Table 5.8 and 5.9 and plotted in Figure 5.18 for the 5x5 and 7x7 PWR fuel pins lattices show less of a difference between the homogeneous and heterogeneous model calculated doses. This suggests that a boundary effect is involved in the competition between heterogeneous channeling and the homogeneous shielding.

Table 5.8: Dose comparison for a 5x5 lattice of PWR fuel bundle pins modeled heterogeneously and homogeneously.

Ring Detector Position	Distance from Center of Lattice (cm)	Heterogeneous Dose (Sv)	Homogeneous Dose (Sv)	Ratio (Hom. / Het.) ± 95% CI
Minimum	4.56	1.5296E-16	1.6888E-16	1.10 ± 0.03
+ 1.0	5.56	1.2024E-16	1.2987E-16	1.08 ± 0.03
+ 4.0	8.56	7.3392E-17	7.9721E-17	1.09 ± 0.02
+ 9.0	13.56	4.5476E-17	4.8818E-17	1.07 ± 0.01
+ 19.0	23.56	2.5476E-17	2.7255E-17	1.07 ± 0.01
100.0	100.0	4.7349E-18	5.0543E-18	1.07 ± 0.01
200.0	200.0	1.6775E-18	1.7850E-18	1.064 ± 0.005

Table 5.9: Dose comparison for a 7x7 lattice of PWR fuel bundle pins modeled heterogeneously and homogeneously.

Ring Detector Position	Distance from Center of Lattice (cm)	Heterogeneous Dose (Sv)	Homogeneous Dose (Sv)	Ratio (Hom. / Het.) ± 95% CI
Minimum	6.35	8.9405E-17	9.5946E-17	1.07 ± 0.03
+ 1.0	7.35	7.3635E-17	7.8461E-17	1.07 ± 0.03
+ 4.0	10.35	4.9458E-17	5.2141E-17	1.05 ± 0.02
+ 9.0	15.35	3.2226E-17	3.4116E-17	1.06 ± 0.01
+ 19.0	25.35	1.8993E-17	1.9888E-17	1.05 ± 0.01
100.0	100.0	3.8132E-18	4.0149E-18	1.05 ± 0.01
200.0	200.0	1.3664E-18	1.4286E-18	1.046 ± 0.005

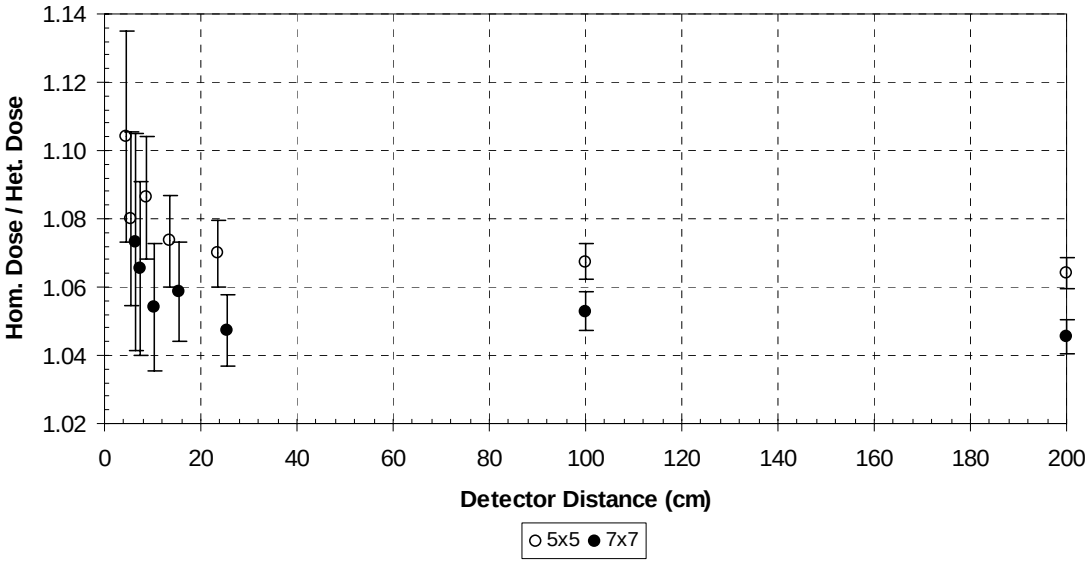

Figure 5.18: Ratio of MCNP calculated doses for homogeneous and heterogeneous models of a 5x5 and 7x7 lattice of PWR fuel pins as a function of detector distance.

As previously discussed, one of the primary benefits from source redistribution as a result of homogenization is the potential for a gamma-ray birth site to be near the boundary of the unit cell, thereby increasing the escape probability of the gamma ray. The escape probability decreases the further the source site is from the lattice boundary. Therefore, for source redistribution to have a larger effect, a significant fraction of the gamma-ray birth sites need to be well within a mean-free path of the edge of the lattice.

The probability of selecting a birth site within a mean-free path of the boundary is proportional to the ratio of the desired birth-site volume to the total volume of the unit cell. Given constant material properties and lattice characteristics, the mean-free path of a photon will not change with the size of the lattice, causing the volume of desirable birth sites to increase less rapidly than the total volume of the unit cell.

Figure 5.19 shows the relationship between the escape probability and volume fraction of desired birth sites for a photon with μ=0.67 cm^{-1}.

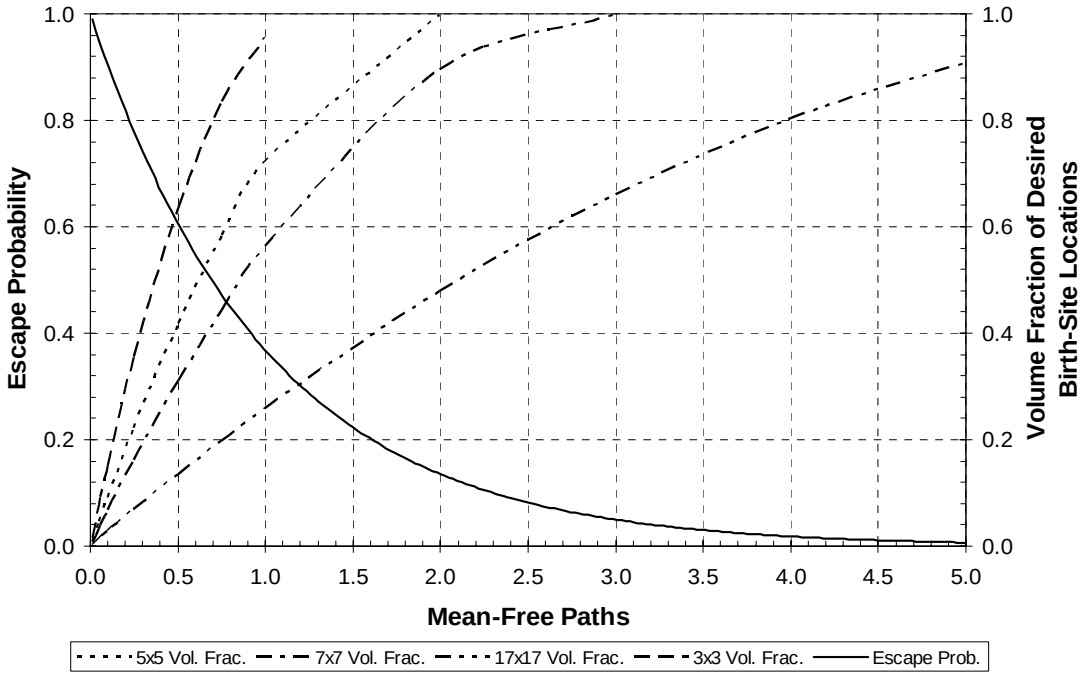

Figure 5.19: Escape probabilities and volume fractions of desired birth sites for a photon with μ=0.67 cm-1 in a homogenized model of 3x3, 5x5, 7x7, and 17x17 PWR fuel pin lattices.

Considering a volume within one half of a mean-free path (61% escape probability) to a boundary, the corresponding volume ratios for a 3x3, 5x5, 7x7, and 17x17 PWR lattices are 0.63, 0.42, 0.31, and 0.13, respectively. The overall effect of increasing the lattice size is to reduce the magnitude of source redistribution in the homogeneous case.

5.3.2 Complete Fuel Bundle Calculations

MCNP models for the entire PWR fuel bundle, as described in the [**Bozkurt**] reference, were created using both heterogeneous and homogeneous materials. An isotopic mass balance of the homogenized materials was performed to ensure that the mass of each isotope was conserved.

The model consists of all the control rod tubes and the instrumentation tube assuming that the control rods themselves are absent and that the instrumentation tube is empty. An air medium surrounds the bundle, pins, control rod tubes and instrumentation tube. It is assumed that air occupies the inside of the control rod tubes and instrumentation tube, as well.

The identical gamma-ray source described in Table 5.4 is used, with the source-sites sampled uniformly from all fuel pins. The radial distribution within a fuel pin is flat and the axial distribution is cosine shaped, as with the small lattice models.

Ring detectors are placed at various radii perpendicular to the vertical axis of the bundle starting at 15.2 cm and extending to 500.0 cm. Three separate calculations were performed with the set of ring detectors at z = 0.0 cm (axial mid-point), z= 100.0 cm, and z = 200.0 cm. Given the axial symmetry of the model, the solution at any height, z, should identically equal the solution at $-z$. The ring detector tallies are modified by the same flux-to-dose function used in the small lattice calculations.

Two axial regions were modeled in the homogeneous case into which masses from the heterogeneous model were uniformly distributed: (1) the fuel region, (2) the top and bottom plenum regions. The volume of the homogeneous fuel region was determined by calculating the dimensions of a parallelepiped having sides equal to 17

unit cells. Each unit cell had length and width dimensions equal to the lattice pitch. The axial height remained the same for both the heterogeneous and homogeneous cases. This resulted in a parallelepiped having dimensions of 21.42 cm x 21.42 cm x 365.76 cm. The mass of all materials located in the fuel region (fuel meat, fuel cladding, control rod cladding, instrumentation tube cladding, and interstitial air) were uniformly distributed into this volume. The same procedure was used for the top and bottom plenum regions and the materials located in these regions (cladding, springs, and interstitial air) were uniformly distributed into this volume. Gamma-ray source sites were sampled uniformly within the x-y plane and sampled according to a cosine-shape in the axial dimension.

A plot on the x-y plane at the bundle mid-point is shown in Figure 5.20, as rendered by the MCNP plotter, with the center portion magnified to provide greater detail. MCNP input decks for the heterogeneous and homogeneous models are provided in Appendix C.

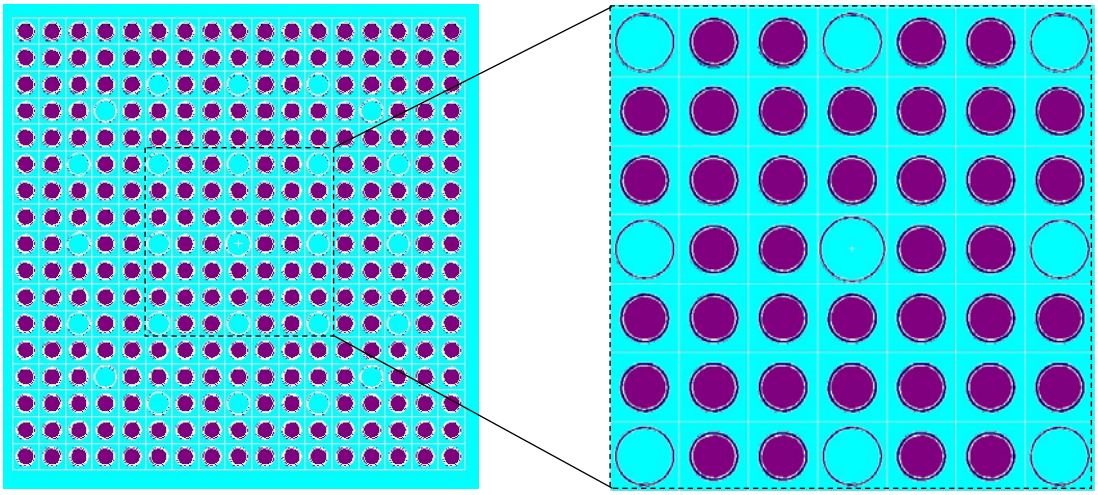

Figure 5.20: MCNP model of the 17x17 PWR fuel bundle with control rod channels and instrument tube at the assembly mid-point, with center section magnified.

Calculated dose rates for the $z = 0$ cm case are shown in Table 5.10. Figure 5.21 shows the dose rate results for the homogeneous and heterogeneous cases along with the ratio of the homogeneous to heterogeneous dose rates. There exists a very slight over prediction of approximately 1% in the homogeneous case but otherwise no significant differences in dose rates were visible as a result of homogenization.

Table 5.10: MCNP calculated dose rates for heterogeneous and homogeneous models of 17x17 fuel bundle at the bundle mid-plane (z = 0).

Detector Radius	Het. Dose Rate (Sv/s)	Rel. Error	Hom. Dose Rate (Sv/s)	Rel. Error	Dose Rate Ratio (Hom. / Het.)	95% CI
15.2	2.0608E-17	0.0103	2.0641E-17	0.0106	1.0016	0.0296
20	1.3985E-17	0.0071	1.4069E-17	0.0074	1.0060	0.0205
25	1.0641E-17	0.0059	1.0757E-17	0.0059	1.0108	0.0167
30	8.6163E-18	0.0052	8.6730E-18	0.005	1.0066	0.0144
40	6.2411E-18	0.0043	6.3030E-18	0.0042	1.0099	0.0120
50	4.8239E-18	0.0037	4.8726E-18	0.0037	1.0101	0.0105
75	2.9775E-18	0.003	3.0079E-18	0.003	1.0102	0.0085
100	2.0619E-18	0.0027	2.0860E-18	0.0027	1.0117	0.0076
200	7.4184E-19	0.0024	7.4760E-19	0.0023	1.0078	0.0066
300	3.7027E-19	0.0024	3.7235E-19	0.0022	1.0056	0.0065
400	2.1711E-19	0.0023	2.1949E-19	0.0023	1.0109	0.0065
500	1.4203E-19	0.0024	1.4339E-19	0.0023	1.0096	0.0066

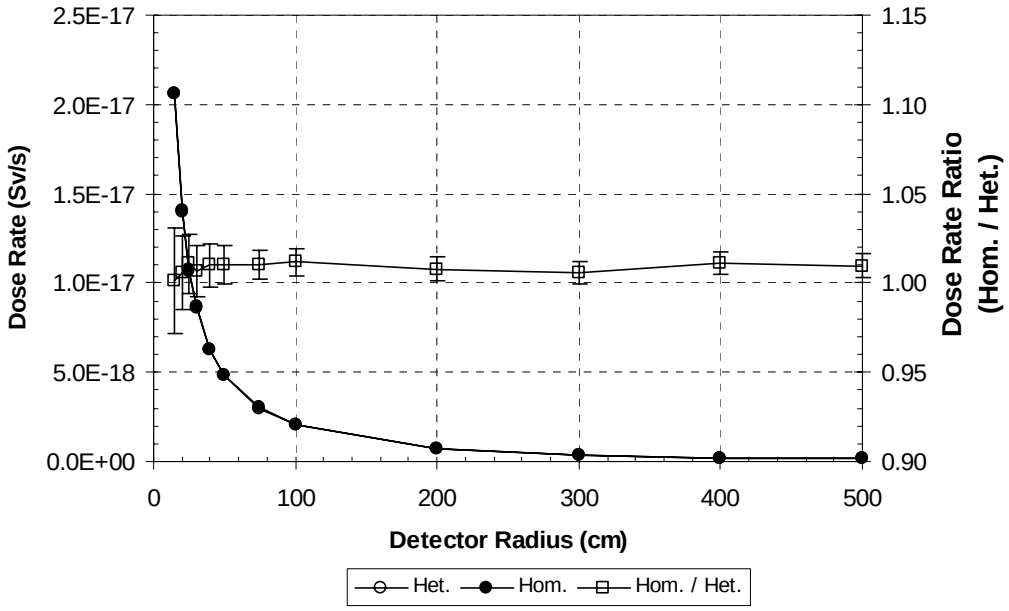

Figure 5.21: MCNP calculated dose rates for heterogeneous and homogeneous models of 17x17 fuel bundle at the bundle mid-plane (z = 0) as a function of detector radius.

This result is in line with the expectations. A large lattice will see less of an effect from source redistribution as a result of homogenization. The channeling effect of the heterogeneous model nearly balances (within about 1%) the increase in dose rate from source redistribution.

Calculated dose rates for the z = 100.0 cm case are shown in Table 5.11. Figure 5.22 shows the dose rate results for the homogeneous and heterogeneous cases along with the ratio of the homogeneous to heterogeneous dose rates. There exists a slight under prediction close to the lattice, but the trend is increasing with detector radius and is approximately unity at 500.0 cm from the center of the lattice.

Table 5.11: MCNP calculated dose rates for heterogeneous and homogeneous models of 17x17 fuel bundle at the bundle mid-plane (z = ±100.0).

Detector Radius	Het. Dose Rate (Sv/s)	Rel. Error	Hom. Dose Rate (Sv/s)	Rel. Error	Dose Rate Ratio (Hom. / Het.)	95% CI
15.2	1.6720E-17	0.0124	1.6128E-17	0.0118	0.9646	0.0343
20	1.1365E-17	0.008	1.0984E-17	0.0081	0.9665	0.0228
25	8.6460E-18	0.0066	8.3723E-18	0.0065	0.9683	0.0186
30	6.9764E-18	0.0056	6.8591E-18	0.006	0.9832	0.0164
40	5.1151E-18	0.0049	4.9718E-18	0.0049	0.9720	0.0139
50	3.9630E-18	0.0043	3.8621E-18	0.0047	0.9745	0.0127
75	2.4403E-18	0.0034	2.3874E-18	0.0033	0.9783	0.0095
100	1.7062E-18	0.0031	1.6721E-18	0.003	0.9800	0.0086
200	6.4422E-19	0.0025	6.3843E-19	0.0025	0.9910	0.0071
300	3.3552E-19	0.0025	3.3552E-19	0.0024	1.0000	0.0069
400	2.0378E-19	0.0023	2.0415E-19	0.0023	1.0019	0.0065
500	1.3547E-19	0.0023	1.3610E-19	0.0023	1.0046	0.0065

The gamma-ray source at this axial height (z = 100.0 cm) is considerably less than at the axial mid-plane (z = 0.0), where the maxima of the cosine-shaped distribution is located. Gamma rays born at locations closer to the mid-plane have to travel nearly vertically in order to contribute to the detector tallies close to the bundle. This eliminates the benefit from radial source redistribution since the photons may travel a significant vertical distance through the lattice. The channeling effect present in the heterogeneous case,

however, facilitates transport of photons both radially and vertically, causing the homogeneous case to under predict the dose rates at these locations.

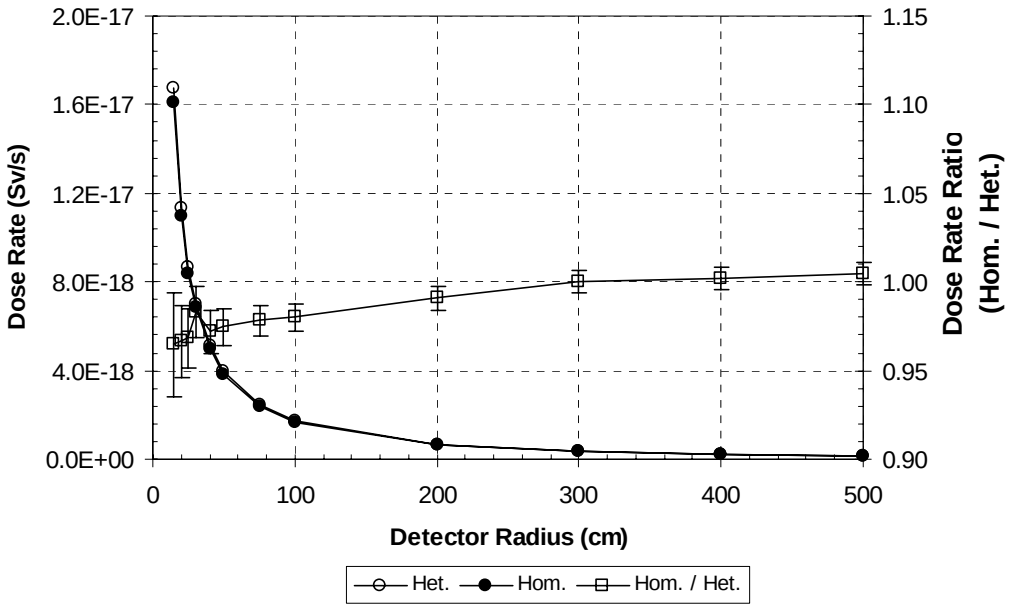

Figure 5.22: MCNP calculated dose rates for heterogeneous and homogeneous models of 17x17 fuel bundle at z = ±100.0 as a function of detector radius.

As the detector radii increase, photons born towards the axial mid-plane have less of a vertical path to the detector and the radial effects of source redistribution again become a factor. At the 300.0 cm detector, the homogeneous and heterogeneous dose rates are very nearly equal with a slight increasing trend noted at the 400.0 cm and 500.0 cm detectors.

The final set of results has the ring detectors at a vertical position of ±200.0 cm, which is slightly greater than that of the fueled region of the bundle. The calculated dose rates and dose rate ratios are shown in Table 5.12. Figure 5.23 shows the dose rate results for the homogeneous and heterogeneous cases along with the ratio of the homogeneous to heterogeneous dose rates.

Table 5.12: MCNP calculated dose rates for heterogeneous and homogeneous models of 17x17 fuel bundle at the bundle mid-plane (z = ±200.0).

Detector Radius	Het. Dose Rate (Sv/s)	Rel. Error	Hom. Dose Rate (Sv/s)	Rel. Error	Dose Rate Ratio (Hom. / Het.)	95% CI
15.2	1.3411E-18	0.0186	1.2657E-18	0.0212	0.9438	0.0562
20	1.4533E-18	0.0156	1.3890E-18	0.0161	0.9558	0.0449
25	1.4521E-18	0.0114	1.3933E-18	0.0125	0.9595	0.0338
30	1.4380E-18	0.0106	1.3564E-18	0.011	0.9432	0.0306
40	1.3134E-18	0.0078	1.2406E-18	0.0082	0.9445	0.0226
50	1.1844E-18	0.0067	1.1130E-18	0.0067	0.9397	0.0190
75	9.2841E-19	0.0048	8.9153E-19	0.005	0.9603	0.0139
100	7.6094E-19	0.0047	7.2931E-19	0.004	0.9584	0.0124
200	4.1090E-19	0.0029	4.0116E-19	0.0029	0.9763	0.0082
300	2.5300E-19	0.0026	2.5036E-19	0.0026	0.9896	0.0074
400	1.6857E-19	0.0028	1.6810E-19	0.0024	0.9972	0.0074
500	1.1805E-19	0.0024	1.1814E-19	0.0024	1.0008	0.0068

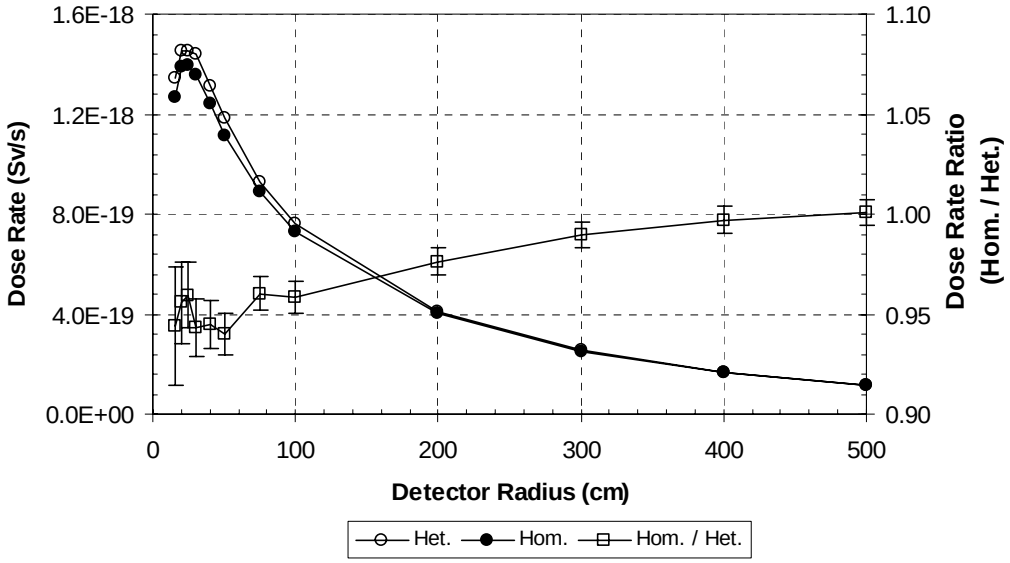

Figure 5.23: MCNP calculated dose rates for heterogeneous and homogeneous models of 17x17 fuel bundle at z = ±200.0 as a function of detector radius.

At this height, gamma rays born at any location in the fuel need to travel a vertical distance through the lattice before contributing to the detectors close to the bundle. As the detector radii increase, the fraction of the vertical distance within the fuel bundle decreases. The peculiar maximum in the calculated dose rates at 25 cm to 30 cm is a

result of the shielding from fuel and plenum regions reducing the dose rate. As the detector radii increase, the shielding decreases faster than the geometric attenuation leading to a maximum between 25 cm and 30 cm. As in the previous case, the channeling effect facilitates the transport of gamma rays trough the lattice vertically leading to a slight under prediction of the homogeneous dose rate. As the detector radii increase further, the vertical distance traveled by gamma rays contributing to the detector tallies decreases. The effect of source redistribution begins to compensate for the lack of channeling in the homogeneous model, explaining the increasing trend in the homogeneous to heterogeneous ratios.

The results of the full PWR fuel bundle analyses demonstrate that the effect of homogenizing the fuel region, consistent with the method of this study, does not significantly affect the calculated dose rates on the outside of the bundle. The largest effects are noted at locations away from the axial mid-point and close to the bundle. Within three to five meters distance of the bundle, the dose rates of the homogeneous and heterogeneous models are nearly identical.

CHAPTER 6
DISCUSSION AND CONCLUSIONS

The focus of this work was to isolate the channeling effect on gamma-ray transmission through fuel pin lattices in air. Both calculational and experimental measurement results were generated to demonstrate the effect. The effect of the material homogenization approximation on calculational results was also studied to determine what error is introduced in the results using this simplification. The unique characteristics of the RPI RCF allowed for the direct measurement of activated fuel pins in lattices of unirradiated fuel pins in an air medium.

A critical element to this work was to establish a convenient method of determining the after-shutdown delayed fission-product gamma-ray source. Using the DELBG code, a technique for easily determining the delayed fission-product gamma-ray source was developed. This allowed for quickly determining the source for point-kernel and Monte Carlo calculations of the gamma-ray transmission through fuel pin lattices given any power history.

The point-kernel code, LATDOSE, was developed to demonstrate the lattice channeling effect on gamma-ray transmission. LATDOSE was specifically designed to accommodate a wide range of pin lattice configurations, allowing for parameters such as number of pins, lattice pitch, fuel and clad dimensions, number of energy groups, and gamma-ray source to be entered by the user. LATDOSE output contains data on the contribution of each pin in the lattice to the detector as well as an overall flux at the detector, as a function of detector position relative to the lattice, for every energy group. LATDOSE was very useful in determining the expected behavior of the gamma-ray flux for both the heterogeneous material and homogeneous material cases.

The predictions of LATDOSE were verified and its limitations explored using the MCNP Monte Carlo transport code. MCNP was used to model the actual experimental measurements of fission-product gamma-ray transmission through SPERT fuel pin lattices at the RCF. The MCNP models incorporated sophisticated geometry modeling to allow quick and easy generation of different lattice configurations and detector positions relative to the lattice. The position and intensity of the gamma-ray source was modeled with a high level of detail. Both pulse-height and track-length estimator flux tallies in the crystal volume of the detector were used. The pulse-height tally provides the closest comparison to the measurements performed with the actual physical detector. Given the nature of the pulse-height tally, most non-analog variance reduction techniques could not be used and heavy reliance was placed on source directional biasing, which helped to improve the MCNP calculation figure of merit.

Experimental measurements of the channeling effect through lattices constructed from RCF SPERT fuel pins using a typical RCF lattice plate were performed. An experimental apparatus was designed and constructed to hold the lattice plates and pins in position relative to a shielded detector with a collimator. The apparatus could rotate the lattice through 45 degrees relative to the detector, in 5 degree increments. The entire experimental apparatus was very flexible and could accommodate a variety of lattices. A technique to correct the experimental data for the constantly changing fission-product source was developed, allowing the changes due to lattice channeling to be isolated from the reduction in source strength due to decay.

A series of measurements were conducted, including "exploratory" measurements, in order to refine the apparatus and procedure for measuring the

channeling effect. Based on these early runs, improvements to the decay-correction scheme and collimator design were implemented.

The channeling effect as measured by the final set of experiments on 3x3, 5x5, and 7x7 SPERT fuel pin lattices reproduced the expected results from the calculations. Differences in the magnitude of the measured and calculated channeling effect are attributed in part to various sources of experimental errors. An analysis of the sources of experimental error was performed and quantified. For some cases, the experimental error was shown to be quite large. The measurements and calculations of SPERT fuel pin lattices demonstrate that as the source pin is placed in increasingly large lattices of pins, the magnitude of the channeling effect decreases.

In order to isolate the effect of calculated gamma-ray transmission through lattices when a material homogenization simplification is applied to the model, MCNP and LATDOSE calculations were performed with homogenized materials. Since the channeling effect is an attribute of the heterogeneity of the lattice, material homogenization effectively removes the effect. Competing with this is the effect of re-distributing the source. In the heterogeneous model, the gamma-ray birth sites are limited to the highly attenuating medium of the fuel pin. In the homogeneous model, the source volume is increased to include the entire unit cell. Since the material of the unit cell is a homogeneous mix of high and low attenuating materials, the resulting unit cell attenuation coefficient is lower than the fuel. The overall effect of source redistribution is to reduce the "self-shielding" of gamma rays in the fuel pin.

It was shown that source redistribution is significant only in cases where a large fraction of the gamma-ray birth sites are located close to the lattice edge. As the lattice

increases in size, the volume for these sites decreases relative to the volume of the entire lattice. Since the source is assumed to be uniformly distributed within the lattice volume, the probability of a gamma ray being born in a particular volume is equal to its volume fraction. As the lattice becomes large, the effect of source redistribution becomes less significant.

The competing effects of source redistribution and removing the channeling on the calculated dose rate outside a typical PWR fuel pin lattice was investigated using MCNP. Several calculations were performed using a single pin, small lattices of pins, and finally a 17x17 pin standard PWR fuel bundle. Comparisons of the heterogeneous and homogeneous dose rates showed that for the single pin and small lattices, the homogenization of materials resulted in an over prediction of the dose rate on the outside of the lattice. This effect decreased as the lattice became larger and the heterogeneous and homogeneous dose rates for the 17x17 case are nearly identical.

This is significant in that if the analyst is interested only in the total dose outside a fuel bundle, it may not be necessary to include all the detail of the heterogeneous model. Additionally, this work supports the current approach used in calculating gamma-ray dose to the pressure vessel and the response of gamma-ray detectors external to the core where, in both cases, the fuel bundles are generally modeled as homogeneous regions. However, if the dose rate on the outside of a lattice of fuel pins, as a function of angle, is desired then full heterogeneous modeling is required.

CHAPTER 7
RECOMMENDATIONS FOR FUTURE WORK

Although the DELBG code provided the sufficient level of information necessary for this work, a reasonable extension to the source modeling could be achieved using the ORIGEN code. In addition to providing an additional check of the DELBG results, the use of ORIGEN would provide greater detail on the after-shutdown inventory of fission products. This would be a necessary extension to this work for isolating radiation from particular fission-product nuclides.

The LATDOSE code may also modified to better model the source within a fuel pin. Currently, the entire source is modeled as a point in the center of the pin. LATDOSE could be modified so that the source would be distributed on an r-θ grid within the fuel meat, with a user supplied probability distribution function. An additional loop over source sites on the grid would be necessary for each pin to get the total contribution to the detector.

Additional modifications to LATDOSE could include the generation of response matrices for gamma-ray tomography. Appropriate subroutines could be added to solve the over-determined system of equations and provide comparisons to experimental measurements. Expanding LATDOSE in this capacity and pursuing its application to tomography is a rich area of research, which can be easily supported by experimental measurements at the RPI RCF.

Experimental measurements at the RPI RCF should continue and be expanded to include lattices of more than one activated pin, lattices with pins of varying activation levels, and lattices with pins removed from certain positions.

However, improvements to the measurement apparatus are warranted. Experimental error analysis determined that with the current uncertainties in detector and lattice position, large errors are possible. Therefore, it is necessary to improve the design of the apparatus so that the detector can be more easily and precisely positioned and the lattice rotation can be more precisely controlled.

A final area where this work may be extended would include the use of a germanium detector in place of the NaI(Tl) detector. The germanium detector could provide the capability to identify and track the transmission of radiation from specific isotopes through the lattice. This capability would complement the use of ORIGEN and improve the decay-correction algorithm of experimental data, once the precise nuclide and decay constant is identified.

REFERENCES

[**ANSI/ANS-6.1.1**] "Neutron and Gamma-Ray Fluence-to-Dose Factors," ANSI/ANS-6.1.1-1990 Draft, Rev. 4, American National Standards Institute (1990).

[**ANSI/ANS-6.4.3**] "Gamma-Ray Attenuation Coefficients and Buildup Factors for Engineering Materials," ANSI/ANS – 6.4.3 – 1991, American Nuclear Society, Illinois, (1992).

[**Bozkurt**] A. Bozkurt, N. Tsoulfanidis, "Modeling Gamma-Ray Dose Rate From A Spent Pressurized Water Reactor Fuel Assembly", Nuclear Technology, Vol. 119, (1997).

[**Briesmeister**] J. F. Briesmeister, Editor, "MCNP^{TM} - A General Monte Carlo N-Particle Transport Code, Version 4C," Los Alamos National Laboratory, Los Alamos, New Mexico (2000).

[**Carter**] L. L. Carter, R. A. Schwarz, "MCNP Visual Editor Computer Code Manual," Supplement to MCNP5 code package CCC-710, Radiation Safety Information Computational Center (RSICC), Oak Ridge, TN (2003).

[**Chart**] J. R. Parrington, H. D. Knox, S. L. Breneman, E. M. Baum, F. Feiner, "Nuclides and Isotopes, Fifteenth Edition," General Electric Co. and KAPL, Inc. (1996).

[**Chilton**] A. B. Chilton, J. K. Shultis, and R. E. Faw, "Principles of Radiation Shielding, Prentice-Hall," Englewood Cliffs, New Jersey (1984).

[**Donovan**] T. J. Donovan, "Monte Carlo Neutral Particle Transport through a Binary Stochastic Mixture Using Chord Length Sampling," Ph.D. Thesis, Rensselaer Polytechnic Institute, Troy, NY (2003).

[**Duderstadt**] J. J. Duderstadt, L. J. Hamilton, "Nuclear Reactor Analysis," John Wiley and Sons, NY (1976).

[**Evans**] R. D. Evans, "The Atomic Nucleus," McGraw-Hill Book Company, NY (1955).

[**Fisher**] P. C. Fisher and L. B. Engle, *Phys. Rev.*, **134**, B796 (1964).

[**Galayda**] M. N. Galayda, "Measurement and Analysis of the Effects of Large Voids in Light Water Reactors," Ph.D. Thesis, Rensselaer Polytechnic Institute, Troy, NY (1997).

[**Harris1**] D. R. Harris, R. R. Rohr, and F. Rodriquez-Vera, "Combined Use of the RPI Reactor for Training and Critical Experiments," Trans. Am. Nucl. Soc., **61**, 95 (1990).

[**Harris2**] D. R. Harris, F. Rodriquez-Vera, and F. E. Wicks, "Refueling the RPI reactor Critical Facility with Low Enrichment Fuel," *Proc. Int. Mtg. Reduced Enrichment for Research and Test Reactors*, Petten, Netherlands, October 14 – 16, 1986, R. Reidel Publishing Company, Dordrecht (1986).

[**Harris3**] D. R. Harris and J. A. Mitchell, "Measurements and Calculations of Neutron Migration and its Anisotropy in Lattices of Fuel Rods in Light Water," Nuclear Science and Engineering, **44**, 221 (1971).

[**Hubbell**] J. H. Hubble, "Photon Cross Sections, Attenuation Coefficients, and Energy Absorption Coefficients from 10 keV to 100 GeV," *Nat. Stand. Ref. Data Ser., Nat. Bur. Stand.,* **29**, (1969).

[**Jacobsson1**] S. Jacobsson, C. Andersson, A. Hakansson, A. Backlin, "A Tomographic Method For Verification of the Integrity of Spent Nuclear Fuel Assemblies – I: Simulation Studies," Nuclear Technology, Vol. 135, (2001).

[**Jacobsson2**] S. Jacobsson, A. Hakansson, P. Jansson, A. Backlin, "A Tomographic Method For Verification of the Integrity of Spent Nuclear Fuel Assemblies – II: Experimental Investigation," Nuclear Technology, Vol. 135, (2001).

[**Jaeger**] R.G. Jaeger, Editor, "Engineering Compendium on Radiation Shielding, Volume I," Springer – Verlag, New York (1968).

[**Kak]** A. C. Kak and M. Slaney, "Principles of Computerized Tomographic Imaging," IEEE Press, NY (1988).

[**Knoll**] G. F. Knoll, "Radiation Detection and Measurement, Second Edition," John Wiley and Sons, New York (1989).

[**Lee]** J. Y. Lee, H. D. Choi, "Pin Power Distribution Determined by Analyzing the Rotational Gamma Scanning Data of HANARO Fuel Bundle," Journal of the Korean Nuclear Society, Vol. 30, No. 5, (1998).

[**Maienschein**] F. C. Maienschein, *et al., op. cit.,* R. W. Peelle, *et al.,* "The Spectra of Gamma-Rays Associated with the Thermal-Neutron Fission of ^{235}U," IAEA Symposium on Pile Neutron Research in Physics, Vienna (1962).

[**Matsson**] I. Matsson, B. Grapengiesser, "Developments in Gamma Scanning of Irradiated Nuclear Fuel," Appl. Radiat. Isot., Vol. 48, No. 10-12 (1997).

[**NIST**] J. H. Hubbel and S. M. Seltzer, "Tables of X-Ray Mass Attenuation Coefficients and Mass Energy-Absorption Coefficients from 1 keV to 20 MeV for Elements $Z = 1$ to 92 and 48 Additional Substances of Dosimetric Interest," Version 1.03, Available: http://physics.nist.gov/PhysRefData/XrayMassCoef, National Institute of Standards and Technology, MD (2004).

[**Perkins**] J. F. Perkins, US Army Missile Command, Redstone Arsenal, Alabama, Report No. RR-TR-63-11 (1963).

[**Price**] B. T. Price, C. C. Horton, K. T. Spinney, "Radiation Shielding," Pergamon Press, NY (1957).

[**Rockwell**] T. Rockwell, Editor, "Reactor Shielding Design Manual," McGraw-Hill Book Company, Inc., (1956).

[**Shultis**] J. K. Shultis, and R. E. Faw, "Radiation Shielding," Prentice Hall PTR, NJ, (1996).

[**Trefethen**] L. N. Trefethen, D. Bau, III, "Numerical Linear Algebra," Society for Industrial and Applied Mathematics, PA, (1997).

[**Stephens**] J. E. Stephens, "Absolute Power Measurement of the RPI RCF Nuclear Reactor Using Delayed Gamma Data," MS. Thesis, Rensselaer Polytechnic Institute, Troy, NY (2002).

[**Wilson**] W. B. Wilson, T. R. England, R. J. LaBauve, and D. C. George, "DKPOWR: A Code for Calculating Decay Power, Energy, Activity, and $\beta + \gamma$ Spectra in LWR Fuel Using Fission Pulse Functions," LA-UR-85-157, Los Alamos National Laboratory, NM (1985).

APPENDIX A
DELBG SOURCE CODE LISTING, INPUT FILE EXAMPLE AND DATA LIBRARY

A.1 DELBG Source Code Listing

```
      PROGRAM DELBG
C=====================================================================
C Program to compute delayed fission product  betas and gammas.
C Original code by D. R. Harris, 1998
C Modified by T. H. Trumbull, 2004
C=====================================================================
      DIMENSION NIB(18,6),NIG(19,6)
     1,AB(24,18,6),CB(24,18,6),AG(24,19,6),CG(24,19,6)
     2,ELB(18),EUB(18),EAB(18),ELG(19),EUG(19),EAG(19)
     3,TP(10),TL(10),TU(10),RR(10,6),LA(3),KP(10),JT(20)
     4,TT(21),EG(19,21),RG(19,21),SG(19,21),TG(19,21)
     5,EB(18,21),RB(18,21),SB(18,21),TB(18,21)
C
C Job Input:
      OPEN(5,FILE='DELBG.INP')
C Job Output:
      OPEN(6,FILE='DELBG.OUT')
C Delayed beta and gamma data for Th232f,U233t,U235t,U238f,Pu239t,Pu241t
      OPEN(7,FILE='DELBG.LIB')
C
      NM=6
      WRITE(6,40)
      WRITE(6,25)
      READ (5,10)JT           !job title
      WRITE(6,20)JT
      READ (5,12)KG           !KG=3 gamma only,=2 beta only,=1 lib only
      WRITE(6,22)KG           !gear control
      IF(KG.EQ.1)WRITE(6,41)NM
      DO IM=1,NM              !must read beta spectra data from library
       IF(KG.EQ.1)WRITE(6,48)IM
       READ (7,13)X,X,N,N,N,NEB,LA
       write(*,*)'beta'
       write(*,13)x,x,n,n,n,neb,la
       IF(KG.EQ.1)WRITE(6,49)
       IF(KG.EQ.1)WRITE(6,23)X,X,N,N,N,NEB,LA
       DO IE=1,NEB
        READ (7,13)ELB(IE),EUB(IE),N,N,N,I
        EAB(IE)=.5*(ELB(IE)+EUB(IE))
        IF(KG.EQ.1)WRITE(6,50)IE,EAB(IE)
        IF(KG.EQ.1)WRITE(6,23)ELB(IE),EUB(IE),N,N,N,I
        READ (7,13)T,T,N,N,N,NIB(IE,IM)
        IF(KG.EQ.1)WRITE(6,51)
        IF(KG.EQ.1)WRITE(6,23)T,T,N,N,N,NIB(IE,IM)
        READ (7,14)(AB(II,IE,IM),CB(II,IE,IM),II=1,NIB(IE,IM))
        IF(KG.EQ.1)WRITE(6,52)
        IF(KG.EQ.1)WRITE(6,24)(AB(II,IE,IM),CB(II,IE,IM),II=1,NIB(IE,IM
     1   ))
        ENDDO                 !IE
       IF(KG.EQ.1)WRITE(6,53)IM !note gamma data follow beta data for
       READ (7,13)X,X,N,N,N,NEG,LA  !each IM
       write(*,*)'gamma'
       write(*,13)x,x,n,n,n,neg,la
```

```
       IF(KG.EQ.1)WRITE(6,54)
       IF(KG.EQ.1)WRITE(6,23)X,X,N,N,N,NEG,LA
       DO IE=1,NEG            !must read gamma spectra data from library
        READ (7,13)ELG(IE),EUG(IE),N,N,N,I
        EAG(IE)=.5*(ELG(IE)+EUG(IE))
        IF(KG.EQ.1)WRITE(6,55)IE,EAG(IE)
        IF(KG.EQ.1)WRITE(6,23)ELG(IE),EUG(IE),N,N,N,I
        READ (7,13)T,T,N,N,N,NIG(IE,IM)
        IF(KG.EQ.1)WRITE(6,56)
        IF(KG.EQ.1)WRITE(6,23)T,T,N,N,N,NIG(IE,IM)
        READ (7,14)(AG(II,IE,IM),CG(II,IE,IM),II=1,NIG(IE,IM))
        IF(KG.EQ.1)WRITE(6,57)
        IF(KG.EQ.1)WRITE(6,24)(AG(II,IE,IM),CG(II,IE,IM),II=1,NIG(IE,IM
     1   ))
        ENDDO                 !IE
       ENDDO                  !IM
      IF(KG.EQ.1)STOP         !end library data
C BEGIN JOB DATA
      READ (5,12)NP           !number of reaction schedules.
      READ (5,12)NT           !number of report times,
  100 WRITE(6,58)NP,NT,KG
      DO IP=1,NP              !data for reaction schedule IP
       READ (5,12)KP(IP)      !control for type of reaction schedule
       WRITE(6,22)KP(IP)
       READ (5,11)TL(IP),TU(IP),TP(IP) !reaction schedule IP start time
       WRITE(6,21)TL(IP),TU(IP),TP(IP) !stop time, period for KP(IP)=2
       READ (5,*)(RR(IP,IM),IM=1,NM)  !reaction rates for materials
       WRITE(6,21)(RR(IP,IM),IM=1,NM)
       ENDDO
      READ (5,*)(TT(IT),IT=1,NT) !report times in report schedule
      WRITE(6,21)(TT(IT),IT=1,NT)
C JOB CALCULATIONS
      WRITE(6,25)
      GO TO(200,130,140),KG
C BETA SPECTRA
  130 DO IE=1,NEB             !energy groups betas
       DO IT=1,NT             !report times
        EB(IE,IT)=0.
        DO IP=1,NP            !power history blocks
         DO IM=1,NM           !materials
          DO II=1,NIB(IE,IM)  !terms
           F1=CB(II,IE,IM)*(TT(IT)-TU(IP))
           F2=CB(II,IE,IM)*(TT(IT)-TL(IP))
           F3=EXP(-F1)
           F4=EXP(-F2)
           F5=F3-F4
           IF(KP(IP).EQ.1)THEN !flat power block
            EB(IE,IT)=EB(IE,IT)+RR(IP,IM)*AB(II,IE,IM)*F5/CB(II,IE,IM)
            ELSE              !rising power block
            F6=CB(II,IE,IM)+1./TP(IP)
            EB(IE,IT)=EB(IE,IT)+RR(IP,IM)*AB(II,IE,IM)*F3/F6
            ENDIF
           ENDDO              !II
          ENDDO               !IM
         ENDDO                !IP
         RB(IE,IT)=EB(IE,IT)/EAB(IE) !beta number rate in IE at TT(IT)
        ENDDO                 !IT
       ENDDO                  !IE
C COMPUTE BETAS ABOVE ELB(IG)
      DO IT=1,NT
       DO IE=1,NEB
        SB(IE,IT)=0.
        TB(IE,IT)=0.
```

```
        DO I1=IE,NEG
         SB(IE,IT)=SB(IE,IT)+RB(I1,IT) !beta number above ELB(IE)
         TB(IE,IT)=TB(IE,IT)+EB(I1,IT) !beta energy above ELB(IE)
         ENDDO                 !I1
        ENDDO                  !IE
       ENDDO                   !IT
C OUTPUT BETA RESULTS
      DO IE=1,NEB              !beta energy in IE
       WRITE(6,62)IE,ELB(IE),EUB(IE),EAB(IE)
       WRITE(6,21)(EB(IE,IT),IT=1,NT)
       ENDDO
      DO IE=1,NEB              !beta energy above ELB(IE)
       WRITE(6,63)IE,ELB(IE),EUB(IE),EAB(IE)
       WRITE(6,21)(TB(IE,IT),IT=1,NT)
       ENDDO
      DO IE=1,NEB              !beta number in IE
       WRITE(6,64)IE,ELB(IE),EUB(IE),EAB(IE)
       WRITE(6,21)(RB(IE,IT),IT=1,NT)
       ENDDO                   !IE
      DO IE=1,NEB              !betas number above ELB(IE)
       WRITE(6,65)IE,ELB(IE),EUB(IE),EAB(IE)
       WRITE(6,21)(SB(IE,IT),IT=1,NT)
       ENDDO                   !IE
      GO TO 200                !end beta calculations
C GAMMA SPECTRA
  140 DO IT=1,NT               !report times
       TOTG=0.0
       TOTG2=0.0
       DO IE=1,NEG             !energy groups gammas
        EG(IE,IT)=0.
        DO IP=1,NP             !power history blocks
         DO IM=1,NM            !materials
          DO II=1,NIG(IE,IM)   !terms in sum
           F1=CG(II,IE,IM)*(TT(IT)-TU(IP))
           IF(F1.LT.0.0)F1=0.0 ! ****** JES ******
           F2=CG(II,IE,IM)*(TT(IT)-TL(IP))
           F3=EXP(-F1)
           F4=EXP(-F2)
           F5=F3-F4
           IF(KP(IP).EQ.1)THEN !flat power block
            EG(IE,IT)=EG(IE,IT)+RR(IP,IM)*AG(II,IE,IM)*F5/CG(II,IE,IM)
            ELSE               !rising power block
            F6=CG(II,IE,IM)+1./TP(IP)
            EG(IE,IT)=EG(IE,IT)+RR(IP,IM)*AG(II,IE,IM)*F3/F6
            ENDIF
          ENDDO                !II
         ENDDO                 !IM
        ENDDO                  !IP
        RG(IE,IT)=EG(IE,IT)/EAG(IE) !gamma number rate
        TOTG=TOTG+RG(IE,IT)
        IF(IE.GE.7)TOTG2=TOTG2+RG(IE,IT)
       ENDDO                   !IE
       WRITE(*,*)TT(IT),TOTG,TOTG2
      ENDDO                    !IT
C COMPUTE GAMMAS ABOVE ELG(IG)
      DO IT=1,NT
       DO IE=1,NEG
        SG(IE,IT)=0.
        TG(IE,IT)=0.
        DO I1=IE,NEG
         SG(IE,IT)=SG(IE,IT)+RG(I1,IT) !gamma number above ELG(IE)
         TG(IE,IT)=TG(IE,IT)+EG(I1,IT) !gamma energy above ELG(IE)
         ENDDO                 !I1
```

```
        ENDDO                !IE
       ENDDO                 !IT
C OUTPUT GAMMA RESULTS
      DO IE=1,NEG            !gamma energy in IE
       WRITE(6,66)IE,ELG(IE),EUG(IE),EAG(IE)
       WRITE(6,21)(EG(IE,IT),IT=1,NT)
       ENDDO
      DO IE=1,NEG            !gamma energy above ELG(IE)
       WRITE(6,67)IE,ELG(IE),EUG(IE),EAG(IE)
       WRITE(6,21)(TG(IE,IT),IT=1,NT)
       ENDDO                 !IE
      DO IE=1,NEG            !gamma number in IE
       WRITE(6,68)IE,ELG(IE),EUG(IE),EAG(IE)
       WRITE(6,21)(RG(IE,IT),IT=1,NT)
       ENDDO                 !IE
      DO IE=1,NEG            !gamma number above ELG(IE)
       WRITE(6,69)IE,ELG(IE),EUG(IE),EAG(IE)
       WRITE(6,21)(SG(IE,IT),IT=1,NT)
       ENDDO                 !IE
C Send special output formatted for THT MCNP model:
      DO IT=1,NT
       WRITE(6,1111) IT,(RG(IE,IT),IE=1,NEG)
      ENDDO
C Make histogram formatted output:
       WRITE(6,1112) IE,(ELG(IE),EUG(IE), IE=1,NEG)
      DO IT=1,NT
         WRITE(6,1112) IT,(RG(IE,IT),RG(IE,IT), IE=1,NEG)
       ENDDO
  200  STOP
1111  FORMAT(I4,19(2x,E12.5))
1112  FORMAT(I4,38(2x,E12.5))
   10 FORMAT(20A4)
   11 FORMAT(6E12.5)
   12 FORMAT(I8)
   13 FORMAT(2E11.4,4I11,A3,2A4)
   14 FORMAT(6E11.4)
   20 FORMAT(20A4)
   21 FORMAT(6E12.5)
   22 FORMAT(6I12)
   23 FORMAT(2E11.4,4I11,A3,2A4)
   24 FORMAT(6E11.4)
   25 FORMAT(1H )
   26 FORMAT(I5,2E11.4,6I5)
   40 FORMAT('DELBG NOV98 DRH')
   41 FORMAT('DELBG LIBRARY  NM= ',I4)
   48 FORMAT('BETA SPECTRA DATA FOR NUCLIDE IM= ',I4)
   49 FORMAT('X,X,N,N,N,NEB,LA')
   50 FORMAT('ELB(IE),EUB(IE),N,N,N,I FOR IE= ',I4,'  EAB(IE)= ',E11.4)
   51 FORMAT('T,T,N,N,N,NIB(IE,IM)')
   52 FORMAT('(AB(II,IE,IM),CB(II,IE,IM),II=1,NIB(IE,IM)')
   53 FORMAT('GAMMA SPECTRA DATA FOR NUCLIDE IM= ',I4)
   54 FORMAT('X,X,N,N,N,NEG,LA')
   55 FORMAT('ELG(IE),EUG(IE),N,N,N,I FOR IE= ',I4,'  EAG(IE)= ',E11.4)
   56 FORMAT('T,T,N,N,,N,NIG(IE,IM)')
   57 FORMAT('(AG(II,IE,IM),CG(II,IE,IM),II=1,NIG(IE,IM)')
   58 FORMAT('JOB DATA NP= ',I4,' NT= ',I4,' KG= ',I4)
   59 FORMAT('POWER BLOCK TL(IP),TU(IP),TP(IP) IP= ',I4,' KP(IP)= ',I4)
   60 FORMAT('(RR(IP,IM),IM=1,6)')
   61 FORMAT('REPORT TIMES (TT(IT),IT=1,NT)')
   62 FORMAT('EB(IE,IT),IT=1,NT IE=',I3,' ELB,EUB,EAB',3E12.5)
   63 FORMAT('TB(IE,IT),IT=1,NT IE=',I3,' ELB,EUB,EAB',3E12.5)
   64 FORMAT('RB(IE,IT),IT=1,NT IE=',I3,' ELB,EUB,EAB',3E12.5)
   65 FORMAT('SB(IE,IT),IT=1,NT IE=',I3,' ELB,EUB,EAB',3E12.5)
```

```
   66 FORMAT('EG(IE,IT),IT=1,NT IE=',I3,' ELG,EUG,EAG',3E12.5)
   67 FORMAT('TG(IE,IT),IT=1,NT IE=',I3,' ELG,EUG,EAG',3E12.5)
   68 FORMAT('RG(IE,IT),IT=1,NT IE=',I3,' ELG,EUG,EAG',3E12.5)
   69 FORMAT('SG(IE,IT),IT=1,NT IE=',I3,' ELG,EUG,EAG',3E12.5)
      STOP
      END
C DELBG Variable Definitions
C  Abbreviate: coeff for coefficient, mat for material, group for
C     energy group
C AB(II,IE,IM)=beta energy coeff term II for group IE for mat IM
C AG(II,IE,IM)=gamma energy coeff term II for group IE for mat IM
C CB(II,IE,IM)=beta energy decay const term II for group IE for mat IM
C CG(II,IE,IM)=gamma energy decay const term II for group IE for mat IM
C EAG(IE)=average energy in gamma group IE
C ELB(IE),EUB(IE)=lower and upper energies of beta group IE
C ELG(IE),EUG(IE)=lower and upper energies of gamma group IE
C EB(IE,IT)=beta energy in group IE at report time TT(IT)
C EG(IE,IT)=gamma energy in group IE at report time TT(IT)
C KG=1 library,=2 beta spectra,=3 gamma spectra. gear control
C NEB=number beta groups,NEG=number gamma groups
C NIB(IE,IM),NIG(IE,IM)=number terms for betas,gammas in group IE & mat IM
C NM=number materials,NP=number reaction schedules,NT=number report times
C RB(IE,IT)=number rate betas in IE at report time TT(IT)
C RG(IE,IT)=number rate gammas in IE at report time TT(IT)
C RR(IP,IM)=reaction rate for mat IM in reaction schedule IP
C SB(IE,IT)=sum of betas above ELB(IE) at report time TT(IT)
C SG(IE,IT)=sum of gammas above ELG(IE) at report time TT(IT)
C TB(IE,IT)=sum of beta energy above ELB(IE) at report time TT(IT)
C TG(IE,IT)=sum of gamma energy above ELG(IE) at report time TT(IT)
C TL(IP),TU(IP)=lower and upper times for reaction schedule IP
C TP(IP)=rising reaction rate period (sec) for reaction schedule IP
C TT(IT)=ITth report time for report schedule
```

A.2 DELBG Input File Example

```
RCF Delayed Gamma for input to MCNP
3                                                  ! 2=beta, 3=gamma
1                                                  ! number of reaction schedules
3                                                  ! number of report times
2                                                  ! 1=S.S., 2=period
0. 200.00 27.00                                    ! t(start),t(end),period
0. 0. 3.6661E8  0. 0. 0.                           !See note below.
400. 1408.0 2416.0                                 !report times after SCRAM


Note: Values are reaction rates [fiss/sec] for Th232(fast), U233(therm),
U235(therm), U238(fast), Pu239(therm), Pu241(therm), in that order.  The
fiss/sec value has been multiplied by 0.38% to account for fissions in the
center fuel pin only.

Exp3D: 1/15/04
83 W*s, 27 sec period, 3.11 W peak
3.11 [W] * 1 [J/s/W] * 1 /1.60219E-13 [J/MeV] * 1 / 201.2 [MeV/fission] *
0.38E-2 = 3.6661E8
```

A.3 DELBG Data Library

```
0.         0.                  0          0          0         18th232fbspec
0.00000+ 0 2.00000- 1          0          0          0          1th232fbspec
1.00000- 4 1.00000+ 9          0          0          0         15th232fbspec
7.92161-12 8.10645-10 2.57865-11 9.38046- 9 2.25982-10 3.25274- 8th232fbspec
2.23186- 9 1.52071- 7 1.18207- 8 7.07689- 7 2.59590- 8 2.78465- 6th232fbspec
1.54149- 7 1.56223- 5 9.78637- 7 7.02329- 5 3.69643- 6 3.26282- 4th232fbspec
1.50089- 5 1.17557- 3 5.86006- 5 6.48832- 3 2.95881- 4 2.89213- 2th232fbspec
5.34399- 4 1.26821- 1 1.76597- 3 5.26375- 1 8.43406- 4 2.59038+ 0th232fbspec
2.00000- 1 4.00000- 1          0          0          0          2th232fbspec
1.00000- 4 1.00000+ 9          0          0          0         15th232fbspec
1.34120-11 8.11286-10 1.93260-12 6.88811- 9 8.76906-11 3.19010- 8th232fbspec
2.90400- 9 1.72808- 7 1.76428- 8 7.05916- 7 3.70514- 8 3.80372- 6th232fbspec
4.85288- 7 1.61546- 5 2.08359- 6 6.98386- 5 8.97524- 6 3.18685- 4th232fbspec
3.46335- 5 1.15957- 3 1.17806- 4 6.39964- 3 5.02965- 4 2.76703- 2th232fbspec
9.58153- 4 1.29738- 1 2.08334- 3 5.24400- 1 1.53041- 3 2.45356+ 0th232fbspec
4.00000- 1 6.00000- 1          0          0          0          3th232fbspec
1.00000- 4 1.00000+ 9          0          0          0         15th232fbspec
6.44616-12 8.32287-10 2.42491-12 1.04579- 8 1.07215-10 3.15424- 8th232fbspec
3.23196- 9 1.70605- 7 2.22816- 8 8.02434- 7 2.04230- 7 8.11988- 6th232fbspec
1.05537- 6 2.83684- 5 5.42767- 6 1.51211- 4 3.29525- 5 6.86631- 4th232fbspec
9.64436- 5 3.17070- 3 5.60772- 4 1.49408- 2 1.29853- 3 5.77749- 2th232fbspec
3.68204- 3 2.90305- 1 3.69125- 3 1.11753+ 0 1.65290- 3 3.70739+ 0th232fbspec
6.00000- 1 8.00000- 1          0          0          0          4th232fbspec
1.00000- 4 1.00000+ 9          0          0          0         15th232fbspec
6.20476-12 7.57535-10 3.21104-11 2.08351- 8 1.47684-10 3.46992- 8th232fbspec
3.29651- 9 1.56348- 7 1.35674- 8 6.72308- 7 4.39679- 8 3.93225- 6th232fbspec
6.27323- 7 1.59047- 5 2.35485- 6 6.52343- 5 1.42110- 5 3.04138- 4th232fbspec
5.78029- 5 1.26129- 3 3.31651- 4 6.52122- 3 1.47663- 3 2.79401- 2th232fbspec
3.39198- 3 1.31679- 1 7.51382- 3 5.23696- 1 5.70872- 3 2.44287+ 0th232fbspec
8.00000- 1 1.00000+ 0          0          0          0          5th232fbspec
1.00000- 4 1.00000+ 9          0          0          0         14th232fbspec
7.91408-12 7.58739-10 2.11135-10 2.85623- 8 3.45645- 9 1.59295- 7th232fbspec
1.30972- 8 1.08296- 6 2.73705- 7 1.12365- 5 1.40731- 6 3.83178- 5th232fbspec
7.46346- 6 1.66781- 4 3.52646- 5 6.70003- 4 1.62228- 4 3.39610- 3th232fbspec
1.16420- 3 1.53374- 2 2.85006- 3 5.97041- 2 1.01310- 2 3.02691- 1th232fbspec
1.15732- 2 9.44020- 1 3.30285- 3 4.31872+ 0 0.00000+ 0 0.00000+ 0th232fbspec
1.00000+ 0 1.20000+ 0          0          0          0          6th232fbspec
1.00000- 4 1.00000+ 9          0          0          0         13th232fbspec
9.15494-12 7.82037-10 2.83514-10 2.94083- 8 2.60696- 9 1.66408- 7th232fbspec
6.79067- 9 1.12651- 6 4.53328- 7 1.63103- 5 2.83618- 6 6.28057- 5th232fbspec
1.74588- 5 3.13964- 4 6.02572- 5 1.30040- 3 4.39070- 4 6.65741- 3th232fbspec
2.49354- 3 2.69987- 2 6.26391- 3 1.34954- 1 1.51349- 2 5.11219- 1th232fbspec
1.17488- 2 2.39754+ 0 0.00000+ 0 0.00000+ 0 0.00000+ 0 0.00000+ 0th232fbspec
1.20000+ 0 1.40000+ 0          0          0          0          7th232fbspec
1.00000- 4 1.00000+ 9          0          0          0         14th232fbspec
9.14770-12 7.54972-10 3.08261-10 2.84629- 8 9.28243-10 1.51777- 7th232fbspec
1.93593- 9 6.93347- 7 4.32589- 9 3.43591- 6 4.81127- 7 1.91210- 5th232fbspec
2.78462- 6 6.40159- 5 1.87563- 5 3.24335- 4 5.87085- 5 1.31683- 3th232fbspec
5.51750- 4 7.04832- 3 2.78456- 3 2.82476- 2 8.06769- 3 1.35971- 1th232fbspec
1.90171- 2 5.29134- 1 1.48469- 2 2.42926+ 0 0.00000+ 0 0.00000+ 0th232fbspec
1.40000+ 0 1.60000+ 0          0          0          0          8th232fbspec
1.00000- 4 1.00000+ 9          0          0          0         14th232fbspec
8.23309-12 7.54628-10 3.31926-10 2.83582- 8 1.13058-10 1.85968- 7th232fbspec
1.02785- 9 7.30442- 7 2.53251- 9 3.46752- 6 4.59446- 7 1.98197- 5th232fbspec
2.59801- 6 6.31001- 5 1.88830- 5 3.35073- 4 5.90771- 5 1.33885- 3th232fbspec
5.75246- 4 7.14676- 3 3.26009- 3 2.89957- 2 1.35085- 2 1.34487- 1th232fbspec
2.37906- 2 5.20585- 1 1.88438- 2 2.43965+ 0 0.00000+ 0 0.00000+ 0th232fbspec
1.60000+ 0 1.80000+ 0          0          0          0          9th232fbspec
1.00000- 4 1.00000+ 9          0          0          0         14th232fbspec
6.28253-12 7.54498-10 3.33066-10 2.82503- 8 1.97478-10 4.49454- 7th232fbspec
```

```
6.91669-10 1.28401- 6 9.60714- 8 1.33237- 5 1.51021- 6 3.99242- 5th232fbspec
5.76851- 6 1.70322- 4 3.33456- 5 6.23638- 4 1.72850- 4 3.40012- 3th232fbspec
1.78554- 3 1.57896- 2 5.21382- 3 6.32599- 2 2.09884- 2 2.97515- 1th232fbspec
2.35308- 2 1.13180+ 0 1.02728- 2 4.11689+ 0 0.00000+ 0 0.00000+ 0th232fbspec
1.80000+ 0 2.00000+ 0          0          0          0         10th232fbspec
1.00000- 4 1.00000+ 9          0          0          0         14th232fbspec
3.68225-12 7.53960-10 3.07736-10 2.81232- 8 1.01174-11 9.59571- 8th232fbspec
2.14856-10 7.22142- 7 6.39273-10 3.35811- 6 3.84889- 7 2.17709- 5th232fbspec
1.91915- 6 6.04550- 5 1.61562- 5 3.55468- 4 5.61923- 5 1.41974- 3th232fbspec
5.45273- 4 7.24547- 3 3.02465- 3 2.84523- 2 1.14972- 2 1.39881- 1th232fbspec
2.89920- 2 5.38448- 1 2.32635- 2 2.41525+ 0 0.00000+ 0 0.00000+ 0th232fbspec
2.00000+ 0 2.20000+ 0          0          0          0         11th232fbspec
1.00000- 4 1.00000+ 9          0          0          0         13th232fbspec
1.27035-12 7.51364-10 2.61106-10 2.80093- 8 1.34688-11 1.27533- 7th232fbspec
3.10046-10 3.46464- 6 3.05508- 7 2.16860- 5 1.67952- 6 5.99195- 5th232fbspec
1.41178- 5 3.69828- 4 5.53904- 5 1.45401- 3 5.14196- 4 7.32210- 3th232fbspec
3.01579- 3 2.81486- 2 1.16559- 2 1.42010- 1 3.16708- 2 5.34933- 1th232fbspec
2.49992- 2 2.42955+ 0 0.00000+ 0 0.00000+ 0 0.00000+ 0 0.00000+ 0th232fbspec
2.20000+ 0 2.40000+ 0          0          0          0         12th232fbspec
1.00000- 4 1.00000+ 9          0          0          0         12th232fbspec
2.06634-13 7.33413-10 2.04217-10 2.83768- 8 8.34988- 8 1.67315- 5th232fbspec
1.27563- 6 4.69102- 5 4.94683- 6 2.52415- 4 2.47698- 5 7.11389- 4th232fbspec
1.51195- 4 3.44696- 3 1.64317- 3 1.57179- 2 5.57414- 3 6.60622- 2th232fbspec
2.49187- 2 2.99347- 1 3.08072- 2 1.12797+ 0 1.29786- 2 4.10383+ 0th232fbspec
2.40000+ 0 2.60000+ 0          0          0          0         13th232fbspec
1.00000- 4 1.00000+ 9          0          0          0         14th232fbspec
1.63432-13 7.30686-10 1.22881-10 2.78871- 8 4.30479-12 5.46050- 8th232fbspec
2.07705-13 1.59558- 7 2.57020- 9 9.36413- 6 1.66908- 7 2.50260- 5th232fbspec
1.31070- 6 5.93121- 5 1.03501- 5 3.81050- 4 5.01222- 5 1.45046- 3th232fbspec
4.84052- 4 7.42672- 3 2.80201- 3 2.86980- 2 1.19783- 2 1.41481- 1th232fbspec
3.41740- 2 5.51528- 1 2.70608- 2 2.40091+ 0 0.00000+ 0 0.00000+ 0th232fbspec
2.60000+ 0 3.00000+ 0          0          0          0         14th232fbspec
1.00000- 4 1.00000+ 9          0          0          0         14th232fbspec
2.90226-13 7.28872-10 6.31896-11 2.77361- 8 2.94039-12 4.99039- 8th232fbspec
3.03238-12 7.21362- 7 1.54501- 9 7.98629- 6 2.15660- 7 3.06095- 5th232fbspec
2.34609- 6 6.12122- 5 1.61753- 5 4.02867- 4 8.63609- 5 1.41097- 3th232fbspec
8.70871- 4 7.32377- 3 5.13938- 3 2.86508- 2 2.34655- 2 1.40391- 1th232fbspec
6.74511- 2 5.53764- 1 5.54707- 2 2.38135+ 0 0.00000+ 0 0.00000+ 0th232fbspec
3.00000+ 0 4.00000+ 0          0          0          0         15th232fbspec
1.00000- 4 1.00000+ 9          0          0          0         14th232fbspec
4.40691-13 7.09668-10 5.74331-13 3.14857- 8 1.09206-12 4.81242- 7th232fbspec
9.42799-11 4.06805- 6 3.38701- 9 1.17246- 5 3.02253- 6 5.92383- 5th232fbspec
1.49036- 6 1.15574- 4 2.26916- 5 4.83210- 4 1.19450- 4 1.52995- 3th232fbspec
1.65516- 3 7.61374- 3 9.17519- 3 3.00103- 2 5.28998- 2 1.40075- 1th232fbspec
1.50527- 1 5.76311- 1 1.24074- 1 2.39106+ 0 0.00000+ 0 0.00000+ 0th232fbspec
4.00000+ 0 5.00000+ 0          0          0          0         16th232fbspec
1.00000- 4 1.00000+ 9          0          0          0         13th232fbspec
1.47587-13 7.28451-10 1.54348-13 2.43216- 7 8.08280-12 2.91218- 6th232fbspec
5.61319-10 1.21132- 5 1.40084- 6 6.75316- 5 1.49774- 7 1.85009- 4th232fbspec
3.59128- 6 7.29777- 4 2.42133- 4 4.57107- 3 1.86588- 3 1.51604- 2th232fbspec
1.82167- 2 7.76286- 2 6.43731- 2 2.84478- 1 9.95626- 2 1.07614+ 0th232fbspec
3.69016- 2 4.13747+ 0 0.00000+ 0 0.00000+ 0 0.00000+ 0 0.00000+ 0th232fbspec
5.00000+ 0 6.00000+ 0          0          0          0         17th232fbspec
1.00000- 4 1.00000+ 9          0          0          0         11th232fbspec
3.59767-14 6.95954-10 2.19063-14 5.25112- 7 1.91173-11 8.16812- 6th232fbspec
2.00699-10 1.69832- 5 3.00407- 8 7.00782- 5 2.19975- 5 3.41292- 3th232fbspec
2.39389- 4 8.58255- 3 2.34891- 3 3.69276- 2 2.41358- 2 1.41695- 1th232fbspec
4.11626- 2 6.26056- 1 2.79714- 2 2.42923+ 0 0.00000+ 0 0.00000+ 0th232fbspec
6.00000+ 0 7.50000+ 0          0          0          0         18th232fbspec
1.00000- 4 1.00000+ 9          0          0          0         11th232fbspec
2.01035-15 6.96410-10 6.34797-15 6.53960- 7 9.31236-11 1.29783- 5th232fbspec
4.68632- 8 1.36045- 3 3.74596- 6 5.27545- 3 2.37788- 4 2.08097- 2th232fbspec
4.14827- 3 7.97422- 2 1.18222- 2 2.66976- 1 1.62365- 2 1.64323+ 0th232fbspec
```

```
-7.64753-11 1.34817- 5 1.15723-11 7.64327- 5 0.00000+ 0 0.00000+ 0th232fbspec
 0.         0.                  0          0          0         19th232fgspec
 0.00000+ 0 1.00000- 1          0          0          0          1th232fgspec
 1.00000- 4 1.00000+ 9          0          0          0         16th232fgspec
 1.12074-13 7.18694-10 5.90589-13 1.34487- 8 1.25728-11 3.13363- 8th232fgspec
 1.83479-10 2.83788- 7 2.83375- 9 9.13999- 7 7.39889- 9 2.91151- 6th232fgspec
 8.23612- 9 8.16273- 6 5.85492- 8 9.86918- 5 6.06404- 7 3.36840- 4th232fgspec
 3.31753- 6 1.33308- 3 6.23954- 5 8.33216- 3 1.68474- 4 2.61585- 2th232fgspec
 1.71939- 4 1.40873- 1 1.75836- 3 6.11075- 1 3.94682- 4 2.61336+ 0th232fgspec
 3.34632- 5 9.50232+ 0 0.00000+ 0 0.00000+ 0 0.00000+ 0 0.00000+ 0th232fgspec
 1.00000- 1 2.00000- 1          0          0          0          2th232fgspec
 1.00000- 4 1.00000+ 9          0          0          0         15th232fgspec
 1.53640-14 5.56759- 9 4.88438-12 2.04697- 8 3.38121-11 3.32284- 8th232fgspec
 1.37917- 9 2.57237- 7 1.04056- 9 9.57658- 7 1.34038- 8 3.31072- 6th232fgspec
 5.14061- 7 5.43383- 5 1.61294- 6 1.99243- 4 7.49553- 6 6.54811- 4th232fgspec
 1.65432- 5 2.80010- 3 2.09308- 4 1.72168- 2 2.67175- 3 7.45528- 2th232fgspec
 7.95545- 3 3.28683- 1 3.29248- 2 1.18417+ 0 1.23917- 2 3.73698+ 0th232fgspec
 2.00000- 1 4.00000- 1          0          0          0          3th232fgspec
 1.00000- 4 1.00000+ 9          0          0          0         15th232fgspec
 2.83322-16 2.58801- 9 2.70677-14 8.16064- 9 4.39267-12 1.26259- 7th232fgspec
 6.25613- 9 6.54976- 7 1.49104- 8 1.72227- 6 9.87049- 8 6.96019- 6th232fgspec
 3.58301- 7 1.89826- 5 4.20299- 5 6.71607- 4 1.83203- 4 4.65961- 3th232fgspec
 2.74808- 3 2.30177- 2 1.29751- 2 1.13291- 1 5.00162- 2 4.54163- 1th232fgspec
 6.36601- 2 2.10074+ 0 1.08579- 5 1.04523- 4-9.50177- 6 9.64993- 5th232fgspec
 4.00000- 1 6.00000- 1          0          0          0          4th232fgspec
 1.00000- 4 1.00000+ 9          0          0          0         16th232fgspec
 5.98983-14 2.26019- 9 9.01548-13 1.00284- 8 2.84600-12 5.73958- 8th232fgspec
 7.63890-10 3.04142- 7 2.81719- 8 6.82579- 7 2.03930- 8 5.55607- 6th232fgspec
 4.07671- 7 1.27199- 5 8.63759- 7 3.18570- 5 1.27235- 5 2.04461- 4th232fgspec
 2.96338- 5 5.78749- 4 2.11241- 4 2.95357- 3 1.38993- 3 1.75609- 2th232fgspec
 1.06262- 2 7.60209- 2 2.26647- 2 2.74215- 1 3.51192- 2 1.15496+ 0th232fgspec
 1.24647- 2 3.78824+ 0 0.00000+ 0 0.00000+ 0 0.00000+ 0 0.00000+ 0th232fgspec
 6.00000- 1 8.00000- 1          0          0          0          5th232fgspec
 1.00000- 4 1.00000+ 9          0          0          0         16th232fgspec
 2.70039-11 7.24978-10 4.75513-12 1.04700- 8 1.72118- 9 1.18769- 7th232fgspec
 1.12973- 8 1.18059- 7 1.70794- 7 2.91145- 6 1.14929- 6 1.39622- 5th232fgspec
 5.65898- 7 7.89218- 5 1.33856- 5 1.93282- 4 3.38206- 5 7.01671- 4th232fgspec
 2.47808- 4 3.28947- 3 2.49420- 3 1.71773- 2 9.71779- 3 6.02584- 2th232fgspec
 3.51866- 2 2.73408- 1 7.73143- 2 1.16289+ 0 3.46509- 2 3.68742+ 0th232fgspec
-6.09811- 9 2.47964- 7 0.00000+ 0 0.00000+ 0 0.00000+ 0 0.00000+ 0th232fgspec
 8.00000- 1 1.00000+ 0          0          0          0          6th232fgspec
 1.00000- 4 1.00000+ 9          0          0          0         16th232fgspec
 5.37033-18 4.45592-12 5.94000-14 2.27632- 8 5.12210-14 3.71542- 8th232fgspec
 8.59244- 9 5.56814- 7 1.29530- 8 7.82592- 7 1.38261- 8 2.81102- 6th232fgspec
 4.99841- 7 2.58848- 5 7.20642- 6 8.97732- 5 3.46066- 5 2.29935- 4th232fgspec
 1.55225- 4 1.43325- 3 4.69124- 4 6.07439- 3 2.88833- 3 3.06729- 2th232fgspec
 1.38718- 2 1.49137- 1 4.21688- 2 5.46078- 1 6.72722- 2 2.70343+ 0th232fgspec
 3.84105- 3 8.31886+ 0 0.00000+ 0 0.00000+ 0 0.00000+ 0 0.00000+ 0th232fgspec
 1.00000+ 0 1.20000+ 0          0          0          0          7th232fgspec
 1.00000- 4 1.00000+ 9          0          0          0         15th232fgspec
 3.42513-18 8.78590-12 2.02430-13 2.17950- 8 1.97728-11 4.01660- 7th232fgspec
 3.82171-10 8.69960- 7 8.59025- 9 3.10110- 6 3.06570- 7 1.62550- 5th232fgspec

 1.17075- 6 3.10550- 5 1.15609- 5 1.88970- 4 7.51544- 5 7.07270- 4th232fgspec
 1.21742- 4 3.01960- 3 1.20335- 3 1.67410- 2 4.31741- 3 5.93570- 2th232fgspec
 1.55556- 2 3.21580- 1 1.41238- 2 8.98890- 1 1.81833- 3 5.71790+ 0th232fgspec
 1.20000+ 0 1.40000+ 0          0          0          0          8th232fgspec
 1.00000- 4 1.00000+ 9          0          0          0         16th232fgspec
 1.34931-18 8.96519-12 1.56499-13 2.71494- 8 1.02779-12 7.79100- 8th232fgspec
 3.90005-11 1.47067- 7 9.18706- 9 2.25374- 6 7.48991- 9 3.46498- 6th232fgspec
 8.20491- 8 1.29191- 5 3.24166- 6 4.70424- 5 6.32670- 6 1.09066- 4th232fgspec
 8.37572- 5 7.73802- 4 1.42356- 4 3.25868- 3 2.29438- 3 1.33036- 2th232fgspec
 4.90054- 3 6.06006- 2 3.45666- 2 3.32154- 1 2.41410- 2 1.08573+ 0th232fgspec
```

```
 5.84137- 3 4.01484+ 0 0.00000+ 0 0.00000+ 0 0.00000+ 0 0.00000+ 0th232fgspec
 1.40000+ 0 1.60000+ 0          0          0          0          9th232fgspec
 1.00000- 4 1.00000+ 9          0          0          0         17th232fgspec
 1.38561-18 8.64588-12 8.85365-12 2.80029- 8 3.52472-13 3.82140- 8th232fgspec
 8.71319- 8 6.30486- 7 2.18257- 6 6.57352- 5 6.24083- 5 3.65841- 4th232fgspec
 3.49765- 3 1.23956- 2 1.92149- 3 6.17180- 2 2.98481- 2 3.14989- 1th232fgspec
 2.18192- 2 9.21496- 1 2.49899- 2 2.96426+ 0-4.21985- 3 6.24252+ 0th232fgspec
-5.00879- 5 9.29309- 4 1.29785- 4 3.56872- 3-2.96005- 9 7.83323- 7th232fgspec
-9.75149- 8 5.23463- 6 2.04281- 7 1.90226- 5 0.00000+ 0 0.00000+ 0th232fgspec
 1.60000+ 0 1.80000+ 0          0          0          0         10th232fgspec
 1.00000- 4 1.00000+ 9          0          0          0         14th232fgspec
 2.29524-19 6.95138-12 1.14202-14 2.18006- 8 1.50108-13 6.41371- 7th232fgspec
 8.92326-10 2.47337- 6 1.55168- 8 1.13838- 5 6.09159- 7 2.92168- 5th232fgspec
 2.12615- 6 1.17143- 4 6.24842- 6 3.30163- 4 5.62826- 5 1.23776- 3th232fgspec
 3.15267- 4 7.41624- 3 9.03997- 4 2.48009- 2 2.80425- 3 1.29973- 1th232fgspec
 9.75772- 3 5.54920- 1 1.90892- 3 2.79408+ 0 0.00000+ 0 0.00000+ 0th232fgspec
 1.80000+ 0 2.00000+ 0          0          0          0         11th232fgspec
 1.00000- 4 1.00000+ 9          0          0          0         14th232fgspec
 1.66428-19 5.94237-12 7.02912-15 2.18008- 8 7.21969-11 6.18274- 7th232fgspec
 4.58110-10 1.82939- 6 1.71977- 9 3.12332- 6 9.35806- 8 2.23714- 5th232fgspec
 3.81965- 6 7.85481- 5 8.47786- 6 3.01017- 4 2.67124- 5 1.20409- 3th232fgspec
 5.41151- 4 9.69030- 3 7.08026- 4 2.32335- 2 5.28654- 3 1.66567- 1th232fgspec
 1.37538- 2 6.13021- 1 2.71695- 2 2.22047+ 0 0.00000+ 0 0.00000+ 0th232fgspec
 2.00000+ 0 2.20000+ 0          0          0          0         12th232fgspec
 1.00000- 4 1.00000+ 9          0          0          0         12th232fgspec
 2.04059-11 2.76219- 8 1.35714-11 2.98631- 8 2.17382- 9 2.36353- 6th232fgspec
 3.65231- 8 2.01755- 5 4.54698- 6 7.80272- 5 1.37394- 5 3.78041- 4th232fgspec
 5.57309- 5 9.91065- 4 4.66762- 4 1.08657- 2 7.51541- 4 2.98035- 2th232fgspec
 2.03985- 3 1.42126- 1 1.14675- 2 5.69732- 1 1.27391- 2 2.30358+ 0th232fgspec
 2.20000+ 0 2.40000+ 0          0          0          0         13th232fgspec
 1.00000- 4 1.00000+ 9          0          0          0         13th232fgspec
 9.69362-15 2.17890- 8 7.18160-21 1.66410- 8 8.71606-12 4.85780- 7th232fgspec
 1.15935- 9 6.35260- 7 2.42180-12 1.17824- 5 4.43166- 6 6.55140- 5th232fgspec
 6.11851- 6 1.40780- 4 1.48580- 5 3.95350- 4 1.33554- 4 6.17110- 3th232fgspec
 7.34261- 4 1.33120- 2 1.18132- 2 3.53760- 1 1.98726- 2 1.60931+ 0th232fgspec
-3.87540- 3 4.24433- 1 0.00000+ 0 0.00000+ 0 0.00000+ 0 0.00000+ 0th232fgspec
 2.40000+ 0 2.60000+ 0          0          0          0         14th232fgspec
 1.00000- 4 1.00000+ 9          0          0          0         16th232fgspec
 5.02375-15 2.17885- 8 9.44113-12 5.08872- 7 5.41742- 9 6.29349- 7th232fgspec
 2.84512- 6 1.04864- 4 6.51087- 6 1.99327- 4 3.32675- 5 8.13479- 4th232fgspec
 6.32677- 4 1.09583- 2 4.93985- 4 3.23540- 2 1.55429- 3 1.15284- 1th232fgspec
 5.01622- 3 5.22610- 1 6.81582- 3 2.54134+ 0-8.38483- 4 3.06557+ 0th232fgspec
-1.55413-10 6.70447- 7-3.44764-10 1.83228- 6 1.00066- 6 1.00894- 5th232fgspec
-9.90588- 7 9.97965- 6 0.00000+ 0 0.00000+ 0 0.00000+ 0 0.00000+ 0th232fgspec
 2.60000+ 0 3.00000+ 0          0          0          0         15th232fgspec
 1.00000- 4 1.00000+ 9          0          0          0         17th232fgspec
 3.72673-15 2.21802- 8 9.67141-15 2.94158- 8 2.95214-10 7.15093- 7th232fgspec
 6.99939- 7 7.51846- 5 6.14830- 6 1.89261- 4 1.57593- 5 6.38825- 4th232fgspec
 1.74366- 4 4.05973- 3 1.50109- 3 1.27423- 2 3.23521- 3 9.58123- 2th232fgspec
 7.98943- 3 3.40147- 1 5.96169- 3 7.44311- 1 7.87824- 4 2.06916+ 1th232fgspec
-4.29278-10 9.05688- 7 2.83474-10 1.13206- 6-9.14035-11 2.51750- 6th232fgspec
 3.00002- 5 1.00000- 5-3.00000- 5 1.00000- 5 0.00000+ 0 0.00000+ 0th232fgspec
 3.00000+ 0 4.00000+ 0          0          0          0         16th232fgspec
 1.00000- 4 1.00000+ 9          0          0          0         17th232fgspec
 7.16649-16 2.17886- 8 6.58884-22 1.18021- 8 3.31748-13 4.33768- 7th232fgspec
 5.24950-11 6.50396- 7 4.28551- 7 8.19749- 5 3.54354- 6 1.51556- 4th232fgspec
 1.51818- 5 4.90882- 4 7.03126- 5 1.88441- 3 8.22745- 4 7.73975- 3th232fgspec
 2.62499- 3 2.72537- 2 1.46004- 2 1.54232- 1 1.87644- 2 5.07525- 1th232fgspec
-2.34956- 3 1.71117+ 0 1.51924- 3 6.49008+ 0-1.03501-11 9.92681- 7th232fgspec
-5.72502-11 5.91667- 6 1.67851-10 1.69655- 5 0.00000+ 0 0.00000+ 0th232fgspec
 4.00000+ 0 5.00000+ 0          0          0          0         17th232fgspec
 1.00000- 4 1.00000+ 9          0          0          0         10th232fgspec
 4.01071-18 4.26508- 6 4.46539- 8 6.78069- 5 2.28752- 8 1.30458- 4th232fgspec
```

```
 2.99508- 7 4.05757- 4 8.11377- 5 3.49744- 3 4.99993- 4 8.48032- 3th232fgspec
 1.79595- 3 3.39318- 2 2.40236- 3 1.24410- 1 4.98964- 3 4.79752- 1th232fgspec
 1.01058- 2 6.07123+ 0 0.00000+ 0 0.00000+ 0 0.00000+ 0 0.00000+ 0th232fgspec
 5.00000+ 0 6.00000+ 0          0          0          0         18th232fgspec
 1.00000- 4 1.00000+ 6          0          0          0         12th232fgspec
 4.81688-19 4.14055- 6 6.32049-21 8.04922- 6 1.83910-15 2.06283- 4th232fgspec
 3.37725-13 6.75621- 4 1.34579- 6 3.18090- 3 3.76265- 5 5.45079- 3th232fgspec
 5.29410- 4 1.37075- 2 8.42440- 4 8.09651- 2 7.69510- 4 1.57389- 1th232fgspec
-5.86237- 4 3.86877- 1 7.79720- 4 4.22563+ 0-4.06474- 4 6.09487+ 0th232fgspec
 6.00000+ 0 7.50000+ 0          0          0          0         19th232fgspec
 1.00000- 4 1.00000+ 9          0          0          0         11th232fgspec
 6.67726-20 4.27179- 6 2.88261-17 5.33528- 4 4.17184- 9 4.87267- 3th232fgspec
 2.08511- 5 8.81261- 3 6.74140- 5 1.53925- 2 1.87976- 4 1.49833- 1th232fgspec
-7.61451- 5 5.07670- 1 1.05597- 4 4.65028+ 0-5.28495- 5 7.68267+ 0th232fgspec
-2.93711- 5 2.50833- 2-6.53965-21 6.84435- 6 0.00000+ 0 0.00000+ 0th232fgspec
 0.         0.          0          0          0         18 u233tbspec
 0.00000+ 0 2.00000- 1          0          0          0          1 u233tbspec
 1.00000- 4 1.00000+ 9          0          0          0         15 u233tbspec
 7.26401-12 7.83710-10 1.59424-11 9.33945- 9 1.50755-10 3.35917- 8 u233tbspec
 2.33134- 9 1.47865- 7 1.31390- 8 7.55297- 7 3.85399- 8 2.71908- 6 u233tbspec
 1.55267- 7 1.51771- 5 8.49991- 7 6.88788- 5 3.55074- 6 3.28256- 4 u233tbspec
 1.22193- 5 1.14958- 3 4.14751- 5 6.47445- 3 1.32851- 4 2.72571- 2 u233tbspec
 1.85912- 4 1.14152- 1 3.40443- 4 5.33765- 1 8.49766- 5 2.53972+ 0 u233tbspec
 2.00000- 1 4.00000- 1          0          0          0          2 u233tbspec
 1.00000- 4 1.00000+ 9          0          0          0         15 u233tbspec
 1.21576-11 7.83925-10 1.40286-12 7.16382- 9 6.45029-11 3.38198- 8 u233tbspec
 2.53469- 9 1.67492- 7 1.68278- 8 6.91469- 7 4.64220- 8 3.23310- 6 u233tbspec
 4.83394- 7 1.51995- 5 1.76440- 6 6.82600- 5 8.99146- 6 3.26948- 4 u233tbspec
 3.09255- 5 1.12140- 3 7.92588- 5 6.39859- 3 2.60819- 4 2.69556- 2 u233tbspec
 4.23061- 4 1.19489- 1 6.33964- 4 5.13562- 1 1.64304- 4 2.51705+ 0 u233tbspec
 4.00000- 1 6.00000- 1          0          0          0          3 u233tbspec
 1.00000- 4 1.00000+ 9          0          0          0         15 u233tbspec
 5.61714-12 8.04167-10 1.73224-12 8.67818- 9 7.20839-11 3.26551- 8 u233tbspec
 2.44994- 9 1.59969- 7 1.60018- 8 6.78531- 7 5.73218- 8 3.53891- 6 u233tbspec
 6.33816- 7 1.51571- 5 1.77940- 6 6.54511- 5 1.28256- 5 3.22140- 4 u233tbspec
 4.56314- 5 1.15547- 3 1.49468- 4 6.42376- 3 5.07135- 4 2.70784- 2 u233tbspec
 9.06926- 4 1.20140- 1 1.38053- 3 5.11418- 1 3.64064- 4 2.50266+ 0 u233tbspec
 6.00000- 1 8.00000- 1          0          0          0          4 u233tbspec
 1.00000- 4 1.00000+ 9          0          0          0         15 u233tbspec
 5.62146-12 7.55211-10 2.06356-11 2.06648- 8 9.57107-11 3.53471- 8 u233tbspec
 2.87994- 9 1.56201- 7 1.19285- 8 6.76418- 7 5.49106- 8 3.60128- 6 u233tbspec
 6.29460- 7 1.51085- 5 2.09573- 6 6.36282- 5 1.48334- 5 3.17164- 4 u233tbspec
 5.24950- 5 1.18826- 3 2.21887- 4 6.49807- 3 7.87593- 4 2.71417- 2 u233tbspec
 1.52228- 3 1.21164- 1 2.36815- 3 5.11089- 1 6.37502- 4 2.48948+ 0 u233tbspec
 8.00000- 1 1.00000+ 0          0          0          0          5 u233tbspec
 1.00000- 4 1.00000+ 9          0          0          0         15 u233tbspec
 7.14512-12 7.53511-10 1.25480-10 2.80233- 8 2.50196- 9 1.46629- 7 u233tbspec
 4.26507- 9 5.38665- 7 1.13238- 8 1.70070- 6 1.92777- 7 8.32424- 6 u233tbspec
 1.23775- 6 3.23769- 5 6.63233- 6 1.57215- 4 3.71569- 5 6.63955- 4 u233tbspec
 1.12160- 4 3.19700- 3 6.85736- 4 1.45508- 2 1.56640- 3 6.00245- 2 u233tbspec
 3.38864- 3 2.82481- 1 4.07807- 3 9.81547- 1 2.66240- 4 6.67676+ 0 u233tbspec
 1.00000+ 0 1.20000+ 0          0          0          0          6 u233tbspec
 1.00000- 4 1.00000+ 9          0          0          0         15 u233tbspec
 8.07794-12 7.54086-10 1.58945-10 2.79570- 8 1.81453- 9 1.46123- 7 u233tbspec
 2.21395- 9 5.22402- 7 5.47835- 9 1.57024- 6 1.38709- 7 9.26366- 6 u233tbspec
 1.31562- 6 3.44827- 5 6.66742- 6 1.58254- 4 3.55832- 5 6.53518- 4 u233tbspec
 1.21770- 4 3.23220- 3 8.33875- 4 1.47600- 2 2.00013- 3 6.09450- 2 u233tbspec
 4.34270- 3 2.78556- 1 2.86357- 3 9.64502- 1 5.15080- 4 4.17890+ 0 u233tbspec
 1.20000+ 0 1.40000+ 0          0          0          0          7 u233tbspec
 1.00000- 4 1.00000+ 9          0          0          0         15 u233tbspec
 8.25097-12 7.54228-10 1.85029-10 2.78913- 8 7.53881-10 1.44424- 7 u233tbspec
 9.39834-10 5.23862- 7 2.90868- 9 1.59538- 6 1.17365- 7 1.06076- 5 u233tbspec
 1.36331- 6 3.62256- 5 6.20565- 6 1.60074- 4 3.53795- 5 6.52653- 4 u233tbspec
```

```
1.25280- 4 3.22044- 3 9.39234- 4 1.49554- 2 2.38237- 3 6.19066- 2 u233tbspec
5.43357- 3 2.79293- 1 3.66311- 3 9.68566- 1 6.60314- 4 4.16000+ 0 u233tbspec
1.40000+ 0 1.60000+ 0          0          0          0          8 u233tbspec
1.00000- 4 1.00000+ 9          0          0          0         15 u233tbspec
7.42944-12 7.54104-10 1.99459-10 2.77909- 8 4.74246-11 1.14714- 7 u233tbspec
4.17733-10 4.49504- 7 1.77260- 9 1.45703- 6 9.57663- 8 1.13021- 5 u233tbspec
1.36849- 6 3.71281- 5 5.39318- 6 1.62305- 4 3.57042- 5 6.56125- 4 u233tbspec
1.26102- 4 3.20018- 3 1.00507- 3 1.52131- 2 3.84553- 3 6.79796- 2 u233tbspec
7.27722- 3 2.61304- 1 4.14469- 3 9.85986- 1 8.71559- 4 4.07715+ 0 u233tbspec
1.60000+ 0 1.80000+ 0          0          0          0          9 u233tbspec
1.00000- 4 1.00000+ 9          0          0          0         15 u233tbspec
5.67378-12 7.53953-10 2.00177-10 2.76605- 8 9.44285-12 7.45876- 8 u233tbspec
2.40332-10 5.12201- 7 1.07043- 9 1.63034- 6 8.34259- 8 1.23113- 5 u233tbspec
1.33341- 6 3.82889- 5 4.45963- 6 1.68554- 4 3.45146- 5 6.63569- 4 u233tbspec
1.24439- 4 3.18516- 3 9.96280- 4 1.53376- 2 2.88917- 3 6.43055- 2 u233tbspec
7.21555- 3 2.80674- 1 5.18816- 3 9.77004- 1 9.39011- 4 4.12976+ 0 u233tbspec
1.80000+ 0 2.00000+ 0          0          0          0         10 u233tbspec
1.00000- 4 1.00000+ 9          0          0          0         15 u233tbspec
3.33468-12 7.53349-10 1.85670-10 2.75007- 8 1.03320-11 6.70965- 8 u233tbspec
8.35697-11 4.56612- 7 4.59296-10 1.48781- 6 7.92298- 8 1.38584- 5 u233tbspec
1.26611- 6 3.98694- 5 3.59759- 6 1.83330- 4 3.23660- 5 6.79237- 4 u233tbspec
1.21138- 4 3.18810- 3 9.63530- 4 1.54272- 2 3.00316- 3 6.56295- 2 u233tbspec
7.77632- 3 2.80982- 1 5.85246- 3 9.80666- 1 1.06034- 3 4.12005+ 0 u233tbspec
2.00000+ 0 2.20000+ 0          0          0          0         11 u233tbspec
1.00000- 4 1.00000+ 9          0          0          0         13 u233tbspec
1.17526-12 7.60460-10 1.62526-10 2.76672- 8 2.61286-11 2.77722- 7 u233tbspec
3.68905-10 3.47790- 6 2.89568- 7 2.15059- 5 1.36053- 6 5.71379- 5 u233tbspec
1.17954- 5 4.03393- 4 5.30105- 5 1.34412- 3 2.98951- 4 6.83848- 3 u233tbspec
1.53502- 3 2.73152- 2 5.23798- 3 1.28686- 1 9.47050- 3 5.21444- 1 u233tbspec
3.09997- 3 2.26784+ 0 0.00000+ 0 0.00000+ 0 0.00000+ 0 0.00000+ 0 u233tbspec
2.20000+ 0 2.40000+ 0          0          0          0         12 u233tbspec
1.00000- 4 1.00000+ 9          0          0          0         13 u233tbspec
2.09602-13 7.39228-10 8.66861-11 2.60617- 8 4.10612-11 3.34556- 8 u233tbspec
4.28069-11 1.70972- 6 7.82777- 8 1.67729- 5 1.12604- 6 4.56223- 5 u233tbspec
1.50258- 5 4.59804- 4 6.79343- 5 1.80439- 3 6.89591- 4 1.16194- 2 u233tbspec
2.65703- 3 5.29176- 2 8.87867- 3 2.65120- 1 5.85367- 3 9.12129- 1 u233tbspec
2.05553- 3 2.04056+ 0 0.00000+ 0 0.00000+ 0 0.00000+ 0 0.00000+ 0 u233tbspec
2.40000+ 0 2.60000+ 0          0          0          0         13 u233tbspec
1.00000- 4 1.00000+ 9          0          0          0         14 u233tbspec
1.67570-13 7.24407-10 5.27999-11 2.56017- 8 2.84269-11 3.30188- 8 u233tbspec
1.45427-11 9.54833- 7 1.16981- 9 8.31958- 6 1.35861- 7 2.35154- 5 u233tbspec
1.06025- 6 5.59809- 5 9.42161- 6 4.45160- 4 4.58596- 5 1.33655- 3 u233tbspec
2.78432- 4 6.73799- 3 1.36427- 3 2.73085- 2 5.30681- 3 1.26043- 1 u233tbspec
9.59059- 3 5.46420- 1 3.57099- 3 1.95512+ 0 0.00000+ 0 0.00000+ 0 u233tbspec
2.60000+ 0 3.00000+ 0          0          0          0         14 u233tbspec
1.00000- 4 1.00000+ 9          0          0          0         14 u233tbspec
2.97291-13 7.21985-10 3.40583-11 2.47863- 8 1.39413-11 3.78757- 8 u233tbspec
1.37359-11 6.27286- 7 5.17522-10 6.60550- 6 1.52074- 7 2.88617- 5 u233tbspec
1.80954- 6 5.73200- 5 1.84225- 5 4.94790- 4 7.64660- 5 1.36796- 3 u233tbspec
4.23677- 4 6.27073- 3 2.50693- 3 2.55982- 2 1.00919- 2 1.25053- 1 u233tbspec
1.83379- 2 5.44340- 1 7.67139- 3 2.04980+ 0 0.00000+ 0 0.00000+ 0 u233tbspec
3.00000+ 0 4.00000+ 0          0          0          0         15 u233tbspec
1.00000- 4 1.00000+ 9          0          0          0         15 u233tbspec
4.61071-13 7.28596-10 2.53154-12 2.20446- 8 5.58685-12 1.87795- 7 u233tbspec
2.74227-12 3.25703- 7 3.37885-11 2.23912- 6 1.90076- 9 1.07966- 5 u233tbspec
2.33013- 6 5.81855- 5 1.97273- 6 1.61607- 4 6.48900- 5 7.74363- 4 u233tbspec
3.14097- 4 3.49842- 3 2.48667- 3 1.51740- 2 1.21131- 2 7.14763- 2 u233tbspec
2.73726- 2 2.67911- 1 3.59099- 2 9.97722- 1 6.01837- 3 4.05774+ 0 u233tbspec
4.00000+ 0 5.00000+ 0          0          0          0         16 u233tbspec
1.00000- 4 1.00000+ 9          0          0          0         13 u233tbspec
1.49630-13 7.09818-10 1.73179-12 2.21273- 7 5.22164-12 1.41441- 6 u233tbspec
2.22447-10 8.60667- 6 1.20692- 8 3.21132- 5 1.09214- 6 7.15610- 5 u233tbspec
5.48780- 6 7.81072- 4 1.43548- 4 4.30767- 3 8.14548- 4 1.43983- 2 u233tbspec
```

```
8.23262- 3 8.10022- 2 1.93520- 2 2.56918- 1 2.29639- 2 1.04156+ 0 u233tbspec
3.29470- 3 3.10829+ 0 0.00000+ 0 0.00000+ 0 0.00000+ 0 0.00000+ 0 u233tbspec
5.00000+ 0 6.00000+ 0          0          0          0         17 u233tbspec
1.00000- 4 1.00000+ 9          0          0          0         13 u233tbspec
3.75094-14 7.13916-10 4.07177-13 4.85749- 7 3.49991-13 1.01794- 6 u233tbspec
1.22478-10 1.13634- 5 1.92931- 8 6.58659- 5 1.63622- 9 9.41151- 5 u233tbspec
3.91390- 7 1.31521- 3 4.70814- 5 4.61523- 3 2.22625- 4 1.56052- 2 u233tbspec
5.26191- 3 8.57377- 2 8.99434- 3 2.43621- 1 9.97814- 3 1.04008+ 0 u233tbspec
1.23569- 3 4.38219+ 0 0.00000+ 0 0.00000+ 0 0.00000+ 0 0.00000+ 0 u233tbspec
6.00000+ 0 7.50000+ 0          0          0          0         18 u233tbspec
1.00000- 4 1.00000+ 9          0          0          0         11 u233tbspec
2.08854-15 7.07352-10 2.13327-13 6.29001- 7 2.38926-11 1.25028- 5 u233tbspec
3.25657-11 6.76702- 5 6.03998- 9 9.52131- 4 2.71463- 7 2.36939- 3 u233tbspec
1.35415- 5 9.64958- 3 3.73173- 4 4.23097- 2 4.09848- 3 1.41688- 1 u233tbspec
2.98118- 3 6.98441- 1 1.33727- 3 2.15199+ 0 0.00000+ 0 0.00000+ 0 u233tbspec
0.         0.                  0          0          0         19 u233tgspec
0.00000+ 0 1.00000- 1          0          0          0          1 u233tgspec
1.00000- 4 1.00000+ 9          0          0          0         15 u233tgspec
1.36570-13 8.82010-10 3.33170-12 2.00440- 8 5.88530-12 4.67310- 8 u233tgspec
1.95650-10 2.88680- 7 5.07310- 9 1.13780- 6 2.92530-10 1.85210- 6 u233tgspec
3.51500- 8 5.44580- 5 7.96860- 8 1.42440- 4 7.02290- 7 7.00550- 4 u233tgspec
1.57550- 6 1.32850- 3 3.40050- 5 1.19620- 2 1.89290- 4 6.32460- 2 u233tgspec
1.70080- 4 4.49640- 1 1.01840- 4 1.77560+ 0 1.09480- 5 1.11080+ 1 u233tgspec
1.00000- 1 2.00000- 1          0          0          0          2 u233tgspec
1.00000- 4 1.00000+ 9          0          0          0         14 u233tgspec
6.65908-14 5.45030- 9 1.73765-11 2.71778- 8 9.78524-11 1.35174- 7 u233tgspec
1.37409- 9 2.97653- 7 1.52553- 8 2.52401- 6 9.77691- 9 5.11409- 6 u233tgspec
2.70048- 7 5.44434- 5 1.62361- 6 1.83796- 4 7.75519- 6 6.23794- 4 u233tgspec
1.38739- 5 2.70508- 3 1.34544- 4 1.50309- 2 1.15664- 3 6.83280- 2 u233tgspec
2.23894- 3 3.03962- 1 3.48683- 3 8.91446- 1 0.00000+ 0 0.00000+ 0 u233tgspec
2.00000- 1 4.00000- 1          0          0          0          3 u233tgspec
1.00000- 4 1.00000+ 9          0          0          0         15 u233tgspec
6.17211-14 7.53376- 9 2.26313-14 1.28519- 8 6.06240-12 1.27473- 7 u233tgspec
8.09133- 9 6.88191- 7 2.86366- 8 1.69360- 6 1.36545- 7 9.00944- 6 u233tgspec
3.36147- 7 1.68060- 5 1.05210- 5 2.68193- 4 5.21458- 5 9.21471- 4 u233tgspec
8.23863- 5 3.12884- 3 4.48561- 4 1.82399- 2 3.26027- 3 5.66480- 2 u233tgspec
8.40570- 3 3.12395- 1 8.53146- 3 9.87157- 1 2.87800- 3 2.95644+ 0 u233tgspec
4.00000- 1 6.00000- 1          0          0          0          4 u233tgspec
1.00000- 4 1.00000+ 9          0          0          0         15 u233tgspec
9.00296-14 3.06475- 9 2.63071-12 9.90187- 9 6.02216-12 2.80792- 8 u233tgspec
2.05205- 9 2.23755- 7 2.28693- 8 6.86792- 7 4.38186- 8 3.92085- 6 u233tgspec
7.24694- 7 1.44442- 5 1.56338- 6 6.21138- 5 2.21291- 5 3.12602- 4 u233tgspec
9.14588- 5 1.42260- 3 2.26280- 4 5.96055- 3 1.42942- 3 3.03240- 2 u233tgspec
1.07651- 2 1.24693- 1 1.47859- 2 4.77667- 1 1.80593- 3 3.62802+ 0 u233tgspec
6.00000- 1 8.00000- 1          0          0          0          5 u233tgspec
1.00000- 4 1.00000+ 9          0          0          0         14 u233tgspec
2.79662-11 7.30506-10 6.22245-12 1.14378- 8 1.66474- 8 1.21020- 7 u233tgspec
2.70155- 7 2.83572- 6 1.44728- 6 1.47083- 5 3.57627- 6 1.07868- 4 u233tgspec
2.17780- 5 2.81309- 4 7.60792- 5 1.45182- 3 3.59453- 4 6.49732- 3 u233tgspec
3.16513- 3 2.99936- 2 6.16395- 3 1.20170- 1 1.29189- 2 5.41803- 1 u233tgspec
6.77788- 3 2.18394+ 0-8.33763- 9 2.16658- 7 0.00000+ 0 0.00000+ 0 u233tgspec
8.00000- 1 1.00000+ 0          0          0          0          6 u233tgspec
1.00000- 4 1.00000+ 9          0          0          0         15 u233tgspec
1.09127-16 1.09908- 9 5.88281-14 1.41503- 8 2.64341-13 2.98962- 8 u233tgspec
6.59174- 9 5.50675- 7 1.35468- 8 7.75005- 7 3.25716- 8 3.00556- 6 u233tgspec
3.37314- 7 1.91392- 5 5.90085- 6 7.64028- 5 4.61597- 5 2.51564- 4 u233tgspec
1.49940- 4 1.40094- 3 2.86610- 4 5.33340- 3 1.41035- 3 3.27760- 2 u233tgspec

7.25785- 3 1.19635- 1 1.36059- 2 6.04210- 1 2.06457- 2 2.44918+ 0 u233tgspec
1.00000+ 0 1.20000+ 0          0          0          0          7 u233tgspec
1.00000- 4 1.00000+ 9          0          0          0         14 u233tgspec
7.88266-17 1.14745- 9 7.45993-13 1.94581- 8 5.04103-13 2.99656- 8 u233tgspec
1.35684-10 4.40006- 7 1.16746- 9 8.48079- 7 1.71713- 8 3.35582- 6 u233tgspec
```

```
 7.92878- 7 2.00180- 5 7.02745- 7 5.54314- 5 2.17826- 5 2.52140- 4 u233tgspec
 1.60481- 4 1.29853- 3 4.14926- 5 1.15362- 2 1.32116- 3 1.53926- 2 u233tgspec
 4.46261- 3 1.53627- 1 1.26069- 2 6.49242- 1 0.00000+ 0 0.00000+ 0 u233tgspec
 1.20000+ 0 1.40000+ 0          0          0          0          8 u233tgspec
 1.00000- 4 1.00000+ 9          0          0          0         15 u233tgspec
 2.54684-16 2.23394- 9 1.54457-14 1.27282- 8 2.79015-13 3.93521- 8 u233tgspec
 3.84998-11 1.48092- 7 9.74474-10 1.00463- 6 3.14804- 8 2.97521- 6 u233tgspec
 3.30713- 7 2.54799- 5 3.35840- 6 5.77770- 5 2.59908- 5 4.35314- 4 u233tgspec
 1.04290- 4 1.35716- 3 5.56609- 4 7.81315- 3 1.13081- 3 2.10988- 2 u233tgspec
 4.09899- 3 1.28962- 1 1.31757- 2 4.98350- 1 2.01049- 3 2.18424+ 0 u233tgspec
 1.40000+ 0 1.60000+ 0          0          0          0          9 u233tgspec
 1.00000- 4 1.00000+ 9          0          0          0         12 u233tgspec
 2.43514-17 1.09246- 9 5.26536-12 2.74073- 8 8.64922-11 3.28153- 7 u233tgspec
 7.22010- 8 6.30875- 7 1.54684- 6 3.33400- 5 3.96226- 5 2.55293- 4 u233tgspec
 4.53223- 4 4.24622- 3 2.05958- 3 2.17467- 2 2.43854- 3 1.74374- 1 u233tgspec
 6.75113- 3 4.60646- 1 6.45495- 3 2.30634+ 0-1.85321- 7 7.63958- 6 u233tgspec
 1.60000+ 0 1.80000+ 0          0          0          0         10 u233tgspec
 1.00000- 4 1.00000+ 9          0          0          0         14 u233tgspec
 1.12240-18 1.88850-11 6.81580-14 2.17920- 8 3.45860-14 1.39630- 7 u233tgspec
 6.89020-13 6.90660- 7 1.42030- 9 2.46660- 6 3.36480- 9 7.35380- 6 u233tgspec
 3.45210- 7 2.19490- 5 3.49520- 6 1.09850- 4 6.39130- 5 1.07980- 3 u233tgspec
 6.70920- 6 1.48930- 3 8.95660- 4 1.08330- 2 2.20900- 3 9.10600- 2 u233tgspec
 1.57970- 3 1.63230- 1 1.38670- 3 7.80110- 1 0.00000+ 0 0.00000+ 0 u233tgspec
 1.80000+ 0 2.00000+ 0          0          0          0         11 u233tgspec
 1.00000- 4 1.00000+ 9          0          0          0         14 u233tgspec
 8.07323-19 1.18830-11 4.12100-14 2.17959- 8 6.19056-11 5.92598- 7 u233tgspec
 5.22517-10 1.66109- 6 3.86579- 9 3.29230- 6 2.25524- 7 2.71831- 5 u233tgspec
 1.72717- 6 6.49869- 5 1.27861- 5 3.10169- 4 3.93215- 5 1.30210- 3 u233tgspec
 2.12693- 4 6.92156- 3 3.65354- 4 1.19662- 2 2.50214- 3 1.71711- 1 u233tgspec
 4.90346- 3 5.15061- 1 5.51717- 3 2.34919+ 0 0.00000+ 0 0.00000+ 0 u233tgspec
 2.00000+ 0 2.20000+ 0          0          0          0         12 u233tgspec
 1.00000- 4 1.00000+ 9          0          0          0         16 u233tgspec
 1.18216-12 2.46878- 8 1.92319-11 2.89070- 8 1.06345-10 9.12296- 7 u233tgspec
 4.30240- 9 2.60621- 6 4.15959- 9 1.15387- 5 3.64740- 7 5.39892- 5 u233tgspec
 3.44024- 6 1.09394- 4 8.22036- 6 4.67462- 4 5.82938- 5 1.05519- 3 u233tgspec
 1.14809- 3 1.27935- 2 1.75015- 3 4.55934- 1 2.86595- 3 2.10531+ 0 u233tgspec
-8.39491- 4 1.59275- 2 4.51161- 4 8.71447- 2 3.00000-14 1.00000- 9 u233tgspec
-3.00000-14 1.00000- 9 0.00000+ 0 0.00000+ 0 0.00000+ 0 0.00000+ 0 u233tgspec
 2.20000+ 0 2.40000+ 0          0          0          0         13 u233tgspec
 1.00000- 4 1.00000+ 9          0          0          0         13 u233tgspec
 5.62675-14 2.17886- 8 1.39481-13 2.74570- 7 9.41960-10 6.31750- 7 u233tgspec
 1.05384- 9 3.36012- 6 1.95504- 6 6.61373- 5 5.35174- 6 1.54683- 4 u233tgspec
 1.53592- 5 5.57690- 4 9.64040- 5 2.33376- 3 3.17356- 4 1.02334- 2 u233tgspec
 4.32592- 4 9.64437- 2 1.49890- 3 3.54448- 1 4.09210- 3 1.42984+ 0 u233tgspec
 5.84139- 4 3.75310+ 0 0.00000+ 0 0.00000+ 0 0.00000+ 0 0.00000+ 0 u233tgspec
 2.40000+ 0 2.60000+ 0          0          0          0         14 u233tgspec
 1.00000- 4 1.00000+ 9          0          0          0         16 u233tgspec
 2.93989-14 2.17886- 8 1.22912-18 1.89990- 8 8.04839-17 1.06783- 7 u233tgspec
 4.35968- 9 6.26498- 7 2.19981- 8 5.78262- 6 2.66359- 6 7.99882- 5 u233tgspec
 1.56220- 5 2.84092- 4 1.28085- 5 1.41413- 3 3.88069- 4 7.74428- 3 u233tgspec
 1.10898- 4 1.85309- 2 5.71404- 4 1.30262- 1 1.11037- 3 6.18185- 1 u233tgspec
 3.62757- 4 2.01565+ 0-2.73853- 8 5.78621- 6 6.27132- 8 3.60836- 5 u233tgspec
 7.11035- 8 3.59778- 5 0.00000+ 0 0.00000+ 0 0.00000+ 0 0.00000+ 0 u233tgspec
 2.60000+ 0 3.00000+ 0          0          0          0         15 u233tgspec
 1.00000- 4 1.00000+ 9          0          0          0         14 u233tgspec
 1.68490-14 2.18310- 8 5.61470-15 2.94930- 8 1.57620-10 6.76400- 7 u233tgspec
 6.13250- 8 3.83560- 5 5.26390- 6 1.64060- 4 6.43900- 5 1.07120- 3 u233tgspec
 1.73970- 5 1.92270- 3 7.69000- 4 9.96950- 3 9.85040- 4 9.71510- 2 u233tgspec
 2.01270- 3 2.65330- 1 2.24270- 3 7.66640- 1-1.67250-10 8.84970- 7 u233tgspec
 1.11800-10 1.09500- 6-1.05350-10 4.77420- 6 0.00000+ 0 0.00000+ 0 u233tgspec
 3.00000+ 0 4.00000+ 0          0          0          0         16 u233tgspec
 1.00000- 4 1.00000+ 9          0          0          0         15 u233tgspec
 4.20302-15 2.17852- 8 8.76872-20 2.21392- 8 3.13437-13 4.62292- 7 u233tgspec
```

```
 4.15525-11 6.35609- 7 3.20784- 7 8.17366- 5 3.76182- 6 1.48360- 4 u233tgspec
 3.00708- 5 7.76483- 4 3.11756- 4 3.32220- 3 1.07827- 3 8.85852- 3 u233tgspec
 1.27022- 3 8.80647- 2 8.91999- 3 2.38641- 1 3.33572- 3 8.98795- 1 u233tgspec
-1.36949- 3 2.12405+ 0-3.67997-12 6.74556- 7-3.37107-11 4.42399- 6 u233tgspec
 4.00000+ 0 5.00000+ 0          0          0          0         17 u233tgspec
 1.00000- 4 1.00000+ 9          0          0          0         11 u233tgspec
 4.44653-18 4.24232- 6 3.20566- 8 6.78099- 5 2.17381- 8 1.28561- 4 u233tgspec
 1.83480- 7 4.33708- 4 5.17918- 5 3.15290- 3 2.79596- 4 7.94271- 3 u233tgspec
 4.47982- 4 2.81777- 2 7.22127- 4 1.22011- 1 2.43831- 3 5.62986- 1 u233tgspec
 3.93970- 4 1.81955+ 0 1.61498- 5 2.40044+ 1 0.00000+ 0 0.00000+ 0 u233tgspec
 5.00000+ 0 6.00000+ 0          0          0          0         18 u233tgspec
 1.00000- 4 1.00000+ 9          0          0          0         14 u233tgspec
 5.72476-18 5.87405- 6 2.46763-14 2.72700- 4 2.14990- 9 1.76130- 3 u233tgspec
 1.00157- 5 4.15950- 3 1.20326- 4 1.08740- 2 1.04501- 4 2.42660- 2 u233tgspec
 7.21067- 4 1.41290- 1 4.08850- 5 1.59138+ 0-9.26330-18 7.07260- 6 u233tgspec
 1.15058-17 1.15860- 5 2.90760-16 2.01810- 5-2.96170-16 1.98900- 5 u233tgspec
 1.90874-22 1.08360- 6-2.72881-22 9.58140- 7 0.00000+ 0 0.00000+ 0 u233tgspec
 6.00000+ 0 7.50000+ 0          0          0          0         19 u233tgspec
 1.00000- 4 1.00000+ 9          0          0          0         11 u233tgspec
 7.78087-20 4.25260- 6 4.88927-18 2.74576- 4 2.30638-16 8.09994- 4 u233tgspec
 5.72003- 6 8.38590- 3 1.88641- 5 1.29606- 2 1.32398- 4 1.69563- 1 u233tgspec
-3.50851- 5 3.52948- 1 1.33347- 5 1.25269+ 0-3.15493- 6 2.19196+ 0 u233tgspec
-9.32907-21 5.18919- 6-5.82061-22 1.41320- 5 0.00000+ 0 0.00000+ 0 u233tgspec
 0.         0.                   0          0          0         18 u235tbspec
 0.00000+ 0 2.00000- 1          0          0          0          1 u235tbspec
 1.00000- 2 1.00000+ 9          0          0          0         18 u235tbspec
 6.43377-12 7.89595-10 1.91310-11 9.47383- 9 1.57815-10 3.25633- 8 u235tbspec
 2.52998- 9 1.50122- 7 1.70776- 8 9.19858- 7 4.20579- 8 3.30710- 6 u235tbspec
 1.83401- 7 1.78011- 5 5.00475- 7 7.04163- 5 2.17922- 6 1.45356- 4 u235tbspec
 8.08710- 6 4.01775- 4 2.30602- 5 1.34482- 3 9.55357- 5 7.22835- 3 u235tbspec
 5.49077- 4 3.39481- 2 1.98155- 3 1.83310- 1 1.69569- 3 6.55070- 1 u235tbspec
-6.75815- 4 8.56217- 1 6.05404- 4 8.47469+ 0-2.32612- 4 4.54971+ 0 u235tbspec
 2.00000- 1 4.00000- 1          0          0          0          2 u235tbspec
 1.00000- 2 1.00000+ 9          0          0          0         19 u235tbspec
 1.06194-11 7.80727-10 1.88989-12 1.14833- 8 6.35076-11 3.18421- 8 u235tbspec
 2.01493- 9 1.58484- 7 1.57570- 8 6.52895- 7 5.44851- 8 3.46341- 6 u235tbspec
 6.06126- 7 1.73086- 5 9.70952- 7 6.24528- 5 3.98365- 6 1.70050- 4 u235tbspec
 1.72694- 5 4.93642- 4 5.40125- 5 1.39328- 3 2.77358- 4 9.58130- 3 u235tbspec
 8.34080- 4 3.73971- 2 9.00517- 4 1.12069- 1 5.94415- 3 4.59269- 1 u235tbspec
-2.49945- 2 7.69293- 1 2.15277- 2 8.76992- 1 1.11010- 2 1.00984+ 1 u235tbspec
-1.12644- 2 9.78846+ 0 0.00000+ 0 0.00000+ 0 0.00000+ 0 0.00000+ 0 u235tbspec
 4.00000- 1 6.00000- 1          0          0          0          3 u235tbspec
 1.00000- 2 1.00000+ 9          0          0          0         18 u235tbspec
 4.74950-12 7.80512-10 2.35653-12 1.19146- 8 7.88819-11 3.14043- 8 u235tbspec
 2.39141- 9 1.69791- 7 1.85409- 8 7.80828- 7 8.22036- 8 4.45289- 6 u235tbspec
 6.78314- 7 1.62367- 5 1.34045- 6 6.34875- 5 9.95036- 6 1.95134- 4 u235tbspec
 6.03186- 5 9.27521- 4 3.86085- 4 7.55496- 3 1.22586- 3 3.45485- 2 u235tbspec
 2.43452- 3 1.38074- 1 2.60110- 3 3.70304- 1 5.65350- 3 1.79234+ 0 u235tbspec
 5.23903- 3 5.80884+ 0-8.99137- 3 3.45827+ 0-1.61056- 6 1.17779- 4 u235tbspec
 6.00000- 1 8.00000- 1          0          0          0          4 u235tbspec
 1.00000- 2 1.00000+ 9          0          0          0         19 u235tbspec
 4.88308-12 7.49858-10 1.90250-11 2.13838- 8 9.87208-11 3.12679- 8 u235tbspec
 4.29956- 9 1.62595- 7 1.43243- 8 7.55871- 7 1.34979- 7 5.46872- 6 u235tbspec
 9.36877- 7 2.15051- 5 5.39472- 6 1.34948- 4 7.59187- 5 5.56545- 4 u235tbspec
 1.30799- 3 9.63546- 3 2.67085- 3 4.49910- 2 9.31510- 3 3.32208- 1 u235tbspec
 7.55117- 4 1.20597+ 1-7.69586- 3 8.49470- 1 9.08125- 3 1.44223+ 0 u235tbspec
-5.84719- 4 9.49329- 3-7.23139- 5 6.67844- 4 8.84352- 5 1.28119- 3 u235tbspec
-1.82359- 9 1.74245- 7 0.00000+ 0 0.00000+ 0 0.00000+ 0 0.00000+ 0 u235tbspec
 8.00000- 1 1.00000+ 0          0          0          0          5 u235tbspec
 1.00000- 2 1.00000+ 9          0          0          0         17 u235tbspec
 6.29202-12 7.68530-10 1.04209-10 2.61371- 8 6.66629-11 3.80924- 8 u235tbspec
 2.50413- 9 1.59102- 7 1.15178- 8 1.02018- 6 6.95693- 7 8.64291- 6 u235tbspec
 1.04436- 5 1.92433- 4 6.63541- 5 9.14207- 4 1.75986- 2 1.07055- 2 u235tbspec
```

```
 2.07147- 2 4.20293+ 0-2.34578- 2 3.43650+ 0-1.87247- 2 1.11639- 2 u235tbspec
 3.23137- 3 1.99115- 2 6.29421- 3 1.26729- 1 1.35216- 2 1.09617+ 0 u235tbspec
-5.36118- 7 9.22708- 6 1.23110- 6 3.09482- 5 0.00000+ 0 0.00000+ 0 u235tbspec
 1.00000+ 0 1.20000+ 0          0          0          0          6 u235tbspec
 1.00000- 2 1.00000+ 9          0          0          0         18 u235tbspec
 7.11162-12 7.70552-10 1.53974-10 2.64092- 8 6.93823-11 4.57704- 8 u235tbspec
 2.15607- 9 1.62334- 7 5.46379- 9 9.59079- 7 6.18978- 8 7.04881- 6 u235tbspec
 4.92729- 7 2.04419- 5 2.25319- 6 6.54795- 5 1.85696- 5 3.28120- 4 u235tbspec
 6.16781- 5 1.22867- 3 2.96475- 4 6.26051- 3 1.57371- 3 1.96703- 2 u235tbspec
 3.57843- 1 1.66257- 1-3.68569- 1 1.70785- 1 2.49062- 2 2.90282- 1 u235tbspec
 7.84659- 3 3.43857+ 0-2.40898- 3 1.01714+ 1-4.07235-10 1.77671- 7 u235tbspec
 1.20000+ 0 1.40000+ 0          0          0          0          7 u235tbspec
 1.00000- 2 1.00000+ 9          0          0          0         19 u235tbspec
 7.26435-12 7.70899-10 1.60477-10 2.61850- 8 8.73595-11 3.81094- 8 u235tbspec
 8.81143-10 1.81084- 7 3.71364- 9 1.33552- 6 1.75353- 7 1.29044- 5 u235tbspec
 1.33924- 6 3.98613- 5 2.51979- 6 1.39940- 4 1.46622- 5 3.66611- 4 u235tbspec
 4.22717- 5 1.03893- 3 1.31079- 4 4.13199- 3 8.08064- 4 1.23887- 2 u235tbspec
 1.91155- 3 3.47298- 2 5.57568- 3 1.25789- 1 3.57041- 3 1.67532- 1 u235tbspec
 2.20373- 2 9.83072- 1-1.46115- 2 1.78324+ 0 8.13159- 3 4.12749+ 0 u235tbspec
-4.06814-11 2.83662- 6 0.00000+ 0 0.00000+ 0 0.00000+ 0 0.00000+ 0 u235tbspec
 1.40000+ 0 1.60000+ 0          0          0          0          8 u235tbspec
 1.00000- 2 1.00000+ 9          0          0          0         18 u235tbspec
 6.4632e-12 7.5825e-10 1.8253e-10 2.6745e-08 8.8851e-11 3.9011e-08 u235tbspec
 3.0972e-10 3.9825e-07 8.1369e-10 9.8404e-07 2.9049e-09 3.2156e-06 u235tbspec
 1.9052e-07 1.4862e-05 1.1070e-06 4.0588e-05 1.1103e-06 8.7256e-05 u235tbspec
 1.7309e-05 3.7893e-04 4.2079e-05 1.0793e-03 9.8690e-05 3.5653e-03 u235tbspec
 8.9678e-04 1.2186e-02 2.5677e-03 4.5219e-02 5.0914e-03 1.0860e-01 u235tbspec
 1.6116e-02 3.8369e-01 3.8124e-02 3.8526e+00-3.0973e-02 4.8785e+00 u235tbspec
 1.60000+ 0 1.80000+ 0          0          0          0          9 u235tbspec
 1.00000- 2 1.00000+ 9          0          0          0         15 u235tbspec
 4.84923-12 7.31447-10 2.13588-10 2.65453- 8 6.44767-11 5.16097- 8 u235tbspec
 1.02822- 9 1.13762- 6 6.46479- 8 1.14766- 5 1.05241- 6 3.50031- 5 u235tbspec
 2.87178- 6 1.53604- 4 2.11406- 3 1.07792- 3 1.84275- 2 1.26265- 1 u235tbspec
-7.58381- 3 1.50166- 1 2.20953- 2 7.81991- 1-2.35588- 3 1.13149- 3 u235tbspec
 3.98787- 4 1.82270- 3 1.57751- 3 1.76382- 2-1.75069-11 4.98043- 8 u235tbspec
 1.80000+ 0 2.00000+ 0          0          0          0         10 u235tbspec
 1.00000- 2 1.00000+ 9          0          0          0         15 u235tbspec
 2.9487e-12 7.7139e-10 1.9803e-10 2.7509e-08 6.5587e-11 3.7314e-08 u235tbspec
 5.3384e-10 1.3224e-06 8.0187e-08 1.4220e-05 1.2065e-06 4.0565e-05 u235tbspec
 2.2814e-05 4.8676e-04 5.8276e-05 1.6703e-03 4.8586e-04 8.9084e-03 u235tbspec
 9.5718e-03 4.3768e-02 1.4375e-02 1.7332e-01 2.2156e-02 1.1929e+00 u235tbspec
-6.9015e-03 4.5785e-02-9.1592e-08 2.3554e-03-2.5218e-11 4.4117e-08 u235tbspec
 2.00000+ 0 2.20000+ 0          0          0          0         11 u235tbspec
 1.00000- 2 1.00000+ 9          0          0          0         16 u235tbspec
 1.02020-12 7.52874-10 1.45184-10 2.62103- 8 7.99533-11 3.55380- 8 u235tbspec
 2.19340-10 2.23942- 6 2.16856- 7 2.05404- 5 1.70731- 6 5.44576- 5 u235tbspec
 2.06718- 5 5.11875- 4 7.75502- 5 2.02914- 3 6.90544- 4 1.26402- 2 u235tbspec
 2.51737- 3 4.54563- 2 1.23254- 2 1.63277- 1 2.17705- 2 7.34103- 1 u235tbspec
 4.17919- 3 8.79711+ 0-1.87033- 4 6.30981- 2-8.83043- 7 6.60527- 5 u235tbspec
-1.94621-11 3.45649- 8 0.00000+ 0 0.00000+ 0 0.00000+ 0 0.00000+ 0 u235tbspec
 2.20000+ 0 2.40000+ 0          0          0          0         12 u235tbspec
 1.00000- 2 1.00000+ 9          0          0          0         16 u235tbspec
 1.9033e-13 7.3832e-10 1.0718e-10 2.5289e-08 5.4825e-11 3.4352e-08 u235tbspec
 1.5533e-10 2.9976e-06 1.4537e-07 2.0311e-05 1.2005e-06 5.4669e-05 u235tbspec
 1.6954e-05 4.6805e-04 5.6508e-05 1.5939e-03 3.9521e-04 9.2822e-03 u235tbspec
 4.1204e-03 4.8440e-02 7.7986e-03 1.6771e-01 1.1159e-02 2.4773e-01 u235tbspec
 2.2571e-02 1.3783e+00-2.2359e-03 8.7497e-02-1.3683e-06 1.3195e-04 u235tbspec
-6.8875e-12 2.1750e-08                                             u235tbspec
 2.40000+ 0 2.60000+ 0          0          0          0         13 u235tbspec
 1.00000- 2 1.00000+ 9          0          0          0         15 u235tbspec
 1.5374e-13 7.2774e-10 8.3626e-11 2.6230e-08 2.3751e-11 4.4446e-08 u235tbspec
 4.1039e-08 1.7522e-05 6.3870e-07 4.3001e-05 2.4773e-05 6.4319e-04 u235tbspec
 1.3452e-03 3.3401e-03 7.3142e-04 1.4200e-02 4.0267e-03 6.9443e-02 u235tbspec
```

```
 3.5517e-02 2.6427e-01-2.0664e-02 2.9136e-01 2.4394e-02 1.2451e+00 u235tbspec
-1.2869e-03 3.4201e-03-6.6594e-12 4.4853e-08 7.1271e-11 2.4090e-06 u235tbspec
 2.60000+ 0 3.00000+ 0          0          0          0         14 u235tbspec
 1.00000- 2 1.00000+ 9          0          0          0         17 u235tbspec
 2.72653-13 7.24277-10 4.13821-11 2.44116- 8 1.70598-11 3.57044- 8 u235tbspec
 1.04464-11 2.32790- 7 1.49501-10 3.55287- 6 1.23995- 8 1.63557- 5 u235tbspec
 1.34011- 6 4.79652- 5 2.91723- 5 5.90512- 4 5.14526- 5 1.35685- 3 u235tbspec
 4.35461- 4 6.81356- 3 1.23630- 2 4.47919- 2 4.51703- 2 6.05292- 1 u235tbspec
 4.57003- 2 3.44576+ 0-2.42460- 2 4.15157+ 0-2.11399- 2 6.30591- 2 u235tbspec
 2.96769- 2 1.05523- 1-4.28662- 7 8.22434- 5 0.00000+ 0 0.00000+ 0 u235tbspec
 3.00000+ 0 4.00000+ 0          0          0          0         15 u235tbspec
 1.00000- 2 1.00000+ 9          0          0          0         17 u235tbspec
 4.1532e-13 7.0980e-10 3.5791e-12 2.0830e-08 1.3461e-12 6.6568e-08 u235tbspec
 1.4247e-11 2.4546e-07 3.4178e-10 5.3606e-06 8.9960e-07 3.9181e-05 u235tbspec
 2.1502e-06 5.1839e-05 4.8370e-05 6.2376e-04 9.9285e-05 1.9480e-03 u235tbspec
 3.1574e-04 6.5395e-03 2.9870e-03 2.1094e-02 3.1737e-02 1.1711e-01 u235tbspec
 1.0021e-01 4.5710e-01 4.8354e-04 3.9402e+00-3.5773e-02 4.7901e-01 u235tbspec
 9.4530e-02 1.6630e+00-1.8043e-06 4.3924e-05                     u235tbspec
 4.00000+ 0 5.00000+ 0          0          0          0         16 u235tbspec
 1.00000- 2 1.00000+ 9          0          0          0         15 u235tbspec
 1.3596e-13 7.0059e-10 2.8716e-12 2.1045e-07 3.9178e-10 9.4432e-06 u235tbspec
 1.9414e-07 4.7747e-05 5.1995e-06 5.2302e-04 4.2774e-05 3.2976e-03 u235tbspec
 3.1323e-04 9.8462e-03 1.9508e-01 7.0715e-02-4.7932e-01 7.8505e-02 u235tbspec
 3.0669e-01 8.6393e-02 7.5047e-02 6.3807e-01 4.9230e-02 1.7120e+00 u235tbspec
-2.0391e-02 7.4579e-01-8.0673e-13 4.4391e-07 5.0148e-12 1.3747e-06 u235tbspec
 5.00000+ 0 6.00000+ 0          0          0          0         17 u235tbspec
 1.00000- 2 1.00000+ 9          0          0          0         15 u235tbspec
 3.3926e-14 6.9587e-10 5.0264e-14 2.3165e-07 1.8908e-13 1.8910e-06 u235tbspec
 1.2508e-10 1.1210e-05 7.3434e-10 3.5617e-05 2.2188e-08 7.6096e-05 u235tbspec
 1.1956e-06 4.7498e-03 2.7889e-05 4.6280e-03 1.5500e-04 2.0958e-02 u235tbspec
 1.4768e-02 1.3989e-01 2.0497e-02 6.0317e-01-1.4228e-02 5.5448e-01 u235tbspec
 2.4804e-02 2.4145e+00-1.5993e-02 3.6736e+00-5.1528e-09 7.1649e-05 u235tbspec
 6.00000+ 0 7.50000+ 0          0          0          0         18 u235tbspec
 1.00000- 4 1.00000+ 5          0          0          0         13 u235tbspec
 1.90934-15 7.06343-10 5.36465-14 8.33849-07 2.33181-11 1.16847-05 u235tbspec
 2.77998-10 6.74779-05 4.54551-08 1.36779-03 1.93885-06 4.87554-03 u235tbspec
 8.71837-05 2.05905-02 2.22677-03 7.64181-02 5.98149-03 1.98977-01 u235tbspec
 8.85817-03 1.04123+00 1.61727-03 5.21095+00-2.36961-10 7.60620-05 u235tbspec
-4.45492-14 9.28661-07                                           u235tbspec
 0.         0.                 0          0          0         19 u235tgspec
 0.00000+ 0 1.00000- 1          0          0          0          1 u235tgspec
 1.00000+ 0 1.00000+ 9          0          0          0         15 u235tgspec
 1.22759-13 8.57900-10 4.44747-13 1.27500- 8 9.40450-12 3.17160- 8 u235tgspec
 3.02229-10 3.40290- 7 6.52773- 9 1.31410- 6 3.31752- 8 5.05420- 6 u235tgspec
 9.47610- 7 3.28330- 4 7.53290- 6 1.42580- 3 6.50660- 5 1.04050- 2 u235tgspec
 4.81790- 4 4.51430- 2 8.86280- 4 3.18670- 1-2.13230- 4 4.56140- 2 u235tgspec
-3.85750- 6 1.42450- 3-3.22550- 8 6.74190- 6 4.74150- 8 3.69510- 5 u235tgspec
 1.00000- 1 2.00000- 1          0          0          0          2 u235tgspec
 1.00000+ 0 1.00000+ 9          0          0          0         16 u235tgspec
 4.08994-14 4.80207- 9 2.48507-12 2.07982- 8 2.30435-11 3.11696- 8 u235tgspec
 1.29539- 9 2.72163- 7 2.77433- 8 2.96336- 6 4.52863- 8 1.46094- 5 u235tgspec
 6.72813- 7 9.23115- 5 5.74375- 6 4.10163- 4 9.15827- 6 1.15814- 3 u235tgspec
 1.12738- 5 3.26615- 3 1.19152- 4 1.32277- 2 7.32318- 4 4.19316- 2 u235tgspec
 1.61932- 3 1.25871- 1 9.44004- 3 7.26918- 1 2.27871- 4 1.04544+ 1 u235tgspec
-4.28825- 9 4.33402- 6 0.00000+ 0 0.00000+ 0 0.00000+ 0 0.00000+ 0 u235tgspec
 2.00000- 1 4.00000- 1          0          0          0          3 u235tgspec
 1.00000+ 0 1.00000+ 9          0          0          0         18 u235tgspec
 4.26180-15 6.14410- 9 1.99080-14 9.62320- 9 3.18790-16 1.54150- 7 u235tgspec
 6.46530-12 1.26210- 7 5.06660- 9 6.48510- 7 1.19300- 8 1.17920- 6 u235tgspec
 5.07500- 8 3.72630- 6 1.22650- 7 2.66240- 5 1.91840- 7 1.31170- 5 u235tgspec
 1.98440- 5 3.28750- 4 5.50310- 5 1.10170- 3 1.18720- 4 7.01130- 3 u235tgspec
 9.77840- 4 1.89860- 2 3.13130- 3 9.15710- 2 1.47530- 2 3.91180- 1 u235tgspec
```

```
 2.05860- 4 1.46340+ 1-7.57400- 3 4.04260- 1 1.26980- 2 1.02560+ 0 u235tgspec
 4.00000- 1 6.00000- 1          0          0          0          4 u235tgspec
 1.00000+ 0 1.00000+ 9          0          0          0         16 u235tgspec
 2.0641e-14 2.1208e-09 8.6363e-13 9.9324e-09 9.5783e-12 2.3625e-08 u235tgspec
 3.1392e-09 2.1099e-07 3.7691e-08 7.2546e-07 5.0324e-07 1.0446e-05 u235tgspec
 1.0387e-06 4.4137e-05 2.0675e-05 2.5977e-04 8.6513e-05 1.4432e-03 u235tgspec
 1.2041e-03 1.3525e-02 7.4620e-03 7.9512e-02 1.0010e-01 4.1851e-01 u235tgspec
-8.1238e-02 4.6537e-01 1.4552e-01 2.0919e+00-1.2322e-01 2.2085e+00 u235tgspec
-1.2425e-08 7.4863e-07                                             u235tgspec
 6.00000- 1 8.00000- 1          0          0          0          5 u235tgspec
 1.00000+ 0 1.00000+ 9          0          0          0         16 u235tgspec
 2.57430-11 7.37583-10 7.41847-12 1.71313- 8 2.86663-11 4.87121- 8 u235tgspec
 1.98380- 8 1.22787- 7 2.61065- 7 2.89413- 6 1.34955- 6 1.48531- 5 u235tgspec
 1.97231- 5 1.96443- 4 7.08852- 5 1.15161- 3 3.10858- 4 4.26471- 3 u235tgspec
 2.30103- 3 2.56084- 2 8.31770- 3 1.48133- 1 1.85069+ 0 1.39462+ 0 u235tgspec
-1.90629+ 0 1.43662+ 0 1.59071- 1 3.24889+ 0-6.48908- 2 4.62249+ 0 u235tgspec
-1.15622- 8 1.97908- 7 0.00000+ 0 0.00000+ 0 0.00000+ 0 0.00000+ 0 u235tgspec
 8.00000- 1 1.00000+ 0          0          0          0          6 u235tgspec
 1.00000+ 0 1.00000+ 9          0          0          0         15 u235tgspec
 1.2590e-17 5.6954e-10 2.9380e-13 2.1218e-08 9.2553e-14 3.3020e-08 u235tgspec
 7.4143e-09 5.6050e-07 1.2727e-08 8.3132e-07 4.3740e-08 4.0352e-06 u235tgspec
 1.0515e-06 3.1786e-05 2.1495e-05 1.6081e-04 2.5592e-05 2.1162e-04 u235tgspec
 2.2354e-04 1.5213e-03 8.8371e-04 1.1083e-02 3.4095e-03 4.9703e-02 u235tgspec
 1.1013e-02 2.1467e-01 4.6310e-02 9.4517e-01 2.5310e-02 4.5419e+00 u235tgspec
 1.00000+ 0 1.20000+ 0          0          0          0          7 u235tgspec
 1.00000+ 0 1.00000+ 9          0          0          0         17 u235tgspec
 9.55363-18 7.04650-10 1.80327-12 2.16700- 8 2.16447-14 2.20660- 8 u235tgspec
 1.91027-11 3.62330- 7 3.36202-10 8.30200- 7 1.09277- 8 2.81540- 6 u235tgspec
 2.44242- 7 1.49680- 5 7.97652- 7 2.92400- 5 1.45782- 5 1.89100- 4 u235tgspec
 1.03671- 4 1.16220- 3 3.97136- 4 6.91210- 3 2.18087- 3 2.69968- 2 u235tgspec
 5.71370- 3 1.06810- 1 1.86988- 2 4.80433- 1 3.73557- 2 1.12876+ 0 u235tgspec
-6.22114- 2 2.84767+ 0 4.89112- 2 4.44034+ 0 0.00000+ 0 0.00000+ 0 u235tgspec
 1.20000+ 0 1.40000+ 0          0          0          0          8 u235tgspec
 1.00000+ 0 1.00000+ 9          0          0          0         17 u235tgspec
 2.4334e-17 1.8242e-09 3.4573e-14 2.0289e-08 1.7197e-13 3.4032e-08 u235tgspec
 3.2149e-11 1.4195e-07 3.0944e-09 1.7746e-06 2.2183e-08 2.8911e-06 u235tgspec
 8.8424e-08 1.2682e-05 3.4424e-06 5.0658e-05 1.3514e-05 2.0028e-04 u235tgspec
 1.0402e-04 1.1859e-03 2.0141e-03 1.1787e-02 6.9995e-03 9.8636e-02 u235tgspec
 1.1280e-01 8.0318e-01-3.3900e-02 7.1828e-01 5.4339e-01 2.0274e+00 u235tgspec
-5.8459e-01 1.8965e+00-1.8868e-04 1.0822e-02                       u235tgspec
 1.40000+ 0 1.60000+ 0          0          0          0          9 u235tgspec
 1.00000- 4 1.00000+ 9          0          0          0         17 u235tgspec
 2.6570e-18 4.3279e-10 4.7430e-12 2.6196e-08 2.4417e-12 3.7414e-08 u235tgspec
 1.4987e-07 6.9164e-07 1.0191e-05 1.5070e-04 1.9128e-04 6.7318e-04 u235tgspec
 1.7837e-03 1.1617e-02 8.9289e-03 2.0815e-01 1.4332e-02 1.5199e+00 u235tgspec
-6.4094e-03 3.3791e-02 8.3906e-03 3.7170e-02-2.1533e-04 8.0703e-04 u235tgspec
 1.1500e-04 1.7557e-03-2.0277e-07 8.9801e-07 1.2735e-07 1.0645e-06 u235tgspec
-1.9114e-07 8.0037e-06 7.0478e-07 2.5678e-05                       u235tgspec
 1.60000+ 0 1.80000+ 0          0          0          0         10 u235tgspec
 1.00000+ 0 1.00000+ 9          0          0          0         18 u235tgspec
 2.6710e-19 6.1818e-11 1.0555e-13 2.1751e-08 4.4174e-14 2.1170e-07 u235tgspec
 1.0719e-12 8.3322e-07 1.1589e-09 2.4182e-06 1.3875e-09 5.2275e-06 u235tgspec
 4.8231e-07 2.3231e-05 3.2805e-06 1.0633e-04 1.2905e-05 4.4019e-04 u235tgspec
 4.8638e-04 1.5009e-03 3.7843e-03 1.2455e-01 1.5983e-02 4.0914e-01 u235tgspec
-1.0404e-01 1.5200e+00 1.0493e-01 1.6934e+00-2.3171e-06 4.7448e+01 u235tgspec
-4.0385e-04 1.4845e-03 5.8888e-04 1.0116e-02 2.0998e-03 3.9908e-02 u235tgspec
 1.80000+ 0 2.00000+ 0          0          0          0         11 u235tgspec
 1.00000+ 0 1.00000+ 9          0          0          0         16 u235tgspec
 2.0240e-19 9.9744e-11 5.8444e-14 2.2077e-08 6.5395e-11 5.9043e-07 u235tgspec
 1.5074e-09 2.8463e-06 2.0690e-09 2.8723e-06 2.1691e-08 2.1099e-05 u235tgspec
 2.7228e-07 2.7335e-05 2.7061e-06 1.0850e-04 1.5206e-05 4.5625e-04 u235tgspec
 5.3376e-05 1.4519e-03 1.5689e-04 6.7883e-03 6.2874e-04 1.4025e-02 u235tgspec
 1.1598e-03 3.4740e-02 6.6383e-03 1.4686e-01 1.8688e-02 6.4508e-01 u235tgspec
```

```
 2.9483e-02 1.7393e+00                                                 u235tgspec
 2.00000+ 0 2.20000+ 0          0          0          0         12 u235tgspec
 1.00000+ 0 1.00000+ 9          0          0          0         14 u235tgspec
 2.6708e-13 2.2744e-08 3.4181e-11 2.8787e-08 2.5620e-09 2.2035e-06 u235tgspec
 3.2478e-10 2.2033e-06 3.6777e-07 4.7797e-05 2.6628e-06 1.1522e-04 u235tgspec
 2.5675e-05 4.9399e-04 8.1033e-05 2.1998e-03 1.1923e-03 1.7362e-02 u235tgspec
 4.0334e-03 9.5312e-02 8.5271e-03 3.7542e-01 1.4756e-01 4.2706e+00 u235tgspec
-1.4154e-01 4.2955e+00-1.0263e-11 2.9964e-08                       u235tgspec
 2.20000+ 0 2.40000+ 0          0          0          0         13 u235tgspec
 1.00000+ 0 1.00000+ 9          0          0          0         15 u235tgspec
 8.7835e-14 2.1741e-08 1.0497e-17 1.8893e-08 1.0159e-16 3.6143e-07 u235tgspec
 4.1161e-12 4.1370e-07 9.3797e-10 6.3515e-07 4.6274e-10 2.4755e-06 u235tgspec
 1.6698e-07 4.1168e-05 2.6794e-06 8.0880e-05 1.3910e-05 3.7084e-04 u235tgspec
 6.7618e-05 2.4032e-03 1.0350e-03 1.4834e-02 5.1409e-03 1.0854e-01 u235tgspec
 1.0347e-01 1.2962e+00 2.3064e-02 3.2060e+00-1.0340e-01 1.6091e+00 u235tgspec
 2.40000+ 0 2.60000+ 0          0          0          0         14 u235tgspec
 1.00000+ 0 1.00000+ 9          0          0          0         14 u235tgspec
 4.5495e-14 2.1737e-08 2.8633e-15 8.1040e-08 3.7735e-10 9.8974e-07 u235tgspec
 4.3193e-09 6.2999e-07 4.9020e-07 5.8337e-05 2.0725e-06 9.8391e-05 u235tgspec
 5.1591e-05 6.0651e-04 1.9503e-04 4.7392e-03 1.1114e-03 2.0314e-02 u235tgspec
 3.1641e-03 9.4485e-02 6.1786e-03 3.3700e-01 1.5024e-05 1.3944e+01 u235tgspec
-3.6000e-05 6.8739e-04-2.0806e-09 2.1823e-06                       u235tgspec
 2.60000+ 0 3.00000+ 0          0          0          0         15 u235tgspec
 1.00000+ 0 1.00000+ 9          0          0          0         16 u235tgspec
 2.4947e-14 2.1733e-08 7.2801e-15 2.7939e-08 7.7674e-11 6.1979e-07 u235tgspec
 3.2805e-07 5.9510e-05 3.0602e-06 2.0175e-04 7.5568e-06 3.2107e-04 u235tgspec
 1.1614e-04 2.3567e-03 1.3662e-03 1.3673e-02 3.3491e-03 5.7573e-02 u235tgspec
 1.5770e-02 2.8257e-01 1.2072e-03 4.1774e+00-3.0443e-02 1.3920e+00 u235tgspec
 3.3832e-02 1.6565e+00-5.5771e-05 3.5126e+00 1.9996e-07 1.6999e-06 u235tgspec
-2.0000e-07 1.7003e-06                                             u235tgspec
 3.00000+ 0 4.00000+ 0          0          0          0         16 u235tgspec
 1.00000- 2 1.00000+ 9          0          0          0         16 u235tgspec
 6.5037e-15 2.1734e-08 2.6685e-18 2.1875e-08 5.3952e-13 4.2656e-07 u235tgspec
 4.0684e-11 6.4123e-07 2.7189e-07 7.4405e-05 3.8190e-06 1.8872e-04 u235tgspec
 5.4667e-05 1.2438e-03 2.8318e-05 1.7669e-03 1.7813e-03 1.1240e-02 u235tgspec
 5.3592e-03 5.8134e-02 1.6242e-02 1.8245e-01 2.9477e-02 6.9138e-01 u235tgspec
-1.6029e-02 1.7766e+00 7.1841e-03 4.4736e+00-2.6914e-12 6.2464e-07 u235tgspec
-3.1530e-11 3.7292e-06                                             u235tgspec
 4.00000+ 0 5.00000+ 0          0          0          0         17 u235tgspec
 1.00000- 2 1.00000+ 9          0          0          0         14 u235tgspec
 2.16760-19 4.14070- 6 6.99520- 9 6.31930- 5 2.26700- 8 7.67050- 5 u235tgspec
 1.79120- 7 4.03400- 4 5.58840- 5 3.65050- 3 2.43150- 4 5.31980- 3 u235tgspec
 1.06340- 3 1.90710- 2 6.51980- 3 9.75960- 2 2.13490- 2 5.19990- 1 u235tgspec
 3.49720- 3 1.11870+ 1-1.34090- 3 1.93100- 1-6.31290- 9 3.98480- 4 u235tgspec
 8.80670- 3 9.94740- 2-9.96680- 3 9.38650- 2 0.00000+ 0 0.00000+ 0 u235tgspec
 5.00000+ 0 6.00000+ 0          0          0          0         18 u235tgspec
 1.00000- 2 1.00000+ 9          0          0          0         16 u235tgspec
 8.81599-20 5.75825- 6 2.17942-15 2.01111- 4 2.46490-13 6.37175- 4 u235tgspec
 1.82130- 7 2.75403- 3 3.24153- 5 5.03643- 3 2.85808- 4 1.13786- 2 u235tgspec
 2.03865- 1 2.01429- 1-2.01229- 1 2.02193- 1 4.29155- 3 4.01372- 1 u235tgspec
-2.90821- 3 4.04482- 1 9.70314- 4 1.20105+ 0-5.32151- 4 1.82423+ 0 u235tgspec
-6.36660-20 7.04290- 6 2.26679- 3 4.10658- 2-1.93919- 3 4.04356- 2 u235tgspec
 1.00001-21 1.00000- 6 0.00000+ 0 0.00000+ 0 0.00000+ 0 0.00000+ 0 u235tgspec
 6.00000+ 0 7.50000+ 0          0          0          0         19 u235tgspec
 1.00000- 4 1.00000+ 9          0          0          0         12 u235tgspec
 3.44840-21 4.26783- 6 8.39004-21 2.10226- 5 3.62256-19 2.05656- 4 u235tgspec
 4.63223-17 6.05335- 4 4.49234- 9 5.32009- 3 1.07130- 5 8.59635- 3 u235tgspec
 1.31924- 5 1.35035- 2 2.51500- 4 1.87459- 1-1.57334- 4 3.25807- 1 u235tgspec
 8.27934- 5 9.56266- 1-1.63636- 5 1.13647+ 0-9.44376-21 2.15828- 5 u235tgspec
 0.         0.                   0          0          0         18 u238fbspec
 0.00000+ 0 2.00000- 1          0          0          0          1 u238fbspec
 1.00000- 4 1.00000+ 9          0          0          0         16 u238fbspec
 4.87604-12 7.81715-10 2.10633-11 9.31886- 9 1.48912-10 3.25725- 8 u238fbspec
```

```
2.36654- 9 1.55566- 7 1.30805- 8 7.61299- 7 4.76336- 8 2.81964- 6 u238fbspec
1.68657- 7 1.46478- 5 6.72963- 7 6.85237- 5 4.84705- 6 3.28838- 4 u238fbspec
1.62044- 5 1.18232- 3 5.98630- 5 6.49690- 3 2.79984- 4 2.90632- 2 u238fbspec
6.58243- 4 1.26464- 1 1.76526- 3 5.37524- 1 7.66546- 4 2.56996+ 0 u238fbspec
4.90771- 5 1.40433+ 1 0.00000+ 0 0.00000+ 0 0.00000+ 0 0.00000+ 0 u238fbspec
2.00000- 1 4.00000- 1          0          0          0          2 u238fbspec
1.00000- 4 1.00000+ 9          0          0          0         16 u238fbspec
7.46262-12 7.59451-10 2.04084-12 1.05769- 8 6.28717-11 3.12183- 8 u238fbspec
1.86096- 9 1.72340- 7 1.55203- 8 6.99564- 7 6.06076- 8 3.38769- 6 u238fbspec
5.11485- 7 1.49257- 5 1.37996- 6 7.06365- 5 1.22068- 5 3.30576- 4 u238fbspec
3.62947- 5 1.09668- 3 1.19284- 4 6.86384- 3 4.80087- 4 2.79622- 2 u238fbspec
1.26279- 3 1.31852- 1 2.40102- 3 5.33452- 1 1.43668- 3 2.43268+ 0 u238fbspec
9.12499- 5 1.49692+ 1 0.00000+ 0 0.00000+ 0 0.00000+ 0 0.00000+ 0 u238fbspec
4.00000- 1 6.00000- 1          0          0          0          3 u238fbspec
1.00000- 4 1.00000+ 9          0          0          0         16 u238fbspec
2.89334-12 7.78106-10 6.98008-12 1.40380- 8 7.62494-11 3.09719- 8 u238fbspec
1.51795- 9 1.65119- 7 1.46205- 8 6.84216- 7 6.61795- 8 3.53374- 6 u238fbspec
6.54161- 7 1.50535- 5 1.65350- 6 6.74328- 5 1.63021- 5 3.24084- 4 u238fbspec
5.29113- 5 1.13367- 3 2.19449- 4 6.82859- 3 9.14444- 4 2.81385- 2 u238fbspec
2.70108- 3 1.32787- 1 5.13164- 3 5.32025- 1 3.12443- 3 2.42399+ 0 u238fbspec
1.98978- 4 1.51049+ 1 0.00000+ 0 0.00000+ 0 0.00000+ 0 0.00000+ 0 u238fbspec
6.00000- 1 8.00000- 1          0          0          0          4 u238fbspec
1.00000- 4 1.00000+ 9          0          0          0         15 u238fbspec
2.83073-12 7.51963-10 1.06185-10 2.54335- 8 9.94631-10 1.26275- 7 u238fbspec
4.91833- 9 4.21650- 7 1.92130- 8 1.41935- 6 2.36588- 7 7.58257- 6 u238fbspec
1.03730- 6 2.86436- 5 7.01658- 6 1.64106- 4 4.48371- 5 6.86480- 4 u238fbspec
1.10152- 4 3.19031- 3 8.22488- 4 1.47238- 2 2.45305- 3 6.25187- 2 u238fbspec
7.44774- 3 2.80435- 1 7.14811- 3 1.06381+ 0 2.88207- 3 4.30176+ 0 u238fbspec
8.00000- 1 1.00000+ 0          0          0          0          5 u238fbspec
1.00000- 4 1.00000+ 9          0          0          0         15 u238fbspec
3.50247-12 7.51865-10 1.49199-10 2.53480- 8 8.59078-10 1.20248- 7 u238fbspec
2.51734- 9 3.49539- 7 1.27515- 8 1.41167- 6 1.73273- 7 7.84113- 6 u238fbspec
1.07102- 6 3.15929- 5 7.37824- 6 1.65304- 4 4.37239- 5 6.79918- 4 u238fbspec
1.31402- 4 3.23581- 3 1.07660- 3 1.48807- 2 3.35852- 3 6.27392- 2 u238fbspec
1.20370- 2 2.88387- 1 1.37165- 2 7.72865- 1 2.17281- 3 1.25613+ 1 u238fbspec
1.00000+ 0 1.20000+ 0          0          0          0          6 u238fbspec
1.00000- 4 1.00000+ 9          0          0          0         15 u238fbspec
3.88210-12 7.52973-10 1.90381-10 2.52499- 8 5.43369-10 1.09041- 7 u238fbspec
1.48886- 9 3.05766- 7 6.24602- 9 1.31886- 6 1.19764- 7 8.77779- 6 u238fbspec
1.02705- 6 3.35051- 5 7.22224- 6 1.67756- 4 4.10869- 5 6.73303- 4 u238fbspec
1.46544- 4 3.23115- 3 1.30866- 3 1.49928- 2 4.48685- 3 6.47725- 2 u238fbspec
1.47754- 2 2.82958- 1 1.46297- 2 1.06921+ 0 5.82667- 3 4.29845+ 0 u238fbspec
1.20000+ 0 1.40000+ 0          0          0          0          7 u238fbspec
1.00000- 4 1.00000+ 9          0          0          0         15 u238fbspec
3.95341-12 7.53176-10 2.22058-10 2.51520- 8 1.84964-10 8.77268- 8 u238fbspec
7.34693-10 2.86190- 7 3.21171- 9 1.33285- 6 8.77536- 8 9.93369- 6 u238fbspec
1.00412- 6 3.51599- 5 6.45541- 6 1.70681- 4 4.06498- 5 6.74583- 4 u238fbspec
1.55211- 4 3.20206- 3 1.45562- 3 1.50701- 2 5.41657- 3 6.59144- 2 u238fbspec
1.84776- 2 2.84311- 1 1.87140- 2 1.07107+ 0 7.39367- 3 4.29721+ 0 u238fbspec
1.40000+ 0 1.60000+ 0          0          0          0          8 u238fbspec
1.00000- 4 1.00000+ 9          0          0          0         15 u238fbspec
3.56806-12 7.53031-10 2.42280-10 2.50331- 8 3.95978-11 5.59749- 8 u238fbspec
3.33335-10 3.74240- 7 1.93002- 9 1.43723- 6 7.28053- 8 1.07487- 5 u238fbspec
9.68198- 7 3.62790- 5 5.45541- 6 1.75236- 4 4.13265- 5 6.78259- 4 u238fbspec
1.59958- 4 3.19260- 3 1.55414- 3 1.52434- 2 9.31764- 3 7.26116- 2 u238fbspec
2.53931- 2 2.72106- 1 2.28573- 2 1.08288+ 0 9.38975- 3 4.27761+ 0 u238fbspec
1.60000+ 0 1.80000+ 0          0          0          0          9 u238fbspec
1.00000- 4 1.00000+ 9          0          0          0         16 u238fbspec
3.06150-12 8.84283-10 9.84834-10 3.11169- 8 5.61886- 8 1.16180- 5 u238fbspec
8.84303- 7 3.62766- 5 1.12833- 6 1.18570- 4 1.54946- 5 3.76996- 4 u238fbspec
7.04207- 5 1.31146- 3 4.83067- 4 7.00620- 3 2.67137- 3 2.78103- 2 u238fbspec
1.39758- 2 1.31997- 1 3.08090- 2 5.41616- 1 2.11390- 2 2.26581+ 0 u238fbspec
1.62303- 4 3.62228+ 1-8.24515-10 3.57001- 8 1.58526-10 7.57407- 8 u238fbspec
```

```
 1.24643- 9 1.28273- 6 0.00000+ 0 0.00000+ 0 0.00000+ 0 0.00000+ 0 u238fbspec
 1.80000+ 0 2.00000+ 0          0          0          0         10 u238fbspec
 1.00000- 4 1.00000+ 9          0          0          0         13 u238fbspec
 1.63586-12 7.48834-10 2.66248-10 2.56157- 8 5.17635-10 1.11201- 6 u238fbspec
 4.27136- 8 1.22446- 5 8.25749- 7 3.80074- 5 3.66176- 6 2.05654- 4 u238fbspec
 3.85037- 5 7.08568- 4 1.58669- 4 3.20769- 3 1.45534- 3 1.52015- 2 u238fbspec
 7.21920- 3 7.00939- 2 2.68020- 2 2.89279- 1 2.99637- 2 1.07308+ 0 u238fbspec
 1.14288- 2 4.28656+ 0 0.00000+ 0 0.00000+ 0 0.00000+ 0 0.00000+ 0 u238fbspec
 2.00000+ 0 2.20000+ 0          0          0          0         11 u238fbspec
 1.00000- 4 1.00000+ 9          0          0          0         15 u238fbspec
 6.21662-13 7.45087-10 1.74990-10 2.37439- 8 6.15896-11 3.70285- 8 u238fbspec
 5.40664-11 5.30325- 7 5.20732-10 4.38897- 6 1.98514- 7 2.12860- 5 u238fbspec
 7.81776- 7 5.47927- 5 1.35480- 5 4.26755- 4 6.81341- 5 1.39548- 3 u238fbspec
 4.77281- 4 7.23771- 3 2.65520- 3 2.90245- 2 1.58050- 2 1.37606- 1 u238fbspec
 3.73455- 2 5.48675- 1 2.44188- 2 2.35782+ 0 8.23034- 4 1.10252+ 1 u238fbspec
 2.20000+ 0 2.40000+ 0          0          0          0         12 u238fbspec
 1.00000- 4 1.00000+ 9          0          0          0         15 u238fbspec
 1.70046-13 7.29186-10 1.28145-10 2.30762- 8 6.38180-11 3.49971- 8 u238fbspec
 2.92974-11 7.07012- 7 2.80081- 9 9.07818- 6 1.38738- 7 2.21964- 5 u238fbspec
 5.82662- 7 5.09646- 5 1.29859- 5 4.57825- 4 6.49222- 5 1.43485- 3 u238fbspec
 4.67494- 4 7.37989- 3 2.61074- 3 2.93099- 2 1.59834- 2 1.38397- 1 u238fbspec
 3.94907- 2 5.53186- 1 2.54951- 2 2.37606+ 0 1.08676- 3 1.30759+ 1 u238fbspec
 2.40000+ 0 2.60000+ 0          0          0          0         13 u238fbspec
 1.00000- 4 1.00000+ 9          0          0          0         15 u238fbspec
 1.47678-13 7.29208-10 9.38895-11 2.28635- 8 3.92220-11 3.24528- 8 u238fbspec
 1.75170-11 2.30269- 7 2.38784- 9 8.72808- 6 7.26733- 8 2.28967- 5 u238fbspec
 5.14350- 7 4.85590- 5 1.30420- 5 4.95487- 4 5.39610- 5 1.40689- 3 u238fbspec
 4.40455- 4 7.13165- 3 2.36062- 3 2.84487- 2 1.57658- 2 1.34717- 1 u238fbspec
 4.00716- 2 5.54884- 1 2.71918- 2 2.28255+ 0 1.12978- 3 1.98598+ 1 u238fbspec
 2.60000+ 0 3.00000+ 0          0          0          0         14 u238fbspec
 1.00000- 4 1.00000+ 9          0          0          0         14 u238fbspec
 2.62335-13 7.27988-10 1.01778-10 2.24407- 8 1.80944-11 4.38470- 8 u238fbspec
 2.88913-11 4.01751- 7 4.92205- 9 1.03622- 5 9.12696- 7 4.74565- 5 u238fbspec
 2.99794- 5 5.78193- 4 9.94091- 5 1.64559- 3 8.44220- 4 7.70246- 3 u238fbspec
 4.64012- 3 3.00815- 2 2.99813- 2 1.36666- 1 8.21043- 2 5.77369- 1 u238fbspec
 5.36709- 2 2.37791+ 0 1.38918- 3 1.69433+ 1 0.00000+ 0 0.00000+ 0 u238fbspec
 3.00000+ 0 4.00000+ 0          0          0          0         15 u238fbspec
 1.00000- 4 1.00000+ 9          0          0          0         17 u238fbspec
 4.14564-13 7.56446-10 3.68709-11 2.37789- 8 9.04051-12 9.18358- 7 u238fbspec
 1.25997- 9 7.74553- 6 1.04928- 7 3.44187- 5 1.20172- 6 6.68361- 5 u238fbspec
 2.42301- 5 5.32621- 4 1.28046- 4 1.41703- 3 1.38474- 3 7.83493- 3 u238fbspec
 8.23088- 3 3.08792- 2 6.12711- 2 1.36639- 1 1.91750- 1 5.98553- 1 u238fbspec
 1.18005- 1 2.39446+ 0 3.08545- 3 1.65611+ 1-1.59032-11 3.26023- 8 u238fbspec
 7.68504-12 7.71897- 8 2.22261-11 2.30904- 7 0.00000+ 0 0.00000+ 0 u238fbspec
 4.00000+ 0 5.00000+ 0          0          0          0         16 u238fbspec
 1.00000- 4 1.00000+ 9          0          0          0         13 u238fbspec
 1.29541-13 6.92593-10 5.66872-12 2.11076- 7 7.26745-11 5.09732- 6 u238fbspec
 3.16680- 9 2.13376- 5 4.35245- 7 7.15347- 5 5.83602- 6 7.24306- 4 u238fbspec
 2.84587- 5 2.77771- 3 5.46058- 4 8.60519- 3 3.34147- 3 3.46996- 2 u238fbspec
 4.34395- 2 1.37976- 1 1.31406- 1 6.06925- 1 6.68813- 2 2.42262+ 0 u238fbspec
 3.22564- 3 8.03097+ 0 0.00000+ 0 0.00000+ 0 0.00000+ 0 0.00000+ 0 u238fbspec
 5.00000+ 0 6.00000+ 0          0          0          0         17 u238fbspec
 1.00000- 4 1.00000+ 9          0          0          0         15 u238fbspec
 3.33178-14 7.19051-10 3.44312-13 3.28462- 7 1.74564-10 1.18552- 5 u238fbspec
 6.70754- 8 7.69645- 5 4.19272- 6 2.28834- 3 1.03802- 4 7.42361- 3 u238fbspec
 1.33845- 3 3.56565- 2 2.22815- 2 1.30017- 1 5.77361- 2 5.74500- 1 u238fbspec
 2.72784- 2 2.45121+ 0-8.71966- 8 8.60926- 5 3.12580- 8 1.09558- 4 u238fbspec
-9.47880-13 5.53960- 7 7.93536-13 7.19168- 7-9.74651-16 2.84685- 9 u238fbspec
 6.00000+ 0 7.50000+ 0          0          0          0         18 u238fbspec
 1.00000- 4 1.00000+ 9          0          0          0         12 u238fbspec
 1.81733-15 6.99165-10 2.89517-15 9.86309- 7 2.90480-11 1.20226- 5 u238fbspec
 1.94390-10 4.29785- 5 9.09378-12 2.52691- 4 4.70876- 8 1.39188- 3 u238fbspec
 2.07081- 6 5.31068- 3 1.39534- 4 2.19076- 2 4.24628- 3 9.02811- 2 u238fbspec
```

```
1.01595- 2 2.73626- 1 1.92196- 2 9.82918- 1 4.05039- 3 4.37665+ 0 u238fbspec
0.         0.                  0          0          0         19 u238fgspec
0.00000+ 0 1.00000- 1          0          0          0          1 u238fgspec
1.00000- 4 1.00000+ 9          0          0          0         15 u238fgspec

1.79791-13 1.25415- 9 3.29328-12 1.85837- 8 9.22192-12 5.84155- 8 u238fgspec
4.56743-10 3.88351- 7 8.79403- 9 1.52278- 6 7.87328- 9 4.98564- 6 u238fgspec
1.37311- 8 3.91138- 5 4.39476- 7 1.99581- 4 2.50496- 6 7.46488- 4 u238fgspec
1.82358- 5 3.92096- 3 4.02342- 4 1.35543- 2 1.82202- 4 4.75037- 2 u238fgspec
8.75574- 3 7.94114- 1-5.39122- 3 9.91245- 1 5.39568- 4 3.28163+ 0 u238fgspec
1.00000- 1 2.00000- 1          0          0          0          2 u238fgspec
1.00000- 4 1.00000+ 9          0          0          0         15 u238fgspec
1.45226-13 4.54672- 9 1.75442-11 2.75970- 8 1.04028-10 1.45863- 7 u238fgspec
1.13129- 9 3.01280- 7 2.06705- 8 2.61374- 6 8.85420- 9 4.99254- 6 u238fgspec
2.08170- 7 6.61829- 5 2.54047- 6 2.22576- 4 1.10481- 5 6.95666- 4 u238fgspec
3.93719- 5 2.77511- 3 2.15051- 4 1.35867- 2 6.87758- 3 8.75182- 2 u238fgspec
1.19911- 2 2.58051- 1 3.68637- 2 1.02424+ 0 8.53861- 3 4.23623+ 0 u238fgspec
2.00000- 1 4.00000- 1          0          0          0          3 u238fgspec
1.00000- 4 1.00000+ 9          0          0          0         15 u238fgspec
5.40735-15 5.49166- 9 4.62844-14 9.88420- 9 6.06165-12 1.24019- 7 u238fgspec
4.93728- 9 6.44425- 7 1.47976- 8 1.22290- 6 5.24535- 8 3.64205- 6 u238fgspec
4.20724- 7 1.42237- 5 1.10596- 5 3.19662- 4 5.87300- 5 7.14560- 4 u238fgspec
1.85007- 4 5.43621- 3 1.55992- 3 1.55630- 2 9.56861- 3 7.30375- 2 u238fgspec
3.78467- 2 2.93236- 1 7.17295- 2 8.91522- 1 3.98185- 2 3.28295+ 0 u238fgspec
4.00000- 1 6.00000- 1          0          0          0          4 u238fgspec
1.00000- 4 1.00000+ 9          0          0          0         16 u238fgspec
4.80676-14 3.41135- 9 1.40439-11 1.47367- 8 6.19270-11 2.91961- 8 u238fgspec
5.97740- 9 2.11742- 7 2.18881- 8 6.78407- 7 4.65306- 8 4.23872- 6 u238fgspec
6.70822- 7 1.39487- 5 1.65125- 6 6.17871- 5 2.80651- 5 3.07395- 4 u238fgspec
1.02490- 4 1.31952- 3 3.93519- 4 7.00234- 3 2.93751- 3 3.27677- 2 u238fgspec
3.53900- 2 1.27352- 1 3.62994- 2 5.37316- 1 2.84205- 2 2.10617+ 0 u238fgspec
1.41004- 3 1.22126+ 1 0.00000+ 0 0.00000+ 0 0.00000+ 0 0.00000+ 0 u238fgspec
6.00000- 1 8.00000- 1          0          0          0          5 u238fgspec
1.00000- 4 1.00000+ 9          0          0          0         14 u238fgspec
2.45216-11 7.30724-10 3.75792-11 2.00355- 8 1.37563- 8 1.20530- 7 u238fgspec
2.94284- 7 2.85665- 6 1.31662- 6 1.45029- 5 2.74253- 6 7.94903- 5 u238fgspec
2.71934- 5 2.76154- 4 1.23752- 4 1.55828- 3 5.77893- 4 6.59036- 3 u238fgspec
5.47957- 3 3.01676- 2 1.53594- 2 1.39199- 1 6.54386- 2 5.91504- 1 u238fgspec
7.33816- 2 2.35105+ 0-6.33959- 9 2.14437- 7 0.00000+ 0 0.00000+ 0 u238fgspec
8.00000- 1 1.00000+ 0          0          0          0          6 u238fgspec
1.00000- 4 1.00000+ 9          0          0          0         16 u238fgspec
7.80912-18 1.00421-10 2.02665-12 2.18052- 8 8.36573-14 5.98386- 8 u238fgspec
7.51101- 9 5.76718- 7 8.98569- 9 7.47183- 7 3.63709- 8 2.75332- 6 u238fgspec
3.66557- 7 2.27659- 5 5.66946- 6 8.58151- 5 4.55099- 5 2.09662- 4 u238fgspec
1.96661- 4 1.69286- 3 3.73829- 4 5.69891- 3 2.24332- 3 2.80511- 2 u238fgspec
2.88321- 2 1.39960- 1 6.55333- 2 6.59459- 1 9.07554- 2 2.88480+ 0 u238fgspec
3.71448- 3 1.06731+ 1 0.00000+ 0 0.00000+ 0 0.00000+ 0 0.00000+ 0 u238fgspec
1.00000+ 0 1.20000+ 0          0          0          0          7 u238fgspec
1.00000- 4 1.00000+ 9          0          0          0         14 u238fgspec
7.36281-18 4.67654-10 1.15773-11 2.17999- 8 9.31421-11 4.59030- 7 u238fgspec
8.73796-10 1.14536- 6 1.38588- 8 3.10541- 6 8.01768- 7 2.12376- 5 u238fgspec
2.27667- 6 7.54470- 5 2.17813- 5 2.90502- 4 1.05230- 4 1.22400- 3 u238fgspec
2.79829- 4 6.18528- 3 1.48214- 3 3.02205- 2 6.87597- 3 1.43795- 1 u238fgspec
2.94095- 2 5.44156- 1 1.59287- 3 5.66511+ 0 0.00000+ 0 0.00000+ 0 u238fgspec
1.20000+ 0 1.40000+ 0          0          0          0          8 u238fgspec
1.00000- 4 1.00000+ 9          0          0          0         15 u238fgspec
2.04299-18 1.35862-10 2.06671-13 2.22693- 8 3.20963-13 5.42032- 8 u238fgspec
2.71362-11 1.55366- 7 1.46737- 9 1.18176- 6 3.29684- 8 2.99810- 6 u238fgspec
4.80513- 7 2.12113- 5 4.99147- 6 6.71479- 5 1.70146- 5 4.49005- 4 u238fgspec
8.34151- 5 1.15838- 3 1.13288- 3 8.73583- 3 2.19807- 3 2.83326- 2 u238fgspec
1.20680- 2 1.46805- 1 4.99948- 2 5.20411- 1 1.40128- 2 2.39085+ 0 u238fgspec
1.40000+ 0 1.60000+ 0          0          0          0          9 u238fgspec
1.00000- 4 1.00000+ 9          0          0          0         16 u238fgspec
```

```
 3.13464-18 3.67220-10 1.66318-12 2.18410- 8 5.26239-12 2.83160- 8 u238fgspec
 9.18463- 8 6.36250- 7 9.16218- 7 4.50854- 5 4.11455- 5 3.23898- 4 u238fgspec
 1.74808- 3 1.24595- 2 1.01915- 1 1.50837- 1-9.21323- 2 1.52448- 1 u238fgspec
 3.39287- 2 5.89398- 1-1.59489- 4 6.48679- 1-2.67624- 8 6.63920- 7 u238fgspec
-4.20428- 7 7.51924- 6 4.27257- 7 8.89169- 6 2.12922- 4 2.15736- 3 u238fgspec
-1.81245- 4 1.87624- 3 0.00000+ 0 0.00000+ 0 0.00000+ 0 0.00000+ 0 u238fgspec
 1.60000+ 0 1.80000+ 0          0          0          0         10 u238fgspec
 1.00000- 4 1.00000+ 9          0          0          0         14 u238fgspec
 3.79429-19 2.90287-10 6.61592-13 2.18013- 8 2.44012-12 5.60275- 7 u238fgspec
 1.59888- 9 2.47537- 6 4.78104- 8 1.37447- 5 8.98255- 7 3.30242- 5 u238fgspec
 5.18229- 6 1.77494- 4 4.52393- 5 8.35406- 4 7.01798- 5 3.46508- 3 u238fgspec
 4.91114- 4 1.39280- 2 1.23472- 3 7.46247- 2 7.81290- 3 3.42064- 1 u238fgspec
 4.99968- 3 8.93876- 1 7.16859- 4 5.82371+ 0 0.00000+ 0 0.00000+ 0 u238fgspec
 1.80000+ 0 2.00000+ 0          0          0          0         11 u238fgspec
 1.00000- 4 1.00000+ 9          0          0          0         13 u238fgspec
 2.57729-19 2.20276-10 3.97626-13 2.18012- 8 1.31859-10 5.84589- 7 u238fgspec
 3.80905- 9 2.68310- 6 8.11285- 8 2.29229- 5 2.04496- 6 9.03220- 5 u238fgspec
 5.96795- 6 2.79795- 4 2.71164- 5 1.13470- 3 3.00931- 4 9.62117- 3 u238fgspec
 5.23080- 4 2.29128- 2 6.34996- 3 1.98537- 1 1.78025- 2 5.77370- 1 u238fgspec
 2.91371- 2 1.99771+ 0 0.00000+ 0 0.00000+ 0 0.00000+ 0 0.00000+ 0 u238fgspec
 2.00000+ 0 2.20000+ 0          0          0          0         12 u238fgspec
 1.00000- 4 1.00000+ 9          0          0          0         13 u238fgspec
 1.17084-12 2.25398- 8 1.96487-11 2.89503- 8 1.55321-10 6.10890- 7 u238fgspec
 4.61374- 9 2.63877- 6 6.60401- 8 2.74797- 5 2.36822- 6 9.11525- 5 u238fgspec
 7.05839- 6 3.22755- 4 5.20954- 5 9.40904- 4 2.59610- 4 1.01735- 2 u238fgspec
 7.00397- 4 3.07563- 2 1.66462- 3 1.63285- 1 8.63488- 3 5.33352- 1 u238fgspec
 6.22037- 3 2.06257+ 0 0.00000+ 0 0.00000+ 0 0.00000+ 0 0.00000+ 0 u238fgspec
 2.20000+ 0 2.40000+ 0          0          0          0         13 u238fgspec
 1.00000- 4 1.00000+ 9          0          0          0         14 u238fgspec
 5.51725-13 2.17885- 8 9.58851-17 2.41482- 8 2.73544-17 2.45460- 8 u238fgspec
 8.31001-10 6.19299- 7 1.14955-10 1.02484- 6 5.30440-10 2.31061- 6 u238fgspec
 1.04839- 6 5.95739- 5 6.20383- 6 1.57720- 4 1.13014- 5 4.52752- 4 u238fgspec
 6.74600- 5 5.03981- 3 5.06830- 4 1.22902- 2 6.55765- 3 3.52561- 1 u238fgspec
 2.16035- 2 1.48349+ 0 2.78118- 3 3.95651+ 0 0.00000+ 0 0.00000+ 0 u238fgspec
 2.40000+ 0 2.60000+ 0          0          0          0         14 u238fgspec
 1.00000- 4 1.00000+ 9          0          0          0         13 u238fgspec
 2.85721-13 2.17980- 8 7.89417-16 2.04040- 8 4.13826- 9 6.30560- 7 u238fgspec
 1.12288- 7 3.98139- 5 4.02753- 6 1.49766- 4 2.31249- 5 8.58493- 4 u238fgspec
 4.95239- 4 1.07583- 2 4.72203- 4 3.20041- 2 1.13279- 3 1.30368- 1 u238fgspec
 6.25555- 3 5.13734- 1 1.52733- 2 2.54956+ 0-1.96182- 3 2.84908+ 0 u238fgspec
-2.64946- 9 3.60131- 6 0.00000+ 0 0.00000+ 0 0.00000+ 0 0.00000+ 0 u238fgspec
 2.60000+ 0 3.00000+ 0          0          0          0         15 u238fgspec
 1.00000- 4 1.00000+ 9          0          0          0         13 u238fgspec
 1.60348-13 2.18094- 8 8.66847-15 5.88272- 8 1.88212-10 6.75108- 7 u238fgspec
 2.05005- 7 7.37322- 5 2.70405- 6 1.47444- 4 1.29507- 5 4.73177- 4 u238fgspec
 1.89840- 4 3.71559- 3 7.86602- 4 1.20084- 2 2.56902- 3 1.15786- 1 u238fgspec
 9.04289- 3 3.60345- 1 6.47873- 3 5.48009- 1-1.12440-10 7.30182- 7 u238fgspec
 2.46361-11 4.74740- 6 0.00000+ 0 0.00000+ 0 0.00000+ 0 0.00000+ 0 u238fgspec
 3.00000+ 0 4.00000+ 0          0          0          0         16 u238fgspec
 1.00000- 4 1.00000+ 9          0          0          0         14 u238fgspec
 4.08959-14 2.17886- 8 8.81928-17 5.28836- 8 1.52119-19 3.29636- 8 u238fgspec
 3.52087-11 6.28966- 7 1.62602- 7 8.27274- 5 2.30598- 6 1.40316- 4 u238fgspec
 2.08237- 5 7.39442- 4 8.87959- 5 3.23974- 3 1.04872- 3 1.30574- 2 u238fgspec
 3.06409- 3 7.40084- 2 2.83784- 2 2.59158- 1 1.13602- 2 8.54484- 1 u238fgspec
-6.27722- 3 1.85516+ 0-2.52385-11 3.87978- 6 0.00000+ 0 0.00000+ 0 u238fgspec
 4.00000+ 0 5.00000+ 0          0          0          0         17 u238fgspec
 1.00000- 4 1.00000+ 9          0          0          0         10 u238fgspec
 9.21174-20 4.46138- 6 1.22927- 8 6.78334- 5 1.54895- 8 1.28546- 4 u238fgspec
 1.09519- 7 4.26359- 4 3.42823- 5 3.52303- 3 2.61493- 4 8.70059- 3 u238fgspec
 4.70106- 4 2.98365- 2 2.10848- 3 1.55799- 1 8.49559- 3 5.09546- 1 u238fgspec
 1.99998- 2 6.16508+ 0 0.00000+ 0 0.00000+ 0 0.00000+ 0 0.00000+ 0 u238fgspec
 5.00000+ 0 6.00000+ 0          0          0          0         18 u238fgspec
 1.00000- 4 1.00000+ 9          0          0          0         14 u238fgspec
```

```
 4.57714-20 6.98637- 6 4.93223-16 2.00263- 4 8.19477-13 6.38602- 4 u238fgspec
 2.83567- 7 3.04320- 3 1.26022- 5 5.00306- 3 1.18079- 4 1.25985- 2 u238fgspec
 2.43667- 3 7.84892- 2-2.85464- 3 8.61137- 2 1.65434- 3 1.40840- 1 u238fgspec
 5.96809- 4 1.64862+ 0-7.39509- 5 1.64064+ 0-4.53527-20 9.27738- 6 u238fgspec
 1.00269-17 5.00043- 5-9.99697-18 4.99975- 5 0.00000+ 0 0.00000+ 0 u238fgspec
 6.00000+ 0 7.50000+ 0          0          0          0         19 u238fgspec
 1.00000- 4 1.00000+ 9          0          0          0         13 u238fgspec
 1.19454-21 4.30253- 6 6.06994-20 1.66481- 4 8.64200-17 5.76814- 4 u238fgspec
 1.88731-16 8.48668- 4 1.52461- 5 8.28207- 3 1.40119- 5 1.27745- 2 u238fgspec
 1.91665- 4 1.63925- 1 1.03184- 5 6.24040+ 0-5.04471- 5 3.30600- 1 u238fgspec
 7.06415- 5 1.26225+ 0-7.30307- 6 3.19969- 2-6.71639- 6 4.81969- 2 u238fgspec
-6.14692-21 5.34505- 5 0.00000+ 0 0.00000+ 0 0.00000+ 0 0.00000+ 0 u238fgspec
 0.         0.                   0          0          0         18pu239tbspec
 0.00000+ 0 2.00000- 1          0          0          0          1pu239tbspec
 1.00000- 2 1.00000+ 9          0          0          0         15pu239tbspec
 5.1191e-12 8.8823e-10 5.8974e-11 1.5831e-08 7.5503e-10 8.5520e-08pu239tbspec
 3.8903e-09 2.9097e-07 3.1200e-08 1.4307e-06 8.9827e-08 6.1941e-06pu239tbspec
 2.2802e-07 2.5726e-05 4.6450e-06 1.8001e-04 2.8996e-05 8.2184e-04pu239tbspec
 4.9291e-05 4.2581e-03 2.5397e-04 1.5128e-02 8.4746e-04 8.1654e-02pu239tbspec
 4.0210e-05 1.4332e-01 3.2109e-05 4.4972e-01 3.2148e-06 9.6887e+00pu239tbspec
 2.00000- 1 4.00000- 1          0          0          0          2pu239tbspec
 1.00000- 2 1.00000+ 9          0          0          0         15pu239tbspec
 6.81527-12 7.59148-10 5.07428-11 2.61796- 8 8.63897-10 1.40503- 7pu239tbspec
 6.73981- 9 4.52471- 7 2.54580- 8 1.39184- 6 2.05725- 7 7.44283- 6pu239tbspec
 1.08767- 6 3.18898- 5 7.33542- 6 1.98009- 4 6.06974- 5 8.68648- 4pu239tbspec
 1.27672- 4 5.06592- 3 5.42134- 4 1.79128- 2 1.03312- 3 5.74564- 2pu239tbspec
 8.25254- 4 2.75293- 1 5.38881- 4 9.17345- 1 6.07629- 5 4.49885+ 0pu239tbspec
 4.00000- 1 6.00000- 1          0          0          0          3pu239tbspec
 1.00000- 2 1.00000+ 9          0          0          0         15pu239tbspec
 2.33079-12 7.84736-10 6.77308-11 2.41264- 8 4.44787-10 1.17443- 7pu239tbspec
 6.46937- 9 4.45982- 7 2.26534- 8 1.39088- 6 1.87611- 7 7.01533- 6pu239tbspec
 9.49216- 7 2.46086- 5 2.37800- 6 1.01187- 4 2.53495- 5 3.93672- 4pu239tbspec
 8.59625- 5 1.49374- 3 4.25857- 4 8.51859- 3 1.12996- 3 3.21880- 2pu239tbspec
 1.60493- 3 8.69050- 2 2.01614- 3 5.18212- 1 4.06753- 4 2.51737+ 0pu239tbspec
 6.00000- 1 8.00000- 1          0          0          0          4pu239tbspec
 1.00000- 2 1.00000+ 9          0          0          0         15pu239tbspec
 2.0487e-12 7.5067e-10 1.1076e-10 2.4183e-08 5.2639e-10 1.1563e-07pu239tbspec
 4.6550e-09 4.2188e-07 2.0023e-08 1.4599e-06 1.8496e-07 7.1921e-06pu239tbspec
 8.8251e-07 2.4582e-05 3.5694e-06 1.1580e-04 3.3907e-05 4.8698e-04pu239tbspec
 6.4981e-05 1.5867e-03 4.8535e-04 7.8459e-03 1.5377e-03 2.7314e-02pu239tbspec
 3.8665e-03 1.3391e-01 1.2547e-03 3.1994e-01 7.1331e-06 6.2456e-01pu239tbspec
 8.00000- 1 1.00000+ 0          0          0          0          5pu239tbspec
 1.00000- 2 1.00000+ 9          0          0          0         15pu239tbspec
 2.43944-12 7.50448-10 1.56783-10 2.40954- 8 4.44099-10 1.07389- 7pu239tbspec
 2.33720- 9 3.52049- 7 1.27859- 8 1.43206- 6 1.04665- 7 6.78052- 6pu239tbspec
 4.65635- 7 1.95729- 5 2.06358- 6 7.23924- 5 2.00605- 5 3.51390- 4pu239tbspec
 7.33757- 5 1.30685- 3 5.36927- 4 7.55384- 3 1.65528- 3 2.86926- 2pu239tbspec
 2.99743- 3 1.04521- 1 6.52529- 3 4.01177- 1 1.81457- 3 1.98333+ 0pu239tbspec
 1.00000+ 0 1.20000+ 0          0          0          0          6pu239tbspec
 1.00000- 2 1.00000+ 9          0          0          0         15pu239tbspec
 2.62999-12 7.52406-10 2.00634-10 2.40201- 8 2.80944-10 9.51936- 8pu239tbspec
 1.34474- 9 3.13751- 7 6.24722- 9 1.34280- 6 4.60791- 8 6.85275- 6pu239tbspec
 3.22969- 7 1.81931- 5 1.57885- 6 6.16935- 5 1.66661- 5 3.38062- 4pu239tbspec
 6.83790- 5 1.31132- 3 5.11118- 4 7.68497- 3 1.82569- 3 2.82676- 2pu239tbspec
 3.93794- 3 1.14006- 1 6.41708- 3 4.67219- 1 1.50690- 3 2.45341+ 0pu239tbspec
 1.20000+ 0 1.40000+ 0          0          0          0          7pu239tbspec
 1.00000- 2 1.00000+ 9          0          0          0         15pu239tbspec
 2.66883-12 7.52918-10 2.36787-10 2.39493- 8 1.11665-10 7.53298- 8pu239tbspec
 6.49896-10 3.01594- 7 3.24386- 9 1.35723- 6 2.11271- 8 6.89477- 6pu239tbspec
 2.82997- 7 1.90492- 5 1.31804- 6 5.99532- 5 1.47646- 5 3.31365- 4pu239tbspec
 6.59682- 5 1.30631- 3 4.80033- 4 7.60527- 3 1.97748- 3 2.85936- 2pu239tbspec
 5.11345- 3 1.19899- 1 8.19755- 3 4.46977- 1 1.71833- 3 3.16095+ 0pu239tbspec
 1.40000+ 0 1.60000+ 0          0          0          0          8pu239tbspec
```

```
1.00000- 2 1.00000+ 9          0          0          0         15pu239tbspec
2.41987-12 7.53232-10 2.60373-10 2.38633- 8 3.71533-11 5.22208- 8pu239tbspec
3.38077-10 3.84169- 7 1.96760- 9 1.47420- 6 1.36373- 8 7.06869- 6pu239tbspec
2.43894- 7 1.94323- 5 1.11618- 6 5.45026- 5 1.34652- 5 3.41691- 4pu239tbspec
6.33494- 5 1.31333- 3 4.10227- 4 7.24307- 3 1.90549- 3 2.75665- 2pu239tbspec
7.42579- 3 1.31710- 1 1.10197- 2 5.37406- 1 2.43059- 3 1.74232+ 0pu239tbspec
1.60000+ 0 1.80000+ 0          0          0          0          9pu239tbspec
1.00000- 2 1.00000+ 9          0          0          0         15pu239tbspec
1.87777-12 7.53711-10 2.67986-10 2.37673- 8 3.36897-11 5.08864- 8pu239tbspec
1.86552-10 4.03387- 7 1.19631- 9 1.59957- 6 6.56991- 9 6.88662- 6pu239tbspec
1.77806- 7 1.97175- 5 8.03950- 7 4.70428- 5 1.24405- 5 3.56309- 4pu239tbspec
6.06704- 5 1.31026- 3 3.74905- 4 7.26973- 3 1.89162- 3 2.88193- 2pu239tbspec
7.17749- 3 1.27489- 1 1.11742- 2 4.60577- 1 2.44118- 3 2.45672+ 0pu239tbspec
1.80000+ 0 2.00000+ 0          0          0          0         10pu239tbspec
1.00000- 2 1.00000+ 9          0          0          0         15pu239tbspec
1.15835-12 7.54866-10 2.58220-10 2.36170- 8 3.22902-11 4.90383- 8pu239tbspec
9.04352-11 3.59291- 7 5.23877-10 1.56969- 6 3.07616- 9 6.88927- 6pu239tbspec
1.60426- 7 2.09139- 5 6.05905- 7 4.81015- 5 1.01749- 5 3.89691- 4pu239tbspec
5.63324- 5 1.23795- 3 3.14638- 4 7.34474- 3 1.64155- 3 2.80609- 2pu239tbspec
7.80966- 3 1.25715- 1 1.16125- 2 4.59348- 1 4.78608- 3 4.15829+ 0pu239tbspec
2.00000+ 0 2.20000+ 0          0          0          0         11pu239tbspec
1.00000- 2 1.00000+ 9          0          0          0         15pu239tbspec
4.89297-13 7.58652-10 2.32400-10 2.34351- 8 2.84767-11 4.66844- 8pu239tbspec
3.24927-11 2.82946- 7 1.05850-10 1.66388- 6 2.46975- 9 8.12848- 6pu239tbspec
1.39753- 7 2.15153- 5 4.28559- 7 4.69506- 5 9.13164- 6 4.24615- 4pu239tbspec
5.45557- 5 1.23605- 3 2.52554- 4 7.19198- 3 1.54673- 3 2.78863- 2pu239tbspec
8.17722- 3 1.32292- 1 1.28439- 2 4.48319- 1 4.23700- 3 4.12198+ 0pu239tbspec
2.20000+ 0 2.40000+ 0          0          0          0         12pu239tbspec
1.00000- 2 1.00000+ 9          0          0          0         14pu239tbspec
1.91543-13 7.65203-10 1.95008-10 2.32046- 8 2.29978-11 5.09633- 8pu239tbspec
2.23602-11 3.52774- 7 2.48796-10 3.78571- 6 3.74383- 8 1.53983- 5pu239tbspec
3.70203- 7 3.89960- 5 8.96423- 6 4.64369- 4 5.01012- 5 1.27417- 3pu239tbspec
1.95808- 4 6.80042- 3 1.47585- 3 2.76430- 2 7.88711- 3 1.37137- 1pu239tbspec
1.33890- 2 4.14283- 1 4.39490- 3 3.47291+ 0 0.00000+ 0 0.00000+ 0pu239tbspec
2.40000+ 0 2.60000+ 0          0          0          0         13pu239tbspec
1.00000- 2 1.00000+ 9          0          0          0         14pu239tbspec
1.70407-13 7.60606-10 1.47439-10 2.28857- 8 1.56079-11 4.91003- 8pu239tbspec
1.59181-11 2.55065- 7 1.88704-10 4.22524- 6 2.04138- 8 1.49223- 5pu239tbspec
3.01002- 7 4.04042- 5 9.33774- 6 5.00883- 4 4.30137- 5 1.33843- 3pu239tbspec
1.14641- 4 5.59227- 3 1.51158- 3 2.74868- 2 7.58626- 3 1.42159- 1pu239tbspec
1.41805- 2 4.89874- 1 4.08519- 3 3.02776+ 0 0.00000+ 0 0.00000+ 0pu239tbspec
2.60000+ 0 3.00000+ 0          0          0          0         14pu239tbspec
1.00000- 2 1.00000+ 9          0          0          0         14pu239tbspec
3.00750-13 7.51415-10 1.55147-10 2.22394- 8 1.03739-11 4.78465- 8pu239tbspec
2.43283-11 2.47652- 7 2.78550-10 4.25721- 6 9.03182- 9 1.26969- 5pu239tbspec
4.66334- 7 4.19893- 5 1.67183- 5 5.57945- 4 6.53776- 5 1.28408- 3pu239tbspec
2.30343- 4 6.21613- 3 2.09746- 3 2.64015- 2 1.45185- 2 1.37604- 1pu239tbspec
2.61846- 2 4.91831- 1 9.53534- 3 3.00029+ 0 0.00000+ 0 0.00000+ 0pu239tbspec
3.00000+ 0 4.00000+ 0          0          0          0         15pu239tbspec
1.00000- 2 1.00000+ 9          0          0          0         14pu239tbspec
4.54253-13 7.37085-10 3.98289-11 2.12077- 8 8.33360-12 9.68602- 8pu239tbspec
2.80758-11 2.72235- 7 1.16865-10 3.45115- 6 6.57608- 9 1.21087- 5pu239tbspec
5.39667- 7 5.19174- 5 2.32898- 5 5.55472- 4 8.70600- 5 1.41423- 3pu239tbspec
4.34458- 4 7.91116- 3 3.39386- 3 3.10711- 2 3.28610- 2 1.56543- 1pu239tbspec
5.80191- 2 7.53865- 1 1.36313- 2 1.43226+ 0 0.00000+ 0 0.00000+ 0pu239tbspec
4.00000+ 0 5.00000+ 0          0          0          0         16pu239tbspec
1.00000- 2 1.00000+ 9          0          0          0         13pu239tbspec
1.45339-13 6.89207-10 6.18868-12 2.07897- 7 6.94113-12 1.67538- 6pu239tbspec
3.33459-10 8.78407- 6 3.96019- 9 2.06861- 5 2.71581- 7 7.05059- 5pu239tbspec
1.92746- 6 4.95601- 4 4.63622- 6 1.57858- 3 7.13254- 5 7.53192- 3pu239tbspec
5.46195- 4 2.27162- 2 1.43721- 2 1.32480- 1 4.12168- 2 6.94959- 1pu239tbspec
1.50993- 2 1.79727+ 0 0.00000+ 0 0.00000+ 0 0.00000+ 0 0.00000+ 0pu239tbspec
5.00000+ 0 6.00000+ 0          0          0          0         17pu239tbspec
```

```
 1.00000- 2 1.00000+ 9          0          0          0         16pu239tbspec
 3.72162-14 7.20340-10 8.31349-13 3.78730- 7 4.29151-10 1.30710- 5pu239tbspec
 1.99189- 8 6.27410- 5 1.15003- 6 1.59505- 3 2.13938- 5 8.36676- 3pu239tbspec
 9.61769- 5 3.22322- 2 1.82993- 3 9.08920- 2 1.11992- 2 2.46440- 1pu239tbspec
 3.23447- 2 1.04790+ 0-1.43057- 2 6.15110- 1 7.55491- 3 5.77132+ 0pu239tbspec
-4.66530- 3 2.81140+ 0-1.39549- 8 6.50960- 5-1.56771-12 5.14290- 7pu239tbspec
 1.45417-12 6.84990- 7 0.00000+ 0 0.00000+ 0 0.00000+ 0 0.00000+ 0pu239tbspec
 6.00000+ 0 7.50000+ 0          0          0          0         18pu239tbspec
 1.00000- 4 1.00000+ 9          0          0          0         15pu239tbspec

 2.02247-15 6.81882-10 4.26636-13 6.30735-07 8.99431-10 1.63083-05pu239tbspec
 5.76412-08 1.52073-03 2.47780-06 6.16627-03 5.85628-05 1.97103-02pu239tbspec
 1.03751-03 7.39598-02 3.19925-03 1.74214-01 1.15261-02 7.93894-01pu239tbspec
-6.31111-03 8.90645-01 2.85479-03 2.87581+00-1.53200-03 3.57001+00pu239tbspec
-9.53371-10 1.75916-05 4.09241-10 3.26377-05-2.67547-13 6.3666 -07pu239tbspec
 0.         0.                   0          0          0         19pu239tgspec
 0.00000+ 0 1.00000- 1          0          0          0          1pu239tgspec
 1.00000- 2 1.00000+ 9          0          0          0         17pu239tgspec
 1.6745e-13 1.0525e-09 5.8682e-13 7.4913e-09 6.5332e-12 3.1930e-08pu239tgspec
 1.5625e-10 2.5329e-07 2.9423e-09 9.5013e-07 1.0248e-08 2.3259e-06pu239tgspec
 7.4364e-09 9.5538e-06 3.4827e-08 9.9562e-05 9.9546e-07 3.2597e-04pu239tgspec
 4.6689e-06 1.4196e-03 2.7058e-05 6.4382e-03 1.9079e-04 1.7863e-02pu239tgspec
 5.6541e-04 9.0850e-02 6.8560e-02 1.5820e+00-7.0293e-02 1.6589e+00pu239tgspec
 4.6816e-03 4.9538e+00-2.1239e-03 7.5006e+00                     pu239tgspec
 1.00000- 1 2.00000- 1          0          0          0          2pu239tgspec
 1.00000- 2 1.00000+ 9          0          0          0         15pu239tgspec
 1.89458-13 4.57827- 9 7.62429-13 1.64707- 8 1.60251-11 2.99703- 8pu239tgspec
 1.10437- 9 2.62687- 7 2.77794- 8 2.90335- 6 5.21332- 8 1.53445- 5pu239tgspec
 7.96255- 7 1.35652- 4 5.55581- 6 4.01915- 4 1.68380- 5 1.53364- 3pu239tgspec
 8.23951- 5 7.61538- 3 8.44159- 4 4.54362- 2 2.43597- 3 2.40069- 1pu239tgspec
 2.00477- 2 1.39564+ 0-8.52702- 3 1.59554+ 0-4.43708- 9 5.91653- 6pu239tgspec
 2.00000- 1 4.00000- 1          0          0          0          3pu239tgspec
 1.00000- 2 1.00000+ 9          0          0          0         18pu239tgspec
 1.90355-14 6.09782- 9 8.13413-14 1.01153- 8 7.53087-14 3.88371- 8pu239tgspec
 1.01884-11 1.49877- 7 5.42052- 9 6.60506- 7 1.79829- 8 1.23476- 6pu239tgspec
 6.33906- 8 4.01443- 6 3.28510- 7 1.36646- 5 2.89838- 7 3.17456- 5pu239tgspec
 2.68194- 5 4.06071- 4 4.97800- 5 8.41963- 4 5.30591- 4 9.42166- 3pu239tgspec
 1.89871- 2 8.05136- 2 1.01522- 1 7.40264+ 0-1.12355- 1 6.86436+ 0pu239tgspec
-2.31142- 2 9.39644- 2 1.20481- 2 1.64589- 1 1.64385- 2 2.36320+ 0pu239tgspec
 4.00000- 1 6.00000- 1          0          0          0          4pu239tgspec
 1.00000- 2 1.00000+ 9          0          0          0         18pu239tgspec
 1.57971-13 4.50135- 9 1.98087-11 1.41032- 8 1.08092-10 2.81701- 8pu239tgspec
 7.88327- 9 2.24862- 7 3.12650- 8 8.42036- 7 4.18292- 7 1.00961- 5pu239tgspec
 1.13232- 6 4.55997- 5 1.93785- 5 2.83545- 4 4.86045- 5 9.43090- 4pu239tgspec
 1.03002- 4 3.51864- 3 5.79016- 4 1.20404- 2 6.22299- 4 2.75575- 2pu239tgspec
 1.02827- 2 1.14705- 1 3.84337- 2 5.04986- 1-1.54785- 2 5.63255- 1pu239tgspec
 4.80456- 3 2.56293+ 0-2.38204- 3 4.64111+ 0-5.74609- 9 7.77343- 7pu239tgspec
 6.00000- 1 8.00000- 1          0          0          0          5pu239tgspec
 1.00000- 2 1.00000+ 9          0          0          0         18pu239tgspec
 2.74342-11 7.27834-10 1.23249-11 1.08688- 8 7.87323-11 2.96621- 8pu239tgspec
 1.46183- 8 1.23964- 7 3.05004- 7 2.82621- 6 8.59388- 7 1.51987- 5pu239tgspec
 2.48657- 6 6.04630- 5 2.04711- 5 2.51572- 4 3.83978- 5 9.02364- 4pu239tgspec
 1.53785- 4 2.90476- 3 4.90311- 4 1.09160- 2 2.28453- 3 4.34068- 2pu239tgspec
 1.23923- 2 2.71597- 1 5.80462- 2 2.33740+ 0-1.24137- 1 4.39308+ 0pu239tgspec
 7.71839- 2 5.73104+ 0-4.95776- 4 2.64233- 1-7.29853- 9 1.96925- 7pu239tgspec
 8.00000- 1 1.00000+ 0          0          0          0          6pu239tgspec
 1.00000- 2 1.00000+ 9          0          0          0         15pu239tgspec
 6.1206e-16 2.2094e-09 3.4148e-12 2.1622e-08 3.0609e-12 1.8763e-07pu239tgspec
 1.4731e-08 6.3076e-07 4.8773e-08 2.9425e-06 4.3669e-07 2.0153e-05pu239tgspec
 2.2331e-05 1.5062e-04 3.4671e-05 3.4208e-04 1.3320e-04 1.3813e-03pu239tgspec
 3.9237e-04 6.9255e-03 7.5488e-03 4.7568e-02 2.1759e-02 5.7720e-01pu239tgspec
 2.0771e-02 3.6488e+00-1.7013e-02 6.9358e-02 1.6860e-02 9.3244e-02pu239tgspec
 1.00000+ 0 1.20000+ 0          0          0          0          7pu239tgspec
```

```
 1.00000- 2 1.00000+ 9          0          0          0         17pu239tgspec
 3.3859e-16 1.8722e-09 1.8905e-11 2.1593e-08 1.0149e-12 3.4973e-08pu239tgspec
 5.9662e-10 5.6083e-07 1.4878e-09 1.4138e-06 1.4052e-08 3.1471e-06pu239tgspec
 9.4636e-08 1.1361e-05 9.3132e-07 3.3545e-05 1.3963e-05 2.2501e-04pu239tgspec
 7.1798e-05 9.8381e-04 1.9070e-04 4.3368e-03 1.3274e-03 2.1329e-02pu239tgspec
 4.9879e-03 1.0003e-01 2.4173e-02 5.3311e-01-1.1548e-02 1.3637e+00pu239tgspec
 3.0240e-03 2.9022e+00-6.8022e-05 3.0109e-02                     pu239tgspec
 1.20000+ 0 1.40000+ 0          0          0          0          8pu239tgspec
 1.00000- 2 1.00000+ 9          0          0          0         16pu239tgspec
 1.0352e-15 2.4205e-09 1.0860e-13 1.6702e-08 3.4005e-13 3.1303e-08pu239tgspec
 1.5554e-11 1.4953e-07 3.5574e-10 6.1772e-07 2.1704e-08 2.4245e-06pu239tgspec
 2.5662e-08 5.1534e-06 1.6731e-06 4.1606e-05 9.0097e-06 1.9128e-04pu239tgspec
 4.9570e-05 7.4254e-04 1.2602e-04 2.8791e-03 1.3260e-03 1.4220e-02pu239tgspec
 2.2441e-03 6.2974e-02 9.5057e-03 2.5601e-01 1.3013e-02 8.2323e-01pu239tgspec
 1.2611e-04 1.5135e+01                                          pu239tgspec
 1.40000+ 0 1.60000+ 0          0          0          0          9pu239tgspec
 1.00000- 2 1.00000+ 9          0          0          0         19pu239tgspec
 6.0106e-17 1.4137e-09 3.4901e-12 2.2068e-08 3.8755e-12 3.0630e-08pu239tgspec
 6.2534e-07 7.4402e-07 7.3727e-05 3.9491e-04 1.3557e-03 1.5216e-02pu239tgspec
 1.8850e-03 7.5887e-02 6.2792e-03 2.2780e-01 1.3810e-02 7.3231e-01pu239tgspec
-7.3087e-03 5.9550e-01 2.4414e-03 1.5332e+00-4.0712e-03 2.3314e+00pu239tgspec
-2.9589e-05 4.1229e-04 1.6258e-04 3.9785e-03-1.6167e-06 8.1584e-07pu239tgspec
 9.9532e-07 8.4564e-07 8.0303e-07 4.5868e-05 2.0934e-07 1.3438e-06pu239tgspec
-1.9847e-07 1.8942e-06                                          pu239tgspec
 1.60000+ 0 1.80000+ 0          0          0          0         10pu239tgspec
 1.00000- 2 1.00000+ 9          0          0          0         18pu239tgspec
 1.4200e-18 1.5489e-10 1.1262e-12 2.1799e-08 2.7907e-13 2.0032e-07pu239tgspec
 8.4361e-12 7.5122e-07 1.7638e-09 2.5564e-06 2.0824e-08 1.1208e-05pu239tgspec
 4.9113e-07 2.7626e-05 4.8142e-06 1.7575e-04 1.4406e-05 5.6450e-04pu239tgspec
 5.8553e-05 1.1823e-03 2.3585e-04 7.0978e-03 1.1685e-03 2.4689e-02pu239tgspec
 1.2700e-02 1.1172e-01-8.1518e-03 1.1933e-01 8.8635e-03 3.7935e-01pu239tgspec
-5.2943e-03 1.2973e+00 2.9344e-03 4.4672e+00-1.1430e-03 3.3071e+00pu239tgspec
 1.80000+ 0 2.00000+ 0          0          0          0         11pu239tgspec
 1.00000- 2 1.00000+ 9          0          0          0         15pu239tgspec
 9.6962e-19 9.5650e-11 6.8324e-13 2.1797e-08 1.7195e-10 5.6579e-07pu239tgspec
 3.9956e-09 2.7015e-06 4.3613e-08 1.7561e-05 6.6437e-07 6.4162e-05pu239tgspec
 7.1490e-06 2.8737e-04 4.7535e-05 1.0093e-03 1.0413e-04 4.6229e-03pu239tgspec
 7.7923e-04 1.6670e-02 1.0915e-03 3.8609e-02 4.8508e-03 1.7399e-01pu239tgspec
 1.0160e-02 5.4955e-01-4.7396e-03 1.1628e+00 3.8801e-03 2.1733e+00pu239tgspec
 2.00000+ 0 2.20000+ 0          0          0          0         12pu239tgspec
 1.00000- 2 1.00000+ 9          0          0          0         16pu239tgspec
 9.3936e-12 2.4651e-08 5.1631e-16 3.0705e-08 1.8383e-12 9.9137e-08pu239tgspec
 9.9849e-11 3.1222e-07 5.0558e-12 1.2595e-06 3.5727e-09 2.0715e-06pu239tgspec
 3.9638e-07 5.4834e-05 9.3002e-06 2.2801e-04 4.7990e-05 8.0952e-04pu239tgspec
 1.2161e-04 4.2004e-03 1.3863e-03 2.2194e-02 5.0886e-03 1.6882e-01pu239tgspec
 3.9323e-03 5.1315e-01 4.9303e-03 3.7547e+00-6.6879e-03 2.0487e+00pu239tgspec
-3.1436e-06 1.9398e-04                                          pu239tgspec
 2.20000+ 0 2.40000+ 0          0          0          0         13pu239tgspec
 1.00000- 2 1.00000+ 9          0          0          0         16pu239tgspec
 9.3957e-13 2.1788e-08 2.5603e-16 3.0705e-08 1.0451e-12 3.5437e-07pu239tgspec
 8.0016e-10 6.1916e-07 2.3439e-10 1.2114e-06 1.8302e-09 5.4110e-06pu239tgspec
 7.3674e-07 5.9504e-05 9.8244e-06 2.0176e-04 3.3026e-05 9.1239e-04pu239tgspec
 2.5824e-04 7.4385e-03 1.4203e-03 2.5338e-02 5.5931e-03 2.1417e-01pu239tgspec
 4.1603e-03 6.7515e-01 4.2629e-03 4.4592e+00-5.7121e-03 2.5447e+00pu239tgspec
-4.2596e-06 1.6831e-04                                          pu239tgspec
 2.40000+ 0 2.60000+ 0          0          0          0         14pu239tgspec
 1.00000- 2 1.00000+ 9          0          0          0         17pu239tgspec
 4.84835-13 2.17840- 8 1.25202-15 2.26292- 8 3.61244-16 2.26357- 8pu239tgspec
 3.37412- 9 6.13882- 7 1.40688- 7 4.25297- 5 4.23160- 6 1.60245- 4pu239tgspec
 4.57193- 5 8.99766- 4 5.98085- 4 1.20557- 2 7.49703- 4 4.24332- 2pu239tgspec
 4.71308- 3 2.01849- 1 3.49330- 3 7.06328- 1-1.03927- 3 1.27744+ 0pu239tgspec
 6.77131- 4 2.27487+ 0-5.64490- 4 3.73776+ 0-1.46923- 5 7.93424- 4pu239tgspec
 1.99026- 7 1.69217- 6-2.00448- 7 1.70487- 6 0.00000+ 0 0.00000+ 0pu239tgspec
```

```
 2.60000+ 0 3.00000+ 0          0          0          0         15pu239tgspec
 1.00000- 2 1.00000+ 9          0          0          0         15pu239tgspec
 2.6798e-13 2.1787e-08 4.3464e-15 2.5531e-08 7.3120e-11 6.2404e-07pu239tgspec
 2.6842e-13 6.8348e-06 6.7762e-09 1.9928e-05 1.3881e-06 1.1579e-04pu239tgspec
 6.8855e-06 3.0985e-04 4.3673e-05 1.2398e-03 1.0702e-02 1.0381e-02pu239tgspec
-1.0976e-02 1.0743e-02 2.7094e-03 2.1161e-02 5.0395e-03 1.6823e-01pu239tgspec
 1.0869e-02 5.7669e-01-5.8094e-03 1.3012e+00 1.9040e-04 1.1616e+01pu239tgspec
 3.00000+ 0 4.00000+ 0          0          0          0         16pu239tgspec
 1.00000- 2 1.00000+ 9          0          0          0         11pu239tgspec
 6.9755e-14 2.1788e-08 6.4648e-17 3.5070e-08 3.3208e-11 6.3082e-07pu239tgspec
 1.8274e-07 9.5235e-05 1.7328e-06 1.4742e-04 3.3545e-05 7.3355e-04pu239tgspec
 1.3924e-04 3.6290e-03 2.0586e-03 1.8077e-02 3.5005e-03 8.5234e-02pu239tgspec
 1.4610e-02 2.3233e-01-1.8515e-11 3.3544e-06                     pu239tgspec
 4.00000+ 0 5.00000+ 0          0          0          0         17pu239tgspec
 1.00000- 2 1.00000+ 9          0          0          0         11pu239tgspec
 7.78088-19 4.14163- 6 8.31114- 9 6.79999- 5 2.35714- 8 1.47786- 4pu239tgspec
 1.95550- 7 6.89631- 4 1.68067- 6 5.20794- 3 1.59112- 4 5.20737- 3pu239tgspec
 7.87545- 4 2.48929- 2 1.76339- 3 1.23610- 1 4.69275- 3 2.86217- 1pu239tgspec
 4.70164- 5 9.94260- 1 2.46301- 5 1.61966+ 1 0.00000+ 0 0.00000+ 0pu239tgspec
 5.00000+ 0 6.00000+ 0          0          0          0         18pu239tgspec
 1.00000- 2 1.00000+ 9          0          0          0         10pu239tgspec
 1.20035-19 4.28878- 6 3.00407-15 2.02205- 4 1.19142-12 6.55211- 4pu239tgspec
 2.95928- 7 3.00640- 3 2.49270- 5 6.33558- 3 2.01190- 4 1.92088- 2pu239tgspec
 9.90698- 6 3.25773- 2 1.32482- 3 1.53864- 1 1.41793- 3 9.21246- 1pu239tgspec
-1.81124-20 5.94536- 6 0.00000+ 0 0.00000+ 0 0.00000+ 0 0.00000+ 0pu239tgspec
 6.00000+ 0 7.50000+ 0          0          0          0         19pu239tgspec
 1.00000- 4 1.00000+ 9          0          0          0         12pu239tgspec
 1.85545-20 4.57245-06 3.30519-17 4.41793-04 5.72023-16 8.97811-04pu239tgspec
 3.86898-06 8.03833-03 1.02786-05 1.22545-02 1.23228-04 1.99914-01pu239tgspec
-4.42133-05 2.53015-01 2.57210-05 1.11151+00-6.96988-06 2.76967+00pu239tgspec
-2.50522-06 1.33733-02-7.29476-21 6.83542-06 2.15247-20 6.22339-05pu239tgspec
 0.         0.                   0          0          0         18pu241tbspec
 0.00000+ 0 2.00000- 1          0          0          0          1pu241tbspec
 1.00000- 4 1.00000+ 9          0          0          0         15pu241tbspec
 5.0181e-12 9.1340e-10 7.3856e-11 1.6167e-08 6.0715e-10 7.9718e-08pu241tbspec
 3.9406e-09 2.9938e-07 3.0280e-08 1.4231e-06 9.1134e-08 6.4041e-06pu241tbspec
 3.3598e-07 3.2033e-05 1.0010e-06 1.6970e-04 1.0205e-05 6.0190e-04pu241tbspec
 1.9859e-05 2.0263e-03 1.8695e-04 1.3365e-02 6.0245e-04 8.3026e-02pu241tbspec
 1.3407e-03 2.6484e-01 6.5911e-05 4.6569e-01 1.3051e-05 9.2266e+00pu241tbspec
 2.00000- 1 4.00000- 1          0          0          0          2pu241tbspec
 1.00000- 2 1.00000+ 9          0          0          0         14pu241tbspec
 6.30358-12 7.47858-10 6.75779-11 2.67630- 8 1.52961- 9 1.85533- 7pu241tbspec
 1.71977- 8 7.31721- 7 6.48446- 8 3.66768- 6 4.30363- 7 1.44176- 5pu241tbspec
 5.60149- 7 3.87136- 5 7.34644- 6 3.50836- 4 3.54697- 5 1.12426- 3pu241tbspec
 1.58271- 4 7.81855- 3 4.60593- 4 2.77698- 2 1.07162- 3 1.45392- 1pu241tbspec
 1.59265- 3 4.11181- 1 1.80721- 4 4.81820+ 0 0.00000+ 0 0.00000+ 0pu241tbspec
 4.00000- 1 6.00000- 1          0          0          0          3pu241tbspec
 1.00000- 2 1.00000+ 9          0          0          0         15pu241tbspec
 1.9777e-12 7.7288e-10 8.7972e-11 2.3961e-08 3.0144e-10 1.1390e-07pu241tbspec
 7.3075e-09 4.6902e-07 2.0323e-08 1.3448e-06 2.1177e-07 7.0839e-06pu241tbspec
 7.4886e-07 2.2411e-05 6.1319e-07 8.4010e-05 2.4193e-05 5.4252e-04pu241tbspec
 7.1308e-05 2.8624e-03 4.8888e-04 1.3515e-02 1.0529e-03 6.0732e-02pu241tbspec
 2.3162e-03 2.2418e-01 3.4196e-03 9.8609e-01 5.1133e-05 2.1786e+00pu241tbspec
 6.00000- 1 8.00000- 1          0          0          0          4pu241tbspec
 1.00000- 2 1.00000+ 9          0          0          0         15pu241tbspec
 1.6608e-12 7.4694e-10 1.4241e-10 2.3822e-08 3.3555e-10 1.0546e-07pu241tbspec
 5.1835e-09 4.3642e-07 1.8331e-08 1.3863e-06 2.2353e-07 7.4861e-06pu241tbspec
 8.0482e-07 2.7571e-05 3.1308e-07 4.1109e-05 2.1653e-05 5.0500e-04pu241tbspec
 6.6107e-05 2.5170e-03 6.1193e-04 1.2470e-02 1.0109e-03 4.5518e-02pu241tbspec
 3.6564e-03 1.7452e-01 7.1443e-03 9.4463e-01 9.7736e-06 1.0861e+00pu241tbspec
 8.00000- 1 1.00000+ 0          0          0          0          5pu241tbspec
 1.00000- 2 1.00000+ 9          0          0          0         15pu241tbspec
 1.9278e-12 7.5100e-10 2.0281e-10 2.3782e-08 2.9580e-10 9.8344e-08pu241tbspec
```

```
2.5178e-09 3.7345e-07 1.1359e-08 1.3405e-06 1.3742e-07 7.2250e-06pu241tbspec
6.8338e-07 2.5560e-05 7.5054e-07 8.3046e-05 2.2565e-05 5.6989e-04pu241tbspec
7.1883e-05 2.9892e-03 4.7177e-04 1.1269e-02 1.0217e-03 3.4158e-02pu241tbspec
3.7900e-03 1.4127e-01 1.5330e-02 9.7504e-01 5.4988e-05 3.8171e+00pu241tbspec
1.00000+ 0 1.20000+ 0          0          0          0           6pu241tbspec
1.00000- 2 1.00000+ 9          0          0          0          15pu241tbspec
2.0306e-12 7.5279e-10 2.5963e-10 2.3698e-08 1.9457e-10 8.5617e-08pu241tbspec
1.3716e-09 3.3379e-07 5.4314e-09 1.2375e-06 9.2149e-08 8.2483e-06pu241tbspec
8.5718e-07 3.3523e-05 7.2400e-07 3.3713e-04 1.7955e-05 5.3793e-04pu241tbspec
7.1834e-05 2.7754e-03 6.9653e-04 1.2810e-02 1.8762e-03 5.5663e-02pu241tbspec
4.6846e-03 1.8834e-01 1.4275e-02 9.9043e-01 1.7977e-04 2.1631e+00pu241tbspec
1.20000+ 0 1.40000+ 0          0          0          0           7pu241tbspec
1.00000- 2 1.00000+ 9          0          0          0          15pu241tbspec
2.0527e-12 7.5266e-10 3.0535e-10 2.3605e-08 8.5428e-11 6.3933e-08pu241tbspec
6.2893e-10 3.1344e-07 2.6730e-09 1.2112e-06 6.3849e-08 9.2235e-06pu241tbspec
7.4935e-07 3.4327e-05 6.5077e-07 3.4218e-04 1.3253e-05 5.0279e-04pu241tbspec
5.4403e-05 2.1759e-03 6.0532e-04 1.1614e-02 1.7542e-03 4.4801e-02pu241tbspec
7.8785e-03 2.0179e-01 1.8116e-02 1.1480e+00 2.2943e-04 2.1559e+00pu241tbspec
1.40000+ 0 1.60000+ 0          0          0          0           8pu241tbspec
1.00000- 2 1.00000+ 9          0          0          0          15pu241tbspec
1.8753e-12 7.5836e-10 3.3843e-10 2.3575e-08 4.0856e-11 4.9490e-08pu241tbspec
3.6279e-10 4.0544e-07 1.5590e-09 1.3324e-06 5.4163e-08 9.9792e-06pu241tbspec
6.7417e-07 3.5307e-05 5.5335e-07 3.4991e-04 1.4018e-05 5.4454e-04pu241tbspec
3.8973e-05 2.0113e-03 4.9858e-04 1.0196e-02 1.7603e-03 4.1680e-02pu241tbspec
7.4355e-03 1.7429e-01 2.6056e-02 1.0488e+00 2.9422e-04 2.1370e+00pu241tbspec
1.60000+ 0 1.80000+ 0          0          0          0           9pu241tbspec
1.00000- 2 1.00000+ 9          0          0          0          15pu241tbspec
1.4636e-12 7.5615e-10 3.4986e-10 2.3482e-08 3.7172e-11 4.9120e-08pu241tbspec
1.7191e-10 3.8030e-07 9.1201e-10 1.3481e-06 3.2030e-08 1.0127e-05pu241tbspec
5.8496e-07 3.5766e-05 4.5251e-07 3.6508e-04 1.6811e-05 6.3744e-04pu241tbspec
6.2362e-05 2.8679e-03 5.5966e-04 1.2838e-02 2.2304e-03 5.4037e-02pu241tbspec
8.9310e-03 2.0704e-01 2.6018e-02 1.0354e+00 3.2205e-04 2.1438e+00pu241tbspec
1.60000+ 0 1.80000+ 0          0          0          0          10pu241tbspec
1.00000- 2 1.00000+ 9          0          0          0          15pu241tbspec
9.1520e-13 7.4816e-10 3.3958e-10 2.3360e-08 3.6937e-11 4.9846e-08pu241tbspec
7.5772e-11 3.5536e-07 3.4699e-10 1.1352e-06 1.6398e-08 9.7801e-06pu241tbspec
3.7976e-07 3.1022e-05 4.5251e-08 5.7141e-04 1.3253e-05 6.0114e-04pu241tbspec
4.7154e-05 2.3260e-03 5.0029e-04 1.2741e-02 1.4915e-03 4.7402e-02pu241tbspec
5.3781e-03 1.3723e-01 2.9123e-02 6.7528e-01 3.2205e-03 4.2876e+00pu241tbspec
2.00000+ 0 2.20000+ 0          0          0          0          11pu241tbspec
1.00000- 2 1.00000+ 9          0          0          0          15pu241tbspec
4.2086e-13 7.6709e-10 3.0936e-10 2.3221e-08 3.3737e-11 5.3546e-08pu241tbspec
3.8155e-11 3.9754e-07 2.4899e-11 8.0388e-07 9.5952e-09 9.5003e-06pu241tbspec
2.5139e-07 2.7428e-05 3.2160e-07 4.7350e-04 1.2165e-05 6.3131e-04pu241tbspec
3.6907e-05 2.2167e-03 3.1610e-04 1.0680e-02 1.2204e-03 3.6899e-02pu241tbspec
8.4732e-03 1.5860e-01 2.5277e-02 7.3870e-01 7.0366e-03 2.2353e+00pu241tbspec
2.20000+ 0 2.40000+ 0          0          0          0          12pu241tbspec
1.00000- 2 1.00000+ 9          0          0          0          14pu241tbspec
1.9465e-13 7.7700e-10 2.5978e-10 2.3015e-08 2.6762e-11 5.0517e-08pu241tbspec
1.6098e-11 2.7963e-07 8.6971e-10 5.3293e-06 1.0094e-08 1.4459e-05pu241tbspec
1.7655e-07 2.6510e-05 1.1516e-05 6.4931e-04 4.3360e-05 2.3750e-03pu241tbspec
1.5539e-04 1.0368e-02 8.7218e-04 2.6363e-02 7.1684e-03 1.3466e-01pu241tbspec
2.1598e-02 5.3999e-01 1.5113e-02 1.8815e+00                     pu241tbspec
2.40000+ 0 2.60000+ 0          0          0          0          13pu241tbspec
1.00000- 2 1.00000+ 9          0          0          0          14pu241tbspec
1.7460e-13 7.5717e-10 2.0154e-10 2.2722e-08 1.8202e-11 5.2986e-08pu241tbspec
1.2333e-11 3.1645e-07 7.8490e-10 5.7889e-06 8.6047e-09 1.3768e-05pu241tbspec
1.5187e-07 3.0145e-05 8.8971e-06 6.3669e-04 3.3119e-05 1.9762e-03pu241tbspec
1.8844e-04 1.0113e-02 9.2624e-04 3.1794e-02 5.4243e-03 1.3892e-01pu241tbspec
8.2750e-03 3.2964e-01 2.9585e-02 1.3010e+00                     pu241tbspec
2.60000+ 0 3.00000+ 0          0          0          0          14pu241tbspec
1.00000- 2 1.00000+ 9          0          0          0          14pu241tbspec
3.0303e-13 7.2818e-10 2.1866e-10 2.2122e-08 8.6955e-12 4.8985e-08pu241tbspec
```

```
2.2200e-11 1.6074e-07 2.2908e-09 6.8771e-06 6.7747e-09 2.8853e-05pu241tbspec
1.6345e-07 2.8330e-05 1.2696e-05 6.3223e-04 5.0544e-05 1.9052e-03pu241tbspec
1.5716e-04 8.2362e-03 1.0156e-03 2.2965e-02 4.7363e-03 8.7476e-02pu241tbspec
2.5230e-02 2.8474e-01 5.8977e-02 1.5504e+00                     pu241tbspec
3.00000+ 0 4.00000+ 0          0          0          0         15pu241tbspec
1.00000- 2 1.00000+ 9          0          0          0         13pu241tbspec
4.6707e-13 7.2764e-10 6.1012e-11 2.1782e-08 2.6841e-11 2.0649e-07pu241tbspec
6.4702e-10 5.4192e-06 7.0193e-09 1.2900e-05 2.1785e-07 4.0247e-05pu241tbspec
2.4521e-05 7.2515e-04 6.5468e-05 2.5526e-03 4.5896e-04 1.2576e-02pu241tbspec
1.7438e-03 3.0181e-02 1.5504e-02 1.2411e-01 3.5966e-02 3.6376e-01pu241tbspec
1.3977e-01 1.1707e+00                                           pu241tbspec
4.00000+ 0 5.00000+ 0          0          0          0         16pu241tbspec
1.00000- 2 1.00000+ 9          0          0          0         12pu241tbspec
1.4865e-13 6.8492e-10 5.4103e-12 2.0751e-07 5.8321e-11 4.3652e-06pu241tbspec

9.7175e-09 2.1683e-05 2.2244e-08 1.4253e-04 1.1396e-06 5.2447e-04pu241tbspec
8.0682e-06 3.5733e-03 2.0966e-04 1.4273e-02 1.9730e-03 6.6171e-02pu241tbspec
4.5663e-03 1.2850e-01 1.5574e-02 3.0025e-01 1.2295e-01 1.3301e+00pu241tbspec
5.00000+ 0 6.00000+ 0          0          0          0         17pu241tbspec
1.00000- 2 1.00000+ 9          0          0          0         13pu241tbspec
3.78294-14 7.10055-10 1.04221-13 2.44597- 7 1.74897-13 1.38300- 6pu241tbspec
4.44035-10 1.29449- 5 3.35695- 9 4.74643- 5 1.51788- 8 1.90373- 4pu241tbspec
6.68819- 8 2.17654- 3 2.34149- 6 4.40514- 3 1.12036- 4 2.93440- 2pu241tbspec
7.97946- 4 1.72705- 1 7.24527- 3 2.10961- 1 4.94387- 2 1.07479+ 0pu241tbspec
4.11312- 4 2.39338+ 0 0.00000+ 0 0.00000+ 0 0.00000+ 0 0.00000+ 0pu241tbspec
6.00000+ 0 7.50000+ 0          0          0          0         18pu241tbspec
1.00000- 4 1.00000+ 9          0          0          0         12pu241tbspec
2.06895-15 6.78524-10 2.42058-14 6.18590- 7 8.71880-11 1.29570- 5pu241tbspec
1.93571-10 3.03401- 5 1.88239-10 8.62785- 5 7.78318- 8 1.71755- 3pu241tbspec
2.62285- 6 6.55928- 3 5.27877- 5 1.78139- 2 8.65601- 4 5.71350- 2pu241tbspec
5.96159- 3 1.67078- 1 1.32341- 2 8.40342- 1 1.11900- 3 5.71856+ 0pu241tbspec
0.         0.                   0          0          0         19pu241tgspec
0.00000+ 0 1.00000- 1          0          0          0          1pu241tgspec
1.00000- 2 1.00000+ 9          0          0          0         16pu241tgspec
1.9382e-13 1.1593e-09 6.3374e-13 7.1378e-09 7.0406e-12 3.1260e-08pu241tgspec
1.3734e-10 2.4762e-07 3.7611e-09 9.7344e-07 1.0101e-08 2.7562e-06pu241tgspec
7.5517e-09 1.1361e-05 5.5109e-08 6.4529e-05 1.1157e-06 3.9283e-04pu241tgspec
5.2429e-06 1.7599e-03 5.4537e-05 9.1289e-03 1.7281e-04 2.0053e-02pu241tgspec
4.8219e-04 9.0511e-02 1.6696e-03 6.6070e-01 5.6212e-06 1.1842e+00pu241tgspec
1.6266e-06 1.5408e+01                                           pu241tgspec
1.00000- 1 2.00000- 1          0          0          0          2pu241tgspec
1.00000- 2 1.00000+ 9          0          0          0         15pu241tgspec
2.34456-13 4.45667- 9 2.17307-12 1.85334- 8 1.83617-11 3.24925- 8pu241tgspec
9.33713-10 2.54778- 7 1.32990- 9 1.01559- 6 2.84457- 8 3.21009- 6pu241tgspec
1.38341- 7 6.19063- 5 1.77466- 6 1.91896- 4 9.30717- 6 5.92354- 4pu241tgspec
2.45409- 5 2.27666- 3 1.73811- 4 1.08154- 2 1.38831- 3 5.38058- 2pu241tgspec
5.09821- 3 3.89570- 1 1.61453- 2 2.04548+ 0 1.39258- 2 3.38490+ 0pu241tgspec
2.00000- 1 4.00000- 1          0          0          0          3pu241tgspec
1.00000- 2 1.00000+ 9          0          0          0         14pu241tgspec
1.59114-15 3.70170- 9 4.41878-14 9.66672- 9 1.42800-13 3.33271- 8pu241tgspec
8.94424-11 2.70292- 7 1.13861- 8 7.96509- 7 4.64208- 8 2.96178- 6pu241tgspec
4.37911- 7 1.34422- 5 1.58245- 5 3.55621- 4 4.94279- 5 6.47960- 4pu241tgspec
3.41450- 4 6.53312- 3 9.78252- 4 1.86173- 2 4.15470- 3 8.25699- 2pu241tgspec
1.57888- 2 5.08542- 1 5.58806- 2 2.52545+ 0 0.00000+ 0 0.00000+ 0pu241tgspec
4.00000- 1 6.00000- 1          0          0          0          4pu241tgspec
1.00000- 2 1.00000+ 9          0          0          0         15pu241tgspec
4.70606-14 3.89261- 9 6.30385-11 1.77221- 8 1.28196-10 3.23166- 8pu241tgspec
5.74148- 9 2.16748- 7 2.26826- 8 6.46534- 7 4.13934- 8 4.73931- 6pu241tgspec
5.48168- 7 1.30176- 5 9.48969- 7 4.58032- 5 2.05242- 5 2.79152- 4pu241tgspec
8.49546- 5 1.25292- 3 1.47293- 4 4.86522- 3 1.63792- 3 2.11183- 2pu241tgspec
1.56508- 2 1.23624- 1 2.52435- 2 6.49639- 1 1.43308- 2 2.08165+ 0pu241tgspec
6.00000- 1 8.00000- 1          0          0          0          5pu241tgspec
1.00000- 2 1.00000+ 9          0          0          0         15pu241tgspec
```

```
 2.78043-11 7.13537-10 3.59793-11 1.62409- 8 6.87199-11 2.77392- 8pu241tgspec
 1.40944- 8 1.26378- 7 2.11306- 7 2.60038- 6 1.35075- 6 1.42459- 5pu241tgspec
 1.46782- 5 1.62800- 4 5.60810- 5 8.39934- 4 3.16581- 4 4.17210- 3pu241tgspec
 1.88651- 3 2.33123- 2 7.27973- 3 1.27410- 1 2.07648- 2 5.67548- 1pu241tgspec
 4.30461- 2 1.82103+ 0-2.94810- 6 9.05437- 4-8.43624- 9 1.88036- 7pu241tgspec
 8.00000- 1 1.00000+ 0          0          0          0          6pu241tgspec
 1.00000- 2 1.00000+ 9          0          0          0         16pu241tgspec
 1.75087-17 5.85728-10 4.94486-12 2.17424- 8 8.71103-14 3.29540- 8pu241tgspec
 1.09415- 8 5.97510- 7 6.21514- 9 7.95048- 7 2.90740- 8 2.79781- 6pu241tgspec
 2.76477- 7 2.06772- 5 7.42718- 6 9.74716- 5 4.24783- 5 2.26097- 4pu241tgspec
 1.28143- 4 1.46427- 3 2.63515- 4 4.77529- 3 1.61359- 3 2.06592- 2pu241tgspec
 1.03546- 2 1.30641- 1 3.74376- 2 8.00948- 1 3.91726- 2 2.52252+ 0pu241tgspec
 7.83933- 4 2.32458+ 1 0.00000+ 0 0.00000+ 0 0.00000+ 0 0.00000+ 0pu241tgspec
 1.00000+ 0 1.20000+ 0          0          0          0          7pu241tgspec
 1.00000- 2 1.00000+ 9          0          0          0         13pu241tgspec
 1.9239e-17 1.1302e-09 2.8523e-11 2.1797e-08 4.1953e-10 5.4464e-07pu241tgspec
 7.8838e-09 2.3884e-06 8.6336e-08 1.0813e-05 1.1881e-06 3.2446e-05pu241tgspec
 1.2211e-05 1.9403e-04 6.9165e-05 9.3328e-04 2.5256e-04 4.1796e-03pu241tgspec
 1.3836e-03 1.8469e-02 4.8182e-03 8.2587e-02 1.1911e-02 3.4785e-01pu241tgspec
 1.2872e-02 6.0249e-01                                             pu241tgspec
 1.20000+ 0 1.40000+ 0          0          0          0          8pu241tgspec
 1.00000- 2 1.00000+ 9          0          0          0         15pu241tgspec
 3.1402e-17 1.7690e-09 3.7997e-13 2.1368e-08 2.5185e-13 3.9767e-08pu241tgspec
 2.2172e-11 1.8487e-07 6.8664e-10 7.7635e-07 2.7391e-08 2.8999e-06pu241tgspec
 4.4844e-07 2.0767e-05 2.3982e-06 5.7707e-05 1.8339e-05 2.7099e-04pu241tgspec
 8.6171e-05 1.2841e-03 7.9331e-04 8.5441e-03 1.9568e-03 2.4193e-02pu241tgspec
 6.6384e-03 1.1683e-01 2.4539e-02 5.4844e-01 1.1270e-02 1.1303e+00pu241tgspec
 1.40000+ 0 1.60000+ 0          0          0          0          9pu241tgspec
 1.00000- 2 1.00000+ 9          0          0          0         16pu241tgspec
 3.49541-18 3.86879-10 4.87900-12 2.21287- 8 4.39048-12 3.01812- 8pu241tgspec
 9.38172- 7 7.52767- 7 1.17592- 4 3.97955- 4 1.54941- 3 1.68551- 2pu241tgspec
 2.81316- 3 7.31063- 2 1.17067- 2 2.67799- 1 9.09305- 3 1.30695+ 0pu241tgspec
-7.31246- 5 4.41905- 4 2.75103- 4 5.03693- 3-1.15114- 6 7.98802- 7pu241tgspec
 1.99913- 7 1.54305- 6 9.21886- 7 4.51705- 5 3.41050- 7 1.00087- 6pu241tgspec
-2.98423- 7 1.67918- 6 0.00000+ 0 0.00000+ 0 0.00000+ 0 0.00000+ 0pu241tgspec
 1.60000+ 0 1.80000+ 0          0          0          0         10pu241tgspec
 1.00000- 2 1.00000+ 9          0          0          0         14pu241tgspec
 5.78961-19 5.58182-10 1.64002-12 2.18500- 8 6.01625-12 5.54722- 7pu241tgspec
 1.35450- 9 2.49918- 6 4.48152- 8 1.36826- 5 9.43737- 7 3.31363- 5pu241tgspec
 7.63633- 6 2.13704- 4 6.82269- 5 9.88596- 4 1.41539- 4 4.71298- 3pu241tgspec
 1.54491- 3 2.06715- 2 1.79394- 3 7.37730- 2 1.15328- 2 1.98557- 1pu241tgspec
 2.29650- 4 4.37980- 1 6.45818- 6 3.28052+ 1 0.00000+ 0 0.00000+ 0pu241tgspec
 1.80000+ 0 2.00000+ 0          0          0          0         11pu241tgspec
 1.00000- 2 1.00000+ 9          0          0          0         13pu241tgspec
 3.81694-19 4.56599-10 1.01179-12 2.18362- 8 2.39299-10 5.65560- 7pu241tgspec
 3.19568- 9 2.76517- 6 5.17710- 8 2.03791- 5 2.18508- 6 1.02981- 4pu241tgspec
 1.21192- 5 4.38793- 4 6.43196- 5 1.33033- 3 7.88918- 4 1.18323- 2pu241tgspec
 1.40535- 3 2.97055- 2 1.10388- 2 1.81636- 1 7.46935- 3 5.52633- 1pu241tgspec
 1.37008- 2 1.66637+ 0 0.00000+ 0 0.00000+ 0 0.00000+ 0 0.00000+ 0pu241tgspec
 2.00000+ 0 2.20000+ 0          0          0          0         12pu241tgspec
 1.00000- 2 1.00000+ 9          0          0          0         13pu241tgspec
 1.82449-12 2.20588- 8 1.92862-11 2.89408- 8 4.22276-10 6.28643- 7pu241tgspec
 4.05479- 9 2.88951- 6 3.30237- 8 2.21167- 5 1.80092- 6 8.95244- 5pu241tgspec
 2.63361- 5 4.99587- 4 6.96169- 5 1.57376- 3 6.65586- 4 1.14687- 2pu241tgspec
 2.29883- 3 3.62207- 2 6.72786- 3 2.22730- 1 7.22065- 3 3.01193- 1pu241tgspec
 2.96352- 4 1.09495+ 0 0.00000+ 0 0.00000+ 0 0.00000+ 0 0.00000+ 0pu241tgspec
 2.20000+ 0 2.40000+ 0          0          0          0         13pu241tgspec
 1.00000- 2 1.00000+ 9          0          0          0         14pu241tgspec
 1.3644e-12 2.1789e-08 2.5968e-15 2.4025e-08 5.3099e-17 1.7434e-08pu241tgspec
 8.3944e-10 6.0865e-07 1.2973e-10 8.6172e-07 3.5140e-10 1.8970e-06pu241tgspec
 6.4981e-08 3.3766e-05 2.4527e-06 9.2932e-05 3.6628e-05 7.1732e-04pu241tgspec
 1.3180e-03 1.2852e-02 1.2766e-04 2.0310e-02 5.6261e-03 1.0540e-01pu241tgspec
 1.1971e-02 5.1138e-01 9.8815e-04 1.1071e+00                     pu241tgspec
```

```
 2.40000+ 0 2.60000+ 0          0          0          0         14pu241tgspec
 1.00000- 2 1.00000+ 9          0          0          0         16pu241tgspec
 7.0262e-13 2.1780e-08 3.6750e-16 2.0486e-08 4.0483e-16 2.1771e-08pu241tgspec
 1.7176e-09 5.4704e-07 1.7751e-07 4.4906e-05 5.1619e-06 1.7335e-04pu241tgspec
 3.0960e-05 1.0297e-03 2.7988e-04 7.7995e-03 1.4778e-03 2.5964e-02pu241tgspec
 2.1192e-03 9.8854e-02 8.8573e-03 3.1497e-01 3.2485e-04 1.1752e+00pu241tgspec
 3.0104e-07 1.0022e-06-2.9969e-07 1.0082e-06 1.4979e-06 4.9976e-06pu241tgspec
-1.5005e-06 5.0020e-06                                             pu241tgspec
 2.60000+ 0 3.00000+ 0          0          0          0         15pu241tgspec
 1.00000- 2 1.00000+ 9          0          0          0         14pu241tgspec
 3.9095e-13 2.1791e-08 5.4169e-15 2.9418e-08 8.3830e-11 6.2800e-07pu241tgspec
 9.4061e-10 1.2570e-05 1.6405e-06 1.1337e-04 1.9730e-05 5.7745e-04pu241tgspec
 1.4012e-05 1.5434e-03 6.6987e-04 9.0665e-03 2.8863e-03 2.4520e-02pu241tgspec
 1.1490e-02 1.9208e-01 1.4294e-02 4.8600e-01-1.0030e-02 9.6478e-01pu241tgspec
 1.4960e-03 4.8756e-03-1.5522e-03 5.1801e-03                       pu241tgspec
 3.00000+ 0 4.00000+ 0          0          0          0         16pu241tgspec
 1.00000- 2 1.00000+ 9          0          0          0         16pu241tgspec
 1.0225e-13 2.1788e-08 7.3079e-15 6.9572e-08 2.5112e-15 8.5609e-08pu241tgspec
 6.4804e-11 7.0120e-07 1.6692e-07 8.9252e-05 2.0691e-06 1.3480e-04pu241tgspec
 3.9067e-05 8.1243e-04 2.7843e-04 5.7171e-03 3.0802e-03 2.1543e-02pu241tgspec
 1.4422e-02 1.3788e-01 3.4985e-02 4.3358e-01-1.9560e-02 9.9882e-01pu241tgspec
-3.5557e-11 9.5103e-07-5.8581e-12 5.3411e-06 3.0011e-06 1.0000e-05pu241tgspec
-3.0011e-06 1.0000e-05                                             pu241tgspec
 4.00000+ 0 5.00000+ 0          0          0          0         17pu241tgspec
 1.00000- 2 1.00000+ 9          0          0          0         11pu241tgspec
 2.1024e-19 4.1887e-06 6.5915e-09 6.8101e-05 2.3395e-07 2.9405e-04pu241tgspec
 1.1098e-06 3.6367e-04 2.9640e-05 2.6620e-03 4.6845e-04 1.1486e-02pu241tgspec
 2.4446e-03 6.0058e-02 3.3276e-02 3.7087e-01-1.7574e-02 4.2695e-01pu241tgspec
 2.9837e-03 5.1334e+00-3.9790e-03 2.6902e+00                       pu241tgspec
 5.00000+ 0 6.00000+ 0          0          0          0         18pu241tgspec
 1.00000- 2 1.00000+ 9          0          0          0         11pu241tgspec
 1.1264e-19 5.9220e-06 2.8794e-13 8.1990e-04 8.2574e-10 9.2328e-04pu241tgspec
 1.5950e-06 2.1833e-03 1.4149e-04 1.0467e-02 6.0148e-04 5.3968e-02pu241tgspec
 3.8953e-03 2.6097e-01 1.0774e-03 5.0365e-01-1.2949e-03 1.1347e+00pu241tgspec
-9.5811e-20 7.3170e-06 3.1297e-19 5.6327e-05                       pu241tgspec
 6.00000+ 0 7.50000+ 0          0          0          0         19pu241tgspec
 1.00000- 4 1.00000+ 9          0          0          0         10pu241tgspec
 3.00269-21 4.15307- 6 1.24756-21 9.53193- 6 6.60448-20 2.05406- 4pu241tgspec
 5.88668-17 6.39032- 4 3.63435- 9 4.43402- 3 1.14050- 5 8.48437- 3pu241tgspec
 4.34461- 6 1.16363- 2 1.17848- 4 2.07039- 1 2.47816- 5 1.89504+ 0pu241tgspec
-1.57509-21 1.31732- 5 0.00000+ 0 0.00000+ 0 0.00000+ 0 0.00000+ 0pu241tgspec
```

APPENDIX B
LATDOSE SOURCE CODE LISTING AND INPUT FILE EXAMPLES

B.1 LATDOSE Source Code Listing

```
      PROGRAM LATDOSE
C-----------------------------------------------------------------------
C                               DESCRIPTION
C
C This code demonstrates the channeling effect of gamma rays through a
C 2-D lattice of fuel pins. A point detector is moved from 0 to 45
C degrees in 1 degree increments, relative to the lower left corner of
C the lattice in order to develop the angular dependence of the dose.
C
C The method of solution is to trace rays from the center of each active
C pin in the lattice, to the detector, and solve for the total distance
C the ray traversed through pin cladding, fuel, and air, along the
C journey.  The Point-Kernel method (without build-up factors) is used
C to calculate the dose from each pin to the detector.
C
C Both 19 group (DELBG) energy spectrum and 7 group
C (Bozkurt & Tsoulfanidis) energy spectrum can be used and any number
C of pins can be specified, provided they are in an NxN matrix on
C constant square pitch, with N<=17.
C
C The output provides the dose contribution from each pin, for each
C detector position, for each energy group, as well as a total dose to
C the detector.  Also provided is a table of NxN numbers showing the
C fraction of the total dose based on pin position in the lattice.
C
C The code can be run in heterogeneous or homogeneous mode.  If
C homogeneous mode is selected, then equivallent smeared attenutation
C coefficients are calculated and the problem is run as a two region
C problem - within the NxN lattice (smeared material), and outside of
C the NxN lattice (air).
C
C                          INPUT AND OUTPUT FILES
C
C Device = 10, File = SETUP
C Data Contained:
C   HET[Logical]
C     = .TRUE. or .FALSE. (.TRUE. = heterogeneous)
C   EGRPS[INTEGER]
C     = Number of energy groups
C   DDIST[REAL]
C     = Detector distance from lower left pin center(cm)
C   NUMPINS[INTEGER]
C     = Total number of pins, NxN.  If not a perfect square,
C       job aborts.
C   RCLAD[REAL]
C     = Pin cladding radius(cm)
C   RFUEL[REAL]
C     = Pin fuel radius(cm)
C   PITCH[REAL]
C     = Pin array pitch(cm)
C   PPOS(NUMPINS)[REAL]
C     = Array of either 1.0's or 0.0's depending on whether
C       the lattice position is occupied by a pin. PPOS(n)
```

```
C       begins in the lower left pin position, increasing left
C       to right, bottom to top.  The data should be organized
C       as rows and columns, NxN.
C   RELSRC(NUMPINS)[REAL]
C     = Array of the relative source strength of the pin in
C       the lattice position.  Same ordering as PPOS array.
C   ATTEN(3)[REAL],SPECTRUM[REAL]
C     = Energy group linear attenuation coefficients for clad,
C       fuel, and air, in that order, followed by the gammas/sec
C       for that energy group.
C
C
C Device = 11, File = LATDOSE.OUT
C Data Contained:
C   X,Y PAIRS FOR PIN CENTERS (0,0 to N,N): Table of X,Y Coordinates
C                                           of pin centers.
C   PINS IN LATTICE POSITIONS (0,0 to N,N): Table of 1's or 0's
C                                           indicating if lattice
C                                           position is occupied by a
C                                           pin (1=yes).
C   LATTICE POSITION RELATIVE SOURCE STRENGTH (0,0 to N,N): Table of
C                                           relative source strengths
C                                           for each lattice position.
C   ENERGY GROUP:         The energy group number.
C    MASS ATTEN. COEFF. =  The mass attenuation coefficients for
C                          clad, fuel, air.
C    SOURCE GAMMAS/SEC =   The source strength for the ith energy group.
C    DETECTOR AT   [X,Y]   The X,Y coordinate of the point detector.
C     DETECTOR POSITION:   The position of the detector in degrees.
C     DOSE FROM PIN [1,NUMPINS] A loop over all pins showing the
C                               calculate dose from each pin to the
C                               point detector.
C     CONTRIBUTION FROM EACH PIN IN LATTICE: Table showing the fraction
C                                            of the total dose from each
C                                            pin in the lattice.
C                                            The table has pin 0,0 in
C                                            the lower left and
C                                            increases left to right
C                                            and bottom to top.
C     TOTAL CLADDING TRAVERSED = The total cladding distance that was
C                                traversed by rays in the problem.
C     TOTAL FUEL TRAVERSED =     The total fuel distance that was
C                                traversed by rays in the problem.
C     TOTAL AIR TRAVERSED =      The total air distance that was
C                                traversed by rays in the problem.
C
C    (Repeat the above output for detector positions 0 - 45)
C   (Repeat the above output for all energy groups)
C
C    DOSE MATRIX (ANGLE X ENERGY GROUP): A table of 46 rows X EGRPS
C                                        columns with the total dose
C                                        from each energy group
C                                        provided for each detector
C                                        angle.
C
C
C
C                           TH Trumbull 08/12/04
C-----------------------------------------------------------------------
      REAL ATTEN(3)
       REAL, ALLOCATABLE ::  AIR(:), CLAD(:), FUEL(:), DOSE(:),
     ;                       PPOS(:),RELSRC(:),FRAC(:),DOSETOT(:,:)
       REAL*8, ALLOCATABLE :: X(:),Y(:)
```

```
      REAL*8 CDIST,FDIST,DTX,DTY,RCLAD,RFUEL
      INTEGER EGRPS,NUMPINS
      LOGICAL CINTER, FINTER, HET
c
c Open SETUP and read some data:
       OPEN(UNIT=10, FILE='SETUP')
       READ(10,*) HET
       READ(10,*) EGRPS
       READ(10,*) DDIST
       READ(10,*) NUMPINS
       READ(10,*) RCLAD
       READ(10,*) RFUEL
       READ(10,*) PITCH
c
c Test to see if NUMPINS is perfect square:
      ROOT = SQRT(FLOAT(NUMPINS))
       IF(ROOT.NE.INT(ROOT))THEN
        WRITE(*,*) "NOT A SQUARE ARRAY!  ABORTING!"
        STOP
       ENDIF
       IPINS=INT(ROOT)
c
c Allocate memory now that array sizes are known:
      ALLOCATE(AIR(NUMPINS),CLAD(NUMPINS),FUEL(NUMPINS),DOSE(NUMPINS),
     ;         PPOS(NUMPINS),RELSRC(NUMPINS),FRAC(NUMPINS),
     ;         DOSETOT(46,EGRPS),X(NUMPINS),Y(NUMPINS))
c Initialize variables:
      CINTER = .FALSE.
      FINTER = .FALSE.
      AIR  = 0.
       CLAD = 0.
       FUEL = 0.
       DOSE = 0.
      DOSETOT = 0.
c The angular mesh is set at 1 degree over 0 to 45 degrees, relative to
c the lower left (0,0) position.
      NUMPOS = 45
c
c Open output file:
      OPEN(UNIT=11,FILE='LATDOSE.OUT')
c
c Generate and write out X,Y coordinates of pins for reference:
       WRITE(11,*) "X,Y PAIRS FOR PIN CENTERS (0,0 to N,N):"
      INUM = 0
      DO IROW = 0,IPINS-1
       DO ICOL = 0,IPINS-1
        INUM = INUM + 1
        X(INUM) = FLOAT(ICOL) * PITCH
        Y(INUM) = FLOAT(IROW) * PITCH
       ENDDO
        ITMP = INUM - IPINS + 1
       write(11,'(<IPINS>(F6.2,",",F6.2,2x))')
     ;      (X(ii),Y(ii), ii=ITMP,INUM)
      ENDDO
       write(11,*)
c
c Set up pin arrangement and relative source strength arrays:
       write(11,*) "PINS IN LATTICE POSITIONS (0,0 to N,N):"
       DO IROW=1,IPINS
        J=IPINS*(IROW-1)
        READ(10,*) (PPOS(J+ICOL),ICOL=1,IPINS)
        write(11,'(<IPINS>(F4.2,2x))') (PPOS(J+ICOL),ICOL=1,IPINS)
       ENDDO
```

```
      write(11,*)
c
      write(11,*) "LATTICE POSITION RELATIVE SOURCE STRENGTH (0,0 to N,N
     ;):"
       DO IROW=1,IPINS
        J=IPINS*(IROW-1)
        READ(10,*) (RELSRC(J+ICOL),ICOL=1,IPINS)
        write(11,'(<IPINS>(F4.2,2x))') (RELSRC(J+ICOL),ICOL=1,IPINS)
       ENDDO
      write(11,*)
c
c Energy groups, the outer-most loop
       DO IGRP = 1,EGRPS
c
        WRITE(11,*) "ENERGY GROUP:",IGRP
c Read mass attenuation coeff. and gammas/sec for group IGRP:
        READ(10,*) (ATTEN(ii),ii=1,3),SPECTRUM
c If doing Homogeneous calculation, smear atten. coeff.
        IF(.not.HET) THEN
c   ----> Smear the attenuation coefficients for clad and fuel:
c         Density: UO2 = 10 g/cc, clad = 7.874, Air = 1.21E-3
c         Calculate weight fractions and smeared attenuation coefficient
          FUELVOL = 3.1416*RFUEL**2.0
           CLADVOL = 3.1416*(RCLAD**2.0 - RFUEL**2.0)
              AIRVOL  = PITCH**2.0 - FUELVOL - CLADVOL
              TOTMASS  =    10.0 * FUELVOL  +
     ;                 7.874 * CLADVOL  +
     ;               1.21E-3 * AIRVOL
          TOTDENS  = TOTMASS / PITCH**2.0
c
           ATTEN(2)=(CLADVOL*ATTEN(1) + FUELVOL*ATTEN(2) +
     ;             AIRVOL*ATTEN(3)) / PITCH**2.0
              ATTEN(1) = 0.
        ENDIF
        WRITE(11,*) "MASS ATTEN. COEFF. =",(ATTEN(ii),ii=1,3)
        WRITE(11,*) "SOURCE GAMMAS/SEC=",SPECTRUM
c Angular Mesh
       DO ILOOP = 0,NUMPOS
        ANG = FLOAT(ILOOP) * 3.1416 / 180.0
        DTX  =  DDIST * COS(ANG)
        DTY  =  DDIST * SIN(ANG)
         write(11,*) "DETECTOR AT",DTX,DTY
c Begin Calculations:
c Loop over all pins to determine fraction of path through air, clad,
c & fuel to get to detector.
c
        DO IPIN = 1,NUMPINS
          IF (RELSRC(IPIN).GT.0)THEN
           IF (HET) THEN
c   ---> Do the heterogeneous solution
            CLAD(IPIN) = RCLAD - RFUEL
            FUEL(IPIN) = RFUEL
            AIR(IPIN) = ((DTX-X(IPIN))**2.0 + (DTY-Y(IPIN))**2.0)**0.5
             DO JPIN = 1,NUMPINS
               IF (X(JPIN).GE.X(IPIN).AND.JPIN.NE.IPIN) THEN
               CALL CROSS(X(IPIN),Y(IPIN),X(JPIN),Y(JPIN),DTX,DTY,
     ;                    RCLAD,RFUEL,IPIN,CDIST,FDIST,CINTER,FINTER)
               CDIST = CDIST * PPOS(IPIN)
                   FDIST = FDIST * PPOS(IPIN)
                IF(CINTER.AND.FINTER)THEN
                 CLAD(IPIN) = CLAD(IPIN) + CDIST - FDIST
                 FUEL(IPIN) = FUEL(IPIN) + FDIST
                ELSEIF(CINTER)THEN
```

```
                CLAD(IPIN) = CLAD(IPIN) + CDIST
               ELSEIF(FINTER)THEN
                write(11,*)"FUEL BUT NO CLAD INTERSECTION???"
                STOP
               ENDIF
              ENDIF
             ENDDO
            AIR(IPIN) = AIR(IPIN) - CLAD(IPIN) - FUEL(IPIN)
           ELSE
c   -----> Do the homogeneous solution
            SIDE = (FLOAT(IPINS)-0.5) * PITCH
            SLOPE = (DTY - Y(IPIN)) / (DTX - X(IPIN)) + 1E-20
            YINT = DTY - SLOPE * DTX
            YS = SLOPE * SIDE + DTY - SLOPE * DTX   !Ray at X plane
            XS = (SIDE - DTY + SLOPE * DTX) / SLOPE !Ray at Y plane
            IF(YS.LE.SIDE)THEN
             XA = SIDE
             YA = YS
            ELSEIF(XS.LE.SIDE)THEN
             XA = XS
             YA = SIDE
            ELSE
             write(11,*) "CANNOT SOLVE RAY EQUATION FOR INTERSECTION."
             write(11,*) "PINX,PINY,XS,YS:",X(IPIN),Y(IPIN),XS,YS
             STOP
            ENDIF
c
           AIR(IPIN) = ((DTX-XA)**2.0 + (DTY-YA)**2.0)**0.5
            FUEL(IPIN) = ((XA - X(IPIN))**2.0 + (YA - Y(IPIN))**2.0)**0.5
            CLAD(IPIN) = 0.0
            ENDIF !End HET or HOM conditional
c
           CALL CALDOSE(AIR(IPIN),CLAD(IPIN),FUEL(IPIN),HET,ATTEN,
     ;           PPOS(IPIN),RELSRC(IPIN),SPECTRUM,DOSE(IPIN))
           DOSETOT(ILOOP+1,IGRP) = DOSETOT(ILOOP+1,IGRP) + DOSE(IPIN)
          ENDIF  !End RELSRC > 0 conditional
         ENDDO   !Go back and do all pins
c Report out
         write(11,*) "DETECTOR POSITION:",ILOOP
         DO I=1,NUMPINS
          write(11,*) "DOSE FROM PIN ",I,"=",DOSE(I)
          FRAC(I) = DOSE(I) / DOSETOT(ILOOP+1,IGRP)
         ENDDO
         write(11,*) "CONTRIBUTION FROM EACH PIN IN LATTICE:"
         DO I=IPINS,1,-1
          write(11,1000) (FRAC((I-1)*IPINS+J),J=1,IPINS)
         ENDDO
         XC = 0.
         XF = 0.
         XA = 0.
         DO I = 1,IPINS
          XC = XC + CLAD(I)
          XF = XF + FUEL(I)
          XA = XA + AIR(I)
         ENDDO
         write(11,1001) XC,XF,XA
         write(11,*)
c Go back and do all detector positions
        ENDDO
c
c Go back and do all energy groups
      ENDDO
c
```

```
c Write out dose matrix: angle X spectrum
       write(11,*)
       write(11,*) "DOSE MATRIX (ANGLE X ENERGY GROUP):"
       DO IANG=1,46
        write(11,'(<EGRPS>(E10.4,2x))') (DOSETOT(IANG,J),J=1,EGRPS)
       ENDDO
c
      CLOSE(10)
      CLOSE(11)
1000  FORMAT(<IPINS>(2x,E10.4))
1001  FORMAT('TOTAL CLADDING TRAVERSED =',F8.4,/,
     ;       '    TOTAL FUEL TRAVERSED =',F8.4,/,
     ;       '     TOTAL AIR TRAVERSED =',F8.4)
      END
c
c---------------------------------------------------------------------
      SUBROUTINE CALDOSE(A,C,F,HET,ATTEN,P,S,SS,D)
c
      REAL ATTEN(3)
       LOGICAL HET
c P: pin or air, S: relative source strength, SS: DELBG Spectrum
       SOURCE = P * S * SS
c
      D = SOURCE / 4.0 / 3.1416    !Constant
     ;  /  (A+C+F)**2.0            !C/r^2
     ;  *  EXP(-ATTEN(1)*C)        !CLAD
     ;  *  EXP(-ATTEN(2)*F)        !FUEL
     ;  *  EXP(-ATTEN(3)*A)        !AIR
           write(*,*) (ATTEN(ii),ii=1,3),D
c
      RETURN
      END
c---------------------------------------------------------------------
      SUBROUTINE CROSS(PTX,PTY,PINX,PINY,DTX,DTY,
     ;                 RCLAD,RFUEL,IPIN,CDIST,FDIST,CINTER,FINTER)
c
      LOGICAL CINTER,FINTER
       DOUBLE PRECISION PTX,PTY,PINX,PINY,DTX,DTY,RCLAD,RFUEL,CDIST,FDIST
     ;                ,XM,YI,A,B,C,XC1,XC2,YC1,YC2,XF1,XF2,YF1,YF2
      CINTER = .FALSE.
      FINTER = .FALSE.
c
      FDIST = 0.
      CDIST = 0.
c Calculate slope (XM) and Y-intercept (YI):
      XM  = (DTY - PTY) / (DTX - PTX)
      YI = DTY - XM * DTX
c Calculate factors to solve quadratic equation:
      A = 1.0 + XM**2.0
      B = -2.0 * PINX + 2.0*XM*(YI-PINY)
      C = PINX**2.0 + (YI - PINY)**2.0 - RCLAD**2.0
c Test for ray intersection with clad:
      IF((B**2.0).GT.(4.0*A*C))THEN
c Solution exists for clad intersection.
       CINTER = .TRUE.
c Calculate roots:
       XC1 = (-B + (B**2.0 - 4.0*A*C)**0.5) / (2.0 * A)
       XC2 = (-B - (B**2.0 - 4.0*A*C)**0.5) / (2.0 * A)
       YC1 = XM * XC1 + YI
       YC2 = XM * XC2 + YI
       CDIST = ((XC1 - XC2)**2.0 + (YC1 - YC2)**2.0)**0.5
c Test for ray intersection with fuel:
       C = PINX**2.0 + (YI - PINY)**2.0 - RFUEL**2.0
```

```
       IF((B**2.0).GT.(4.0*A*C))THEN
c Solution exists for fuel intersection.
         FINTER = .TRUE.
c Calculate roots:
         XF1 = (-B + (B**2.0 - 4.0*A*C)**0.5) / (2.0 * A)
         XF2 = (-B - (B**2.0 - 4.0*A*C)**0.5) / (2.0 * A)
         YF1 = XM * XF1 + YI
         YF2 = XM * XF2 + YI
         FDIST = ((XF1 - XF2)**2.0 + (YF1 - YF2)**2.0)**0.5
       ENDIF
      ENDIF
c Test to see if pin found is in line from source pin to detector:
       IF(CINTER.AND.((PINY.LT.PTY.AND.DTY.GE.PTY).OR.
     ;               (PINY.GT.PTY.AND.DTY.LT.PTY)))THEN
c If pin is behind source pin, relative to detector, then ray does
c not intersect on the way to detector so reset CINTER and FINTER
c to false.
       CINTER = .FALSE.
       FINTER = .FALSE.
       ENDIF
c
c
      RETURN
      END
```

B.2 LATDOSE Input File Examples

B.2.1 19-Energy Group, Heterogeneous 7x7 Lattice with Corner Pin Activated and All Other Pins Unirradiated.

```
.true.                                              !true = heterogeneous model
19                                                  !No. of energy groups
25.97                                               !Distance to detector (cm)
49                                                  !No. of pins in lattice
0.59182                                             !Pin outer radius (cm)
0.5334                                              !Fuel outer radius (cm)
1.55702                                             !Lattice pitch (cm)
1.0 1.0 1.0 1.0 1.0 1.0 1.0                         !1.0 = pin, 0.0 = air
1.0 1.0 1.0 1.0 1.0 1.0 1.0
1.0 1.0 1.0 1.0 1.0 1.0 1.0
1.0 1.0 1.0 1.0 1.0 1.0 1.0
1.0 1.0 1.0 1.0 1.0 1.0 1.0
1.0 1.0 1.0 1.0 1.0 1.0 1.0
1.0 1.0 1.0 1.0 1.0 1.0 1.0
1.0 0.0 0.0 0.0 0.0 0.0 0.0                         !Relative source strengths
0.0 0.0 0.0 0.0 0.0 0.0 0.0
0.0 0.0 0.0 0.0 0.0 0.0 0.0
0.0 0.0 0.0 0.0 0.0 0.0 0.0
0.0 0.0 0.0 0.0 0.0 0.0 0.0
0.0 0.0 0.0 0.0 0.0 0.0 0.0
0.0 0.0 0.0 0.0 0.0 0.0 0.0
6.5629E+02 1.0691E+03 2.7447E-02 1.1574E+06      !Energy group attenuation
1.7923E+00 2.4748E+01 1.6527E-04 1.1463E+06      !coefficients for clad, fuel
1.2421E+00 1.0230E+01 1.6919E-04 2.3127E+06      !and air, source term for
1.0693E+00 3.7912E+00 1.6643E-04 1.8064E+06      !energy group in gamma rays
8.8433E-01 2.0065E+00 1.4166E-04 2.0631E+06      !per second.
1.0668E+00 2.0688E+00 1.7208E-04 2.2249E+06
9.5149E-01 1.5896E+00 1.5431E-04 1.1564E+06
8.6599E-01 1.3300E+00 1.4072E-04 1.0098E+06
6.9340E-01 1.0126E+00 1.1255E-04 7.5411E+05
```

```
5.5483E-01 7.9882E-01 8.9591E-05 5.1452E+05
7.1058E-01 1.0224E+00 1.1419E-04 3.9259E+05
6.7631E-01 9.7494E-01 1.0788E-04 3.2134E+05
6.5137E-01 9.4624E-01 1.0300E-04 2.4343E+05
6.3109E-01 9.2693E-01 9.8824E-05 2.4357E+05
4.5050E-01 6.7347E-01 6.9422E-05 3.0001E+05
3.9106E-01 6.0676E-01 5.8222E-05 3.2226E+05
5.2720E-01 8.5398E-01 7.5252E-05 1.4880E+05
4.9846E-01 8.5488E-01 6.6896E-05 2.9090E+04
4.0157E-01 7.2906E-01 5.0228E-05 1.4994E+03
```

B.2.2 7-Energy Group, Heterogeneous 17x17 PWR Lattice with All Pins Activated to the Same Source Strength.

```
.TRUE.                                               !true = heterogeneous model
7                                                    !No. of energy groups
15.25                                                !Distance to detector (cm)
81                                                   !No. of pins in lattice
0.4575                                               !Pin outer radius (cm)
0.4000                                               !Fuel outer radius (cm)
1.26                                                 !Lattice pitch (cm)
1.0 1.0 1.0 1.0 1.0 1.0 1.0 1.0 1.0                  !1.0 = pin, 0.0 = air
1.0 1.0 1.0 1.0 1.0 1.0 1.0 1.0 1.0
1.0 1.0 1.0 1.0 1.0 1.0 1.0 1.0 1.0
1.0 1.0 1.0 1.0 1.0 1.0 1.0 1.0 1.0
1.0 1.0 1.0 1.0 1.0 1.0 1.0 1.0 1.0
1.0 1.0 1.0 1.0 1.0 1.0 1.0 1.0 1.0
1.0 1.0 1.0 1.0 1.0 1.0 1.0 1.0 1.0
1.0 1.0 1.0 1.0 1.0 1.0 1.0 1.0 1.0
1.0 1.0 1.0 1.0 1.0 1.0 1.0 1.0 1.0
1.0 1.0 1.0 1.0 1.0 1.0 1.0 1.0 1.0                  !Relative source strengths
1.0 1.0 1.0 1.0 1.0 1.0 1.0 1.0 1.0
1.0 1.0 1.0 1.0 1.0 1.0 1.0 1.0 1.0
1.0 1.0 1.0 1.0 1.0 1.0 1.0 1.0 1.0
1.0 1.0 1.0 1.0 1.0 1.0 1.0 1.0 1.0
1.0 1.0 1.0 1.0 1.0 1.0 1.0 1.0 1.0
1.0 1.0 1.0 1.0 1.0 1.0 1.0 1.0 1.0
1.0 1.0 1.0 1.0 1.0 1.0 1.0 1.0 1.0
1.0 1.0 1.0 1.0 1.0 1.0 1.0 1.0 1.0
66.33611903 111.372854 0.002842741 1.511e-2    !Energy group attenuation
0.392459845 0.5820415  6.34899E-05 1.013e-4    !coefficients for clad, fuel
0.31047182  0.458636   4.83687E-05 1.511e-4    !and air, source term for
0.27295221  0.429098   4.01265E-05 3.935e-8    !energy group in gamma rays
0.25425146  0.424882   3.51258E-05 9.640e-23   !per second.
0.240940463 0.4374365  3.01367E-05 2.937e-23
0.242453846 0.5261383  2.29683E-05 4.689e-25
```

APPENDIX C

EXAMPLES OF MCNP INPUT FILES FOR HETEROGENEOUS AND HOMOGENEOUS CALCULATIONS

C.1 Input Files For 7x7 Lattice with Corner Pin Activated

C.1.1 Heterogeneous Example for Lattice at 0 Degrees Rotation

```
Experiment 3 - Single Pin Activation, 7x7 sq. lattice at 0 deg.
c 0.613 pitch lattice in counting apparatus
c ************************************************************
c ********************** New Collimator **********************
c ************************************************************
c
c                        ...Begin Cell Cards...
c ------------------------Outer cell and walls-------------------------
1   0          7:-8:9:-10:11:-12 $Void
2   1  -2.30   1 -7 -3 4 -6 5    $East concrete wall
3   1  -2.30   -2 8 -3 4 -6 5    $West concrete wall
4   1  -2.30   3 -9 -7 8 -6 5    $North concrete wall
5   1  -2.30   -4 10 -7 8 -6 5   $South concrete wall
6   1  -2.30   -7 8 -9 10 -11 6  $Concrete ceiling
7   1  -2.30   -7 8 -9 10 -5 12  $Concrete floor
c ----------------------------Bottom Lattice-----------------------------
8   2  -8.00   -13 19 -14 16 17 -18 23 24 27 (29:30:-31:-32)  $East side
9   2  -8.00    15 -21 -14 16 17 -18 25 26 28 (30:33:-32:-34) $West side
10  2  -8.00   -14 20 -19 21 17 -18 (35:37:-36:-38)           $North side
11  2  -8.00    16 -22 21 -19 17 -18 (35:40:-36:-39)          $South side
12  7 -1.205E-3 -23 17 -18
13  7 -1.205E-3 -24 17 -18
14  7 -1.205E-3 -25 17 -18
15  7 -1.205E-3 -26 17 -18
16  7 -1.205E-3 -27 17 -18
17  7 -1.205E-3 -28 17 -18
18  7 -1.205E-3 -29 -30 31 32 17 -18
19  7 -1.205E-3 -35 -37 36 38 17 -18
20  7 -1.205E-3 -30 -33 32 34 17 -18
21  7 -1.205E-3 -35 -40 36 39 17 -18
c ----------------------------Top Lattice-----------------------------
22  2  -8.00   -13 19 -14 16 -41 42 23 24 27 (29:30:-31:-32)  $East side
23  2  -8.00    15 -21 -14 16 -41 42 25 26 28 (30:33:-32:-34) $West side
24  2  -8.00   -14 20 -19 21 -41 42 (35:37:-36:-38)           $North side
25  2  -8.00    16 -22 21 -19 -41 42 (35:40:-36:-39)          $South side
26  7 -1.205E-3 -23 -41 42
27  7 -1.205E-3 -24 -41 42
28  7 -1.205E-3 -25 -41 42
29  7 -1.205E-3 -26 -41 42
30  7 -1.205E-3 -27 -41 42
31  7 -1.205E-3 -28 -41 42
32  7 -1.205E-3 -29 -30 31 32 -41 42
33  7 -1.205E-3 -35 -37 36 38 -41 42
34  7 -1.205E-3 -30 -33 32 34 -41 42
35  7 -1.205E-3 -35 -40 36 39 -41 42
c ---------------Air around fuel lattice & between plates---------------
36  7 -1.205E-3 -13 -14 15 16 18 -42 (19:20:-21:-22) #84
c                                     (62:-63:-81:-64:65)
c ----------------------Bottom Pin lattice ----------------------
37  0           -19 -20 21 22 17 -18 fill=1
38  0           -43 44 -45 46 u=1 lat=1 fill=-11:11 -11:11 0:0
                 2  6r  3  8r 2  6r
```

```
                2  4r  3 12r 2  4r
                2  2r  3 16r 2  2r
                2  1r  3 18r 2  1r
                2  1r  3 18r 2  1r
                2      3 20r 2
                2      3 20r 2
                       3 183r
                2 3 3 3 3 3 3 3 3 3 3 3 3 3 3 3 3 3 3 3 3 2
                2 3 3 3 3 4 4 4 4 4 4 4 3 3 3 3 3 3 3 3 3 2
                2 3 3 3 3 4 4 4 4 4 4 4 3 3 3 3 3 3 3 3 3 2
                2 2 3 3 3 4 4 4 4 4 4 4 3 3 3 3 3 3 3 3 2 2
                2 2 3 3 3 4 4 4 4 4 4 4 3 3 3 3 3 3 3 3 2 2
                2 2 2 3 3 4 4 4 4 4 4 4 3 3 3 3 3 3 3 2 2 2
                2 2 2 2 2 4 4 4 4 4 4 4 3 3 3 3 3 3 2 2 2 2 2
                2 2 2 2 2 4 4 4 4 4 4 4 3 3 3 3 2 2 2 2 2 2 2
c ==> Universe 2 for regions within grid that are all steel
39  2  -8.00     -49 u=2
40  2  -8.00      49 u=2
c ==> Universe 3 for regions within grid that are drilled out
41  7 -1.205E-3  -51 u=3
42  2  -8.00      51 u=3
c ==> Universe 4 for regions within grid that have pins
43  2  -8.00     -52              u=4 $Pin nipple
44  7 -1.205E-3   52 -51          u=4 $Air between lattice hole & nipple
45  2  -8.00      51              u=4 $Metal of lattice
c
c ----------------------Top Pin lattice ----------------------
46  0           -19 -20 21 22 42 -59 fill=5
47  0           -43 44 -45 46 u=5 lat=1 fill=-11:11 -11:11 0:0
                6  6r  7  8r 6  6r
                6  4r  7 12r 6  4r
                6  2r  7 16r 6  2r
                6  1r  7 18r 6  1r
                6  1r  7 18r 6  1r
                6      7 20r 6
                6      7 20r 6
                       7 183r
                6 7 7 7 7 7 7 7 7 7 7 7 7 7 7 7 7 7 7 7 7 6
                6 7 7 7 7 8 8 8 8 8 8 8 7 7 7 7 7 7 7 7 7 6
                6 7 7 7 7 8 8 8 8 8 8 8 7 7 7 7 7 7 7 7 7 6
                6 6 7 7 7 8 8 8 8 8 8 8 7 7 7 7 7 7 7 7 6 6
                6 6 7 7 7 8 8 8 8 8 8 8 7 7 7 7 7 7 7 7 6 6
                6 6 6 7 7 8 8 8 8 8 8 8 7 7 7 7 7 7 7 6 6 6
                6 6 6 6 6 8 8 8 8 8 8 8 7 7 7 7 7 7 6 6 6 6 6
                6 6 6 6 6 8 8 8 8 8 8 8 7 7 7 7 6 6 6 6 6 6 6
c ==> Universe 6 for regions within grid that are all steel
48  2  -8.00    -49 -41 u=6
49  2  -8.00     49 -41 u=6
50  7 -1.205E-3 -49 41 u=6
51  7 -1.205E-3  49 41 u=6
c ==> Universe 7 for regions within grid that are drilled out
52  7 -1.205E-3 -50 -41 u=7
53  2  -8.00     50 -41 u=7
54  7 -1.205E-3 -50 41 u=7
55  7 -1.205E-3  50 41 u=7
c ==> Universe 8 for regions within grid that have pins
56  5  -1.36     -48 -58        u=8 $Spring region
57  2  -8.00      48 -49 -58    u=8 $Clad
58  7 -1.205E-3   49 -50 -41    u=8 $Air between lattice hole and clad
59  2  -8.00      -41 50        u=8 $Metal of Lattice
60  12 -3.93      -49 58        u=8 $Pin notch region
61  7 -1.205E-3  41 49          u=8 $Air aound top of pin
c
```

```
c ---------------------- Pin lattice ----------------------
62  0           -100 101 -20 102 18 -42 fill=9
63  0           -43 44 -45 46 u=9 lat=1 fill=-11:11 -11:11 0:0
                                10 528r
c
64  2  -8.00      -49  -53        u=10 $Plug
65  7 -1.205E-3    49  -53        u=10 $Air around plug
66  3 -3.99       53 -54 -47     u=10 $Al2O3
67  6  1.83E-6    53 -54 47 -48  u=10 $He around Al2O3
68  2  -8.00      53 -54 48 -49  u=10 $Clad
69  7 -1.205E-3  53  49          u=10 $Air around entire length of pin
70  4 -10.08      54 -55 -47     u=10 $Fuel region
71  6  1.83E-6    54 -55 47 -48  u=10 $He around Al2O3
72  2  -8.00      54 -55 48 -49  u=10 $Clad
73  3  -3.99      55 -56 -47     u=10 $Al2O3
74  6  1.83E-6    55 -56 47 -48  u=10 $He around Al2O3
75  2  -8.00      55 -56 48 -49  u=10 $Clad
76  2  -8.00      56 -57 -47     u=10 $SS spacer
77  6  1.83E-6    56 -57 47 -48  u=10 $He around spacer
78  2  -8.00      56 -57 48 -49  u=10 $Clad
79  5  -1.36      57 -48 -58     u=10 $Spring region
80  2  -8.00      57 48 -49      u=10 $Clad
c -----------------------Air Around Pin Lattice------------------------
81  7 -1.205E-3   22 -102 -19 21 18 -42
82  7 -1.205E-3  -19 100 -20 102 18 -42
83  7 -1.205E-3  -20 21 -101 102 18 -42 #84
c                (62:-63:-81:-64:65)
c -------------------------Lead Shield Volume--------------------------
84  0            81 -61 -62 63 64 -65 fill=11
85  8  -11.35    60 66               u=11 $Top bricks
86  8  -11.35    60 -67              u=11 $Bottom bricks
87  8  -11.35    60 -66 67 -68 70    u=11 $Right brick
88  7 -1.205E-3  60 -66 67 -70       u=11 $Right air volume
89  8  -11.35    60 -66 67 69 -71    u=11 $Left brick
90  7 -1.205E-3  60 -66 67 71        u=11 $Left air volume
c ==> Use this cell when front brick is used:
91  8  -11.35    -60 103 -104        u=11 $Half Front Brick,lead
104 8  -11.35    -60 72 -73          u=11 $Half Front Brick,lead
105 8  -11.35    -60 73 -103 105     u=11 $Fill col. top slit, lead
106 8  -11.35    -60 73 -103 -106    u=11 $Fill col. bot. slit, lead
c
92  7 -1.205E-3 -60 -72              u=11 $Right air volume
93  7 -1.205E-3 -60  104             u=11 $Left air volume
94  7 -1.205E-3 -60 73 -103 -105 106 u=11 $Collimator
c ==> Detector
95  9   -2.94   60 -76 -75           u=11 $Front window Al
96  10  -0.55   76 -78 -79           u=11 $Front window refelctor
97  11  -3.70   78 -77 -80           u=11 $NaI crystal
98  9   -2.94   -75 79 76 -80        u=11 $Al canning
99  10  -0.55   78 77 -79 -80        u=11 $Reflector coating
100  7 -1.205E-3 -66 67 68 -69 80     u=11 $Air cavity behind detector
101  7 -1.205E-3 60 -66 67 68 -69 75 -80 u=11 $Air cavity around detector
c -----------------------Air surrounding apparatus---------------------
102   7 -1.205E-3 -13 -14 15 16 41 -59 (19:20:-21:-22)  $Above top lattice
103  7 -1.205E-3 -1 2 -3 4 5 -6
               (13:14:-15:-16:-17:59) #84
c               (61:62:-63:-64:65)
c ======================================================================

c ======================================================================
c                        ...Begin Surface Cards...
1     px  152.0
2     px -152.0
```

```
3     py  244.0
4     py -244.0
5     pz    0.0
6     pz  285.0
c
7     px  213.0
8     px -213.0
9     py  305.0
10    py -305.0
11    pz  305.0
12    pz  -20.0
c
13    px   33.02
14    py   33.02
15    px  -33.02
16    py  -33.02
17    pz    7.62
18    pz    8.89
19    px   17.90
20    py   17.90
21    px  -17.90
22    py  -17.90
23    c/z  29.21  29.21 1.67    $1 5/16" dia. holes
24    c/z  29.21 -29.21 1.67
25    c/z -29.21  29.21 1.67
26    c/z -29.21 -29.21 1.67
27    c/z  29.21   0    0.635   $0.5" dia. holes
28    c/z -29.21   0    0.635
29    px   25.718               $Control rod cut-outs
30    py    3.731
31    px   18.256
32    py   -3.731
33    px  -18.256
34    px  -25.718
35    px    3.731
36    px   -3.731
37    py   25.718
38    py   18.256
39    py  -25.718
40    py  -18.256
c
41    pz  104.775             $Top lattice plate
42    pz  103.505
c
43    px    0.779             $Pin volume parallelpiped
44    px   -0.779
45    py    0.779
46    py   -0.779
47    cz 0.5334               $Fuel OD
48    cz 0.54102              $Clad ID
49    cz 0.59182              $Clad OD
50    cz 0.635                $0.5" hole
51    cz 0.3175               $0.25" hole
52    cz 0.3137               $Bottom of pin nipple
53    pz 10.795               $Bottom plug
54    pz 11.1125              $Al2O3 Spacer
55    pz 102.5525             $Al2O3 Spacer
56    pz 102.87               $Pad
57    pz 103.1875             $Spring
58    pz 110.1725             $Bottom of pin handling notch area
59    pz 113.3475             $Top of pin
c ---------------------------- Detector Surfaces --------------------------
c
```

```
c ****************************** New Collimator ***************************
c
c     To move detector, add or subtract the distance moved along the y-axis
c     in centimeters from every py plane and correct offset in TR1 card. The
c     TR1 offset = (#pins along y-axis from lattice plate center to active pin)
c                  * PITCH.  EXP3C TR1 offset = 6*PITCH = 9.342 cm.
c
c     The measured distance in EXP3B from center of active pin to the detector
c     face was 20.412 cm.  The reference is the detector face (#60).
c     Offsets are as follows: Surf. #    Offset
c                               61        20.32
c                               76         0.05
c                               78         0.21
c                               80         5.40
c                               81        -5.08
c
60 1   py   25.492              $Front of detector face
61 1   py   45.812              $Back of universe
76 1   py   25.542              $Front window can
78 1   py   25.702              $Front window reflector
80 1   py   30.892              $Al can
81 1   py   15.332              $front of universe
c
62 1   px   10.16
63 1   px  -10.16
64 1   pz   47.9425
65 1   pz   68.2625
66 1   pz   63.1825
67 1   pz   53.0225
68 1   px   -2.95
69 1   px    2.95
70 1   px   -8.03
71 1   px    8.03
c
72 1   px   -5.5563
73 1   px   -0.4765
103 1  px    0.4765
104 1  px    5.5563
105 1  pz   60.6425
106 1  pz   55.5625
c
75 1   c/y   0.0 58.1025 2.855 $Detector Case
77 1   c/y   0.0 58.1025 2.645 $O.D. Crystal
79 1   c/y   0.0 58.1025 2.805 $I.D. Canning
c ---------------------------------------------------------------------
100   px   0.778
101   px -10.114
102   py  7.001
c =====================================================================

c =====================================================================
c                            ...Begin Data Cards...
mode p
imp:p 0 1 104r
c ----------------------------Lattice Rotation-------------------------
c Surface transformation cards for detector relative to lattice
*tr1     0.0000  7.785  0.0000 $Displacment Vector
         0.00   90.00   90.00  $Angle between XYZ & X'
        90.00    0.00   90.00  $Angle between XYZ & Y'
c ----------------------------------Tallies----------------------------
e4    50e-3 180e-3 450e-3 550e-3 1.0
      1.5 2.0 3.0 4.0 5.0 6.0 7.5
c
```

```
c e5    50e-3 180e-3 450e-3 550e-3 1.0
c      1.5 2.0 3.0 4.0 5.0 6.0 7.5
c
e8    0 1.0e-5 50e-3 180e-3 450e-3 550e-3 1.00
        2.0 3.0 4.0 5.0 6.0 7.5
c ==> Cell Flux * Source Particles / sec (from DELBG)
f4:p   97
fm4    1.6148e7
c ==> Point detector at detector face to get collided and uncollided flux
c     (X,Y,Z) position = (r*sin(theta),r*cos(theta),58.1025)
c                  r = 28.197 for EXP3C
c f5:p   0.0 28.197 58.1025 0.0   $ 0 deg.
c
c ==> Pulse ht. Tally in NaI(Tl) detector
f8:p   97
c ---------------------------------Materials---------------------------
c ==> Concrete wt. frac's from NIST (ordinary)
m1     1001 -0.022100
       6000 -0.002485
       8016 -0.574930
      11023 -0.015208
      12000 -0.001266
      13027 -0.019953
      14000 -0.304627
      19000 -0.010045
      20000 -0.042951
      26000 -0.006435
c ==> SS304 wt. fractions from ANL Assay Letter & The Hendrix Group Web Site
m2    27000 -0.00084
      24000 -0.18690
      29000 -0.00170
      26000 -0.68991
      25000 -0.01060
      42000 -0.00200
      28000 -0.09650
       6000 -0.00080
      15000 -0.00045
      16000 -0.00030
      14000 -0.01000
c ==> Al2O3 Compositions & density from Ceradyne's Web Site
m3    13027 2.0
       8016 3.0
c ==> Fuel Composition from ANL Assay Letter (0.32854-U + 0.67146-O)
m4    92233 0.0000009855
      92234 0.0000844348
      92235 0.0159864279
      92236 0.0001550709
      92238 0.3123130809
      8016  0.67146
c ==> Spring region (smeared density = 1.36 g/cc, wt % SS = 99.99%, He = 0.01%)
m5    27000 -0.0008316
      24000 -0.1850310
      29000 -0.0016830
      26000 -0.6830109
      25000 -0.0104940
      42000 -0.0019800
      28000 -0.0955350
       6000 -0.0007920
      15000 -0.0004455
      16000 -0.0002970
      14000 -0.0099000
       2004 -0.01
c ==> He gas region
```

```
m6     2004 1.0
c ==> Dry Air wt. frac's from NIST
m7     6000 -0.000124
       7015 -0.755268
       8016 -0.231781
      18000 -0.012827
c ==> Lead Shielding
m8     82206   0.247
       82207   0.227
       82208   0.526
c ==> Aluminum canning on detector (0.5 mm thk., rho = 147mg/cm^2)
m9     13027   1.000
c ==> Al2O3 Oxide reflector (1.6 mm thk., rho = 88mg/cm^2)
m10    13027   2.0
        8016   3.0
c ==> NaI Detector
m11    11023   0.5
       53127   0.5
c ==> Handling Notch Region (smeared density = 3.93 g/cc, wt% SS = 99.98)
m12   27000 -0.0008398
      24000 -0.1868626
      29000 -0.0016997
      26000 -0.6897720
      25000 -0.0105979
      42000 -0.0019996
      28000 -0.0964807
       6000 -7.9986480E-4
      15000 -0.0004499
      16000 -0.0002999
      14000 -0.0099980
c wt% Air = 0.02
       7015 -1.5105360E-4
       8016 -4.6356200E-5
      18000 -2.6254000E-6
c ----------------------------Source Definition-----------------------
sdef  CEL=D1 POS=0 0 0 AXS=0 0 1 RAD D2 EXT D3 ERG D4 PAR=2
             VEC=0 1 0 DIR D5
si1  L 62:63(0 5 0):70
sp1    1.0
c
si2  0. 0.5335  $Sampling radius of fuel region in a pin
c
c 3"(7.62 cm) Axial Nodes
si3  H    11.1125 18.7325 26.3525 33.9725 41.5925 49.2125 56.8325
          64.4525 72.0725 79.6925 87.3125 94.9325 102.5525
c Relative Total Neutron Flux in axial node - Assume delayed gamma
c flux follows the neutron flux during operation
sp3       0. 0.033 0.058 0.078 0.091 0.109 0.115 0.118 0.114
             0.102 0.084 0.062 0.036
c
c 19 energy group structure in DELBG same for all times:
si4    H 0 .1  .2  .4  .6  .8 1.0 1.2 1.4 1.6 1.8
          2.0 2.2 2.4 2.6 3.0 4.0 5.0 6.0 7.5
c Gammas per second, from DELBG:
c 470 sec after SCRAM: Total Source = 1.6148e7 photons/sec
sp4  0. 0.0717 0.0710 0.1432 0.1119 0.1278 0.1378 0.0716
        0.0625 0.0467 0.0319 0.0243 0.0199 0.0151 0.0151
        0.0186 0.0200 0.0092 0.0018 0.0001
c Source Bias (exponential)
sb5    -31 3
nps 8.0e7
print
```

C.1.2 Heterogeneous Example for Lattice at 25 Degrees Rotation

```
Experiment 3 - Single Pin Activation, 7x7 sq. lattice at 25 deg.
c 0.613 pitch lattice in counting apparatus
c ************************************************************
c ********************** New Collimator **********************
c ************************************************************
c
c                        ...Begin Cell Cards...
c ------------------------Outer cell and walls-------------------------
1   0          7:-8:9:-10:11:-12 $Void
2   1  -2.30   1 -7 -3 4 -6 5    $East concrete wall
3   1  -2.30   -2 8 -3 4 -6 5    $West concrete wall
4   1  -2.30   3 -9 -7 8 -6 5    $North concrete wall
5   1  -2.30   -4 10 -7 8 -6 5   $South concrete wall
6   1  -2.30   -7 8 -9 10 -11 6  $Concrete ceiling
7   1  -2.30   -7 8 -9 10 -5 12  $Concrete floor
c --------------------------Bottom Lattice-----------------------------
8   2  -8.00   -13 19 -14 16 17 -18 23 24 27 (29:30:-31:-32)  $East side
9   2  -8.00    15 -21 -14 16 17 -18 25 26 28 (30:33:-32:-34) $West side
10  2  -8.00   -14 20 -19 21 17 -18 (35:37:-36:-38)           $North side
11  2  -8.00    16 -22 21 -19 17 -18 (35:40:-36:-39)          $South side
12  7 -1.205E-3 -23 17 -18
13  7 -1.205E-3 -24 17 -18
14  7 -1.205E-3 -25 17 -18
15  7 -1.205E-3 -26 17 -18
16  7 -1.205E-3 -27 17 -18
17  7 -1.205E-3 -28 17 -18
18  7 -1.205E-3 -29 -30 31 32 17 -18
19  7 -1.205E-3 -35 -37 36 38 17 -18
20  7 -1.205E-3 -30 -33 32 34 17 -18
21  7 -1.205E-3 -35 -40 36 39 17 -18
c ---------------------------Top Lattice-----------------------------
22  2  -8.00   -13 19 -14 16 -41 42 23 24 27 (29:30:-31:-32)  $East side
23  2  -8.00    15 -21 -14 16 -41 42 25 26 28 (30:33:-32:-34) $West side
24  2  -8.00   -14 20 -19 21 -41 42 (35:37:-36:-38)           $North side
25  2  -8.00    16 -22 21 -19 -41 42 (35:40:-36:-39)          $South side
26  7 -1.205E-3 -23 -41 42
27  7 -1.205E-3 -24 -41 42
28  7 -1.205E-3 -25 -41 42
29  7 -1.205E-3 -26 -41 42
30  7 -1.205E-3 -27 -41 42
31  7 -1.205E-3 -28 -41 42
32  7 -1.205E-3 -29 -30 31 32 -41 42
33  7 -1.205E-3 -35 -37 36 38 -41 42
34  7 -1.205E-3 -30 -33 32 34 -41 42
35  7 -1.205E-3 -35 -40 36 39 -41 42
c ---------------Air around fuel lattice & between plates--------------
36  7 -1.205E-3 -13 -14 15 16 18 -42 (19:20:-21:-22) #84
c                                    (62:-63:-81:-64:65)
c ---------------------Bottom Pin lattice ----------------------
37  0           -19 -20 21 22 17 -18 fill=1
38  0           -43 44 -45 46 u=1 lat=1 fill=-11:11 -11:11 0:0
                 2  6r  3  8r 2  6r
                 2  4r  3 12r 2  4r
                 2  2r  3 16r 2  2r
                 2  1r  3 18r 2  1r
                 2  1r  3 18r 2  1r
                 2      3 20r 2
                 2      3 20r 2
                        3 183r
                 2 3 3 3 3 3 3 3 3 3 3 3 3 3 3 3 3 3 3 3 3 3 2
```

```
                2 3 3 3 3 4 4 4 4 4 4 4 3 3 3 3 3 3 3 3 3 3 2
                2 3 3 3 3 4 4 4 4 4 4 4 3 3 3 3 3 3 3 3 3 3 2
                2 2 3 3 3 4 4 4 4 4 4 4 3 3 3 3 3 3 3 3 3 2 2
                2 2 3 3 3 4 4 4 4 4 4 4 3 3 3 3 3 3 3 3 3 2 2
                2 2 2 3 3 4 4 4 4 4 4 4 3 3 3 3 3 3 3 3 2 2 2
                2 2 2 2 2 4 4 4 4 4 4 4 3 3 3 3 3 3 2 2 2 2 2
                2 2 2 2 2 4 4 4 4 4 4 4 3 3 3 3 2 2 2 2 2 2 2
c ==> Universe 2 for regions within grid that are all steel
39  2  -8.00     -49 u=2
40  2  -8.00      49 u=2
c ==> Universe 3 for regions within grid that are drilled out
41  7 -1.205E-3  -51 u=3
42  2  -8.00      51 u=3
c ==> Universe 4 for regions within grid that have pins
43  2  -8.00     -52              u=4 $Pin nipple
44  7 -1.205E-3   52 -51          u=4 $Air between lattice hole & nipple
45  2  -8.00      51              u=4 $Metal of lattice
c
c ----------------------Top Pin lattice ----------------------
46  0           -19 -20 21 22 42 -59 fill=5
47  0           -43 44 -45 46 u=5 lat=1 fill=-11:11 -11:11 0:0
                 6  6r  7  8r 6  6r
                 6  4r  7 12r 6  4r
                 6  2r  7 16r 6  2r
                 6  1r  7 18r 6  1r
                 6  1r  7 18r 6  1r
                 6      7 20r 6
                 6      7 20r 6
                        7 183r
                 6 7 7 7 7 7 7 7 7 7 7 7 7 7 7 7 7 7 7 7 7 7 6
                 6 7 7 7 7 8 8 8 8 8 8 8 7 7 7 7 7 7 7 7 7 7 6
                 6 7 7 7 7 8 8 8 8 8 8 8 7 7 7 7 7 7 7 7 7 7 6
                 6 6 7 7 7 8 8 8 8 8 8 8 7 7 7 7 7 7 7 7 7 6 6
                 6 6 7 7 7 8 8 8 8 8 8 8 7 7 7 7 7 7 7 7 7 6 6
                 6 6 6 7 7 8 8 8 8 8 8 8 7 7 7 7 7 7 7 7 6 6 6
                 6 6 6 6 6 8 8 8 8 8 8 8 7 7 7 7 7 7 6 6 6 6 6
                 6 6 6 6 6 8 8 8 8 8 8 8 7 7 7 7 6 6 6 6 6 6 6
c ==> Universe 6 for regions within grid that are all steel
48  2  -8.00    -49 -41 u=6
49  2  -8.00     49 -41 u=6
50  7 -1.205E-3 -49 41 u=6
51  7 -1.205E-3  49 41 u=6
c ==> Universe 7 for regions within grid that are drilled out
52  7 -1.205E-3 -50 -41 u=7
53  2  -8.00     50 -41 u=7
54  7 -1.205E-3 -50 41 u=7
55  7 -1.205E-3  50 41 u=7
c ==> Universe 8 for regions within grid that have pins
56  5  -1.36     -48 -58        u=8 $Spring region
57  2  -8.00      48 -49 -58    u=8 $Clad
58  7 -1.205E-3   49 -50 -41    u=8 $Air between lattice hole and clad
59  2  -8.00      -41 50        u=8 $Metal of Lattice
60  12 -3.93      -49 58        u=8 $Pin notch region
61  7 -1.205E-3  41 49          u=8 $Air aound top of pin
c
c ---------------------- Pin lattice ----------------------
62  0           -100 101 -20 102 18 -42 fill=9
63  0           -43 44 -45 46 u=9 lat=1 fill=-11:11 -11:11 0:0
                                  10 528r
c
64  2  -8.00      -49  -53        u=10 $Plug
65  7 -1.205E-3    49  -53        u=10 $Air around plug
66  3 -3.99      53 -54 -47     u=10 $Al2O3
```

```
67  6  1.83E-6   53 -54 47 -48  u=10 $He around Al2O3
68  2  -8.00     53 -54 48 -49  u=10 $Clad
69  7 -1.205E-3  53  49         u=10 $Air around entire length of pin
70  4 -10.08     54 -55 -47     u=10 $Fuel region
71  6  1.83E-6   54 -55 47 -48  u=10 $He around Al2O3
72  2  -8.00     54 -55 48 -49  u=10 $Clad
73  3  -3.99     55 -56 -47     u=10 $Al2O3
74  6  1.83E-6   55 -56 47 -48  u=10 $He around Al2O3
75  2  -8.00     55 -56 48 -49  u=10 $Clad
76  2  -8.00     56 -57 -47     u=10 $SS spacer
77  6  1.83E-6   56 -57 47 -48  u=10 $He around spacer
78  2  -8.00     56 -57 48 -49  u=10 $Clad
79  5  -1.36     57 -48 -58     u=10 $Spring region
80  2  -8.00     57 48 -49      u=10 $Clad
c ----------------------Air Around Pin Lattice-------------------------
81  7 -1.205E-3   22 -102 -19 21 18 -42
82  7 -1.205E-3  -19 100 -20 102 18 -42
83  7 -1.205E-3  -20 21 -101 102 18 -42 #84
c -------------------------Lead Shield Volume--------------------------
84  0            81 -61 -62 63 64 -65 fill=11
85  8  -11.35    60 66               u=11 $Top bricks
86  8  -11.35    60 -67              u=11 $Bottom bricks
87  8  -11.35    60 -66 67 -68 70    u=11 $Right brick
88  7 -1.205E-3  60 -66 67 -70       u=11 $Right air volume
89  8  -11.35    60 -66 67 69 -71    u=11 $Left brick
90  7 -1.205E-3  60 -66 67 71        u=11 $Left air volume
c ==> Use this cell when front brick is used:
91  8  -11.35    -60 103 -104        u=11 $Half Front Brick,lead
104 8  -11.35    -60 72 -73          u=11 $Half Front Brick,lead
105 8  -11.35    -60 73 -103 105     u=11 $Fill col. top slit, lead
106 8  -11.35    -60 73 -103 -106    u=11 $Fill col. bot. slit, lead
c
92  7 -1.205E-3 -60 -72             u=11 $Right air volume
93  7 -1.205E-3 -60  104            u=11 $Left air volume
94  7 -1.205E-3 -60 73 -103 -105 106 u=11 $Collimator
c ==> Detector
95  9   -2.94   60 -76 -75          u=11 $Front window Al
96  10  -0.55   76 -78 -79          u=11 $Front window refelctor
97  11  -3.70   78 -77 -80          u=11 $NaI crystal
98  9   -2.94   -75 79 76 -80       u=11 $Al canning
99  10  -0.55   78 77 -79 -80       u=11 $Reflector coating
100  7 -1.205E-3 -66 67 68 -69 80     u=11 $Air cavity behind detector
101  7 -1.205E-3 60 -66 67 68 -69 75 -80 u=11 $Air cavity around detector
c ----------------------Air surrounding apparatus---------------------
102   7 -1.205E-3 -13 -14 15 16 41 -59 (19:20:-21:-22)  $Above top lattice
103  7 -1.205E-3 -1 2 -3 4 5 -6
                (13:14:-15:-16:-17:59) #84
c                (61:62:-63:-64:65)
c ====================================================================

c ====================================================================
c                        ...Begin Surface Cards...
1     px  152.0
2     px -152.0
3     py  244.0
4     py -244.0
5     pz    0.0
6     pz  285.0
c
7     px  213.0
8     px -213.0
9     py  305.0
10    py -305.0
```

```
11    pz  305.0
12    pz  -20.0
c
13    px   33.02
14    py   33.02
15    px  -33.02
16    py  -33.02
17    pz    7.62
18    pz    8.89
19    px   17.90
20    py   17.90
21    px  -17.90
22    py  -17.90
23    c/z  29.21  29.21 1.67    $1 5/16" dia. holes
24    c/z  29.21 -29.21 1.67
25    c/z -29.21  29.21 1.67
26    c/z -29.21 -29.21 1.67
27    c/z  29.21   0    0.635   $0.5" dia. holes
28    c/z -29.21   0    0.635
29    px   25.718               $Control rod cut-outs
30    py    3.731
31    px   18.256
32    py   -3.731
33    px  -18.256
34    px  -25.718
35    px    3.731
36    px   -3.731
37    py   25.718
38    py   18.256
39    py  -25.718
40    py  -18.256
c
41    pz  104.775             $Top lattice plate
42    pz  103.505
c
43    px    0.779             $Pin volume parallelpiped
44    px   -0.779
45    py    0.779
46    py   -0.779
47    cz 0.5334               $Fuel OD
48    cz 0.54102              $Clad ID
49    cz 0.59182              $Clad OD
50    cz 0.635                $0.5" hole
51    cz 0.3175               $0.25" hole
52    cz 0.3137               $Bottom of pin nipple
53    pz 10.795               $Bottom plug
54    pz 11.1125              $Al2O3 Spacer
55    pz 102.5525             $Al2O3 Spacer
56    pz 102.87               $Pad
57    pz 103.1875             $Spring
58    pz 110.1725             $Bottom of pin handling notch area
59    pz 113.3475             $Top of pin
c ---------------------------- Detector Surfaces --------------------------
c
c ****************************** New Collimator ***************************
c
c     To move detector, add or subtract the distance moved along the y-axis
c     in centimeters from every py plane and correct offset in TR1 card. The
c     TR1 offset = (#pins along y-axis from lattice plate center to active pin)
c                  * PITCH.  EXP3C TR1 offset = 5*PITCH = 7.785 cm.
c
c     The measured distance in EXP3B from center of active pin to the detector
c     face was 20.412 cm.  The reference is the detector face (#60).
```

```
c     Offsets are as follows: Surf. #    Offset
c                               61        20.32
c                               76         0.05
c                               78         0.21
c                               80         5.40
c                               81        -5.08
c
60 1   py   25.492              $Front of detector face
61 1   py   45.812              $Back of universe
76 1   py   25.542              $Front window can
78 1   py   25.702              $Front window reflector
80 1   py   30.892              $Al can
81 1   py   15.332              $front of universe
c
62 1   px   10.16
63 1   px  -10.16
64 1   pz   47.9425
65 1   pz   68.2625
66 1   pz   63.1825
67 1   pz   53.0225
68 1   px   -2.95
69 1   px    2.95
70 1   px   -8.03
71 1   px    8.03
c
72 1   px   -5.5563
73 1   px   -0.4765
103 1  px    0.4765
104 1  px    5.5563
105 1  pz   60.6425
106 1  pz   55.5625
c
75 1   c/y   0.0 58.1025 2.855 $Detector Case
77 1   c/y   0.0 58.1025 2.645 $O.D. Crystal
79 1   c/y   0.0 58.1025 2.805 $I.D. Canning
c ---------------------------------------------------------------------
100   px   0.778
101   px -10.114
102   py  7.001
c =====================================================================

c =====================================================================
c                             ...Begin Data Cards...
mode p
imp:p 0 1 104r
c ----------------------------Lattice Rotation-------------------------
c Surface transformation cards for detector relative to lattice
*tr1     0.0000  7.785  0.0000 $Displacment Vector
        25.00   65.00   90.00  $Angle between XYZ & X'
       115.00   25.00   90.00  $Angle between XYZ & Y'
c ---------------------------------Tallies-----------------------------
e4    50e-3 180e-3 450e-3 550e-3 1.0
      1.5 2.0 3.0 4.0 5.0 6.0 7.5
c
c e5    50e-3 180e-3 450e-3 550e-3 1.0
c      1.5 2.0 3.0 4.0 5.0 6.0 7.5
c
e8    0 1.0e-5 50e-3 180e-3 450e-3 550e-3 1.00
        2.0 3.0 4.0 5.0 6.0 7.5
c ==> Cell Flux * Source Particles / sec (from DELBG)
f4:p   97
fm4    1.6148e7
c ==> Point detector at detector face to get collided and uncollided flux
```

```
c     (X,Y,Z) position = (r*sin(theta),r*cos(theta),58.1025)
c                  r = 28.197 for EXP3C
c f5:p   -8.627 26.285 58.1025 0.0   $ 25 deg.
c
c ==> Pulse ht. Tally in NaI(Tl) detector
f8:p   97
c ---------------------------------Materials---------------------------
c ==> Concrete wt. frac's from NIST (ordinary)
m1     1001 -0.022100
       6000 -0.002485
       8016 -0.574930
      11023 -0.015208
      12000 -0.001266
      13027 -0.019953
      14000 -0.304627
      19000 -0.010045
      20000 -0.042951
      26000 -0.006435
c ==> SS304 wt. fractions from ANL Assay Letter & The Hendrix Group Web Site
m2    27000 -0.00084
      24000 -0.18690
      29000 -0.00170
      26000 -0.68991
      25000 -0.01060
      42000 -0.00200
      28000 -0.09650
       6000 -0.00080
      15000 -0.00045
      16000 -0.00030
      14000 -0.01000
c ==> Al2O3 Compositions & density from Ceradyne's Web Site
m3    13027 2.0
       8016 3.0
c ==> Fuel Composition from ANL Assay Letter (0.32854-U + 0.67146-O)
m4    92233 0.0000009855
      92234 0.0000844348
      92235 0.0159864279
      92236 0.0001550709
      92238 0.3123130809
      8016  0.67146
c ==> Spring region (smeared density = 1.36 g/cc, wt % SS = 99.99%, He = 0.01%)
m5    27000 -0.0008316
      24000 -0.1850310
      29000 -0.0016830
      26000 -0.6830109
      25000 -0.0104940
      42000 -0.0019800
      28000 -0.0955350
       6000 -0.0007920
      15000 -0.0004455
      16000 -0.0002970
      14000 -0.0099000
       2004 -0.01
c ==> He gas region
m6     2004 1.0
c ==> Dry Air wt. frac's from NIST
m7     6000 -0.000124
       7015 -0.755268
       8016 -0.231781
      18000 -0.012827
c ==> Lead Shielding
m8     82206   0.247
       82207   0.227
```

```
       82208   0.526
c ==> Aluminum canning on detector (0.5 mm thk., rho = 147mg/cm^2)
m9     13027   1.000
c ==> Al2O3 Oxide reflector (1.6 mm thk., rho = 88mg/cm^2)
m10    13027   2.0
        8016   3.0
c ==> NaI Detector
m11    11023   0.5
       53127   0.5
c ==> Handling Notch Region (smeared density = 3.93 g/cc, wt% SS = 99.98)
m12   27000 -0.0008398
      24000 -0.1868626
      29000 -0.0016997
      26000 -0.6897720
      25000 -0.0105979
      42000 -0.0019996
      28000 -0.0964807
       6000 -7.9986480E-4
      15000 -0.0004499
      16000 -0.0002999
      14000 -0.0099980
c wt% Air = 0.02
       7015 -1.5105360E-4
       8016 -4.6356200E-5
      18000 -2.6254000E-6
c ------------------------------Source Definition-----------------------
sdef  CEL=D1 POS=0 0 0 AXS=0 0 1 RAD D2 EXT D3 ERG D4 PAR=2
            VEC=-0.423 0.906 0 DIR D5
si1  L 62:63(0 5 0):70
sp1    1.0
c
si2  0. 0.5335  $Sampling radius of fuel region in a pin
c
c 3"(7.62 cm) Axial Nodes
si3  H    11.1125 18.7325 26.3525 33.9725 41.5925 49.2125 56.8325
          64.4525 72.0725 79.6925 87.3125 94.9325 102.5525
c Relative Total Neutron Flux in axial node - Assume delayed gamma
c flux follows the neutron flux during operation
sp3       0. 0.033 0.058 0.078 0.091 0.109 0.115 0.118 0.114
             0.102 0.084 0.062 0.036
c
c 19 energy group structure in DELBG same for all times:
si4    H 0 .1  .2  .4  .6  .8 1.0 1.2 1.4 1.6 1.8
          2.0 2.2 2.4 2.6 3.0 4.0 5.0 6.0 7.5
c Gammas per second, from DELBG:
c 470 sec after SCRAM: Total Source = 1.6148e7 photons/sec
sp4  0. 0.0717 0.0710 0.1432 0.1119 0.1278 0.1378 0.0716
        0.0625 0.0467 0.0319 0.0243 0.0199 0.0151 0.0151
        0.0186 0.0200 0.0092 0.0018 0.0001
c Source Bias (exponential)
sb5    -31 3
nps 5.0e7
print
```

C.1.3 Heterogeneous Example for Lattice at 45 Degrees Rotation

```
Experiment 3 - Single Pin Activation, 7x7 sq. lattice at 45 deg.
c 0.613 pitch lattice in counting apparatus
c ************************************************************
c ********************** New Collimator **********************
c ************************************************************
c
c                        ...Begin Cell Cards...
c ------------------------Outer cell and walls-------------------------
1   0          7:-8:9:-10:11:-12 $Void
2   1  -2.30   1 -7 -3 4 -6 5    $East concrete wall
3   1  -2.30   -2 8 -3 4 -6 5    $West concrete wall
4   1  -2.30   3 -9 -7 8 -6 5    $North concrete wall
5   1  -2.30   -4 10 -7 8 -6 5   $South concrete wall
6   1  -2.30   -7 8 -9 10 -11 6  $Concrete ceiling
7   1  -2.30   -7 8 -9 10 -5 12  $Concrete floor
c --------------------------Bottom Lattice-----------------------------
8   2  -8.00   -13 19 -14 16 17 -18 23 24 27 (29:30:-31:-32)  $East side
9   2  -8.00    15 -21 -14 16 17 -18 25 26 28 (30:33:-32:-34) $West side
10  2  -8.00   -14 20 -19 21 17 -18 (35:37:-36:-38)           $North side
11  2  -8.00    16 -22 21 -19 17 -18 (35:40:-36:-39)          $South side
12  7 -1.205E-3 -23 17 -18
13  7 -1.205E-3 -24 17 -18
14  7 -1.205E-3 -25 17 -18
15  7 -1.205E-3 -26 17 -18
16  7 -1.205E-3 -27 17 -18
17  7 -1.205E-3 -28 17 -18
18  7 -1.205E-3 -29 -30 31 32 17 -18
19  7 -1.205E-3 -35 -37 36 38 17 -18
20  7 -1.205E-3 -30 -33 32 34 17 -18
21  7 -1.205E-3 -35 -40 36 39 17 -18
c ---------------------------Top Lattice-----------------------------
22  2  -8.00   -13 19 -14 16 -41 42 23 24 27 (29:30:-31:-32)  $East side
23  2  -8.00    15 -21 -14 16 -41 42 25 26 28 (30:33:-32:-34) $West side
24  2  -8.00   -14 20 -19 21 -41 42 (35:37:-36:-38)           $North side
25  2  -8.00    16 -22 21 -19 -41 42 (35:40:-36:-39)          $South side
26  7 -1.205E-3 -23 -41 42
27  7 -1.205E-3 -24 -41 42
28  7 -1.205E-3 -25 -41 42
29  7 -1.205E-3 -26 -41 42
30  7 -1.205E-3 -27 -41 42
31  7 -1.205E-3 -28 -41 42
32  7 -1.205E-3 -29 -30 31 32 -41 42
33  7 -1.205E-3 -35 -37 36 38 -41 42
34  7 -1.205E-3 -30 -33 32 34 -41 42
35  7 -1.205E-3 -35 -40 36 39 -41 42
c ---------------Air around fuel lattice & between plates--------------
36  7 -1.205E-3 -13 -14 15 16 18 -42 (19:20:-21:-22) #84
c                                    (62:-63:-81:-64:65)
c ---------------------Bottom Pin lattice ----------------------
37  0           -19 -20 21 22 17 -18 fill=1
38  0           -43 44 -45 46 u=1 lat=1 fill=-11:11 -11:11 0:0
                 2  6r  3  8r 2  6r
                 2  4r  3 12r 2  4r
                 2  2r  3 16r 2  2r
                 2  1r  3 18r 2  1r
                 2  1r  3 18r 2  1r
                 2      3 20r 2
                 2      3 20r 2
                        3 183r
                 2 3 3 3 3 3 3 3 3 3 3 3 3 3 3 3 3 3 3 3 3 3 2
```

```
                2 3 3 3 3 4 4 4 4 4 4 4 3 3 3 3 3 3 3 3 3 3 2
                2 3 3 3 3 4 4 4 4 4 4 4 3 3 3 3 3 3 3 3 3 3 2
                2 2 3 3 3 4 4 4 4 4 4 4 3 3 3 3 3 3 3 3 3 2 2
                2 2 3 3 3 4 4 4 4 4 4 4 3 3 3 3 3 3 3 3 3 2 2
                2 2 2 3 3 4 4 4 4 4 4 4 3 3 3 3 3 3 3 3 2 2 2
                2 2 2 2 2 4 4 4 4 4 4 4 3 3 3 3 3 3 2 2 2 2 2
                2 2 2 2 2 4 4 4 4 4 4 4 3 3 3 3 2 2 2 2 2 2 2
c ==> Universe 2 for regions within grid that are all steel
39  2  -8.00     -49 u=2
40  2  -8.00      49 u=2
c ==> Universe 3 for regions within grid that are drilled out
41  7 -1.205E-3  -51 u=3
42  2  -8.00      51 u=3
c ==> Universe 4 for regions within grid that have pins
43  2  -8.00     -52              u=4 $Pin nipple
44  7 -1.205E-3   52 -51          u=4 $Air between lattice hole & nipple
45  2  -8.00      51              u=4 $Metal of lattice
c
c ----------------------Top Pin lattice ----------------------
46  0           -19 -20 21 22 42 -59 fill=5
47  0           -43 44 -45 46 u=5 lat=1 fill=-11:11 -11:11 0:0
                 6  6r  7  8r 6  6r
                 6  4r  7 12r 6  4r
                 6  2r  7 16r 6  2r
                 6  1r  7 18r 6  1r
                 6  1r  7 18r 6  1r
                 6      7 20r 6
                 6      7 20r 6
                        7 183r
                 6 7 7 7 7 7 7 7 7 7 7 7 7 7 7 7 7 7 7 7 7 7 6
                 6 7 7 7 7 8 8 8 8 8 8 8 7 7 7 7 7 7 7 7 7 7 6
                 6 7 7 7 7 8 8 8 8 8 8 8 7 7 7 7 7 7 7 7 7 7 6
                 6 6 7 7 7 8 8 8 8 8 8 8 7 7 7 7 7 7 7 7 7 6 6
                 6 6 7 7 7 8 8 8 8 8 8 8 7 7 7 7 7 7 7 7 7 6 6
                 6 6 6 7 7 8 8 8 8 8 8 8 7 7 7 7 7 7 7 7 6 6 6
                 6 6 6 6 6 8 8 8 8 8 8 8 7 7 7 7 7 7 6 6 6 6 6
                 6 6 6 6 6 8 8 8 8 8 8 8 7 7 7 7 6 6 6 6 6 6 6
c ==> Universe 6 for regions within grid that are all steel
48  2  -8.00    -49 -41 u=6
49  2  -8.00     49 -41 u=6
50  7 -1.205E-3 -49 41 u=6
51  7 -1.205E-3  49 41 u=6
c ==> Universe 7 for regions within grid that are drilled out
52  7 -1.205E-3 -50 -41 u=7
53  2  -8.00     50 -41 u=7
54  7 -1.205E-3 -50 41 u=7
55  7 -1.205E-3  50 41 u=7
c ==> Universe 8 for regions within grid that have pins
56  5  -1.36     -48 -58        u=8 $Spring region
57  2  -8.00      48 -49 -58    u=8 $Clad
58  7 -1.205E-3   49 -50 -41    u=8 $Air between lattice hole and clad
59  2  -8.00      -41 50        u=8 $Metal of Lattice
60  12 -3.93      -49 58        u=8 $Pin notch region
61  7 -1.205E-3  41 49          u=8 $Air aound top of pin
c
c ---------------------- Pin lattice ----------------------
62  0           -100 101 -20 102 18 -42 fill=9
63  0           -43 44 -45 46 u=9 lat=1 fill=-11:11 -11:11 0:0
                                  10 528r
c
64  2  -8.00      -49  -53        u=10 $Plug
65  7 -1.205E-3    49  -53        u=10 $Air around plug
66  3 -3.99      53 -54 -47     u=10 $Al2O3
```

```
67  6  1.83E-6   53 -54 47 -48  u=10 $He around Al2O3
68  2  -8.00     53 -54 48 -49  u=10 $Clad
69  7 -1.205E-3  53  49         u=10 $Air around entire length of pin
70  4 -10.08     54 -55 -47     u=10 $Fuel region
71  6  1.83E-6   54 -55 47 -48  u=10 $He around Al2O3
72  2  -8.00     54 -55 48 -49  u=10 $Clad
73  3  -3.99     55 -56 -47     u=10 $Al2O3
74  6  1.83E-6   55 -56 47 -48  u=10 $He around Al2O3
75  2  -8.00     55 -56 48 -49  u=10 $Clad
76  2  -8.00     56 -57 -47     u=10 $SS spacer
77  6  1.83E-6   56 -57 47 -48  u=10 $He around spacer
78  2  -8.00     56 -57 48 -49  u=10 $Clad
79  5  -1.36     57 -48 -58     u=10 $Spring region
80  2  -8.00     57 48 -49      u=10 $Clad
c ----------------------Air Around Pin Lattice-------------------------
81  7 -1.205E-3   22 -102 -19 21 18 -42
82  7 -1.205E-3  -19 100 -20 102 18 -42
83  7 -1.205E-3  -20 21 -101 102 18 -42 #84
c -------------------------Lead Shield Volume--------------------------
84  0            81 -61 -62 63 64 -65 fill=11
85  8  -11.35    60 66               u=11 $Top bricks
86  8  -11.35    60 -67              u=11 $Bottom bricks
87  8  -11.35    60 -66 67 -68 70    u=11 $Right brick
88  7 -1.205E-3  60 -66 67 -70       u=11 $Right air volume
89  8  -11.35    60 -66 67 69 -71    u=11 $Left brick
90  7 -1.205E-3  60 -66 67 71        u=11 $Left air volume
c ==> Use this cell when front brick is used:
91  8  -11.35    -60 103 -104        u=11 $Half Front Brick,lead
104 8  -11.35    -60 72 -73          u=11 $Half Front Brick,lead
105 8  -11.35    -60 73 -103 105     u=11 $Fill col. top slit, lead
106 8  -11.35    -60 73 -103 -106    u=11 $Fill col. bot. slit, lead
c
92  7 -1.205E-3 -60 -72             u=11 $Right air volume
93  7 -1.205E-3 -60  104            u=11 $Left air volume
94  7 -1.205E-3 -60 73 -103 -105 106 u=11 $Collimator
c ==> Detector
95  9   -2.94   60 -76 -75          u=11 $Front window Al
96  10  -0.55   76 -78 -79          u=11 $Front window refelctor
97  11  -3.70   78 -77 -80          u=11 $NaI crystal
98  9   -2.94   -75 79 76 -80       u=11 $Al canning
99  10  -0.55   78 77 -79 -80       u=11 $Reflector coating
100  7 -1.205E-3 -66 67 68 -69 80     u=11 $Air cavity behind detector
101  7 -1.205E-3 60 -66 67 68 -69 75 -80 u=11 $Air cavity around detector
c ----------------------Air surrounding apparatus---------------------
102   7 -1.205E-3 -13 -14 15 16 41 -59 (19:20:-21:-22)  $Above top lattice
103  7 -1.205E-3 -1 2 -3 4 5 -6
               (13:14:-15:-16:-17:59) #84
c               (61:62:-63:-64:65)
c ====================================================================

c ====================================================================
c                        ...Begin Surface Cards...
1     px  152.0
2     px -152.0
3     py  244.0
4     py -244.0
5     pz    0.0
6     pz  285.0
c
7     px  213.0
8     px -213.0
9     py  305.0
10    py -305.0
```

```
11    pz  305.0
12    pz  -20.0
c
13    px   33.02
14    py   33.02
15    px  -33.02
16    py  -33.02
17    pz    7.62
18    pz    8.89
19    px   17.90
20    py   17.90
21    px  -17.90
22    py  -17.90
23    c/z  29.21  29.21 1.67    $1 5/16" dia. holes
24    c/z  29.21 -29.21 1.67
25    c/z -29.21  29.21 1.67
26    c/z -29.21 -29.21 1.67
27    c/z  29.21   0    0.635   $0.5" dia. holes
28    c/z -29.21   0    0.635
29    px   25.718               $Control rod cut-outs
30    py    3.731
31    px   18.256
32    py   -3.731
33    px  -18.256
34    px  -25.718
35    px    3.731
36    px   -3.731
37    py   25.718
38    py   18.256
39    py  -25.718
40    py  -18.256
c
41    pz  104.775             $Top lattice plate
42    pz  103.505
c
43    px    0.779             $Pin volume parallelpiped
44    px   -0.779
45    py    0.779
46    py   -0.779
47    cz 0.5334               $Fuel OD
48    cz 0.54102              $Clad ID
49    cz 0.59182              $Clad OD
50    cz 0.635                $0.5" hole
51    cz 0.3175               $0.25" hole
52    cz 0.3137               $Bottom of pin nipple
53    pz 10.795               $Bottom plug
54    pz 11.1125              $Al2O3 Spacer
55    pz 102.5525             $Al2O3 Spacer
56    pz 102.87               $Pad
57    pz 103.1875             $Spring
58    pz 110.1725             $Bottom of pin handling notch area
59    pz 113.3475             $Top of pin
c ---------------------------- Detector Surfaces --------------------------
c
c ****************************** New Collimator ***************************
c
c     To move detector, add or subtract the distance moved along the y-axis
c     in centimeters from every py plane and correct offset in TR1 card. The
c     TR1 offset = (#pins along y-axis from lattice plate center to active pin)
c                  * PITCH.  EXP3C TR1 offset = 5*PITCH = 7.785 cm.
c
c     The measured distance in EXP3B from center of active pin to the detector
c     face was 20.412 cm.  The reference is the detector face (#60).
```

```
c     Offsets are as follows: Surf. #    Offset
c                               61        20.32
c                               76         0.05
c                               78         0.21
c                               80         5.40
c                               81        -5.08
c
60 1   py   25.492              $Front of detector face
61 1   py   45.812              $Back of universe
76 1   py   25.542              $Front window can
78 1   py   25.702              $Front window reflector
80 1   py   30.892              $Al can
81 1   py   15.332              $front of universe
c
62 1   px   10.16
63 1   px  -10.16
64 1   pz   47.9425
65 1   pz   68.2625
66 1   pz   63.1825
67 1   pz   53.0225
68 1   px   -2.95
69 1   px    2.95
70 1   px   -8.03
71 1   px    8.03
c
72 1   px   -5.5563
73 1   px   -0.4765
103 1  px    0.4765
104 1  px    5.5563
105 1  pz   60.6425
106 1  pz   55.5625
c
75 1   c/y   0.0 58.1025 2.855 $Detector Case
77 1   c/y   0.0 58.1025 2.645 $O.D. Crystal
79 1   c/y   0.0 58.1025 2.805 $I.D. Canning
c ---------------------------------------------------------------------
100   px   0.778
101   px -10.114
102   py  7.001
c =====================================================================

c =====================================================================
c                             ...Begin Data Cards...
mode p
imp:p 0 1 104r
c ----------------------------Lattice Rotation-------------------------
c Surface transformation cards for detector relative to lattice
*tr1     0.0000  7.785  0.0000 $Displacment Vector
        45.00   45.00   90.00  $Angle between XYZ & X'
       135.00   45.00   90.00  $Angle between XYZ & Y'
c ---------------------------------Tallies-----------------------------
e4    50e-3 180e-3 450e-3 550e-3 1.0
      1.5 2.0 3.0 4.0 5.0 6.0 7.5
c
c e5    50e-3 180e-3 450e-3 550e-3 1.0
c      1.5 2.0 3.0 4.0 5.0 6.0 7.5
c
e8    0 1.0e-5 50e-3 180e-3 450e-3 550e-3 1.00
        2.0 3.0 4.0 5.0 6.0 7.5
c ==> Cell Flux * Source Particles / sec (from DELBG)
f4:p   97
fm4    1.6148e7
c ==> Point detector at detector face to get collided and uncollided flux
```

```
c     (X,Y,Z) position = (r*sin(theta),r*cos(theta),58.1025)
c                  r = 28.197 for EXP3C
c f5:p   -14.433 22.218 58.1025 0.0   $ 0 deg.
c
c ==> Pulse ht. Tally in NaI(Tl) detector
f8:p   97
c ---------------------------------Materials---------------------------
c ==> Concrete wt. frac's from NIST (ordinary)
m1     1001 -0.022100
       6000 -0.002485
       8016 -0.574930
      11023 -0.015208
      12000 -0.001266
      13027 -0.019953
      14000 -0.304627
      19000 -0.010045
      20000 -0.042951
      26000 -0.006435
c ==> SS304 wt. fractions from ANL Assay Letter & The Hendrix Group Web Site
m2    27000 -0.00084
      24000 -0.18690
      29000 -0.00170
      26000 -0.68991
      25000 -0.01060
      42000 -0.00200
      28000 -0.09650
       6000 -0.00080
      15000 -0.00045
      16000 -0.00030
      14000 -0.01000
c ==> Al2O3 Compositions & density from Ceradyne's Web Site
m3    13027 2.0
       8016 3.0
c ==> Fuel Composition from ANL Assay Letter (0.32854-U + 0.67146-O)
m4    92233 0.0000009855
      92234 0.0000844348
      92235 0.0159864279
      92236 0.0001550709
      92238 0.3123130809
      8016  0.67146
c ==> Spring region (smeared density = 1.36 g/cc, wt % SS = 99.99%, He = 0.01%)
m5    27000 -0.0008316
      24000 -0.1850310
      29000 -0.0016830
      26000 -0.6830109
      25000 -0.0104940
      42000 -0.0019800
      28000 -0.0955350
       6000 -0.0007920
      15000 -0.0004455
      16000 -0.0002970
      14000 -0.0099000
       2004 -0.01
c ==> He gas region
m6     2004 1.0
c ==> Dry Air wt. frac's from NIST
m7     6000 -0.000124
       7015 -0.755268
       8016 -0.231781
      18000 -0.012827
c ==> Lead Shielding
m8     82206   0.247
       82207   0.227
```

```
       82208   0.526
c ==> Aluminum canning on detector (0.5 mm thk., rho = 147mg/cm^2)
m9     13027   1.000
c ==> Al2O3 Oxide reflector (1.6 mm thk., rho = 88mg/cm^2)
m10    13027   2.0
        8016   3.0
c ==> NaI Detector
m11    11023   0.5
       53127   0.5
c ==> Handling Notch Region (smeared density = 3.93 g/cc, wt% SS = 99.98)
m12   27000 -0.0008398
      24000 -0.1868626
      29000 -0.0016997
      26000 -0.6897720
      25000 -0.0105979
      42000 -0.0019996
      28000 -0.0964807
       6000 -7.9986480E-4
      15000 -0.0004499
      16000 -0.0002999
      14000 -0.0099980
c wt% Air = 0.02
       7015 -1.5105360E-4
       8016 -4.6356200E-5
      18000 -2.6254000E-6
c ------------------------------Source Definition-----------------------
sdef  CEL=D1 POS=0 0 0 AXS=0 0 1 RAD D2 EXT D3 ERG D4 PAR=2
             VEC=-1 1 0 DIR D5
si1  L 62:63(0 5 0):70
sp1    1.0
c
si2  0. 0.5335  $Sampling radius of fuel region in a pin
c
c 3"(7.62 cm) Axial Nodes
si3  H    11.1125 18.7325 26.3525 33.9725 41.5925 49.2125 56.8325
          64.4525 72.0725 79.6925 87.3125 94.9325 102.5525
c Relative Total Neutron Flux in axial node - Assume delayed gamma
c flux follows the neutron flux during operation
sp3       0. 0.033 0.058 0.078 0.091 0.109 0.115 0.118 0.114

             0.102 0.084 0.062 0.036
c
c 19 energy group structure in DELBG same for all times:
si4    H 0 .1  .2  .4  .6  .8 1.0 1.2 1.4 1.6 1.8
         2.0 2.2 2.4 2.6 3.0 4.0 5.0 6.0 7.5
c Gammas per second, from DELBG:
c 470 sec after SCRAM: Total Source = 1.6148e7 photons/sec
sp4  0. 0.0717 0.0710 0.1432 0.1119 0.1278 0.1378 0.0716
        0.0625 0.0467 0.0319 0.0243 0.0199 0.0151 0.0151
        0.0186 0.0200 0.0092 0.0018 0.0001
c Source Bias (exponential)
sb5    -31 3
nps 5.0e7
print
```

C.1.4 Homogeneous Example for Lattice at 45 Degrees Rotation

```
Experiment 3 Homogeneous - Single Pin Activation, 7x7 sq. lattice at 45 deg.
c 0.613 pitch lattice in counting apparatus
c ************************************************************
c ********************** New Collimator **********************
c ************************************************************
c
c                        ...Begin Cell Cards...
c ------------------------Outer cell and walls-------------------------
1   0          7:-8:9:-10:11:-12 $Void
2   1  -2.30   1 -7 -3 4 -6 5    $East concrete wall
3   1  -2.30   -2 8 -3 4 -6 5    $West concrete wall
4   1  -2.30   3 -9 -7 8 -6 5    $North concrete wall
5   1  -2.30   -4 10 -7 8 -6 5   $South concrete wall
6   1  -2.30   -7 8 -9 10 -11 6  $Concrete ceiling
7   1  -2.30   -7 8 -9 10 -5 12  $Concrete floor
c --------------------------Bottom Lattice-----------------------------
8   2  -8.00   -13 19 -14 16 17 -18 23 24 27 (29:30:-31:-32)  $East side
9   2  -8.00    15 -21 -14 16 17 -18 25 26 28 (30:33:-32:-34) $West side
10  2  -8.00   -14 20 -19 21 17 -18 (35:37:-36:-38)           $North side
11  2  -8.00    16 -22 21 -19 17 -18 (35:40:-36:-39)          $South side
12  7 -1.205E-3 -23 17 -18
13  7 -1.205E-3 -24 17 -18
14  7 -1.205E-3 -25 17 -18
15  7 -1.205E-3 -26 17 -18
16  7 -1.205E-3 -27 17 -18
17  7 -1.205E-3 -28 17 -18
18  7 -1.205E-3 -29 -30 31 32 17 -18
19  7 -1.205E-3 -35 -37 36 38 17 -18
20  7 -1.205E-3 -30 -33 32 34 17 -18
21  7 -1.205E-3 -35 -40 36 39 17 -18
c ---------------------------Top Lattice-----------------------------
22  2  -8.00   -13 19 -14 16 -41 42 23 24 27 (29:30:-31:-32)  $East side
23  2  -8.00    15 -21 -14 16 -41 42 25 26 28 (30:33:-32:-34) $West side
24  2  -8.00   -14 20 -19 21 -41 42 (35:37:-36:-38)           $North side
25  2  -8.00    16 -22 21 -19 -41 42 (35:40:-36:-39)          $South side
26  7 -1.205E-3 -23 -41 42
27  7 -1.205E-3 -24 -41 42
28  7 -1.205E-3 -25 -41 42
29  7 -1.205E-3 -26 -41 42
30  7 -1.205E-3 -27 -41 42
31  7 -1.205E-3 -28 -41 42
32  7 -1.205E-3 -29 -30 31 32 -41 42
33  7 -1.205E-3 -35 -37 36 38 -41 42
34  7 -1.205E-3 -30 -33 32 34 -41 42
35  7 -1.205E-3 -35 -40 36 39 -41 42
c ---------------Air around fuel lattice & between plates--------------
36  7 -1.205E-3 -13 -14 15 16 18 -42 (19:20:-21:-22) #84
c                                    (62:-63:-81:-64:65)
c ---------------------Bottom Pin lattice ----------------------
37  0           -19 -20 21 22 17 -18 fill=1
38  0           -43 44 -45 46 u=1 lat=1 fill=-11:11 -11:11 0:0
                 2  6r  3  8r 2  6r
                 2  4r  3 12r 2  4r
                 2  2r  3 16r 2  2r
                 2  1r  3 18r 2  1r
                 2  1r  3 18r 2  1r
                 2      3 20r 2
                 2      3 20r 2
                        3 183r
                 2 3 3 3 3 3 3 3 3 3 3 3 3 3 3 3 3 3 3 3 3 3 2
```

```
                2 3 3 3 3 4 4 4 4 4 4 4 3 3 3 3 3 3 3 3 3 3 2
                2 3 3 3 3 4 4 4 4 4 4 4 3 3 3 3 3 3 3 3 3 3 2
                2 2 3 3 3 4 4 4 4 4 4 4 3 3 3 3 3 3 3 3 3 2 2
                2 2 3 3 3 4 4 4 4 4 4 4 3 3 3 3 3 3 3 3 3 2 2
                2 2 2 3 3 4 4 4 4 4 4 4 3 3 3 3 3 3 3 3 2 2 2
                2 2 2 2 2 4 4 4 4 4 4 4 3 3 3 3 3 3 2 2 2 2 2
                2 2 2 2 2 4 4 4 4 4 4 4 3 3 3 3 2 2 2 2 2 2 2
c ==> Universe 2 for regions within grid that are all steel
39  2  -8.00     -49 u=2
40  2  -8.00      49 u=2
c ==> Universe 3 for regions within grid that are drilled out
41  7 -1.205E-3  -51 u=3
42  2  -8.00      51 u=3
c ==> Universe 4 for regions within grid that have pins
43  2  -8.00     -52              u=4 $Pin nipple
44  7 -1.205E-3   52 -51          u=4 $Air between lattice hole & nipple
45  2  -8.00      51              u=4 $Metal of lattice
c
c ----------------------Top Pin lattice ----------------------
46  0           -19 -20 21 22 42 -59 fill=5
47  0           -43 44 -45 46 u=5 lat=1 fill=-11:11 -11:11 0:0
                 6  6r  7  8r 6  6r
                 6  4r  7 12r 6  4r
                 6  2r  7 16r 6  2r
                 6  1r  7 18r 6  1r
                 6  1r  7 18r 6  1r
                 6      7 20r 6
                 6      7 20r 6
                        7 183r
                 6 7 7 7 7 7 7 7 7 7 7 7 7 7 7 7 7 7 7 7 7 7 6
                 6 7 7 7 7 8 8 8 8 8 8 8 7 7 7 7 7 7 7 7 7 7 6
                 6 7 7 7 7 8 8 8 8 8 8 8 7 7 7 7 7 7 7 7 7 7 6
                 6 6 7 7 7 8 8 8 8 8 8 8 7 7 7 7 7 7 7 7 7 6 6
                 6 6 7 7 7 8 8 8 8 8 8 8 7 7 7 7 7 7 7 7 7 6 6
                 6 6 6 7 7 8 8 8 8 8 8 8 7 7 7 7 7 7 7 7 6 6 6
                 6 6 6 6 6 8 8 8 8 8 8 8 7 7 7 7 7 7 6 6 6 6 6
                 6 6 6 6 6 8 8 8 8 8 8 8 7 7 7 7 6 6 6 6 6 6 6
c ==> Universe 6 for regions within grid that are all steel
48  2  -8.00    -49 -41 u=6
49  2  -8.00     49 -41 u=6
50  7 -1.205E-3 -49 41 u=6
51  7 -1.205E-3  49 41 u=6
c ==> Universe 7 for regions within grid that are drilled out
52  7 -1.205E-3 -50 -41 u=7
53  2  -8.00     50 -41 u=7
54  7 -1.205E-3 -50 41 u=7
55  7 -1.205E-3  50 41 u=7
c ==> Universe 8 for regions within grid that have pins
56  5  -1.36     -48 -58        u=8 $Spring region
57  2  -8.00      48 -49 -58    u=8 $Clad
58  7 -1.205E-3   49 -50 -41    u=8 $Air between lattice hole and clad
59  2  -8.00      -41 50        u=8 $Metal of Lattice
60  12 -3.93      -49 58        u=8 $Pin notch region
61  7 -1.205E-3  41 49          u=8 $Air aound top of pin
c
c ---------------------- Pin lattice ----------------------
62  0           -100 101 -20 102 18 -42 fill=9
63  0           -43 44 -45 46 u=9 lat=1 fill=-11:11 -11:11 0:0
                                  10 528r
c
64  13  -3.6270    -53          u=10  $Plug
c
65  14  -2.0666     53 -54      u=10  $Al2O3 Spacer
```

```
c
66  15  -4.3083     54 -55      u=10  $Fuel Region
c
67  16  -2.0666     55 -56      u=10  $Al2O3 Spacer
c
68  17  -3.5439     56 -57      u=10  $SS Spacer
c
69  18  -1.1122         57      u=10  $Spring
c -----------------------Air Around Pin Lattice-------------------------
81  7 -1.205E-3   22 -102 -19 21 18 -42
82  7 -1.205E-3  -19 100 -20 102 18 -42
83  7 -1.205E-3  -20 21 -101 102 18 -42 #84
c -------------------------Lead Shield Volume--------------------------
84  0            81 -61 -62 63 64 -65 fill=11
85  8  -11.35    60 66               u=11 $Top bricks
86  8  -11.35    60 -67              u=11 $Bottom bricks
87  8  -11.35    60 -66 67 -68 70    u=11 $Right brick
88  7 -1.205E-3  60 -66 67 -70       u=11 $Right air volume
89  8  -11.35    60 -66 67 69 -71    u=11 $Left brick
90  7 -1.205E-3  60 -66 67 71        u=11 $Left air volume
c ==> Use this cell when front brick is used:
91  8  -11.35    -60 103 -104        u=11 $Half Front Brick,lead
104 8  -11.35    -60 72 -73          u=11 $Half Front Brick,lead
105 8  -11.35    -60 73 -103 105     u=11 $Fill col. top slit, lead
106 8  -11.35    -60 73 -103 -106    u=11 $Fill col. bot. slit, lead
c
92  7 -1.205E-3 -60 -72              u=11 $Right air volume
93  7 -1.205E-3 -60  104             u=11 $Left air volume
94  7 -1.205E-3 -60 73 -103 -105 106 u=11 $Collimator
c ==> Detector
95  9   -2.94   60 -76 -75           u=11 $Front window Al
96  10  -0.55   76 -78 -79           u=11 $Front window refelctor
97  11  -3.70   78 -77 -80           u=11 $NaI crystal
98  9   -2.94   -75 79 76 -80        u=11 $Al canning
99  10  -0.55   78 77 -79 -80        u=11 $Reflector coating
100  7 -1.205E-3 -66 67 68 -69 80     u=11 $Air cavity behind detector
101  7 -1.205E-3 60 -66 67 68 -69 75 -80 u=11 $Air cavity around detector
c ----------------------Air surrounding apparatus---------------------
102   7 -1.205E-3 -13 -14 15 16 41 -59 (19:20:-21:-22)  $Above top lattice
103  7 -1.205E-3 -1 2 -3 4 5 -6
                (13:14:-15:-16:-17:59) #84
c                (61:62:-63:-64:65)
c ======================================================================

c ======================================================================
c                         ...Begin Surface Cards...
1     px  152.0
2     px -152.0
3     py  244.0
4     py -244.0
5     pz    0.0
6     pz  285.0
c
7     px  213.0
8     px -213.0
9     py  305.0
10    py -305.0
11    pz  305.0
12    pz  -20.0
c
13    px   33.02
14    py   33.02
15    px  -33.02
```

```
16    py  -33.02
17    pz    7.62
18    pz    8.89
19    px   17.90
20    py   17.90
21    px  -17.90
22    py  -17.90
23    c/z  29.21  29.21 1.67    $1 5/16" dia. holes
24    c/z  29.21 -29.21 1.67

25    c/z -29.21  29.21 1.67
26    c/z -29.21 -29.21 1.67
27    c/z  29.21   0    0.635   $0.5" dia. holes
28    c/z -29.21   0    0.635
29    px   25.718               $Control rod cut-outs
30    py    3.731
31    px   18.256
32    py   -3.731
33    px  -18.256
34    px  -25.718
35    px    3.731
36    px   -3.731
37    py   25.718
38    py   18.256
39    py  -25.718
40    py  -18.256
c
41    pz  104.775             $Top lattice plate
42    pz  103.505
c
43    px    0.779             $Pin volume parallelpiped
44    px   -0.779
45    py    0.779
46    py   -0.779
c 47    cz 0.5334               $Fuel OD
48    cz 0.54102              $Clad ID
49    cz 0.59182              $Clad OD
50    cz 0.635                $0.5" hole
51    cz 0.3175               $0.25" hole
52    cz 0.3137               $Bottom of pin nipple
53    pz 10.795               $Bottom plug
54    pz 11.1125              $Al2O3 Spacer
55    pz 102.5525             $Al2O3 Spacer
56    pz 102.87               $Pad
57    pz 103.1875             $Spring
58    pz 110.1725             $Bottom of pin handling notch area
59    pz 113.3475             $Top of pin
c --------------------------- Detector Surfaces --------------------------
c
c ***************************** New Collimator **************************
c
c     To move detector, add or subtract the distance moved along the y-axis
c     in centimeters from every py plane and correct offset in TR1 card. The
c     TR1 offset = (#pins along y-axis from lattice plate center to active pin)
c                  * PITCH.  EXP3C TR1 offset = 5*PITCH = 7.785 cm.
c
c     The measured distance in EXP3B from center of active pin to the detector
c     face was 20.412 cm.  The reference is the detector face (#60).
c     Offsets are as follows: Surf. #    Offset
c                               61        20.32
c                               76         0.05
c                               78         0.21
c                               80         5.40
```

```
c                                81        -5.08
c
60 1   py   25.492              $Front of detector face
61 1   py   45.812              $Back of universe
76 1   py   25.542              $Front window can
78 1   py   25.702              $Front window reflector
80 1   py   30.892              $Al can
81 1   py   15.332              $front of universe
c
62 1   px   10.16
63 1   px  -10.16
64 1   pz   47.9425
65 1   pz   68.2625
66 1   pz   63.1825
67 1   pz   53.0225
68 1   px   -2.95
69 1   px    2.95
70 1   px   -8.03
71 1   px    8.03
c
72 1   px   -5.5563
73 1   px   -0.4765
103 1  px    0.4765
104 1  px    5.5563
105 1  pz   60.6425
106 1  pz   55.5625
c
75 1   c/y   0.0 58.1025 2.855 $Detector Case
77 1   c/y   0.0 58.1025 2.645 $O.D. Crystal
79 1   c/y   0.0 58.1025 2.805 $I.D. Canning
c ---------------------------------------------------------------------
100   px   0.778
101   px -10.114
102   py  7.001
c =====================================================================

c =====================================================================
c                             ...Begin Data Cards...
mode p
imp:p 0 1 93r
c ---------------------------Lattice Rotation-------------------------
c Surface transformation cards for detector relative to lattice
*tr1     0.0000  7.785  0.0000 $Displacment Vector
        45.00    45.00   90.00  $Angle between XYZ & X'
        135.00   45.00   90.00  $Angle between XYZ & Y'
c ---------------------------------Tallies-----------------------------
e4    50e-3 180e-3 450e-3 550e-3 1.0
      1.5 2.0 3.0 4.0 5.0 6.0 7.5
c
c e5    50e-3 180e-3 450e-3 550e-3 1.0
c      1.5 2.0 3.0 4.0 5.0 6.0 7.5
c
e8    0 1.0e-5 50e-3 180e-3 450e-3 550e-3 1.00
        2.0 3.0 4.0 5.0 6.0 7.5
c ==> Cell Flux * Source Particles / sec (from DELBG)
f4:p   97
fm4    1.6148e7
c ==> Point detector at detector face to get collided and uncollided flux
c     (X,Y,Z) position = (r*sin(theta),r*cos(theta),58.1025)
c                  r = 28.197 for EXP3C
c f5:p   0.0 28.197 58.1025 0.0   $ 0 deg.
c
c ==> Pulse ht. Tally in NaI(Tl) detector
```

```
f8:p   97
c ---------------------------------Materials---------------------------
c ==> Concrete wt. frac's from NIST (ordinary)
m1     1001 -0.022100
       6000 -0.002485
       8016 -0.574930
      11023 -0.015208
      12000 -0.001266
      13027 -0.019953
      14000 -0.304627
      19000 -0.010045
      20000 -0.042951
      26000 -0.006435
c ==> SS304 wt. fractions from ANL Assay Letter & The Hendrix Group Web Site
m2    27000 -0.00084
      24000 -0.18690
      29000 -0.00170
      26000 -0.68991
      25000 -0.01060
      42000 -0.00200
      28000 -0.09650
       6000 -0.00080
      15000 -0.00045
      16000 -0.00030
      14000 -0.01000
c ==> Spring region (smeared density = 1.36 g/cc, wt % SS = 99.99%, He = 0.01%)
m5    27000 -0.0008316
      24000 -0.1850310
      29000 -0.0016830
      26000 -0.6830109
      25000 -0.0104940
      42000 -0.0019800
      28000 -0.0955350
       6000 -0.0007920
      15000 -0.0004455
      16000 -0.0002970
      14000 -0.0099000
       2004 -0.01
c ==> Dry Air wt. frac's from NIST
m7     6000 -0.000124
       7015 -0.755268
       8016 -0.231781
      18000 -0.012827
c ==> Lead Shielding
m8     82206   0.247
       82207   0.227
       82208   0.526
c ==> Aluminum canning on detector (0.5 mm thk., rho = 147mg/cm^2)
m9     13027   1.000
c ==> Al2O3 Oxide reflector (1.6 mm thk., rho = 88mg/cm^2)
m10    13027   2.0
        8016   3.0
c ==> NaI Detector
m11    11023   0.5
       53127   0.5
c ==> Handling Notch Region (smeared density = 3.93 g/cc, wt% SS = 99.98)
m12   27000 -0.0008398
      24000 -0.1868626
      29000 -0.0016997
      26000 -0.6897720
      25000 -0.0105979
      42000 -0.0019996
      28000 -0.0964807
```

```
       6000 -7.9986480E-4
      15000 -0.0004499
      16000 -0.0002999
      14000 -0.0099980
c wt% Air = 0.02
       7015 -1.5105360E-4
       8016 -4.6356200E-5
      18000 -2.6254000E-6
c ==> Smeared materials
m13   27000 -8.3985E-04
      24000 -1.8687E-01
      29000 -1.6997E-03
      26000 -6.8978E-01
      25000 -1.0598E-02
      42000 -1.9996E-03
      28000 -9.6482E-02
      6000  -7.9988E-04
      15000 -4.4992E-04
      16000 -2.9995E-04
      14000 -9.9982E-03
      7015  -1.3718E-04
      8016  -4.2100E-05
      18000 -2.3299E-06
c
m14   27000 -2.4229E-04
      24000 -5.3910E-02
      29000 -4.9035E-04
      26000 -1.9900E-01
      25000 -3.0575E-03
      42000 -5.7688E-04
      28000 -2.7835E-02
      6000  -2.3079E-04
      15000 -1.2980E-04
      16000 -8.6533E-05
      14000 -2.8844E-03
      13027 -3.7647E-01
      8016  -3.3484E-01
      2004  -6.2390E-08
      7015  -2.4066E-04
      18000 -4.0873E-06
c
m15   27000 -0.000116175
      24000 -2.5849E-02
      29000 -2.3512E-04
      26000 -9.5417E-02
      25000 -1.4660E-03
      42000 -2.7661E-04
      28000 -1.3346E-02
      6000  -1.1064E-04
      15000 -6.2237E-05
      16000 -4.1491E-05
      14000 -1.3830E-03
      92233 -2.2257E-06
      92234 -1.9151E-04
      92235 -3.6414E-02
      92236 -3.5473E-04
      92238 -7.2050E-01
      8016  -0.104117649
      2004  -2.9915E-08
      7015  -0.000115484
      18000 -1.96132E-06
c
m16   27000 -2.4229E-04
```

```
      24000 -5.3910E-02
      29000 -4.9035E-04
      26000 -1.9900E-01
      25000 -3.0575E-03
      42000 -5.7688E-04
      28000 -2.7835E-02
      6000  -2.3079E-04
      15000 -1.2980E-04
      16000 -8.6533E-05
      14000 -2.8844E-03
      13027 -3.7647E-01
      8016  -3.3484E-01
      2004  -6.2390E-08
      7015  -2.4066E-04
      18000 -4.0873E-06
c
m17   27000 -8.3984E-04
      24000 -1.8687E-01
      29000 -1.6997E-03
      26000 -6.8978E-01
      25000 -1.0598E-02
      42000 -0.001999628
      28000 -9.6482E-02
      6000  -7.9987E-04
      15000 -4.4992E-04
      16000 -2.9994E-04
      14000 -9.9981E-03
      2004  -3.6383E-08
      7015  -1.4035E-04
      8016  -4.3070E-05
      18000 -2.3835E-06
c
m18   27000 -8.3561E-04
      24000 -1.8592E-01
      29000 -1.6911E-03
      26000 -6.8630E-01
      25000 -1.0545E-02
      42000 -1.9895E-03
      28000 -9.5996E-02
      6000  -7.9589E-04
      15000 -4.4765E-04
      16000 -0.000298432
      14000 -9.9477E-03
      2004  -4.6344E-03
      7015  -4.4720E-04
      8016  -1.3724E-04
      18000 -7.5950E-06
c ----------------------------Source Definition-----------------------
sdef  CEL=D1 POS=0 0 0 AXS=0 0 1 RAD D2 EXT D3 ERG D4 PAR=2
            VEC=-1 1 0 DIR D5
si1  L 62:63(0 5 0):66
sp1    1.0
c
si2  0. 1.102 $Sampling radius of fuel region in a pin
c
c 3"(7.62 cm) Axial Nodes
si3  H    11.1125 18.7325 26.3525 33.9725 41.5925 49.2125 56.8325
          64.4525 72.0725 79.6925 87.3125 94.9325 102.5525
c Relative Total Neutron Flux in axial node - Assume delayed gamma
c flux follows the neutron flux during operation
sp3       0. 0.033 0.058 0.078 0.091 0.109 0.115 0.118 0.114
             0.102 0.084 0.062 0.036
c
```

```
c 19 energy group structure in DELBG same for all times:
si4    H 0 .1  .2  .4  .6  .8 1.0 1.2 1.4 1.6 1.8
          2.0 2.2 2.4 2.6 3.0 4.0 5.0 6.0 7.5
c Gammas per second, from DELBG:
c 470 sec after SCRAM: Total Source = 1.6148e7 photons/sec
sp4  0. 0.0717 0.0710 0.1432 0.1119 0.1278 0.1378 0.0716
        0.0625 0.0467 0.0319 0.0243 0.0199 0.0151 0.0151
        0.0186 0.0200 0.0092 0.0018 0.0001
c Source Bias (exponential)
sb5    -31 3
nps 5.0e7
print
```

C.2 Input Files For 17x17 PWR Lattice

C.2.1 Heterogeneous Example

```
BTSHETX: Recreate Bozkurt and Tsoulfanidis Experiment
c 17 x 17 PWR array
c       Instrument tube and control rod channels modeled.
c       Top and bottom axial fuel blankets modeled.
c       Heterogeneous geometry - new axial source PDF.
c       Compositions and flux to dose function from paper.
c       Continuous PDF for source energy sampling.
c       Power law on source sampling of pin radius
c --- Begin Cell Definitions
c
1   0             1:2:-3                                  $Outside model
2   1 -1.296E-3  -1 -2 3 (4:-5:6:-7:8:-9)                 $Outside bundle
3   0            -4 5 -6 7 -8 9 fill=1                    $Bundle boundary
4   0            -10 11 -12 13 u=1 lat=1
                          fill=-8:8 -8:8 0:0
                2 2 2 2 2 2 2 2 2 2 2 2 2 2 2 2 2
                2 2 2 2 2 2 2 2 2 2 2 2 2 2 2 2 2
                2 2 2 2 2 4 2 2 4 2 2 4 2 2 2 2 2
                2 2 2 4 2 2 2 2 2 2 2 2 2 4 2 2 2
                2 2 2 2 2 2 2 2 2 2 2 2 2 2 2 2 2
                2 2 4 2 2 4 2 2 4 2 2 4 2 2 4 2 2
                2 2 2 2 2 2 2 2 2 2 2 2 2 2 2 2 2
                2 2 2 2 2 2 2 2 2 2 2 2 2 2 2 2 2
                2 2 4 2 2 4 2 2 3 2 2 4 2 2 4 2 2
                2 2 2 2 2 2 2 2 2 2 2 2 2 2 2 2 2
                2 2 2 2 2 2 2 2 2 2 2 2 2 2 2 2 2
                2 2 4 2 2 4 2 2 4 2 2 4 2 2 4 2 2
                2 2 2 2 2 2 2 2 2 2 2 2 2 2 2 2 2
                2 2 2 4 2 2 2 2 2 2 2 2 4 2 2 2
                2 2 2 2 2 4 2 2 4 2 2 4 2 2 2 2 2
                2 2 2 2 2 2 2 2 2 2 2 2 2 2 2 2 2
                2 2 2 2 2 2 2 2 2 2 2 2 2 2 2 2 2
c -- Fuel Pin
5   2 -10.5      -14 -21 22    u=2     $UO2
6   4 -0.972     -14  21       u=2     $Upper sprng. plenum
7   4 -0.972     -14 -22       u=2     $Lower sprng. plenum
8   0             14 -15       u=2     $Gap
9   3 -6.5        15 -16       u=2     $Clad
10  1 -1.296E-3   16           u=2     $Air
c -- Instrument tube
11  1 -1.296E-3  -17           u=3
12  3 -6.5        17 -18       u=3
13  1 -1.296E-3   18           u=3
```

```
c -- Control Rod Channel
14  1 -1.296E-3  -19          u=4
15  3 -6.5        19 -20      u=4
16  1 -1.296E-3   20          u=4

c --- Begin Surface Definitions
1   cz  520.0        $Model limit, radial
2   pz  300.0        $Model limit, top
3   pz -300.0        $Model limit, bot.
c
4   px  10.71        $Fuel assy., east edge
5   px -10.71        $Fuel assy., west edge
6   py  10.71        $Fuel assy., north edge
7   py -10.71        $Fuel assy., south edge
8   pz  193.40       $Fuel assy., top edge
9   pz -193.40       $Fuel assy., bot. edge
c
10  px  0.631        $Lattice elem., east edge
11  px -0.631        $Lattice elem., west edge
12  py  0.631        $Lattice elem., north edge
13  py -0.631        $Lattice elem., south edge
c
14  cz  0.3918       $Fuel pellet radius (0.0082 cm. pellet/clad gap)
15  cz  0.4000       $Fuel pin clad inner radius
16  cz  0.4572       $Fuel pin clad outer radius
c
17  cz  0.56136      $Instr. tube inner radius (0.04064 cm. clad thk.)
18  cz  0.602        $Instr. tube outer radius
c
19  cz  0.50546      $Cntrl. rod tube inner radius (0.04064 cm. clad thk.)
20  cz  0.5461       $Cntrl. rod tube outer radius
c
21  pz  182.88       $Top of fueled region of fuel pin
22  pz -182.88       $Bot. of fueled region of fuel pin

c --- Begin Data Cards
mode p
phys:p 2j 1
imp:p 0 1 14r
e0     1.0 2.0 3.0 4.0 5.0 7.5 20.0
f5z:p  0.0   15.2   0.0
       0.0   20.0   0.0
       0.0   25.0   0.0
       0.0   30.0   0.0
       0.0   40.0   0.0
       0.0   50.0   0.0
       0.0   75.0   0.0
       0.0  100.0   0.0
       0.0  200.0   0.0
       0.0  300.0   0.0
       0.0  400.0   0.0
       0.0  500.0   0.0
de5   0.01 0.015 0.02 0.03 0.04
      0.05 0.06  0.08 0.10
      0.15 0.20  0.30 0.40
      0.50 0.60  0.80 1.00 1.50
      2.00 3.00  4.00 5.00
      6.00 8.00 10.00 12.00
df5   0.062e-12 0.157e-12 0.238e-12 0.329e-12 0.365e-12
      0.384e-12 0.400e-12 0.451e-12 0.533e-12
      0.777e-12 1.030e-12 1.560e-12 2.060e-12
      2.540e-12 2.990e-12 3.830e-12 4.600e-12 6.240e-12
      7.660e-12 10.200e-12 12.500e-12 14.700e-12
```

```
      16.700e-12 20.800e-12 24.700e-12 28.900e-12
c
c -- Source Definition
sdef CELL=3:4:5 POS=0 0 0 AXS=0 0 1 RAD D1 EXT D2 ERG D3 PAR=2
c -- Radial probability p(x)=Cx^r, r=1
si1  0.0  0.392
c
c -- Axial probability calculated from p(z)=4.5[1+cos(pi*z/335.28)]
si2    -182.8 -175 -170 -160 -150 -140 -130 -120 -110 -100 -90
       -80 -70 -60 -50 -40 -30 -20 -10  0
        10 20 30 40 50 60 70 80 90 100 110 120 130 140 150
        160 170 175 182.8
sp2     0 0.01434 0.01555 0.01633 0.01789 0.01945
        0.02098 0.02247 0.02391 0.02529 0.02659
        0.02781 0.02892 0.02993 0.03083 0.03160
        0.03224 0.03274 0.03311 0.03333 0.03340
        0.03333 0.03311 0.03274 0.03224 0.03160
        0.03083 0.02993 0.02892 0.02781 0.02659
        0.02529 0.02391 0.02247 0.02098 0.01945
        0.01789 0.01633 0.01555
c -- Energy spectrum taken as discrete distribution
si3   H   0 1.0 2.0 3.0 4.0 5.0 7.5 20.0
sp3       0 1.511e-2  1.013e-4 1.511e-4 3.935e-8 9.640e-23
          2.937e-23 4.689e-25
c -- Air
m1     8000 -0.2315
       7000 -0.7552
      18000 -0.0133
c -- UO2
m2     8000 -0.1185
      92000 -0.8815
c -- Zirc
m3    40000 -0.9850
      50000 -0.0120
      26000 -0.0030
c -- Plenum composition (homog. spring)
m4    26000 -0.6950
      24000 -0.1900
      25000 -0.0200
      28000 -0.0950
c
c
nps 1e6
print -85 -86 -128
```

C.2.2 Homogeneous Example

```
BTSHOMX: Recreate Bozkurt and Tsoulfanidis Experiment
c 17 x 17 PWR array
c       Homogeneous model with all materials in fuel region uniformly blended
c       and all materials in the spring plenum regions uniformly blended.
c
c --- Begin Cell Definitions
c
1   0             1:2:-3                                  $Outside model
2   1 -1.296E-3  -1 -2 3 (4:-5:6:-7:8:-9)                 $Outside bundle
c -- Fuel Region
3   2 -3.5383    -4 5 -6 7 -10 11
c -- Plenum Regions
4   3 -0.8945    -4 5 -6 7 -8 10
5   3 -0.8945    -4 5 -6 7  9 -11

c --- Begin Surface Definitions
1   cz  520.0        $Model limit, radial
2   pz  300.0        $Model limit, top
3   pz -300.0        $Model limit, bot.
c
4   px  10.71        $Fuel assy., east edge
5   px -10.71        $Fuel assy., west edge
6   py  10.71        $Fuel assy., north edge
7   py -10.71        $Fuel assy., south edge
8   pz  193.40       $Fuel assy., top edge
9   pz -193.40       $Fuel assy., bot. edge
c
10  pz  182.88       $Top of fueled region of fuel pin
11  pz -182.88       $Bot. of fueled region of fuel pin

c --- Begin Data Cards
mode p
phys:p 2j 1
imp:p 0 1 1 1 1
e0     1.0 2.0 3.0 4.0 5.0 7.5 20.0
f5z:p  0.0   15.2   0.0
       0.0   20.0   0.0
       0.0   25.0   0.0

       0.0   30.0   0.0
       0.0   40.0   0.0
       0.0   50.0   0.0
       0.0   75.0   0.0
       0.0  100.0   0.0
       0.0  200.0   0.0
       0.0  300.0   0.0
       0.0  400.0   0.0
       0.0  500.0   0.0
de5   0.01 0.015 0.02 0.03 0.04
      0.05 0.06  0.08 0.10
      0.15 0.20  0.30 0.40
      0.50 0.60  0.80 1.00 1.50
      2.00 3.00  4.00 5.00
      6.00 8.00 10.00 12.00
df5   0.062e-12 0.157e-12 0.238e-12 0.329e-12 0.365e-12
      0.384e-12 0.400e-12 0.451e-12 0.533e-12
      0.777e-12 1.030e-12 1.560e-12 2.060e-12
      2.540e-12 2.990e-12 3.830e-12 4.600e-12 6.240e-12
      7.660e-12 10.200e-12 12.500e-12 14.700e-12
      16.700e-12 20.800e-12 24.700e-12 28.900e-12
```

```
c
c -- Source Definition
sdef CELL=3 X=D1 Y=D2 Z=D3 ERG=D4 PAR=2
c -- Radial probability: equal probable throughout smear
si1  -10.7 10.7
sp1   0    1
si2  -10.7 10.7
sp2   0    1
c
c -- Axial probability calculated from p(z)=4.5[1+cos(pi*z/335.28)]
si3    -200 -182.8 -175 -170 -160 -150 -140 -130 -120 -110 -100
       -90 -80 -70 -60 -50 -40 -30 -20 -10  0
        10 20 30 40 50 60 70 80 90 100 110 120 130 140 150
        160 170 175 182.8
sp3     0 0.01434 0.01555 0.01633 0.01789 0.01945
        0.02098 0.02247 0.02391 0.02529 0.02659
        0.02781 0.02892 0.02993 0.03083 0.03160
        0.03224 0.03274 0.03311 0.03333 0.03340
        0.03333 0.03311 0.03274 0.03224 0.03160
        0.03083 0.02993 0.02892 0.02781 0.02659
        0.02529 0.02391 0.02247 0.02098 0.01945
        0.01789 0.01633 0.01555 0.01434
c -- Energy spectrum taken as discrete distribution
si4   H   0 1.0 2.0 3.0 4.0 5.0 7.5 20.0
sp4       0 1.511e-2  1.013e-4 1.511e-4 3.935e-8 9.640e-23
          2.937e-23 4.689e-25
c -- Air
m1     8000  -0.2315
       7000  -0.7552
      18000  -0.0133
c -- Fuel Region
m2     92000 -0.7259
        8000 -0.0976
       40000 -0.1737
       50000 -0.0021
       26000 -0.0005
        7000 -0.0002
c -- Plenum Region
m3     26000 -0.2117
       24000 -0.0573
       25000 -0.0060
       28000 -0.0286
       40000 -0.6870
       50000 -0.0084
        8000 -0.0002
        7000 -0.0008
c
c
nps 1e6
print -85 -86 -128
```